

UV-photo rearrangement and isomerization with adsorption and UHPLC PAT-monitoring in continuous micro-flow

Citation for published version (APA):

Shahbazali, E. (2018). *UV-photo rearrangement and isomerization with adsorption and UHPLC PAT-monitoring in continuous micro-flow*. [Phd Thesis 1 (Research TU/e / Graduation TU/e), Chemical Engineering and Chemistry]. Technische Universiteit Eindhoven.

Document status and date:

Published: 18/09/2018

Document Version:

Publisher's PDF, also known as Version of Record (includes final page, issue and volume numbers)

Please check the document version of this publication:

- A submitted manuscript is the version of the article upon submission and before peer-review. There can be important differences between the submitted version and the official published version of record. People interested in the research are advised to contact the author for the final version of the publication, or visit the DOI to the publisher's website.
- The final author version and the galley proof are versions of the publication after peer review.
- The final published version features the final layout of the paper including the volume, issue and page numbers.

[Link to publication](#)

General rights

Copyright and moral rights for the publications made accessible in the public portal are retained by the authors and/or other copyright owners and it is a condition of accessing publications that users recognise and abide by the legal requirements associated with these rights.

- Users may download and print one copy of any publication from the public portal for the purpose of private study or research.
- You may not further distribute the material or use it for any profit-making activity or commercial gain
- You may freely distribute the URL identifying the publication in the public portal.

If the publication is distributed under the terms of Article 25fa of the Dutch Copyright Act, indicated by the "Taverne" license above, please follow below link for the End User Agreement:

www.tue.nl/taverne

Take down policy

If you believe that this document breaches copyright please contact us at:

openaccess@tue.nl

providing details and we will investigate your claim.

UV-Photo Rearrangement and Isomerization with Adsorption and UHPLC-PAT Monitoring in Continuous Micro-flow

Elnaz Shahbazali

Elnaz Shahbazali

UV-Photo Rearrangement and Isomerization with
Adsorption and UHPLC- PAT Monitoring in Continuous Micro-flow



UV-Photo Rearrangement and Isomerization with Adsorption and UHPLC-PAT Monitoring in Continuous Micro-flow

PROEFSCHRIFT

ter verkrijging van de graad van doctor aan de Technische Universiteit Eindhoven, op gezag van de rector magnificus prof.dr.ir. F.P.T. Baaijens, voor een commissie aangewezen door het College voor Promoties, in het openbaar te verdedigen op dinsdag 18 september 2018 om 11:00 uur

door

Elnaz Shahbazali

geboren te Tehran, Iran

Dit proefschrift is goedgekeurd door de promotoren en de samenstelling van de promotiecommissie is als volgt:

voorzitter:	prof.dr.ir. E.J.M. Hensen
1 ^e promotor:	prof.dr. V. Hessel
co-supervisor(s):	prof.dr. J. Meuldijk dr. T. Noël
leden:	dr. S.C.J. Meskers prof.dr.rer.nat. H. Löwe (Johannes Gutenberg Universitat Mainz) prof.dr.ir. M. van Sint Annaland prof.dr. M. Honing (Maastricht University)

Het onderzoek of ontwerp dat in dit proefschrift wordt beschreven is uitgevoerd in overeenstemming met de TU/e Gedragscode Wetenschapsbeoefening.

This research is funded by the European Research Council (ERC) advanced grant on “Novel Process Windows – Boosted Micro Process Technology” under grant agreement number 267443.

UV-Photo Rearrangement and Isomerization with Adsorption and UHPLC-PAT Monitoring in Continuous Micro-flow

© Elnaz Shahbazali

Eindhoven University of Technology, 2018

Cover designed by Elnaz Shahbazali and Loes Kema

A catalogue record is available from the Eindhoven University of Technology Library

ISBN 978-90-386-4580-3

Printed by GVO drukkers & vormgevers B.V.

To my family

" تعصب در دانش و فلسفه مانند هر تعصب دیگری نشانه خامی و بی مایگی است و همیشه به زیان حقیقت تمام می شود."

ابن سینا

Table of content

Summary	i
1 Introduction	1
1.1 Continuous flow chemistry	2
1.2 Novel process window as an enabling tool	3
1.3 Photo-flow	5
1.4 UV-photo flow chemistry	8
1.4.1 UV-light sources	9
1.4.2 Photo-microreactor material	10
1.5 Scope and outline of the thesis	11
1.6 References	14
2 Impact Factor Analysis of the Claisen Rearrangement, in Batch and in Flow	19
2.1 Impact Factor Analysis of the Claisen Rearrangement in Batch and in Flow	20
2.2 Mechanistic analysis of the Claisen rearrangement – quantum-mechanistic modelling and most modern spectrometric analysis	20
2.3 Factors impacting the rearrangement – a comparison of batch and flow processing	22
2.3.1 Substituent effects	22
2.3.2 Solvent effects	24
2.3.3 Catalytic effects	27
2.3.4 Temperature effects	28
2.3.5 Non-thermal activation effects: Photochemistry	30
2.3.6 Pressure effects	32
2.3.7 Concentration effects	33
2.3.8 Reaction time effects	33
2.4 Conclusions	33
2.5 References	35
3 Connected Nucleophilic Substitution-Claisen Rearrangement in Flow – Analysis for Kilo-Lab Process Solutions with Orthogonality	41
3.1 Introduction	43
3.2 Experimental procedures	45
3.2.1 Microchannel experiments	45
3.2.2 Packed bed experiments	46
3.2.3 Other experiments	47
3.3 Results and Discussion	48
3.3.1 Orthogonality of product and auxiliary materials between the two reactions	48
3.3.2 Homogeneous base removal	49
3.3.3 Liquid-liquid extraction and acid absorption	50
3.3.4 Heterogeneous base	52
3.3.5 Dilution	58
3.3.6 Orthogonality check via photo-Claisen rearrangement approach	61
3.4 Conclusions	61
3.5 Acknowledgment	63

3.6	References	64
3.7	Supplementary Material	68
S1	General reagent information	68
S2	Analytical procedures for Claisen rearrangement and nucleophilic substitution experiment	69
S3.1	Batch nucleophilic substitution reaction	69
S3.2	Amberlyst A26 characterization	69
S3.3	Analysis for batch reactions	69
S4	Solvent selection	70
4	Photo-Claisen Rearrangement of Allyl Phenyl Ether in Micro-Flow: Influence of Phenyl Core Substituents and Vision on Orthogonality	73
4.1	Introduction	75
4.2	Results and discussion	76
4.2.1	Parametric sensitivities of the photo-Claisen rearrangement of allyl phenyl ether in micro-flow	76
4.2.2	Orthogonality – Process simplification connecting to a prior nucleophilic substitution	82
4.2.3	Meta-substituent effect on <i>para</i> - to <i>ortho</i> -isomer distribution for the photo-Claisen Rearrangement of allyl phenyl ether in micro-flow	83
4.2.4	Substitution effects in photo micro-flow	84
4.2.5	Substitution effects in photo batch as comparison	85
4.2.6	High-temperature photo micro-flow	85
4.3	Conclusions	87
4.4	Acknowledgment	87
4.5	References	88
4.6	Supplementary Material	91
S.1	General reagent information	91
S.2	Experimental section	91
S.3	General analysis information	91
S.4	Synthesis of 3-substituted allyl phenyl ethers	92
5	UV-Photo Flow Intensification - Taylor Flow for Enhancing Photo-Microreactors	95
5.1	Introduction	97
5.2	Experimental section	99
5.2.1	General Taylor flow experiments	99
5.2.2	Taylor flow experiments in MCFI	100
5.3	Results and Discussion	100
5.3.1	Concentration effect on Photo-Claisen Rearrangement	100
5.3.2	Introducing the Taylor flow Concept into Photoreaction	102
5.3.3	Light confinement effect in Taylor flow	105
5.3.4	Taylor flow in MCFI	108
5.4	Conclusion	111
5.5	References	114
5.6	Supplementary Material	116
S.1	General reagent information	116
S.2	General analysis information	116
6	UV-Photo Flow Photostatistics-Actinometry Measurements in Flow	117
6.1	Introduction	119
6.2	Theoretical description	120

6.2.1	Actinometry: Concept & experimental setup	120
6.2.2	Theoretical description photon flux	123
6.3	Experimental section	125
6.3.1	Reactor configurations	125
6.3.2	Actinometer Synthesis	126
6.4	Results & discussion	127
6.4.1	Ferrioxalate synthesis	127
6.4.2	Light source	128
6.4.3	Results & discussion for the three configurations	128
6.4.4	Comparison between the different configurations of the microreactor with respect to the lamp	132
6.5	Conclusions	133
6.6	References	135
6.7	Supplementary Material	136
S1	General reagent information	136
S.2	Light Source	136
S.3	Post-irradiation treatment	136
S.4	Continuous flow system	137
S.5	Characterization	138
7	UV-Photo Flow on-line Analytics - Coupled UHPLC and Potential for Design of Experiments	141
7.1	Introduction	143
7.2	Experimental Part	146
7.2.1	Experimental setup	146
7.2.2	Experimental conditions of sampling and chromatographic separation.	147
7.3	Results and Discussion	147
7.3.1	Online sampling and analytic time distribution	147
7.3.2	Timing of sampling, analysis, and settling time for next experiment	147
7.3.3	Sampling volume	149
7.3.4	Sampling reliability and robustness	150
7.3.5	Analysis of the confidence in the results obtained	153
7.3.6	Statistical approach of the Photo-Claisen reaction parameters	155
7.4	Conclusions	157
7.5	Acknowledgements	158
7.6	References	159
8	UV-Photo Flow Application- Isomerization of <i>cis</i>-Cyclooctene to <i>trans</i>-Cyclooctene	165
8.1	Introduction	167
8.2	Continuous Flow Setup	169
8.3	Theoretical study	170
8.3.1	Photoisomerization of cis to trans-cyclooctene	170
8.3.2	Kinetics of the photoisomerization	170
8.3.3	Adsorption Isotherm	171
8.3.4	Langmuir isotherm	171
8.3.5	Packed bed Modeling	171
8.3.6	Mass transfer resistance and intrinsic adsorption rate	172
8.3.7	Breakthrough curve prediction	173
8.3.8	Modeling the combination of the photo-microreactor and the adsorption column	174

8.4	Results and Discussion	175
8.4.1	Kinetic study of photoisomerisation	175
8.4.2	Adsorption isotherm	176
8.4.3	Adsorption kinetics	177
8.4.4	Packed bed	179
8.4.5	Process design for integration of a photo-microreactor and adsorption for the isomerization of cis-cyclooctene in to trans-cyclooctene	179
8.4.6	Process configurations	180
8.4.7	Validation of the model in the combination of photo-microreactor and adsorption column	189
8.5	Conclusions	187
8.6	Acknowledgements	188
8.7	References	189
8.8	Supplementary Material	192
S1	Experimental section	192
S2	Kinetics of photoisomerisation	194
S3	Internal mass transfer resistance calculation	194
S4	External mass transfer resistance calculation	198
9	Micro-flow Photosynthesis of New Dienophiles for Inverse-Electron-Demand Diels-Alder Reactions. Application for Pretargeted <i>in vivo</i> PET Imaging	201
9.1	Introduction	202
9.2	Syntheses	203
9.3	Conclusions	205
9.4	References	206
9.5	Supplementary material	207
9.5.1	Material and general methods	207
9.5.2	Syntheses	207
10	Conclusions	219
10.1	Conclusions and Research Highlights	220
10.1.1	Conclusions	220
10.1.2	Research Highlights	221
11	Metallic Nanoparticles Made in Flow and their Catalytic Applications in Organic Synthesis	225
		225
	List of Publications	227
	Acknowledgement	231
	About the author	235

Summary

The research presented in this thesis focuses on continuous micro-flow processing of two UV photo-induced reactions under Novel Process Windows (NPW) - the Claisen rearrangement and the *cis*- to *trans*-cyclooctene (TCO) isomerization. The main focus is to develop integrated process design solutions under the given highly chemically intensified (under Novel Process Window) conditions - very fast reaction, and high-c smallest volumes. Therefore, it covers two intensification principles of NPW, chemical intensification and process-design intensification.

The Claisen rearrangement can lead to different isomers, whether thermal or photo-chemical pathways are chosen. NPW provides access to entirely new parameter sets – the NPW chosen here are new chemical transformation by photo or thermal activation. The options provided by NPW are investigated in the above given situation and high conversion at unusual high concentration.

The photo and thermal micro-flow syntheses can be combined to the nucleophilic ether formation of the Claisen substrate and together provide opportunity in increased chemical diversity, which is also process-design intensification.

Chapter 1 gives an overview of continuous flow chemistry particularly UV-photo flow chemistry. Also, it introduces more in details of NPW principles. Chapter 2 provides an analysis of different impact factors such as choice of substituent, catalyst, temperature, pressure, concentration, flow rates, and solvent. It is well-known that flow processing offers profound opportunities for studying these factors which are known to have large impact on the Claisen rearrangement done in batch.

In chapter 3, the selectivity issue of the two-step synthesis of phenol to 2-allylphenol by thermal-Claisen rearrangement is tackled. It is explained that the combining of two synthetic organic pathways could create orthogonality problems. The root of orthogonality issues were discussed and experimentally verified. It is revealed that the issues are related to two major reasons. The first one was due to the reagent compatibility. And the second one was related to the nature of the reaction kinetics. To deal with, five alternative approaches were considered and among all four approaches were chosen to compare with each other, giving each one's pros and cons. The comparison was done based on prominently the reaction yield, volumetric efficiency, energy consumption, and steadiness of the operation.

The photo-Claisen rearrangement of aromatic substrates gives the *para*-isomer which is not yielded by the thermal pathway. In chapter 4, photo-Claisen rearrangement of allyl phenyl ether in microreactor is studied. In order to do that, first some relevant parametric sensitivities of photo-Claisen rearrangement was addressed. Thanks to the small dimension of microreactors, the reaction time could be reduced from hours to 8 min or less. It was shown that operation at

relatively high concentration, 0.05 M, (compared to the batch mode) was achieved. In the same chapter, increasing molecular diversity was explored by applying 3-substituted phenols as precursor to undergo photo-Claisen rearrangement. The results demonstrated formation of 4-allyl product in addition to the *ortho*- and *para*- allyl products. Also, combination of high-temperature and photo was tackled. Yet, this did not improve the reaction performance, but rather led to more photo degradation. Finally, combining of nucleophilic substitution and photo-Claisen rearrangement did not show a major orthogonality issue.

In photoreactors to go for high concentration is usually a bottleneck. In chapter 5 the concept of applying two phase flow in order to open a new path in photo-flow chemistry is investigated. Here, the concept of Taylor flow (gas-liquid two phase flow) gives a promise to go for even higher concentrations due to the very small film thickness provided compared to one-phase flow microfluidics. The effective mixing zone in the liquid slug may provide reactant refreshment in the thin layer film around the gas slug, enhancing the quantum efficiency of the photoreaction. A set of experiments gives evidence hereabout.

A procedure for photon flux measurements, by means of actinometry experiments using ferrioxalate in microreactors is developed in chapter 6. The determination of photon fluxes were considered for configurationally different systems, including a capillary tower, placing the reactor directly on the UV-lamp and a coil flow inverter. The capillary tower is the mostly-used configuration in this thesis. Winding microreactor on the UV-lamp is tested in chapter 3. The coil flow inverter capillary tower is applied in chapter 4. According to the results, the amount of photon absorbed by the configuration that the reactor was placed on the lamp was higher. Between coil flow inverter and capillary tower, there was not a huge difference, though coil flow inverter showed slightly more photon absorption.

Chapter 7 describes the coupling of flow chemistry and continuous online analytics with the aim to develop Process Analytical Technology (PAT) methodology under the given NPW conditions. The low volumes typical for micro-flow pose challenges for sampling operations in analytics. In this chapter, a fast process was combined with a modified ultra-high-performance liquid chromatography (UHPLC) system allowing for very fast sampling and analysis. Low-volume online sampling was introduced here for UHPLC analysis of the photo-Claisen rearrangement in micro-flow. Chances and challenges were critically reviewed, including the reproducibility and robustness of the sampling.

In the last part of this thesis, integrated micro-flow adsorption was developed for product separation, with option to do that in recycle mode. This was investigated first for the Claisen rearrangement in chapter 3, and thereafter more in depth for the TCO photo-isomerization in chapter 8. Here, the thermodynamic equilibrium was shifted by inserting an in-flow separation in a recycling flow mode, which makes better use of the given photoenergy (transport

intensification). In this part the full theoretical study of in-flow separation in a recycling flow mode has been investigated. Moreover, in chapter 9 different process design to reach optimum yield of TCO derivatives that is valuable in PET imaging is proposed and experimentally tested. Finally, chapter 10 gives an overview of the research highlights described in previous chapters of this dissertation.

In conclusion, this thesis aimed at a study of a chemical reaction under highly intensified micro-flow conditions under the sponsorships of novel process windows (NPW). The thesis was performed together with 4 others (and a post-doc research) in the framework of an ERC Advanced Grant and was the last to start. This thesis made the first consideration to NPW transfer intensification with regard to micro-flow separation. More than the proof-of-concept for integrated reaction and separation explored in the thesis of Dr. I. Vural-Gürsel (ISBN: 978-90-386-3957-4), deep theoretical analysis thereof is given, the question of orthogonality been tackled, and recycle flow introduced to account for the need of multiple-stage operation.

CHAPTER 1

Introduction

1.1 Continuous flow chemistry

Since the first chemical reaction carried out in the old-fashioned chemistry lab, chemists have been utilizing the same fundamental concept of the lab equipment. Still, scientists conduct most of the reaction synthesis in the famous round-bottom flask which is still considered as the applicable equipment to perform small scale reactions in batch mode. Though, the lab equipment seems to be very efficient for small scale and lab tests, considering them for industrial scale is not appropriate. Because only scaling up according to the size of larger vessels would rather make the chemical reaction inefficient due to the lack of heat and mass transfer performance. Therefore, to have more efficient bulk production, petrochemical industries have scaled up the laboratory glasswares to more effective operational units such as pipes and tubes that could afford the continuous operation [1].

Comparing to bulk-chemical industries, fine-chemistry industries and specially pharmaceuticals, still perform most of their production in the so-called batch mode using stirred tanks. This is due to the fact that their production rate is smaller and up to now the focus was more to synthesize the right active pharmaceutical ingredient (API), i.e. product design rather than the process design. Nevertheless, such a vision for scaling up the production line, often leads to inefficient production. Having a poor degree of control over the transport phenomena which can lead to safety issues in (large scale) stirred tank reactors is the main challenge in the batch mode production [2].

Recently, continuous flow chemistry has attracted the most attention since it can be considered as a potential to diminish the risks involved by conventional batch scale up for more efficient mode of scale up [3]–[6]. In fine-chemical industries since the process of synthesizing the final product is quite sensitive, it is very important to have complete control over heat and mass transfer. To overcome this, a new technology of continuous flow, micro-flow chemistry, has broadened the view towards better and more efficient control of chemical synthesis. The key features in microreactors are the high surface-to-volume ratio, reduced diffusional length scales and reducing chemical reaction time which can offer smaller time constant for mass and heat transfer properties as compared to traditional batch reactors. Keeping the transport phenomena under good control may lead to preventing accumulation of unwanted byproducts (which can in some cases be hazardous material) or preventing a consecutive reaction of the desired product. The advantages of the decreased time constant for heat transfer can be very important for instance in multiphase reactors. The improved heat transfer in microreactors diminishes the chance of the formation of so-called local “hot-spots”, as compared to batch reactors. Accordingly, the product selectivity is improved by performing exothermic, (multiphase) reactions in a microreactor. Furthermore, the small-sized microreactors have safety advantages in the use of toxic, harmful or expensive chemicals. Besides, microfluidic synthesis techniques

operate at steady state and give superior control over reaction conditions, such as reagent addition, mixing, and temperature. Another interesting feature of them is that online monitoring can be implemented, allowing a quick parameter-space study for kinetic studies which allows quick optimization [1], [7].

Applying the flow chemistry concept even in lab scale, not only allow us to create better synthesis platform but also it makes it easier to transfer the small lab scale to the larger production scale [8]. To elaborate more, scaling up from lab scale to a larger scale involves less redesigning of reaction parameters since both are in continuous mode. Also, mixing in flow systems is relatively well characterized in comparison to batch vessels. Scaling up of microreactors can be achieved in a number of ways, such as numbering up the reactors in parallel or by increasing the reactor diameter. Also, combination of the techniques are possible. It is important that mixing characterization and fluid dynamics remains the same throughout the scale up process.

Although micro-flow chemistry has a lot advantages, it is not suitable for all the chemical reactions. Roberge *et al.* analyzed 22 different reactions in fine chemicals and found out that performing in micro-flow can be beneficial for 50% of the reactions [9]. Based on their outcomes, they classified the reactions in to 4 classes, A, B, C, D. Class A is related to the reactions that are very fast and exothermic. In this type of reaction having good control of heat transfer minimizes the formation of hot zones resulting in higher selectivity towards the final product and less byproduct formation. Class B are reactions that are exothermic but slower (less than 10 min) than class A reactions. Again it is important to have good mass and heat transfer. Slower reactions due to the kinetic limitation are categorized as class C. Class C reactions may result in some safety issues such as thermal accumulation and autocatalysis. Class D represents very slow reactions with a time frame of hours or even days. These reactions can be enhanced by increasing intrinsic rate by applying harsh process conditions [9].

In 2005, the American Chemical Society Green Chemistry Institute (ACS GCI) founded the so-called Pharmaceutical Roundtable [10], [11]. The Pharmaceutical Roundtable is a multi-industrial “think tank” including the leading pharmaceutical manufacturers which intended to improve the sustainability and environmental aspects of the production processes [10]. According to their report continuous processing and process intensification have been chosen as key green engineering research areas. Moreover, the main outcomes from the operation of continuous manufacturing would be process safety, better environmental impact and enhanced quality of the product.

1.2 Novel process window as an enabling tool

The concept of Novel Process Window (NPW) first time was introduced by Hessel *et al.* in 2008 [4], [12], [13]. NPW is a new technological platform in the micro-flow area. It is based on two

aspects of process design and improvement (Figure 1.1). The first aspect is related to chemical intensification, where intrinsic reaction rate can be increased by applying harsh reaction conditions [14]–[19]. This can be explained by boosting the reaction by orders of magnitude by massive increase in temperature, pressure and/or concentration. According to Arrhenius equation increasing the temperature accelerate the reaction rate. Due to the high heat transfer efficiency in the microreactors, they provide rapid increase in temperature and therefore pressure in a safe mode. In order to keep the reaction medium in liquid phase which is important for some reactions, increasing temperature has to be coupled with an increasing pressure. The mechanical stability of the microreactors allows to perform harsh conditions and a safe mode. Solvent less or even solvent free reactions benefit from the high concentration of the reactant. Also, low used amounts of solvent would simplify the separation processes and leads to greener processes.

The second aspect of NPW is process-design intensification [20], [21]. In this section, integration of different reactions and their influence on each other is considered in a way that the whole process becomes simpler and more intensified. Although this would seem to happen in the conventional processes, intensification in micro-flow would go even much further because miniaturization in micro-flow would lead to a completely new level of intensification.

Besides those mentioned aspects, there is chemical transformation which is at the interface of chemical and process-design intensification [22]–[24]. Chemical transformation would profit from both aspects of intensification. For instance, connecting of multi-step processes by omitting intermediate separation whenever is possible [24].

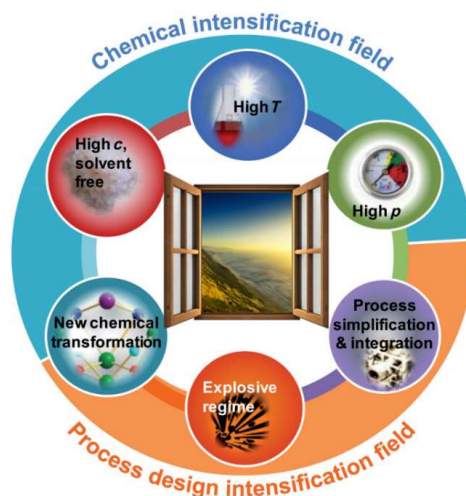


Figure 1.1 Schematic representation of Novel Process Windows [12] Reprinted with kind permission of Wiley-VCH, Weinheim.

1.3 Photo-flow

Among other types of organic chemistry, photo-flow chemistry also has received a lot of attention during the last decade not only in research environments but also from industry, since it has several advantages comparing with conventional batch processes [25]–[30]. The advantages that were stated earlier for flow chemistry, especially for microreactors, are applicable for photo-flow chemistry as well, such as the high surface-to-volume ratio, reduced diffusional dimensions, reducing chemical reaction time, the possibility to avoid accumulation of hazardous intermediates, higher selectivities, and etc. The key point in microreactors is the miniaturization of the reactor dimensions and therefore the reaction media (Figure 1.2). To elaborate more on how these advantages of photoreactors are correlated with their performance, further clarifications are provided below [31].

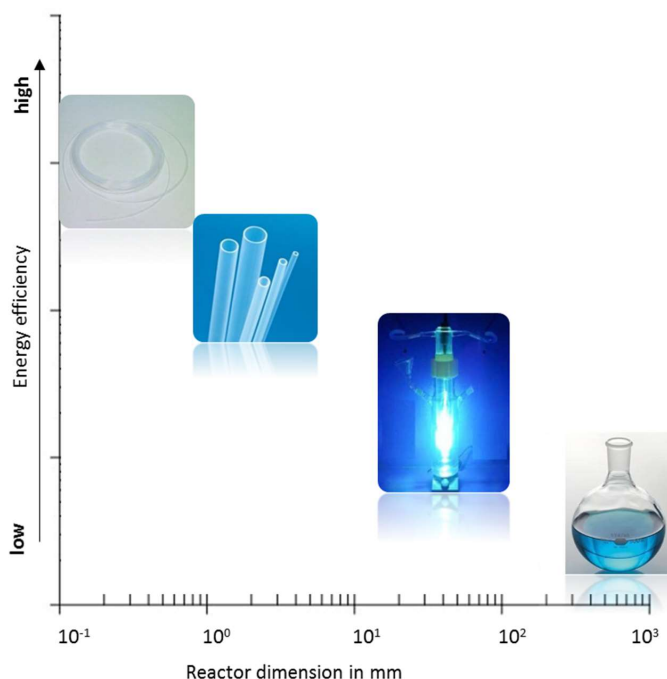


Figure 1.2. Comparison of batch and continuous flow reactor based on energy efficiency

Irradiation of the reaction media. In photochemistry the most important driving force is the photon absorption. According to Bouguer–Lambert–Beer law (Equation 1.1), absorption depends on the molar extinction coefficient (ϵ), the concentration of the absorbing species (C), and the path length (l).

$$T = \frac{I}{I_0} = 10^{-\varepsilon c l} \quad (1.1)$$

Also, it shows that light intensity (I) and transmittance (T) is reduced by increasing the path length of light propagation. This means that the first layers of reactant molecules that are close to the reactor wall receive the most significant amount of the incident light. The effect of characteristic dimensions of photoreactors on light absorption is illustrated for photo-Claisen rearrangement of allyl phenyl ether in Figure 1.3. As it can be seen, the light intensity reduces rapidly as the penetration path of the light is increasing. Another important measure is the photon flux which is defined as the amount of photons received per unit time. Even if this number has the same order of magnitude in both batch and microreactors, dividing this number by the volume of the reactor gives the photon flux density which is an important reactor parameter. Considering a batch volume of 50 ml and a microreactor of 0.5 ml, the photonflux density in microreactor is 100 times higher than in batch. This explain very well why photoreaction in microreactors can be greatly boosted compared with batch reactors [26].

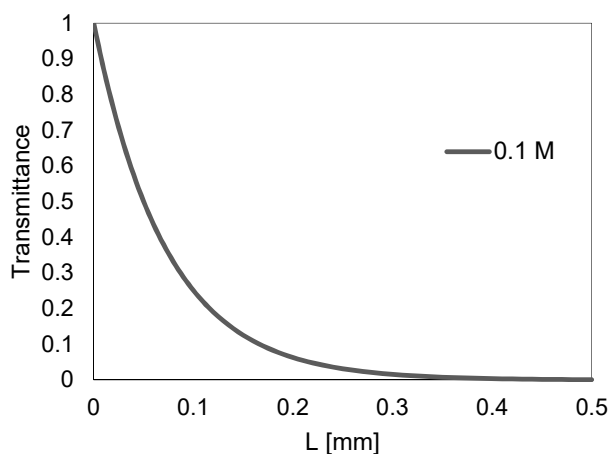


Figure 1.3 Bouguer-Lambert-Beer law and the Transmission (%) of light as a function of distance for photo-Claisen rearrangement of Allyl phenyl ether in 1-butanol (0.1 M)

Scale-up capability. Scale-up and reaching high productivity of photoreactions is a tough challenge, owing to Bouguer-Lambert-Beer law and consequently photon transport limitation. In fact, scaling up a small scale photoreactor by increasing all dimensions of the reactor cannot provide the same performance [27], [32]–[34]. Therefore, more efficient scale-up can be given by microreactors. In order to preserve the advantage of microreactors, it is crucial to keep the light penetration path (diameter of the microchannel) as small as possible. Instead scale-up can be done by either increase the throughput while keeping the residence time constant (longer reactor) or numbering-up. The first option, although it seems to be more applicable, has some

drawbacks. Higher flow rates in longer reactors lead to higher pressure drops and energy dissipation. Moreover, a higher productivity can be obtained by numbering-up the microreactors, which is applying several microreactors in parallel. Numbering-up can be internal or external. The external numbering-up can be obtained by introducing several microreactor systems (together with the pump and the rest of control system) in parallel [34]. The internal numbering-up can be carried out by numbering-up the reactor itself and using flow distributor system and equalizing the flow rate in each reactor [35]. Although the internal numbering-up looks more cost efficient, it also has some disadvantages. A small disturbance in pressure drop can result in flow maldistribution and therefore the performance of the individual reactors would be different.

Enhanced selectivity. In batch system, the photon homogeneity in the reaction mixture is much less than in the microreactor. Therefore, prolonged light exposure can lead to the consecutive reactions or even degradation of the molecules that are closer to the light source. However, as mentioned earlier, generally, microreactors can enhance the selectivities [36]. In photomicroreactors, this feature is mostly correlated to the lower required irradiation time since the molecules spent less time in the reaction zone.

Improved mixing. In a microreactor, the flow pattern is governed by laminar flow. In laminar flow, the fluid is moving in parallel layers and mixing is mostly driven by molecular diffusion. The characteristic mixing time in microchannel can be obtained by Einstein-Smoluchovski equation (Equation 1.2).

$$t_m = \frac{L^2}{D} \quad (1.2)$$

where, L is the diffusion path length and D is the molecular diffusivity. According to equation 1.2, with the same reaction mixture, the smaller the diffusion path length, the better the mixing is. Therefore, better mixing helps in improving the selectivity as well [31], [37].

Efficient heat transfer. High temperatures inside the reaction medium, can result in unwanted-byproducts via a thermal route. In photoreactions, especially UV-photoreactions, part of the energy of the UV-light is converted in to thermal energy [38]. Therefore, UV-lamps can be a source of heat for the reaction mixture. In microreactors due to the high-surface-to volume ratio, heat transfer is much more efficient compared to the conventional batchwise operated stirred tanks.

Multiphase reaction. Multiphase reactions deal with the combination of two or more immiscible phases (e.g. gas-liquid or liquid-liquid reactions). If the reaction rate is limited by the mass transfer from one phase to the other, it is important to provide high interfacial area. Comparing with batch processes, in microreactors, due to their small dimension, a larger specific interfacial area is available providing efficient mass transfer between two immiscible phases [39], [40].

Multistep reaction. Usually in organic synthesis including photochemistry, there are several fundamental reaction steps involved to form the final product. Performing all these individual steps in the conventional batch mode is very complex and time consuming. Recently, with the aid of flowchemistry, all these steps can be combined in one stream line and carried out in a cascade mode [41]. Such a continuous flow process would be very time beneficial and requires less manpower [42]. Also, this improvement has become even more popular due to the novel in-line analytical tools which provide an even faster process control [43]. Another advantage of performing multistep reactions in flow mode, is preventing accumulation of hazardous intermediates, since those intermediate products react further as soon as they have been formed in flow [44], [45].

Safety. As stated earlier, the key advantage of microreactors is preventing accumulation of highly reactive or hazardous intermediates. Therefore performing the reaction in a microreactor leads to a safer mode. In addition, better heat and mass transfer in microreactors avoids hot zones and consequently less runaway.

1.4 UV-photo flow chemistry

Ultraviolet (UV) radiation is electromagnetic radiation with a wavelength ranging from 10 nm to 400 nm, shorter than that of visible light but longer than X-rays. UV radiation is present in sunlight but less than 10% of the total light output of the sun is UV light radiation. Therefore, the UV-radiation intensity in sunlight is quite low. Similar to other wavelength ranges, UV energy can activate reagents to undergo a photochemical transformation. This can occur directly or by means of catalyst. The energy level of UV irradiation is quite high as compared to the higher wavelength radiation; 598-342 kJ/mol attributed to 200-350 nm, respectively [26].

As stated UV light can activate the organic molecules directly. Among all photochemical synthesis, photocycloaddition is the most applied reaction which leads to formation of carbon-carbon bonds in cyclic form. Therefore, many flow photochemists have chosen photocycloaddition as a platform to apply it in flow mode [46]–[48]. Booker-Milburn *et al.* reported on the [2+2] photocycloaddition of maleimide and n-hexyne in microreactor [46]. They made a higher throughput by using a flow reactor with an internal diameter of 2.7 mm ID continuously in 24h and they produced more than 680 g of the target product. Performing a similar type of a photocycloaddition in a batch reactor yielded only 0.63 gr of product after 1 hr [49], implying that in the flow mode, Booker-Milburn *et al.* were able to produce 44 times more than in a conventional batch reactor. More photocycloaddition reactions have been carried out in microreactors, one can be referred to [26]. Another direct light absorption photoreactions is photochemical rearrangement [50]. Photochemical rearrangement usually transforms simple molecules into more complex mostly cyclic molecules. The photochemical rearrangement 4-

hydroxycyclobutenones to produce 5H-furanones was carried out in a flowreactor (1 mm ID) to achieve 99% yield in 90 min by Harrowven *et al.* [51]. In contrast, the same photochemical rearrangement in a batch mode resulted in undesired photo degradation of the product and a yield 27% after 4 hr was obtained [51]. Moreover, photo-microreactors were applied to perform a variety of photocyclizations, for instance, to synthesize pyridocarbazole, phenanthrenes and helicenes, etc [52], [53]. Seeberger *et al.* conducted synthesis of pyridocarbazoles in a continuous flow mode and compared the results with the batch operation [53]. In continuous flow mode it was possible to reach 95% yield in less than 20 min. However, in batch mode it was more challenging, since due to the long reaction time, (more than 5 hrs) a significant amount of byproducts were formed which made the isolation of the desired product not very efficient. More photoreactions have been carried out in microreactors, here, only some examples were given.

1.4.1 UV-light sources

A proper selection of a light source for photochemical reactions is very crucial and it is important to have the overlap between the emission spectrum of the light source and the absorption characteristics of photo-reactive reagent. Other important characteristics for choosing a suitable light source are energy efficiency, cost, fitting the dimensions to the photoreactor setup and finally the life time of the light source.

The most-commonly used UV-light sources are arc lamps and among them the most famous one is the mercury-discharge lamp which contains mercury vapor in a vacuum glass bulb. UV emission of this type of UV- light comes from excitation of mercury atoms through electrical discharge. Low pressure, medium pressure and high pressure are three kinds of mercury UV light sources. Low and medium pressure mercury lights are mostly used where low and mid. UV-wavelengths are needed while high pressure UV-light would give broader spectrum and cover mostly up to 600 nm, though less intense in UVC wavelength (100–280 nm). Also, medium and high pressure UV lamps produce quite amounts of heat and usually require a cooling system prevent overheating of the reactor mixture (Figure 1.3(a)).

Recently, amalgam lamps have been introduced in to industry which promise to give longer life and high performance compared to low-pressure lamps [54], [55]. The main emission wavelength is around 254 nm. They generate very little heat and are very cost efficient. The unique coating prevents the unwanted loss of transmission of the quartz glass which occurs in conventional UV lamps and keeps UV output at a continuously high level (Figure 1.3(b)) [23], [43], [48].

Lately, light-emitting diodes (LEDs) have also become very common to apply in photo-flow chemistry. LEDs are semiconductors and can provide a selective and very narrow emission band (± 20 nm). So according to the application (emission wavelength from 310 to 700 nm), the proper LED can be used. The major importance of the light with a narrow energy band gap is that the

byproduct formation is mitigated. Furthermore, energy losses in LEDs are very low, making them very energy and cost efficient (Figure 1.3(c)) [56], [57].

Another type of UV lights is fluorescent black light that emits long-wave (UVA 310-450 nm) UV light. The fluorescent light, is emitted by a low-pressure mercury-vapor gas-discharge lamp that applies fluorescence to produce visible light. An electric current in the gas excites mercury vapor, which produces short-wave UV light. The phosphor coating on the inner side of the lamp absorbs the monochromatic mercury irradiation and emit less energetic UV light. These lamps are not easy to match with any kinds of flow reactors, because of mismatching of the lamp configuration with the reactor setup there might be some energy losses (Figure 1.3(d)) [58], [59].

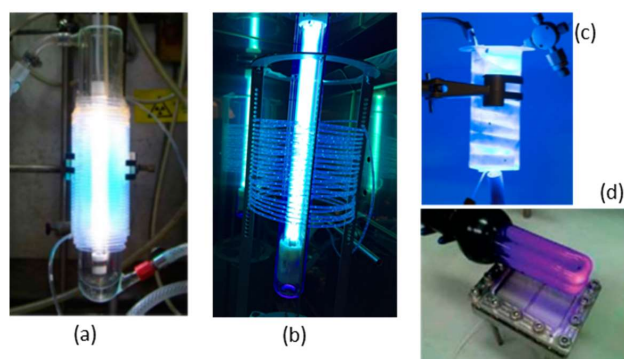


Figure 1.3. Different UV-light source. (a)Mercury lamp with coiled capillary reactor. (b)Amalgam lamp within microreactor setup. (c)Blue LEDs wrapped microreactor setup. (d) Black light 360 nm. Reprinted with kind permission of © 2016 American Chemical Society. [31]

1.4.2 Photo-microreactor material

Photo-microreactors should be fabricated from a material that is transparent for the desired wavelength, allowing to reach to the reaction medium. Otherwise, they act as a filter for certain wavelengths. In Table 1.1, a list of the most common photo-microreactor materials is given. Glass is one of the material choices for photoreactors. For the batch vessels, glass is quite suitable. However, fabrication of glass microreactors requires a complex technique such as clean room facilities. Also, fragility nature of glass capillary tubing renders its operation quite difficult. Being incompatible with strong basic solution and high temperatures are other weak points of glass microreactors.

Polymer-based materials have been very popular as a choice for photo-microreactor material [60]. The polymer-based materials such as poly(methyl methacrylate) (PMMA), polydimethylsiloxane (PDMS), perfluoroalkoxyalkane (PFA) or polytetrafluoroethylene (PTFE) are

very easy to handle, cheap and bearing good light transmission. However, they may not be suitable when being exposed to organic solvents for a prolonged time.

Fluorinated polymers (e.g., PTFE, PFA and FEP) offer a high chemical stability and enhanced optical properties [61]. Also, they can tolerate relatively high pressures and temperatures. These materials are produced as capillary tubing in a wide range of dimensions with relatively low cost. Nevertheless, for UV applications, after prolonged irradiation times, these polymers may decompose.

Table 1.1. Different material applied to fabricate photo-microreactor

Reactor material	Wavelength (nm) cutoff at 50% transmittance
Quartz glass [62]	170
Vycor glass	220
Corex glass	260
Pyrex glass	275
PMMA (polymethylmethacrylate)[63], [64]	248
PDMS (polydimethylsiloxane)	255
PTFE (polytetrafluoroethylene) [65]	200
PFA (perfluoroalkoxyalkane)	180
FEP (perfluoroethylenepropylene)	180

1.5 Scope and outline of the thesis

The research reported in this thesis focuses on continuous micro-flow processing of two UV photo-induced reactions under Novel Process Windows (NPW) - the Claisen rearrangement and the *cis*- to *trans*-cyclooctene (TCO) isomerization. The overarching goal of this thesis is the integration of the photo flow reaction towards second flow reaction (two-step), analytics (PAT), and separation (adsorption). While a number of photo flow reaction studies are concerned with photo and chemical intensification, and so is this one, the unique point is the process-design intensification of a photo flow reaction by the three aforementioned measures under Novel Process window conditions, i.e. very fast reactions, and high concentration in small volumes [4].

The Claisen rearrangement can lead to different isomers, depending on whether thermal or photo-chemical pathways are chosen. NPW provides access to entirely new parameter sets – the NPW chosen here are new chemical transformations by photo or thermal activation. The options provided by NPW are investigated in the above given situation and a high conversion at an unusual high concentration.

The photo and thermal micro-flow syntheses can be combined to the nucleophilic ether formation of the Claisen substrate and together provide the opportunity in increased chemical diversity, which is also process-design intensification.

Beyond its synthetic power, the Claisen rearrangement is among the best fundamentally investigated reactions. The mechanism of this rearrangement has been examined for more than one century in batch processes under various operating conditions. As by the time flow chemistry was introduced and showed very promising potentials in chemistry, it was aimed as well to conduct the Claisen rearrangement in flow. **Chapter 2** provides an analysis of different impact factors such as choice of substituent, catalyst, temperature, pressure, concentration, flow rates, and solvent. It is well-known that flow processing offers profound opportunities for studying these factors which are known to have large impact on the Claisen rearrangement conversion performed in batch.

In **chapter 3**, the selectivity issue of the two-step synthesis of phenol to 2-allylphenol by thermal-Claisen rearrangement is tackled. It is explained that the combining of two synthetic organic pathways could create orthogonality problems. The root of orthogonality issues were discussed and experimentally verified. It is revealed that the issues are related to two major reasons. The first one was due to the reagent compatibility. And the second one was related to the nature of the reaction kinetics. To deal with, five alternative approaches were considered and among all, four approaches were chosen to be compared with each other, giving each one's pros and cons. The comparison was prominently done based on the reaction yield, volumetric efficiency, energy consumption, and steadiness of the operation.

The photo-Claisen rearrangement of aromatic substrates gives the *para*-isomer which is not yielded by thermal operation. In **chapter 4**, the photo-Claisen rearrangement of allyl phenyl ether is studied in a microreactor. In order to do that, first some relevant parametric sensitivities of photo-Claisen rearrangement were addressed. Thanks to the small dimension of microreactors, the reaction time could be reduced from hours to 8 min or less. It was shown that operation at a relatively high concentration of allyl phenyl ether, i.e. 0.05 M, (compared to the batch mode) was possible. In the same chapter, increasing molecular diversity was explored by applying 3-substituted phenols as precursor to undergo a photo-Claisen rearrangement. The results demonstrated the formation of a 4-allyl product in addition to the *ortho*- and *para*- allyl products. Also, combination of a high-temperature and UV irradiation was tackled. Yet, this did not improve the reaction performance, but rather led to more photo degradation of the reactant and products. Finally, combining nucleophilic substitution and photo-Claisen rearrangement did not show a major orthogonality issue.

Applying high reactant concentration is usually a bottleneck in photoreactors. In **chapter 5** the concept of applying two phase flow in order to open a new path in photo-flow chemistry is

investigated. Here, the concept of Taylor flow (gas-liquid two phase flow) gives a promise to go for even higher concentrations due to the very small film thickness provided as compared to single-phase flow microfluidics. The effective mixing zone in the liquid slug may provide reactant refreshment in the thin layer film around the gas slug, enhancing the quantum efficiency of the photoreaction. A set of experiments gives evidence hereabout.

A procedure for photon flux measurements, by means of actinometry using ferrioxalate in microreactors is developed in **chapter 6**. The determination of photon fluxes was considered for configurationally different systems, including a capillary tower, placing the reactor directly around the UV-lamp and a coil flow inverter. The capillary tower is the most frequently-used configuration in this thesis. Winding microreactor on the UV-lamp is tested in **chapter 4**. The coil flow inverter capillary tower is applied in **chapter 5**. According to the results, the amount of photons absorbed by the configuration that the reactor was positioned around the lamp was higher than the other configurations. Between the coil flow inverter and the capillary tower, there was not a huge difference. However, the coil flow inverter showed slightly more photon absorption.

Chapter 7 describes the coupling of flow chemistry and continuous online analysis with the aim to develop a Process Analytical Technology (PAT) methodology under the given NPW conditions. The small volumes typical for micro-flow pose challenges for sampling operations in analytics. In this chapter, a fast process was combined with a modified ultra-high-performance liquid chromatography (UHPLC) system allowing for very fast sampling and analysis. Low-volume online sampling was introduced here for UHPLC analysis of the photo-Claisen rearrangement in micro-flow. Chances and challenges were critically reviewed, including the reproducibility and robustness of the sampling.

In the last part of this thesis, integrated micro-flow adsorption was developed for product separation, with option to do that in recycle mode. This was investigated first for the Claisen reaction in **chapter 3**, and thereafter more in depth for the *trans*-cyclooctene (TCO) photoisomerization in **chapter 8**. Here, the thermodynamic equilibrium was shifted by inserting an in-flow separation in a recycling flow mode, which makes better use of the given photoenergy (transport intensification). In this part the full theoretical study of in-flow separation in a recycling flow mode has been investigated. Moreover, in **chapter 9** different process design to reach optimum yield of TCO derivatives that is valuable in PET imaging is proposed and experimentally tested.

1.6 References

- [1] S. G. Newman and K. F. Jensen, "The role of flow in green chemistry and engineering," *Green Chemistry*. 2013.
- [2] S. K. Teoh, C. Rathi, and P. Sharratt, "Practical Assessment Methodology for Converting Fine Chemicals Processes from Batch to Continuous," *Org. Process Res. Dev.*, 2016.
- [3] M. B. Plutschack, B. Pieber, K. Gilmore, and P. H. Seeberger, "The Hitchhiker's Guide to Flow Chemistry," *Chemical Reviews*. 2017.
- [4] V. Hessel, D. Kralisch, N. Kockmann, T. Noël, and Q. Wang, "Novel process windows for enabling, accelerating, and uplifting flow chemistry," *ChemSusChem*, vol. 6, no. 5. pp. 746–789, 2013.
- [5] K. Jähnisch, V. Hessel, H. Löwe, and M. Baerns, "Chemistry in Microstructured Reactors," *Angewandte Chemie - International Edition*. 2004.
- [6] K. F. Jensen, "Microreaction engineering — is small better?," *Chem. Eng. Sci.*, vol. 56, no. 2, pp. 293–303, 2001.
- [7] A. Williamson, "XLV. Theory of ætherification," *London, Edinburgh, Dublin Philos. Mag. J. Sci.*, vol. 37, no. 251, pp. 350–356, Nov. 1850.
- [8] L. Malet-Sanz and F. Susanne, "Continuous flow synthesis. a pharma perspective," *Journal of Medicinal Chemistry*. 2012.
- [9] D. M. Roberge, L. Ducry, N. Bieler, P. Cretton, and B. Zimmermann, "Microreactor technology: A revolution for the fine chemical and pharmaceutical industries?," *Chem. Eng. Technol.*, 2005.
- [10] ACS GCI. American Chemical Society Green Chemistry Institute Pharmaceutical Roundtable. Available: <https://www.acs.org/content/acs/en/greenchemistry/industry-business/pharmaceutical.html>.
- [11] C. Wiles and P. Watts, "Continuous process technology: A tool for sustainable production," *Green Chemistry*. 2014.
- [12] V. Hessel, "Novel Process Windows - Gate to Maximizing Process Intensification via Flow Chemistry," *Chem. Eng. Technol.*, vol. 32, no. 11, pp. 1655–1681, Nov. 2009.
- [13] T. Illg, V. Hessel, P. Löb, and J. C. Schouten, "Novel Process Window for the safe and continuous synthesis of tert.-butyl peroxy pivalate in a micro-reactor," *Chem. Eng. J.*, 2011.
- [14] T. Razzaq and C. O. Kappe, "Continuous flow organic synthesis under high-temperature/pressure conditions," *Chem. An Asian J.*, vol. 5, no. 6, pp. 1274–1289, Jun. 2010.
- [15] "Overview Contents: Chem. Eng. Technol. 11/2009," *Chem. Eng. Technol.*, vol. 32, no. 11, p. 1643, Oct. 2009.
- [16] T. Razzaq, T. N. Glasnov, and C. O. Kappe, "Accessing novel process windows in a high-temperature/pressure capillary flow reactor," *Chem. Eng. Technol.*, vol. 32, no. 11, pp. 1702–1716, 2009.
- [17] D. R. Snead and T. F. Jamison, "End-to-end continuous flow synthesis and purification of diphenhydramine hydrochloride featuring atom economy, in-line separation, and flow of molten ammonium salts," *Chem. Sci.*, 2013.
- [18] H. Kawanami *et al.*, "Highly selective non-catalytic Claisen rearrangement in a high-pressure and high-

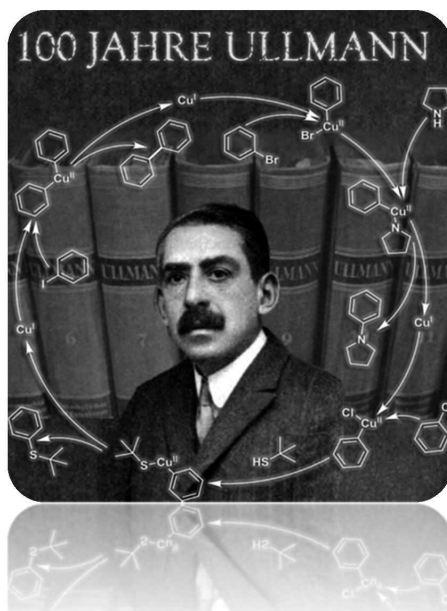
- temperature water microreaction system," *Chem. Eng. J.*, 2011.
- [19] M. Damm, T. N. Glasnov, and C. O. Kappe, "Translating high-temperature microwave chemistry to scalable continuous flow processes," *Org. Process Res. Dev.*, 2010.
- [20] V. Hessel, I. Vural Gürsel, Q. Wang, T. Noël, and J. Lang, "Potential Analysis of Smart Flow Processing and Micro Process Technology for Fastening Process Development: Use of Chemistry and Process Design as Intensification Fields," *Chem. Eng. Technol.*, vol. 35, no. 7, pp. 1184–1204, Jul. 2012.
- [21] I. Vural-Gürsel, Q. Wang, T. Noël, V. Hessel, and J. T. Tinge, "Improving Energy Efficiency of Process of Direct Adipic Acid Synthesis in Flow Using Pinch Analysis," *Ind. Eng. Chem. Res.*, 2013.
- [22] D. Ott, S. Borukhova, and V. Hessel, "Life cycle assessment of multi-step rufinamide synthesis - From isolated reactions in batch to continuous microreactor networks," in *Green Chemistry*, 2016.
- [23] E. Shahbazali, T. Noel, and H. Volker, "Photo-claisen rearrangement of allyl phenyl ether in micro-flow: influence of phenyl core substituents and vision on orthogonality," *J. Flow Chem.*, vol. 6, no. 3, pp. 252–259, 2016.
- [24] E. Shahbazali, M. Spapens, H. Kobayashi, S. Ookawara, T. Noël, and V. Hessel, "Connected nucleophilic substitution-Claisen rearrangement in flow – Analysis for kilo-lab process solutions with orthogonality," *Chem. Eng. J.*, vol. 281, pp. 144–154, 2015.
- [25] J. P. Knowles, L. D. Elliott, and K. I. Booker-Milburn, "Flow photochemistry: Old light through new windows," *Beilstein Journal of Organic Chemistry*, vol. 8, pp. 2025–2052, 2012.
- [26] Y. Su, N. J. W. Straathof, V. Hessel, and T. Noël, "Photochemical transformations accelerated in continuous-flow reactors: Basic concepts and applications," *Chemistry - A European Journal*, vol. 20, no. 34, pp. 10562–10589, 2014.
- [27] M. Oelgemoeller, "Highlights of Photochemical Reactions in Microflow Reactors," *Chemical Engineering and Technology*. 2012.
- [28] M. Oelgemöller and O. Shvydkiv, "Recent advances in microflow photochemistry," *Molecules*. 2011.
- [29] E. E. Coyle and M. Oelgemöller, "Micro-photochemistry: photochemistry in microstructured reactors. The new photochemistry of the future?," *Photochem. Photobiol. Sci.*, vol. 7, no. 11, p. 1313, 2008.
- [30] Y. Matsushita *et al.*, "Recent progress on photoreactions in microreactors," *Pure Appl. Chem.*, 2007.
- [31] D. Cambié, C. Bottecchia, N. J. W. Straathof, V. Hessel, and T. Noël, "Applications of Continuous-Flow Photochemistry in Organic Synthesis, Material Science, and Water Treatment," *Chemical Reviews*, vol. 116, no. 17, pp. 10276–10341, 2016.
- [32] E. E. Coyle and M. Oelgemöller, "Micro-photochemistry: Photochemistry in microstructured reactors. The new photochemistry of the future?," *Photochemical and Photobiological Sciences*. 2008.
- [33] L. D. Elliott *et al.*, "Batch versus flow photochemistry: A revealing comparison of yield and productivity," *Chem. - A Eur. J.*, 2014.
- [34] M. Oelgemöller, N. Hoffmann, and O. Shvydkiv, "From 'lab & light on a chip' to parallel microflow photochemistry," in *Australian Journal of Chemistry*, 2014.
- [35] Y. Su, K. Kuijpers, V. Hessel, and T. Noël, "A convenient numbering-up strategy for the scale-up of gas–liquid photoredox catalysis in flow," *React. Chem. Eng.*, vol. 1, no. 1, pp. 73–81, 2016.
- [36] A. Talla *et al.*, "Metal-Free Photocatalytic Aerobic Oxidation of Thiols to Disulfides in Batch and Continuous-Flow," *Adv. Synth. Catal.*, 2015.

- [37] R. L. Hartman, J. P. McMullen, and K. F. Jensen, "Deciding whether to go with the flow: Evaluating the merits of flow reactors for synthesis," *Angewandte Chemie - International Edition*. 2011.
- [38] H. P. L. Gemoets, Y. Su, M. Shang, V. Hessel, R. Luque, and T. Noël, "Liquid phase oxidation chemistry in continuous-flow microreactors," *Chemical Society Reviews*. 2016.
- [39] C. J. Mallia and I. R. Baxendale, "The Use of Gases in Flow Synthesis," *Organic Process Research and Development*. 2016.
- [40] T. Noël and V. Hessel, "Membrane microreactors: Gas-liquid reactions made easy," *ChemSusChem*, 2013.
- [41] D. Webb and T. F. Jamison, "Continuous flow multi-step organic synthesis," *Chemical Science*. 2010.
- [42] S. V. Ley, D. E. Fitzpatrick, R. J. Ingham, and R. M. Myers, "Organic synthesis: March of the machines," *Angewandte Chemie - International Edition*. 2015.
- [43] M. Escribà-Gelonch, E. Shahbazali, M. Honing, and V. Hessel, "Quality-In(Process)Line (QuProLi) process intensification for a micro-flow UV-photo synthesis enabled by online UHPLC analysis," *Tetrahedron*, 2018.
- [44] S. T. R. Müller and T. Wirth, "Diazo compounds in continuous-flow technology," *ChemSusChem*. 2015.
- [45] B. Gutmann, D. Cantillo, and C. O. Kappe, "Continuous-Flow Technology-A Tool for the Safe Manufacturing of Active Pharmaceutical Ingredients," *Angew. Chemie Int. Ed.*, 2015.
- [46] B. D. A. Hook, W. Dohle, P. R. Hirst, M. Pickworth, M. B. Berry, and K. I. Booker-Milburn, "A practical flow reactor for continuous organic photochemistry," *J. Org. Chem.*, 2005.
- [47] M. D. Lainchbury, M. I. Medley, P. M. Taylor, P. Hirst, W. Dohle, and K. I. Booker-Milburn, "A Protecting Group Free Synthesis of (±)-Neostenine via the [5 + 2] Photocycloaddition of Maleimides," *J. Org. Chem.*, vol. 73, no. 17, pp. 6497–6505, Sep. 2008.
- [48] K. G. Maskill, J. P. Knowles, L. D. Elliott, R. W. Alder, and K. I. Booker-Milburn, "Complexity from simplicity: Tricyclic aziridines from the rearrangement of pyrroles by batch and flow photochemistry," *Angew. Chemie - Int. Ed.*, 2013.
- [49] K. I. Booker-Milburn, J. K. Cowell, F. Delgado Jiménez, A. Sharpe, and A. J. White, "Stereoselective intermolecular [2+2] photocycloaddition reactions of tetrahydrophthalic anhydride and derivatives with alkenols and alkynols," *Tetrahedron*, 1999.
- [50] N. Hoffmann, "Photochemical reactions as key steps in organic synthesis," *Chemical Reviews*. 2008.
- [51] D. C. Harrowven, M. Mohamed, T. P. Gonçalves, R. J. Whitby, D. Bolien, and H. F. Sneddon, "An efficient flow-photochemical synthesis of 5H-furanones leads to an understanding of torquoselectivity in cyclobutenone rearrangements," *Angew. Chemie - Int. Ed.*, 2012.
- [52] Q. Lefebvre, M. Jentsch, and M. Rueping, "Continuous flow photocyclization of stilbenes – scalable synthesis of functionalized phenanthrenes and helicenes," *Beilstein J. Org. Chem.*, 2013.
- [53] D. T. McQuade *et al.*, "Continuous synthesis of pyridocarbazoles and initial photophysical and bioprobe characterization," *Chem. Sci.*, 2013.
- [54] "Amalgam lamp." [Online]. Available: <https://www.dinies.com/english/uv-lights.html>.
- [55] "Amalgam lamp." [Online]. Available: https://www.heraeus.com/en/hng/home_hng/home_noblelight.aspx.

- [56] Y. Matsushita, N. Ohba, S. Kumada, K. Sakeda, T. Suzuki, and T. Ichimura, "Photocatalytic reactions in microreactors," *Chem. Eng. J.*, 2007.
- [57] S. Silvestrini, T. Carofiglio, and M. Maggini, "Shape-selective growth of silver nanoparticles under continuous flow photochemical conditions," *Chem. Commun.*, 2013.
- [58] A. Sugimoto, T. Fukuyama, Y. Sumino, M. Takagi, and I. Ryu, "Microflow photo-radical reaction using a compact light source: application to the Barton reaction leading to a key intermediate for myriceric acid A," *Tetrahedron*, vol. 65, no. 8, pp. 1593–1598, 2009.
- [59] A. Sugimoto, Y. Sumino, M. Takagi, T. Fukuyama, and I. Ryu, "The Barton reaction using a microreactor and black light. Continuous-flow synthesis of a key steroid intermediate for an endothelin receptor antagonist," *Tetrahedron Lett.*, vol. 47, no. 35, pp. 6197–6200, 2006.
- [60] L. Vaccaro, D. Lanari, A. Marrocchi, and G. Strappaveccia, "Flow approaches towards sustainability," *Green Chem.*, vol. 16, no. 8, pp. 3680–3704, 2014.
- [61] A. C. Gutierrez and T. F. Jamison, "Scalable and Robust Synthesis of CpRu(MeCN)₃PF₆ via Continuous Flow Photochemistry," *J. Flow Chem.*, 2012.
- [62] J. P. McMullen and K. F. Jensen, "Integrated Microreactors for Reaction Automation: New Approaches to Reaction Development," *Annu. Rev. Anal. Chem.*, 2010.
- [63] S. Kuhn, T. Noël, L. Gu, P. L. Heider, and K. F. Jensen, "A Teflon microreactor with integrated piezoelectric actuator to handle solid forming reactions," *Lab Chip*, 2011.
- [64] H. Lu, M. A. Schmidt, and K. F. Jensen, "Photochemical reactions and on-line UV detection in microfabricated reactors," *Lab Chip*, 2001.
- [65] M. K. Yang, R. H. French, and E. W. Tokarsky, "Optical properties of Teflon® AF amorphous fluoropolymers," *J. Micro/Nanolithography, MEMS MOEMS*, 2008.

CHAPTER 2

Impact Factor Analysis of the Claisen Rearrangement, in Batch and in Flow



Cover of CIT special issue 100 Jahre Ullmanns Enzyklopädie der Technischen Chemie. December, 2014. Volume 86, Issue 12. Pages 1993–2243, produced by SFP group, TU/e

This chapter is based on three review papers:

Zelentsov, S., Hessel, V., Shahbazali, E., Noël, T., ChemBioEng. Reviews, 1, (2014) 5, 230-240

Hessel, V., Shahbazali, E., Noël, T., Zelentsov, S., ChemBioEng. Reviews, 1, (2014) 6, 244-261

Hessel, V., Shahbazali, E., Noël, T. & Zelentsov, S., Chemie, Ingenieur, Technik, 86 (2014) 12, 2160-2179

2.1 Impact Factor Analysis of the Claisen Rearrangement in Batch and in Flow

The Claisen rearrangement has been profoundly investigated by many researchers. Beyond its synthetic power, the Claisen rearrangement is among the best fundamentally investigated reactions [1]–[6]. The mechanism of this rearrangement has been examined for more than one century in batch processes under various operating conditions. As by the time flow chemistry was introduced and showed great potentials in chemistry, it was aimed as well to conduct the Claisen rearrangement in flow.

This chapter provides an analysis of different impact factors such as the choice of substituent, catalyst, temperature, pressure, concentration, flow rates, and solvent. It is well-known that flow processing offers profound opportunities for studying these factors which are known to have large impact on the Claisen rearrangement done in batch.

2.2 Mechanistic analysis of the Claisen rearrangement – quantum-mechanistic modelling and most modern spectrometric analysis

With time considerable insight into reaction mechanisms and their transition states was provided. Since recently, modern analytical techniques and theoretical/quantum chemistry add more detailed and firm evidence of the proposed mechanism. Direct proofs of the existence of intermediates (and therefore finally proposed respective transition states) are nowadays possible both by advanced experimental and theoretical methods [5]–[8].

Ultra-short pulsed laser spectroscopy gives very detailed and individual information about all major species on the reaction trajectory, including the transition state, through vibration analysis of many groups within on molecule [5], [8]–[10]. This equals the comprehensive functional-group analysis known from Raman spectra of molecules in their ground state; yet now on a femto-second time scale allowing to catch even the most-short lived species.

A spectrogram of the Claisen rearrangement induced by 5 fs pulses in the visible region is shown in Figure 2.1 [8], [11]. The positions of the corresponding molecular vibrations appeared after the 5 fs pulses irradiation agreed well with the Raman data for allyl vinyl ether (AVE). The deformation vibration of the methylene group and the C–O–C symmetric stretching vibration of the ether group have disappeared after about 800 fs delay. It means that the C₄-O bond is weakened or broken at the first step of the reaction. Shifts of the vibrations of the C = C bonds stretching modes also suggest that the C₄ - O bond is weakened. Just after the 5 fs pulses irradiation the C = C bond stretching vibration of the vinyl and that of the allyl groups appears at *ca.* 1650 cm⁻¹. The C₄ - O bond weakening causes delocalization and localization of electronic density on allyl and vinyl groups, respectively. Therefore, the C = C bond stretching vibration

observed at 1650 cm^{-1} splits into a red-shifted at *ca.* 1570 cm^{-1} and in a blue-shifted vibration at *ca.* 1700 cm^{-1} .

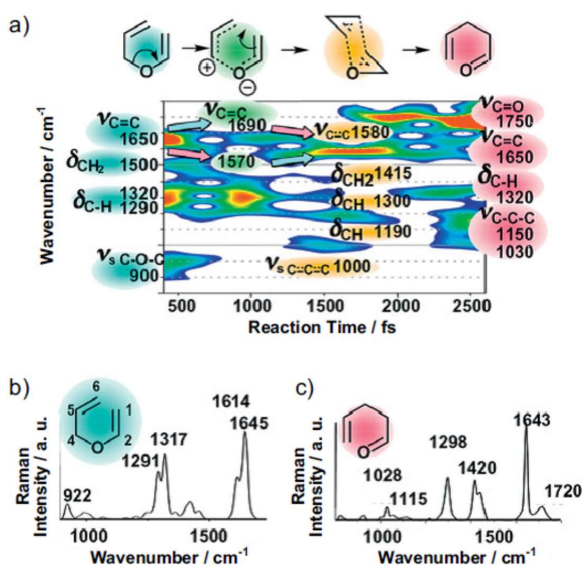


Figure 2.1. Raman spectrogram of a Claisen rearrangement induced by the 5 fs laser pulses in the visible region (a) and Raman spectrum of allyl vinyl ether (b) and of allyl acetaldehyde (c) [11] (reproduced by permission of the Chemical Society of Japan).

The $C_5 = C_6$ bond stretching vibration of the allyl group is shifted from 1570 to 1580 cm^{-1} , and the $C_1 = C_2$ bond stretching vibration of the vinyl group is shifted from 1690 to 1580 cm^{-1} . In addition after 1500 fs delay, the electron transfer from the vinyl to the allyl group makes the $C = C$ bonds of both the allyl and vinyl group to become equivalent and observable at 1580 cm^{-1} , which implies that aromatic-like $C = C$ bonds are formed [11]. This result shows that the generated intermediate has an aromatic-like six-membered structure. Finally, the $C_4 - O$ bond break and the $C_1 - C_6$ bond formation proceed simultaneously to generate allyl acetaldehyde being assigned due to appearance of molecular vibrations after 2000 fs delay.

In this way, massive evidence is provided about the major bond changes which are the supposed critical structures on a reaction coordinate and most notably which structure can be assigned as the transition state (Figure 2.1). Complementary to that, quantum-mechanical calculations can yield bond distances and other geometric information which give a more direct answer, since it mirrors the key characteristic of the critical species involved, rather than arguing over the boundary conditions [12]–[14]. The application of the modern quantum chemical methods can provide not only geometrical parameters being close to experimental ones but they can correctly forecast the activation parameters of a chemical reaction such as activation energy and reaction

enthalpy [15], [16]. Both the novel experimental and theoretical approaches allow to break down the multiple interpretations options to one mechanism and one transition state for a given reaction under given conditions.

2.3 Factors impacting the rearrangement – a comparison of batch and flow processing

Different means are known to control the Claisen rearrangement [17]. Key to such a control of the reaction is a special stabilization or destabilization of the transition state (TS).

In the last decade microreactor technology was much further developed and even applied on industrial scale [18]–[23], including the Claisen rearrangement [24]–[27]. The novel synthesis tool opens doors to new process chemistries, in particular under harsh conditions. Novel process windows widened the synthetic possibilities and toolbox of the chemist [28]–[31]; adding chemical intensification to the prior developed heat and mass transfer intensification. These define novel process windows for the Claisen rearrangement.

Microreactors commonly facilitate the use of alternative activation for a number of reasons and indeed such novel process windows were tested in flow [28]–[31]. The use of the microreactor or microfluidics concept might be considered as the simplest way to solve the shortcomings of the existing industrial realization of the Claisen-like processes [24]–[27], [32], [33].

2.3.1 Substituent effects

Batch processing

Castro *et al.*[1] has compiled literature data to investigate the substituent influence on the Claisen rearrangement of AVE.

An acceleration of the rearrangement was given by electron donating groups O, -NH₂, -F, -CH₃ at position 1 or by -OSi(CH₃)₃, -CH₃, F in position 2 or by -CH₃, -OCH₃ in positions 4 or 6, or if there were electron withdrawing groups -CN, -CO₂⁻, -CO₂CH₃, -CF₃ in position 2 or by -CN, -CF₃ in position 4 or -CN in position 5 [1]. On the other hand, a retardation is given for electron donating groups -CH₃, -OCH₃ in position 5 or electron withdrawing groups -CN, -CO₂CF₃ at position 1 or a -CN group at position 6.

White and Wolfarth [34] showed that electron-donating groups and polar solvents increase the rate of the reaction. The rates of rearrangement of four allyl p-X-phenyl ethers in three solvents were compared. The rate constants were correlated by using the Hammett equation and σ^+ values [35]. Gajewski [36] assumes that the structure of the TS adopts the features of the substrate or products depending on exothermic properties of the reaction. It will have an

associative or dissociative character according to the way that the substituent can stabilize such TS.

In order to determine the impact of the substitution at the *para*-position for the Claisen rearrangement of allyl phenyl ether (APE), kinetic and thermodynamic parameters of substituted allyl aryl ethers were calculated at the B3LYP/6-311G** level [37]. The results obtained in [37] are shown in Table 2.1.

The calculated activation energies for the rearrangement and following proton shift reactions are 33.33 and 52.16 kcal mol⁻¹, respectively. Negative values for the activation entropy confirm existence of the concerted mechanism for the Claisen rearrangement and the proton shift reaction. The Hammett ρ value of -1.34 was obtained in the first step. A negative ρ value indicates that the electron donating groups slightly increase the rate of the first step. A positive Hammett ρ value of 2.51 for proton shift reaction indicates that electron withdrawing groups increase the rate of reaction.

Table 2.1. Thermal Gibbs free energies ($\Delta_r G^\ominus$), thermal enthalpies ($\Delta_r H^\ominus$), entropies ($\Delta_r S^\ominus$), activation energies (E_a) at 298.15 K and 1.0 atm, thermal Gibbs free energies for TS (ΔG^\ddagger), entropies for TS (ΔS^\ddagger), and pre-exponential factor (A) calculated at B3LYP/6-311G** level of theory for the Claisen rearrangement of allyl phenyl ethers having substituent in *para*-position [37].

substituent	$\Delta_r G^\ominus$ kcal mol ⁻¹	$\Delta_r H^\ominus$ kcal mol ⁻¹	$\Delta_r S^\ominus$ cal mol ⁻¹ K ⁻¹	E_a kcal mol ⁻¹	ΔG^\ddagger kcal mol ⁻¹	ΔS^\ddagger cal mol ⁻¹ K ⁻¹	logA
H	10.93	11.39	1.55	34.03	34.80	-4.57	12.23
NO ₂	13.51	14.16	2.19	34.64	35.28	-4.13	12.32
CN	13.46	14.01	1.86	34.54	35.08	-3.82	12.39
CHO	11.89	12.45	1.88	34.16	34.80	-4.13	12.32
F	10.96	11.43	1.60	33.58	34.35	-4.55	12.23
Cl	11.46	11.96	1.67	33.86	34.53	-4.23	12.30
NH ₂	9.96	10.30	1.16	32.28	33.01	-4.45	12.25
NHCH ₃	8.78	9.10	1.08	31.46	32.07	-4.04	12.34
OH	9.61	9.94	1.11	32.57	33.43	-4.85	12.17
OCH ₃	8.57	8.91	1.14	32.08	32.88	-4.67	12.21
CH ₃	10.74	10.35	-1.32	33.43	34.90	-6.90	11.72

Quantum chemical calculations of the TS structures in the *ortho*-aryl-Claisen rearrangement through the chair and boat models were performed [34]. TS structures as shown in Figure 2.2 resulted.

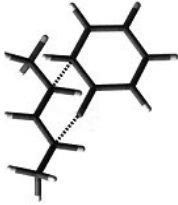

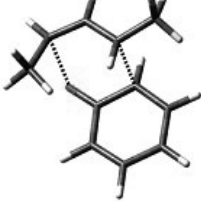
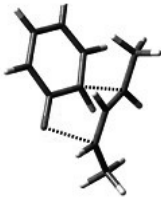

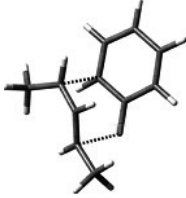
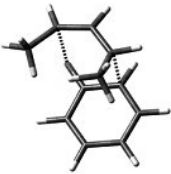
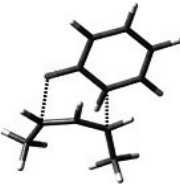
			
<u>1</u> (chair) R(C-O) _{break} =0.226 nm R(C-C) _{form} =0.225 nm	<u>2</u> (boat) R(C-O) _{break} =0.239 nm R(C-C) _{form} =0.229 nm	<u>3</u> (chair) R(C-O) _{break} =0.230 nm R(C-C) _{form} =0.225 nm	<u>4</u> (boat) R(C-O) _{break} =0.241 nm R(C-C) _{form} =0.233 nm
			
<u>5</u> (chair) R(C-O) _{break} =0.229 nm R(C-C) _{form} =0.229 nm	<u>6</u> (boat) R(C-O) _{break} =0.232 nm R(C-C) _{form} =0.233 nm	<u>7</u> (chair) R(C-O) _{break} =0.237 nm R(C-C) _{form} =0.229 nm	<u>8</u> (boat) R(C-O) _{break} =0.231 nm R(C-C) _{form} =0.234 nm

Figure 2.2. Transition state structures obtained by a kinetic study [34] (reproduced by permission of Elsevier).

2.3.2 Solvent effects

Batch processing

A solvent used for a chemical reaction takes an important role on both mechanism and kinetics [38], [39]. An excellent review describing solvent effects on the Claisen rearrangement was published by Gajewski [39]. General comprehensive discussion of the solvent influence can be found in work written by Schmid [40].

Hughes *et al.* [41] seem to be the first who presented satisfactory qualitative explanation of solvent effects on reactivity by concept of an activated complex solvation. In other words[29], solvent effects on the rate constant depend on the relative stabilization of the reactant molecule and corresponding TS causing the activated complex solvation [42]. Hughes *et al.* stated that an increase in polarity causes an increase in reaction rate when the TS is more polar than the initial reagent and causes a decrease when it is less polar. There is more evidence that polar solvents accelerate the Claisen rearrangement[43]–[45]. The acceleration of the Claisen reaction with polarity increasing is evident on the base of data shown in Table 2.2 [46].

Table 2.2. Influence of solvents on rate constants for the Claisen rearrangement of allyl vinyl ether [44].

Solvent	k [10^{-5} s^{-1}]
CF ₃ CH ₂ OH	4.7
50% H ₂ O-MeOH	3.6
25% H ₂ O-MeOH	1.4
MeOH	0.72
25% H ₂ O-DMSO	0.82
10% H ₂ O-DMSO	0.50
C ₂ H ₅ OH	0.51
i-PrOH	0.42
MeCN	0.25
CH ₃ COCH ₃	0.18
Benzene	0.17
Cyclohexane	0.084

Not only polarity is responsible for the acceleration. It has been found out long ago that the Claisen rearrangement acceleration can be caused by hydrogen bond formation[47]–[50]. The acceleration of the Claisen rearrangement in polar protic solvents can partly be attributed to their hydrogen-bonding capacity [48], [49]. Using quantum mechanical computational methods, Jorgensen has developed a model to explain the aqueous acceleration of the Claisen rearrangement involving hydrogen bond interactions between two water molecules and the core heteroatom of the AVE in the optimized TS structure. Monte Carlo calculations and free-energy perturbation theory have demonstrated [51] that in the case of water the rate enhancement is derived from the ability of the interfacial water molecules to stabilize a polar TS *via* enhanced hydrogen bonding at the oil/water interface.

Flow processing

Due to their small internal volumes, flow reactors do not need the presence of a solvent for filling reasons or as dilution media to control potential exothermic heat releases. Thus, solvent-free or high-concentration operation is quite common. The solvent selection for high temperature windows is not restricted anymore by the solvent's boiling point and low-boiling solvents can be used at high temperature desired [52].

Following these lines, the Claisen rearrangement of APE to *ortho*-allyl phenol (*ortho*-AP) was performed in subcritical water (SCW) [85, 86]. In a solvent-free conventional method, *ortho*-AP was produced with 85% yield at 220°C, ambient pressure, and at a reaction time of 6 h. While in a similar batch process, but using SCW, the yield of *ortho*-AP was 84% in addition to shorter reaction time of 10 min at 240°C and 3.4 MPa. Table 2.3 shows the comparison of these two methods with the microreactor case is shown in Table 3 [53].

The reaction time in the flow reactor is further decreased to about 2.5 min, while the yield is still notably further increases. This example shows clearly how the combination of tailored solvent and flowreactor can lead to the opening of a novel process window with increased intensification. This approach is considered environmentally benign and is useful for the green organic synthesis [53].

Table 2.3. The Claisen rearrangement in subcritical water (microreactor mode) [53]

Solvent	Concentration /mol kg ⁻¹	Temperature /°C	Pressure /MPa	Reaction time/ s	Selectivity /(%)	Yield /(%)
Non	6.90	265	5	360	68	37
Subcritical water	0.77	265	5	81	74	73
Subcritical water	0.27	265	5	149	98	98

Concerning the use of organic solvents, a solvent screening study by Kobayashi *et al.* [24] revealed that 1-butanol was the optimal reaction solvent for this transformation in flow. The study shows that even smart differences in the solvents used, as, for example in the case of different isomers (1- and 2-propanol), have a detectable impact. Solvent-free reaction conditions were feasible for the Claisen rearrangement and provided quantitative yields of the target product at 280°C and 100 bar. The use of high pressure enables the superheated processing giving the base for the use of the high temperature.

Firestone and others [54] have observed an increase of the reactivity in solvents of different viscosity. At 130°C the relative rates of the Claisen rearrangement of APE are 1.00, 0.98, 1.13, and 1.36 in n-octane, isooctane, n-octacosane, and Nujol, whose relative viscosities at 100°C are 1.00, 0.94, 4.92, and 11.8, respectively. Addition of polyethylene to the Nujol raises the relative viscosity to 48.5 and relative rate to 1.70.

Complexing and chelating agents can provide anisotropic reaction environments (microcavity) within solvents and consequently can (significantly) alter the product distribution. The photo-

Claisen rearrangement of APE in aqueous solutions containing β -cyclodextrin leads to *para*- and *ortho*-allyl phenols and phenol as main products [55].

2.3.3 Catalytic effects

Batch processing

The most undesirable drawback of the Claisen rearrangement is the need for the relatively high temperature that is necessary to perform the reaction effectively. A general way to overcome the drawback is to use a catalyst. An excellent review on catalysis in the Claisen rearrangement has been published [6]. Numerous substances such as transition-metal complexes, Lewis acids, Brønsted acids, bases, water etc. have been developed to catalyze the Claisen rearrangement [6].

Maruoka *et al.* [56], [57] have shown that the reaction rates of the AVE derivatives increase in the presence of aluminum complexes. The catalysis on the basis of copper (II) complexes was also described [58]. A catalyst containing palladium metal has also been developed [59]. The last reaction was found to proceed with involvement of the boat-like TS due to the coordination of palladium atom to both olefinic bonds. Metal-containing catalysts are generally able to enhance the rate of the Claisen rearrangement. However there are other very effective catalysts having the organic nature.

Consistent with the hypothesis of Jorgensen mentioned above for the solvent effects, compounds capable of dual hydrogen-bonding such as ureas and thioureas demonstrated modest rate accelerations in Claisen rearrangement reactions [60]. A greater catalytic effect was found for *N,N'*-diphenylguanidinium ion associated with the non-coordinating BArF⁻ counterion [61].

Flow processing

It is known from batch synthesis that the primary Claisen product allyl phenol (from allyl phenyl ether) can react further to the corresponding furan by cyclization or add phenyl rings (from decomposition of the Claisen reactant) to the double bond [62] (see also [63]).

With such motivation, it was aimed to investigate the effect of Lewis acids on the overall rate as well as on the rate of the individual steps as given above for the same reaction [84]. APE, 0.5 M in ethanol, was converted using a microcapillary (ID: 500 μm ; length: 10 m) operated at temperature of 240°C and pressure of 125 bar. BF₃ was the Lewis catalyst at 10% concentration.

Indeed, a considerable activation boost is given when rising residence time which achieves almost 60% and 100% conversion in less than 4 and 20 min, respectively [84]. Yet, the furan turned out to be the main product. Thus, the BF₃ Lewis catalyst led to reaction acceleration towards allyl

phenol, but even to more promoted conversion of the product to furan by subsequent cyclization.

2.3.4 Temperature effects

Batch processing

The activation energies of the great majority of the classical Claisen rearrangements are in the range of 27.0-32.0 kcal mol⁻¹ [51], [57], [64], [65]. Some values are presented in Table 2.4. In addition, the activation energy of the classical Claisen rearrangement of APE was calculated by B3LYP/6-311 + G** calculation to be 35 kcal/mol, which is in good agreement with earlier reports [66], [67]. The activation energy values imply that elevated temperatures (up to 300°C) are crucial to achieve full conversion of APE in the Claisen rearrangement.

Table 2.4. Activation parameters of the Claisen rearrangement

Ether name	Activation energy, E _a , kcal mol ⁻¹	Pre-exponential factor, A [10 ¹¹ s ⁻¹]	Gibbs' free energy, ΔG [‡] _{453.15 K} , kcal mol ⁻¹	Literature
Allyl vinyl ether	30.6	5	33.3	[42]
Allyl isopropenyl ether	29.3	5.4	31.9 ± 0.3	[46]
1-Methylallyl vinyl ether	27.87	1.0 ± 0.03	31.0 ± 0.1	[47]
2-Methylallyl vinyl ether	29.10 ± 0.17	1.0 ± 0.2	32.9 ± 0.2	[48]
Allyl phenyl ether	31.6			[49]

The use of very high temperatures in the Claisen rearrangement allows to decrease reaction durability significantly. However, such processing is rather difficult to attain under conventional batch conditions and may deteriorate selectivity.

Flow processing

Razzaq *et al.* applied the high-temperature/pressure to perform the Claisen rearrangement of APE [68]. In addition, the high-temperature/pressure flow system allowed them to study this rearrangement in low boiling point solvents in or near their supercritical state (Figure 2.3).

In contrast to observations under batch conditions, the best results are obtained in flow mode with longer chain alcohols. Based on experimental data, Kobayashi *et al.* [52] have calculated the activation energies for the Claisen rearrangement and these values follow the same reaction

order as observed in batch: ethanol>1-butanol>1-hexanol. Yet, the sequence could reflect also the different thermal expansion of the solvents [26].

Microwave (MW) heating provides an alternative to the fluidic microreactor heating [90, 91]. Damm *et al.* [69] made a comparison between batch MW and conventionally heated flow scale-up protocols for three selected model reactions. Compared to a standard MW batch reactor, higher temperatures and pressures can be attained in a microreactor, therefore allowing further significant process intensification [69]. Conventional processing at the reflux temperature of the solvent requires reaction times of ca. 2-3 days (110 °C, Diels-Alder reaction in toluene). Using sealed vessel MW heating on a small scale (2 mL) at up to 270 °C these reaction times could be reduced to a few seconds or minutes [69].

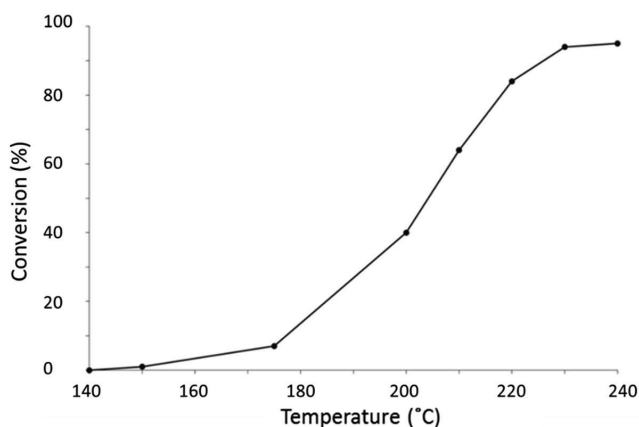


Figure 2.3. Temperature effect on the Claisen rearrangement of allyl phenyl ether under continuous flow conditions (100 bar, 1.0 mL min⁻¹ flow rate, 4 mL coil, 4 min residence time) [68] (reproduced by permission of Elsevier).

Moseley *et al.* [70] applied an automated stop-flow microwave for six pharmaceutically relevant reactions. Moreover, in another work, Moseley *et al.* [94] presented results of the same above mentioned reactions in a continuous flow microwave reactor.

Kirschning *et al.* have used a microreactor packed with iron oxide magnetic nanoparticles and applied radiofrequency heating [71]. These nanoparticles generate heat when they are exposed to a constantly changing magnetic field (25 kHz). The Claisen rearrangement flow synthesis was performed at 170°C and gave 85% yield of the product. Only 62% yield was obtained by conventional heating.

2.3.5 Non-thermal activation effects: Photochemistry

Batch processing

The photo-Claisen rearrangement was studied in the case of the UV photochemical dissociation of APE in solution [3], [7], [72]. Ultrafast UV pump broadband probe methods offer means of studying of early stages of competing routes involved in the photo-Claisen rearrangement [72].

The spectrogram of the photo-Claisen rearrangement of APE is shown in Figure 2.4 [72]. At the first step, the O–C(allyl) bond scission occurs on 90 ps timescale after excitation to the S_1 state of APE. Bleaching of the vibrations at 1495, 1586 and 1598 cm^{-1} takes place. Vibrations at 1415, 1516 and 1670 cm^{-1} appear, with those at 1415 and 1516 cm^{-1} appearing immediately. The cooling decay is observed with a time constant of 94 ps. The vibration at 1670 cm^{-1} shows different kinetic behavior developing with a time constant of 150 ps. The vibration was consistent with both the allyl substituted 2,4- and 2,5-cyclohexadienones. The kinetic behavior of the reactions was consistent with the proposed geminate recombination of the phenoxyl and allyl radicals formed after the initial photochemical dissociation. Unfortunately the predicted signals of the C=O stretching vibration in the two cyclohexadienones were indistinguishable within the available spectral resolution. The proposed reaction scheme of the photo-Claisen rearrangement is shown in Figure 2.4.

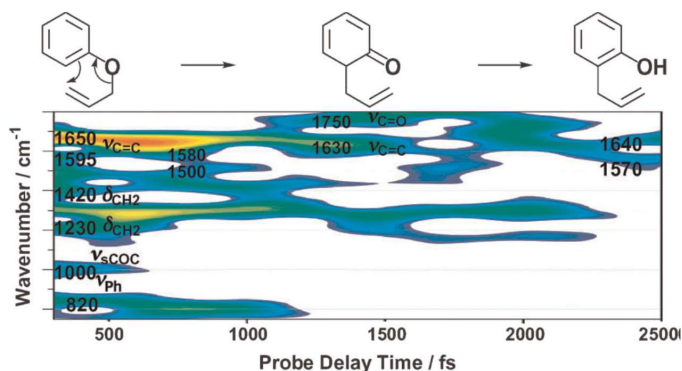


Figure 2.4. Raman spectrogram of the photo-Claisen rearrangement of allyl phenyl ether [72](reproduced by permission of Elsevier).

Immediately after photo-irradiation the only observable vibrations belonged to APE. All of the C_6 symmetric benzene stretching vibration (1000 cm^{-1}), the C–O–C symmetric stretching vibration of the ether group (1030 cm^{-1}), the twisting vibration of the methylene group (1230 cm^{-1}), and the wagging vibration of the methylene group (1420 cm^{-1}) disappeared at about 700 fs. The disappearance of these vibrations implies that the C₄–O bond is weakened at the first step of the reaction. At probe delay times of from 500 to 750 fs the vibrations of the phenyl group were red

shifted from 1595 to 1500 cm^{-1} and the vibrations of the allyl group were red shifted from 1650 to 1580 cm^{-1} . These results indicate that a six-member structure with aromatic bonds is formed in the second step of the reaction. After the probe delay time of 1000 fs a new band appeared at 1750 cm^{-1} that can be assigned to the C=O group. The appearance of this band verifies that the keto-intermediate is generated in the third step of the reaction. Instability of the keto-intermediate leads to keto–enol tautomerization. Therefore, after the probe delay time of 2000 fs the vibrations of the C=O group disappeared and the phenol product was formed.

Flow processing

Maeda *et al.* compared the batch and flow variant of the Photo-Claisen rearrangement [27]. In the batch process, irradiation of a benzene solution containing 2-[(2,4,6-trimethylphenoxy)methyl]-1-(methoxycarbonyl)naphthalene, was carried out for 8 h, led to formation of the cyclohexa-2,4-dienone derivative (22 %) as the photo-Claisen-type rearrangement product along with the *meta*-rearrangement product (19 %), 1-methoxycarbonyl-2-methylnaphthalene (9 %), and the dimeric product 1,2-bis[1-(methoxycarbonyl)naphthalen-2-yl]ethane (12 %). When the same photoreaction was carried out using a flow reactor (0.03 mL/h), 75 % conversion of the initial compound was achieved in 2.2 min residence time. The quantum yield in photochemical flow reactors is generally much higher than in batch owing to the small illuminated dimensions. The reaction time was dramatically shortened in comparison with that using the batch system.

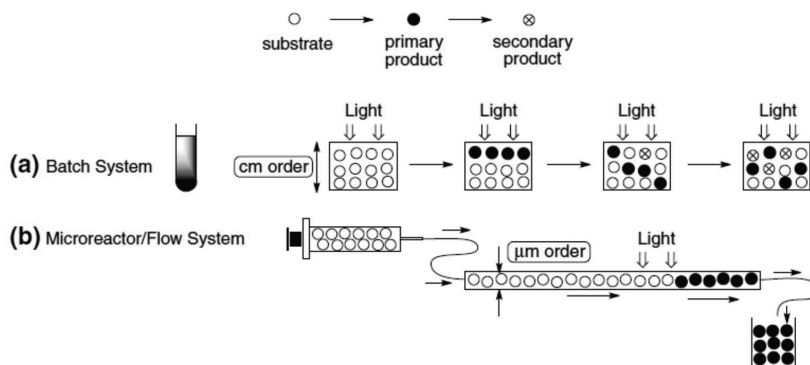


Figure 2.5. Schematic explanation of the difference in product selectivity observed between batch and flow reactors [27] (reproduced by permission of Springer).

Maeda *et al.* proposed that a radical pair plays the key role in the mechanism of the flow Photo-Claisen rearrangement [27]. Both "in-cage" and "out-of-cage" radical reactions contribute to the final mixture of products. A *meta*-rearrangement product is formed by a secondary reaction. The high conversion and selectivity found are attributed to more efficient light absorption in thin layers [67] and the suppression of the secondary reactions. Figure 2.5 explains the last

hypothesis: the primary photoproduct formed in the flow system is quickly removed from the irradiated area, and as a result, the formation of a secondary product is diminished.

2.3.6 Pressure effects

Batch processing

Another important physical parameter that can affect the reaction rate of the Claisen rearrangement is pressure [73]–[79]. Typically, transformations that are accompanied by a decrease in volume (activation volume) are accelerated when pressure is strongly increased (e.g. by 3 orders of magnitude).

It can be shown [73]–[79] that

$$RT \cdot \left(\frac{\partial \ln k}{\partial P} \right)_T = -\Delta V^\ddagger \quad (2.1)$$

Here k is reaction rate constant, P is pressure, R is Boltzmann's constant, T is temperature, and ΔV^\ddagger is activation volume.

The Claisen rearrangements display a negative activation volume ranging from -13 to -6 $\text{cm}^3\text{mol}^{-1}$ [78]. In the case of the Claisen rearrangement ΔV^\ddagger of AVE and allyl *para*-cresol ether in non-polar solvents is -18 $\text{cm}^3\text{mol}^{-1}$ and of allyl *meta*-methoxyphenyl ether in alcohol-water is -15 $\text{cm}^3\text{mol}^{-1}$. The Claisen rearrangement can be accelerated by elevated pressures since high pressure favors the cyclic TS [79].

Flow processing

As mentioned in Section 2.3.2, the Claisen rearrangement was performed at high temperature/pressure, very close to the critical conditions for the solvent. With EtOH as a solvent and at a reaction temperature of 280°C , the Claisen rearrangement was executed at varying pressures between 75 and 200 bar [68]. Essentially, no significant dependence of the conversion on pressure was observed.

However, using another solvent and at still higher pressure, some slight pressure effects were observed by Kobayashi *et al.*, as the reaction time was reduced [52], [80]. In the pressure range from 50 to 300 bar, the yield for the Claisen rearrangement was enhanced from 52 to 67% and further increase can be expected once high pressures can be achieved in a microreactor. In addition, it was observed that the reaction is enhanced by the use of protic solvents, probably due to the catalyzing effect of hydrogen bonding.

What needs to be taken into account, is the volume compression of liquids under pressure. Although liquids are generally considered as incompressible fluids, at the elevated pressures and

temperatures employed in this study this simplification is not valid anymore. There exists a significant difference in residence time of almost 30 s between the experiments performed at 50 and 300 bar [64].

2.3.7 Concentration effects

Flow processing

Being a unimolecular reaction it is not surprising not to see strong concentration effects on the Claisen rearrangement yield [52]. Yet, solvent-free processing can make considerable difference to high-c solvent processing which is likely to be caused by the difference in the reaction medium parameters such as dielectric constant and viscosity (for solvent-free processing, reactant and product provide the reaction medium).

2.3.8 Reaction time effects

Flow processing

Long exposure times of reaction mixtures at high temperatures in batch reactions are problematic and may cause the formation of many impurities. Shortening reaction time through using high reaction temperatures is a way to achieve high selectivity, while not comprising conversion. Often flow processing is mandatory for this [26].

2.4 Conclusions

To summarize what has been presented throughout this review, the latter were grouped with regard to the mechanistic and transition-state analysis. Table 2.5 contains a comparison of process windows for old and novel processing of the Claisen rearrangement (modified variant of the table shown in [47]).

Table 2.5. Comparison of known and novel process windows for the Claisen rearrangement.

Process Window	Batch-based (known) results	Flow-based (novel) results
High temperature	Medium conversion at 300°C	Full conversion at 300°C
High pressure	Invariant and kept at ambient pressure (1 atm.)	15% yield increase by increasing pressure from 50 to 300 bar
Increased concentration/Solvents	<ol style="list-style-type: none"> 1. Selectivity losses for high-c and solvent-free processing 2. Solvents are commonly processed up to boiling point and at ambient pressure 	<ol style="list-style-type: none"> 1. High selectivity for high-c and solvent-free processing 2. New solvation properties accessible, e.g. for 1-butanol at high-T 3. Solvent-free conditions result in full conversion at 280°C
Safety	Limits in usage of high temperatures and pressures	Safe high-p and high-T processing
Process integration	Claisen rearrangements make use of the (limited range) of commercially available products	Coupled two-step flow syntheses in an easy manner and without intermediate production isolation = increased chemical diversity

2.5 References

- [1] A. M. M. Castro, "Claisen rearrangement over the past nine decades," *Chem. Rev.*, 2004.
- [2] J. Rehbein and M. Hiersemann, "Claisen rearrangement of aliphatic allyl vinyl ethers from 1912 to 2012: 100 years of electrophilic catalysis," *Synthesis (Germany)*. 2013.
- [3] F. Galindo, "The photochemical rearrangement of aromatic ethers: A review of the Photo-Claisen reaction," *Journal of Photochemistry and Photobiology C: Photochemistry Reviews*, vol. 6, no. 2–3. pp. 123–138, 2005.
- [4] B. Ganem, "The Mechanism of the Claisen Rearrangement: Déjà Vu All Over Again," *Angew. Chemie Int. Ed. English*, 1996.
- [5] I. Iwakura, Y. Kaneko, S. Hayashi, A. Yabushita, and T. Kobayashi, "The reaction mechanism of claisen rearrangement obtained by transition state spectroscopy and single direct-dynamics trajectory," *Molecules*, 2013.
- [6] K. C. Majumdar, S. Alam, and B. Chattopadhyay, "Catalysis of the Claisen rearrangement," *Tetrahedron*. 2008.
- [7] S. J. Harris *et al.*, "Comparing molecular photofragmentation dynamics in the gas and liquid phases," *Physical Chemistry Chemical Physics*. 2013.
- [8] I. Iwakura, "The experimental visualisation of molecular structural changes during both photochemical and thermal reactions by real-time vibrational spectroscopy," *Phys. Chem. Chem. Phys.*, 2011.
- [9] R. A. Mathies, C. H. Brito Cruz, W. T. Pollard, and C. V. Shank, "Direct observation of the femtosecond excited-state cis-trans isomerization in bacteriorhodopsin," *Science (80-.)*, 1988.
- [10] A. Stingl, R. Szipöcs, C. Spielmann, and F. Krausz, "Generation of 11-fs pulses from a Ti:sapphire laser without the use of prisms," *Opt. Lett.*, 1994.
- [11] I. Iwakura, A. Yabushita, and T. Kobayashi, "Direct Observation of the Molecular Structural Changes during the Claisen Rearrangement Including the Transition State," *Chem. Lett.*, 2010.
- [12] H. B. Schlegel, "Exploring Potential Energy Surfaces for Chemical Reactions: An Overview of Some Practical Methods," *J. Comput. Chem.*, 2003.
- [13] F. Neese, A. Hansen, F. Wennmohs, and S. Grimme, "Accurate theoretical chemistry with coupled pair models," *Acc. Chem. Res.*, 2009.
- [14] J. Jung, S. Re, Y. Sugita, and S. Ten-No, "Improved constrained optimization method for reaction-path determination in the generalized hybrid orbital quantum mechanical/molecular mechanical calculations," *J. Chem. Phys.*, 2013.
- [15] N. Moghadam, S. Liu, S. Srinivasan, M. C. Grady, M. Soroush, and A. M. Rappe, "Computational study of chain transfer to monomer reactions in high-temperature polymerization of Alkyl acrylates," *J. Phys. Chem. A*, 2013.
- [16] P. J. Silva and M. J. Ramos, "Computational insights into the photochemical step of the reaction catalyzed by protochlorophyllide oxidoreductase," *Int. J. Quantum Chem.*, 2011.
- [17] D. S. Karanewsky and Y. Kishi, "New conditions for controlled Claisen rearrangements of allyl aryl ethers," *J. Org. Chem.*, vol. 41, no. 18, pp. 3026–3027, Sep. 1976.

- [18] T. Noël and S. L. Buchwald, "Cross-coupling in flow.," *Chem. Soc. Rev.*, vol. 40, no. 10, pp. 5010–29, Oct. 2011.
- [19] J. Wegner, S. Ceylan, and A. Kirschning, "Ten key issues in modern flow chemistry.," *Chem. Commun. (Camb)*, vol. 47, no. 16, pp. 4583–92, Apr. 2011.
- [20] R. L. Hartman, J. P. McMullen, and K. F. Jensen, "Deciding whether to go with the flow: Evaluating the merits of flow reactors for synthesis," *Angewandte Chemie - International Edition*. 2011.
- [21] D. Webb and T. F. Jamison, "Continuous flow multi-step organic synthesis," *Chemical Science*. 2010.
- [22] K. Geyer, T. Gustafsson, and P. Seeberger, "Developing Continuous-Flow Microreactors as Tools for Synthetic Chemists," *Synlett*, vol. 2009, no. 15, pp. 2382–2391, Aug. 2009.
- [23] S. V. Ley, "The changing face of organic synthesis," *Tetrahedron*, 2010.
- [24] H. Kobayashi *et al.*, "The impact of Novel Process Windows on the Claisen rearrangement," *Tetrahedron*, vol. 69, no. 14, pp. 2885–2890, 2013.
- [25] M. Sato *et al.*, "Highly-selective and high-speed Claisen rearrangement induced with subcritical water microreaction in the absence of catalyst," *Green Chem.*, vol. 11, no. 6, p. 763, 2009.
- [26] L. Kong, Q. Lin, X. Lv, Y. Yang, Y. Jia, and Y. Zhou, "Efficient Claisen rearrangement of allylpara-substituted phenyl ethers using microreactors," *Green Chem.*, vol. 11, no. 8, pp. 1108–1111, 2009.
- [27] H. Maeda, S. Nashihara, H. Mukae, Y. Yoshimi, and K. Mizuno, "Improved efficiency and product selectivity in the photo-Claisen-type rearrangement of an aryl naphthylmethyl ether using a microreactor/flow system," *Res. Chem. Intermed.*, vol. 39, no. 1, pp. 301–310, 2013.
- [28] V. Hessel, I. Vural Gürsel, Q. Wang, T. Noël, and J. Lang, "Potential Analysis of Smart Flow Processing and Micro Process Technology for Fastening Process Development: Use of Chemistry and Process Design as Intensification Fields," *Chem. Eng. Technol.*, vol. 35, no. 7, pp. 1184–1204, Jul. 2012.
- [29] V. Hessel, "Novel Process Windows - Gate to Maximizing Process Intensification via Flow Chemistry," *Chem. Eng. Technol.*, vol. 32, no. 11, pp. 1655–1681, Nov. 2009.
- [30] V. Hessel, B. Cortese, and M. H. J. M. De Croon, "Novel process windows – Concept, proposition and evaluation methodology, and intensified superheated processing," *Chem. Eng. Sci.*, vol. 66, no. 7, pp. 1426–1448, Apr. 2011.
- [31] V. Hessel, D. Kralisch, N. Kockmann, T. Noël, and Q. Wang, "Novel process windows for enabling, accelerating, and uplifting flow chemistry," *ChemSusChem*, vol. 6, no. 5, pp. 746–789, 2013.
- [32] J. A. Rinc, M. Barberis, M. Gonz, M. D. Johnson, and J. K. Niemeier, "Safe , Convenient ortho-Claisen Thermal Rearrangement Using a Flow Reactor," pp. 1428–1432, 2011.
- [33] X. P. Ma, Z. M. Li, and Q. R. Wang, "Rapid formation of β -allyl substituted isotetronic acid derivatives via Claisen rearrangement using a microfluidic device," *Chinese Chem. Lett.*, vol. 22, no. 2, pp. 167–170, 2011.
- [34] T. R. Ramadhar and R. A. Batey, "Resolving the mechanistic origins of E/Z-selectivity differences for the ortho-aryl-Claisen [3,3]-sigmatropic rearrangement through DFT calculations," *Comput. Theor. Chem.*, vol. 974, no. 1, pp. 76–78, 2011.
- [35] M. B. Smith and J. March, *March's Advanced Organic Chemistry: Reactions, Mechanisms, and Structure: Sixth Edition*, vol. 9780471720. John Wiley and Sons, 2006.
- [36] J. J. Gajewski and K. E. Gilbert, "Empirical approach to substituent effects in [3,3]-sigmatropic shifts

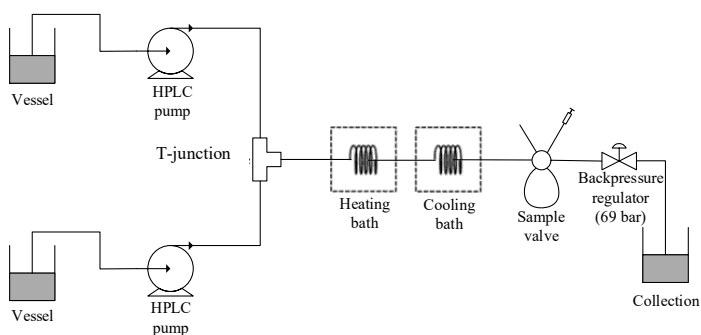
- utilizing the thermochemistry of coupled nonconcerted alternative paths," *J. Org. Chem.*, vol. 49, no. 1, pp. 11–17, Jan. 1984.
- [37] S. R. Emamian, M. . Aghaie, M. R. . Zardoost, E. . Zahedi, and K. Zare, "Kinetic and thermodynamic study of substituent effect on the Claisen rearrangement of para-substituted SI aryl ether: a Hammett study via DFT," *J. Phys. Theor. Chem.*, vol. 6, pp. 183–192, 2009.
- [38] C. Reichardt, "SOLVENT EFFECTS ON CHEMICAL REACTIVITY," *Pure Appl.Chern*, vol. 54, no. 10, pp. 1867–1884, 1982.
- [39] J. J. Gajewski, "The Claisen Rearrangement. Response to Solvents and Substituents: The Case for Both Hydrophobic and Hydrogen Bond Acceleration in Water and for a Variable Transition State," *Acc. Chem. Res.*, vol. 30, no. 5, pp. 219–225, May 1997.
- [40] S. G., "Nanoclusters – Building Blocks for Future Nanoelectronic Devices?," *Adv. Eng. Mater.*, vol. 3, no. 10, pp. 737–743, Oct. 2001.
- [41] E. D. Hughes and C. K. Ingold, "55. Mechanism of substitution at a saturated carbon atom. Part IV. A discussion of constitutional and solvent effects on the mechanism, kinetics, velocity, and orientation of substitution," *J. Chem. Soc.*, p. 244, 1935.
- [42] M. J. Blandamer and J. Burgess, "Solvation of transition metal complexes: thermochemical approaches," *Transit. Met. Chem.*, vol. 13, no. 1, pp. 1–18, 1987.
- [43] E. Brandes, P. A. Grieco, and J. J. Gajewski, "Effect of polar solvents on the rates of Claisen rearrangements: assessment of ionic character," *J. Org. Chem.*, vol. 54, no. 3, pp. 515–516, 1989.
- [44] D. L. Severance and W. L. Jorgensen, "Effects of hydration on the Claisen rearrangement of allyl vinyl ether from computer simulations," *J. Am. Chem. Soc.*, vol. 114, no. 27, pp. 10966–10968, 1992.
- [45] M. M. Davidson, I. H. Hillier, R. J. Hall, and N. A. Burton, "Effect of Solvent on the Claisen Rearrangement of Allyl Vinyl Ether Using ab initio Continuum Methods," *J. Am. Chem. Soc.*, vol. 116, no. 20, pp. 9294–9297, 1994.
- [46] B. Gutmann, D. Cantillo, and C. O. Kappe, "Continuous-Flow Technology-A Tool for the Safe Manufacturing of Active Pharmaceutical Ingredients," *Angew. Chemie Int. Ed.*, 2015.
- [47] A. Lee, J. D. Stewart, J. Clardy, and B. Ganem, "New insight into the catalytic mechanism of chorismate mutases from structural studies," *Chemistry and Biology*, vol. 2, no. 4. pp. 195–203, 1995.
- [48] C. Uyeda and E. N. Jacobsen, "Enantioselective Claisen rearrangements with a hydrogen-bond donor catalyst," *J. Am. Chem. Soc.*, vol. 130, no. 29, pp. 9228–9229, 2008.
- [49] M. Kirsten, J. Rehbein, M. Hiersemann, and T. Strassner, "Organocatalytic Claisen Rearrangement: Theory and Experiment," *J. Org. Chem.*, vol. 72, no. 11, pp. 4001–4011, May 2007.
- [50] Y. Huang, A. K. Unni, A. N. Thadani, and V. H. Rawal, "Hydrogen bonding: single enantiomers from a chiral-alcohol catalyst," *Nature*, vol. 424, no. 6945, p. 146, 2003.
- [51] O. Acevedo and K. Armacost, "Claisen Rearrangements: Insight into Solvent Effects and 'on Water' Reactivity from QM/MM Simulations," *J. Am. Chem. Soc.*, vol. 132, no. 6, pp. 1966–1975, Feb. 2010.
- [52] H. Kobayashi *et al.*, "The impact of Novel Process Windows on the Claisen rearrangement," *Tetrahedron*, vol. 69, no. 14, pp. 2885–2890, 2013.
- [53] H. Kawanami *et al.*, "Highly selective non-catalytic Claisen rearrangement in a high-pressure and high-temperature water microreaction system," *Chem. Eng. J.*, 2011.

- [54] A. M. Sanchez, A. V Veglia, and R. H. de Rossi, "β-Cyclodextrin effects on photo-Claisen rearrangement of allyl phenyl ether," *Can. J. Chem.*, vol. 75, no. 8, pp. 1151–1155, Aug. 1997.
- [55] T. Razzaq, T. N. Glasnov, and C. O. Kappe, "Accessing novel process windows in a high-temperature/pressure capillary flow reactor," *Chem. Eng. Technol.*, 2009.
- [56] A. F. Shamsutdinov, T. F. Shamsutdinov, D. V. Chachkov, A. G. Shamov, and G. M. Khrapkovskii, "The influence of molecular structure on the change of the arrhenius factor of gas-phase elimination of nitric acid from nitroalkanes," *Int. J. Quantum Chem.*, vol. 107, no. 13, pp. 2343–2352, May 2007.
- [57] K. Maruoka, H. Banno, and H. Yamamoto, "Asymmetric Claisen rearrangement catalyzed by chiral organoaluminum reagent," *J. Am. Chem. Soc.*, vol. 112, no. 21, pp. 7791–7793, Oct. 1990.
- [58] K. Maruoka, S. Saito, and H. Yamamoto, "Molecular Design of a Chiral Lewis Acid for the Asymmetric Claisen Rearrangement," *J. Am. Chem. Soc.*, vol. 117, no. 3, pp. 1165–1166, Jan. 1995.
- [59] A. C. Varas, T. Noël, Q. Wang, and V. Hessel, "Copper(I)-catalyzed azide-alkyne cycloadditions in microflow: catalyst activity, high-T operation, and an integrated continuous copper scavenging unit.," *ChemSusChem*, vol. 5, no. 9, pp. 1703–7, Sep. 2012.
- [60] D. P. Curran and L. H. Kuo, "Acceleration of a dipolar Claisen rearrangement by Hydrogen bonding to a soluble diaryl^urea," *Tetrahedron Lett.*, vol. 36, no. 37, pp. 6647–6650, 1995.
- [61] C. Uyeda and E. N. Jacobsen, "Transition-State Charge Stabilization through Multiple Non-covalent Interactions in the Guanidinium-Catalyzed Enantioselective Claisen Rearrangement," *J. Am. Chem. Soc.*, vol. 133, no. 13, pp. 5062–5075, Apr. 2011.
- [62] S. G. Waghlikar, S. Mayadevi, N. E. Jacob, and S. Sivasanker, "Claisen rearrangement of allyl phenyl ether over zeolites beta, mordenite and Y," *Microporous Mesoporous Mater.*, vol. 95, no. 1, pp. 8–16, 2006.
- [63] N. T. Mathew, S. Khaire, S. Mayadevi, R. Jha, and S. Sivasanker, "Rearrangement of allyl phenyl ether over Al-MCM-41," *J. Catal.*, vol. 229, no. 1, pp. 105–113, 2005.
- [64] A. Lubineau and J. Augé, "Water as Solvent in Organic Synthesis BT - Modern Solvents in Organic Synthesis," P. Knochel, Ed. Berlin, Heidelberg: Springer Berlin Heidelberg, 1999, pp. 1–39.
- [65] S. D. Copley and J. R. Knowles, "The conformational equilibrium of chorismate in solution: implications for the mechanism of the non-enzymic and the enzyme-catalyzed rearrangement of chorismate to prephenate," *J. Am. Chem. Soc.*, vol. 109, no. 16, pp. 5008–5013, Aug. 1987.
- [66] R. R. Knowles and E. N. Jacobsen, "Attractive noncovalent interactions in asymmetric catalysis: Links between enzymes and small molecule catalysts," *Proc. Natl. Acad. Sci.*, vol. 107, no. 48, p. 20678 LP-20685, Nov. 2010.
- [67] B. Gómez, P. K. Chattaraj, E. Chamorro, R. Contreras, and P. Fuentealba, "A Density Functional Study of the Claisen Rearrangement of Allyl Aryl Ether, Allyl Arylamine, Allyl Aryl Thio Ether, and a Series of Meta-Substituted Molecules through Reactivity and Selectivity Profiles," *J. Phys. Chem. A*, vol. 106, no. 46, pp. 11227–11233, Nov. 2002.
- [68] C. R. Strauss, "On Scale Up of Organic Reactions in Closed Vessel Microwave Systems," *Org. Process Res. Dev.*, vol. 13, no. 5, pp. 915–923, Sep. 2009.
- [69] J. D. Moseley and E. K. Woodman, "Scaling-Out Pharmaceutical Reactions in an Automated Stop-Flow Microwave Reactor," *Org. Process Res. Dev.*, vol. 12, no. 5, pp. 967–981, Sep. 2008.
- [70] F. Bergamelli, M. Iannelli, J. A. Marafie, and J. D. Moseley, "A Commercial Continuous Flow

- Microwave Reactor Evaluated for Scale-Up," *Org. Process Res. Dev.*, vol. 14, no. 4, pp. 926–930, Jul. 2010.
- [71] S. C. Stouten, T. Noël, Q. Wang, and V. Hessel, "A View Through Novel Process Windows," *Aust. J. Chem.*, vol. 66, no. 2, pp. 121–130, 2013.
- [72] I. Iwakura, A. Yabushita, and T. Kobayashi, "Non-thermal reaction triggered by a stimulated Raman process using 5-fs laser pulses in the electronic ground state: Claisen rearrangement of allyl phenyl ether," *Chem. Phys. Lett.*, 2011.
- [73] F. W. Schuler and G. W. Murphy, "The Kinetics of the Rearrangement of Vinyl Allyl Ether¹," *J. Am. Chem. Soc.*, vol. 72, no. 7, pp. 3155–3159, Jul. 1950.
- [74] L. Stein and G. W. Murphy, "Kinetics of the Rearrangement of Isopropenyl Allyl Ether¹," *J. Am. Chem. Soc.*, vol. 74, no. 4, pp. 1041–1043, Feb. 1952.
- [75] H. M. Frey and B. M. Pope, "The thermal unimolecular isomerisation of 2-methylallyl vinyl ether," *J. Chem. Soc. B Phys. Org.*, no. 0, pp. 209–210, 1966.
- [76] L. Kupczyk-Subotkowska, W. H. Saunders, and H. J. Shine, "Claisen rearrangement of allyl phenyl ether: heavy-atom kinetic isotope effects and bond orders in the transition structure," *J. Am. Chem. Soc.*, vol. 110, no. 21, pp. 7153–7159, Oct. 1988.
- [77] S. Yamabe, S. Okumoto, and T. Hayashi, "Transition Structures for the Aromatic Claisen Rearrangements by the Molecular Orbital Method," *J. Org. Chem.*, vol. 61, no. 18, pp. 6218–6226, Jan. 1996.
- [78] R. Van Eldik, T. Asano, and W. J. Le Noble, "Activation and reaction volumes in solution. 2," *Chem. Rev.*, vol. 89, no. 3, pp. 549–688, May 1989.
- [79] K. R. Brower, "The Volume Change of Activation in the Claisen and Curtius Rearrangements," *J. Am. Chem. Soc.*, vol. 83, no. 21, pp. 4370–4372, Nov. 1961.
- [80] W. Wu, G. Qian, X.-G. Zhou, and W.-K. Yuan, "Peroxidization of methyl ethyl ketone in a microchannel reactor," *Chem. Eng. Sci.*, vol. 62, no. 18, pp. 5127–5132, 2007.

CHAPTER 3

Connected Nucleophilic Substitution-Claisen Rearrangement in Flow – Analysis for Kilo-Lab Process Solutions with Orthogonality



This chapter is based on:

Shahbazali, E., Spapens, M. R. P., Kobayashi, H., Ookawara, S., Noël, T., Hessel, V., Chem. Eng. Journal 281 (2015) 144–154

Abstract

The two-step synthesis of phenol to 2-allylphenol in micro-flow has been investigated. This synthesis involves a nucleophilic substitution (S_N2) reaction of phenol with allyl bromide towards allyl phenyl ether followed by a thermal Claisen rearrangement of allyl phenyl ether to 2-allylphenol. This carbon-carbon bond forming reaction route would provide a valuable path towards complex molecules. Flow cascades have turned into a powerful approach to provide chemical diversity (process-design intensification). This is enabled by chemical intensification of the Claisen rearrangement in micro-flow, by reducing the reaction time to minutes without the need of a catalyst. While both individual reaction steps have been optimized separately in earlier research, an initially directly connected two-step synthesis gave a low selectivity.

Accordingly, the main topic investigated is how to achieve orthogonality in case of reagent mismatch between the two reactions. First, four flow process protocols using three different kinds of in-flow separation and one kinetic approach, are developed on laboratory scale. From there, process design sheets for kilolab processing set-ups of the suited approaches are developed which shed first light on their industrial practice. In particular, it has been found that the main causes for the drop in selectivity are the presence of the base DBU and the reactant allyl bromide during the Claisen rearrangement. Three of the four investigated separation approaches demonstrated the ability to improve the overall yield - acid-base extraction, acid absorption by using ion exchange resin, using a heterogeneous base, and dilution as kinetic approach. Finally, for every option, the proposed respective production set-up, anticipated advantages and drawbacks are given to facilitate a decision.

3.1 Introduction

The rearrangement of allyl vinyl ethers into γ,δ -unsaturated carbonyl compounds was developed by Claisen in 1912 [1, 2]. In general it presents the simplest example of so called [3,3]-sigmatropic shifts. After its development the rearrangement has been widely studied [3]. Commonly, a concerted pathway is assumed [3]. Kinetic experiments by Schuler [4] demonstrated the unimolecularity of the Claisen rearrangement. The Claisen rearrangement is feasible for a large variety of aliphatic and aromatic ethers and has become one of the most synthetically useful reactions of organic chemistry [5, 6]. Substituted allyl vinyl ethers undergo Claisen rearrangement to give the unsaturated aldehydes with quantitative yields and a high degree of stereoselectivity [7, 8].

In the last two decades, microreactor technology has emerged. The technology is meanwhile mature for applications and is even applied on industrial scale [9], including investigations of the Claisen rearrangement in flow [10-13]. It has almost become routine for chemical reactor engineers and, recently, an even larger number of chemists have been attracted by the novel synthesis tool. A major point for the chemists is that the new tool opens doors to new chemistries, in particular under so far non-accessible operation regimes such as harsh conditions. Novel process windows have widened the synthetic possibilities and have become typical for whole flow chemistry [14-17]. They add chemical intensification to the prior developed transfer intensification of microreactors. This is most evident from the order-of-magnitude shrinkage in reaction time; most conveniently done by short-time, high-temperature processing at high pressure to prevent evaporation or boiling.

This was also applied to the Claisen rearrangement which is already conventionally, a typical high-temperature reaction. Here, novel process windows have been identified as follows. Higher yields were obtained for the product 2-allyl-4-chlorophenol and other *para*-substituted phenyl allyl ethers in flow as compared to batch at the same temperature of 200°C [10, 18]. Flow residence times amount to only 24 min as opposed to reaction times of 3 h in batch.

While concentration effects are not strong due to the unimolecular nature of the reaction, solvent-free processing can still make a considerable difference [10]. An important benefit of the new high temperature-high pressure window is that solvent selection is not restricted anymore by the solvent's boiling point. Low-boiling solvents can be used in flow at the desired high temperature when superheated operation is chosen, and replace former costly high-temperature solvents [10]. Following these lines, the Claisen rearrangement of allyl phenyl ether to *ortho*-allyl phenol (o-AP) was performed in subcritical water [11, 19]. In a conventional water-free method, o-AP was produced with 85% yield at 220°C, ambient pressure, and at a reaction time of 6 h. While in a similar batch process, but using subcritical water, the reaction time shortened significantly to 10 min at 240°C and 3.4 MPa, giving a yield of 84%. With flow, the

reaction time was further reduced to 2.5 min. A comprehensive investigation of solvent effects on the Claisen rearrangement to give *ortho*-allyl phenol showed that among alkanol solvents 1-butanol was optimal and even small differences between isomers (1- and 2-propanol) were visible [10] (see also [12]). In this superheated way and without need for advanced supercritical operation, the reaction time was further shrunk to 4 min (quantitative yield, 280°C and 100 bar).

As a net result, space-time yields obtained with micro-flow reactors are typically significantly higher (up to a factor of 80) than in batch reactors [20]. The impact of pressure is ambiguously documented [18]. A detailed discussion is given whether pressure can have kinetic effect or relates to physical phenomena such as volume expansion under temperature and compressibility under pressure [10] (see also [17, 21-23]).

A detailed comparison of the Claisen rearrangement in batch and in flow was given; see Table 10 in [24].

Besides such chemical intensification, a second major flow chemistry motivation is the connection of flow processes into a chain. This is part of process integration and we have termed the effects thereof as process-design intensification. Such flow cascade is a biomimetic analogue of nature's metabolic and signaling pathways [25]. Cascades in batch have attracted attention also in chemistry [26]. Also in flow, cascades have turned into a powerful and speedy approach for providing complex products. Subsecond organometallic flash chemistries [27, 28], deliver – without any separation - a 3- or 4-step product in about one second [29, 30]. Flow syntheses have been described with many more, longer-timed steps to yield complex molecules, e.g. natural products [31-33]. However, here, interim flow separations are needed, mostly by scavenger cartridges [34]. A full orthogonality of all reactions cannot be achieved anymore.

The latter is our motivation of the work reported in this chapter. Rather aiming at an orthogonality for a multi(>5)-step flow synthesis providing analytical amounts of a complex molecule, we investigate a comparatively simple two-step flow synthesis, yet under considerations of engineering it finally to a scale which can provide substantial amounts of product – e.g. sufficient for an industrial kilo-lab (in pharmacy).

Concerning our chemistry, we took phenol as a frequently used building block, a cheap and widely available chemical which is converted into allyl phenyl ether by a Williamson ether synthesis (a nucleophilic substitution). The formed ether is then reacted to 2-allyl phenol using the Claisen rearrangement (see Figure 3.1). The same reaction path is also available for use with a number of functional groups positioned on the phenol substrate [35], increasing the number of possible applications of this synthesis.

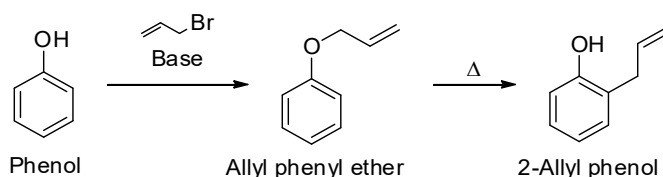


Figure 3.1. Two-step synthesis of 2-allyl phenol from phenol

Earlier in this group, in addition to the thermal Claisen rearrangement, the Williamson ether synthesis of phenol to allyl phenyl ether has been optimized in micro-flow. A conversion of 80% was obtained after 4 minutes residence time using n-butanol as a solvent and the organic homogeneous base DBU as a base at 100°C [36]. However, attempts to directly connect the Williamson ether synthesis to the Claisen rearrangement have been initially unsuccessful. A subsequent Claisen rearrangement resulted in an undesirably low yield, with formation of a dark colored product and numerous different side products; see the ‘Results and Discussion’ section in this chapter.

The objective of the work reported in this chapter is to find process conditions which allow performing a two-step flow synthesis at an overall yield threshold of 80%. This is based on experimental evidence from the single Williamson ether synthesis having an almost quantitative yield and from the Claisen rearrangement having about 80% yield. During this study, the application in continuous production has been considered. Important factors here are the price of required chemicals and equipment, the complexity of operation, the overall productivity of the set-up and the energy requirements.

3.2 Experimental procedures

3.2.1 Microchannel experiments

Microchannel experiments have been executed in the reactor set-up depicted in Figure 3.2. The reactant mixtures are pumped using HPLC pumps (Knauer Azura P4.15). The two pumps are connected to a T-junction (Valco). The stream is then led through a Hastelloy-C® capillary tube reactor (ID 0.03", OD 1/16", 3.3 m). 2.3 m of this reactor length is immersed in a heating bath (Lauda C6 CS) containing thermal oil (Lauda Ultra 300) with a set temperature. The remaining 1 m is immersed in a cooling bath (Lauda Ecoline StarEdition RE104) filled with demineralized water at 15 °C. The mixture then flows through a 6-port sample valve (VICI) with a sample loop of 100 µl, in order to take samples before the back pressure regulator, where circulation might occur due to internal volume. After the sample valve, a back pressure regulator is attached, either of the type Bronkhorst EL-PRESS or the type IDEX cartridge, both set at 69 bar.

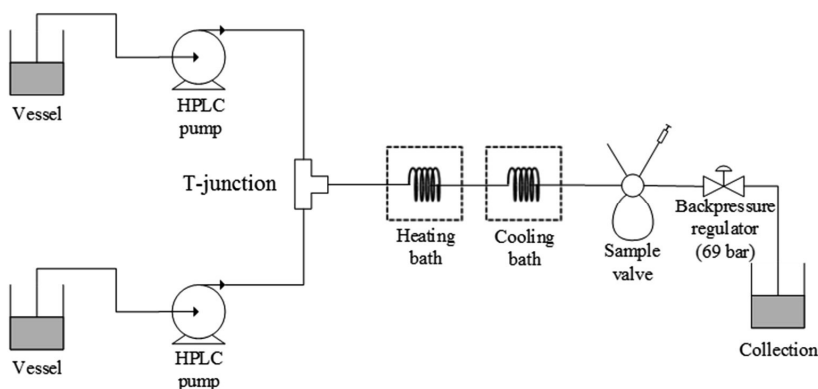


Figure 3.2. Schematic overview of the used microchannel set-up

In a typical Claisen rearrangement experiment, allyl phenyl ether (1.68 g, 12.5 mmol) and the internal standard for HPLC analysis benzonitrile (0.258 g, 2.5 mmol) are dissolved in 25 ml n-butanol as solvent. This solution is introduced into the setup at 15.72 ml/h (space time = 4 min) at 69 bar and 300 °C.

In a typical nucleophilic substitution experiment, phenol (2.35 g, 25 mmol) and the internal standard for HPLC analysis benzonitrile (0.516 g, 5 mmol) are dissolved in 10 ml n-butanol as solvent. Subsequently, while cooling to 0 °C, DBU (7.61 g, 50 mmol) is added slowly. This mixture is further diluted with n-butanol to give 25 ml solution. Then, in a separate vessel, allyl bromide (6.05 g, 50 mmol) is dissolved in 25 ml n-butanol as solvent. The two solutions are introduced into the set-up with two HPLC pumps connected to the T-junction, using a flow rate of 7.86 ml/h per pump (space time = 4 min).

3.2.2 Packed bed experiments

The packed bed reactor used for experiments is a stainless steel 316 tube (ID 0.18", OD 1/4", 10.3 cm) with frits attached to both ends with a pore diameter of 20 μm to hold the packing. The packed bed reactor set-up utilizes the same equipment as the microchannel set-up, but is now configured as depicted in Figure 3.3 (see also Supplementary Material). A single HPLC pump is connected with a capillary tube to the packed bed reactor, which is immersed in the regulated heating bath. For temperatures under or equal to 80 °C, the Lauda Ecoline StarEdition RE104 with demineralized water is used; for temperatures higher than 80 °C, the Lauda C6 CS with Lauda Ultra 300 oil is used. Optionally, a second identical packed bed reactor is directly connected in series to the first packed bed reactor with a short capillary tube and immersed in the same heating bath. After the last packed bed, a back pressure regulator of the type IDEX cartridge set

at 6.9 bar is optionally connected. All packed bed space times have been determined assuming that the solid volume fraction ϵ_{sol} is equal to 0.50.

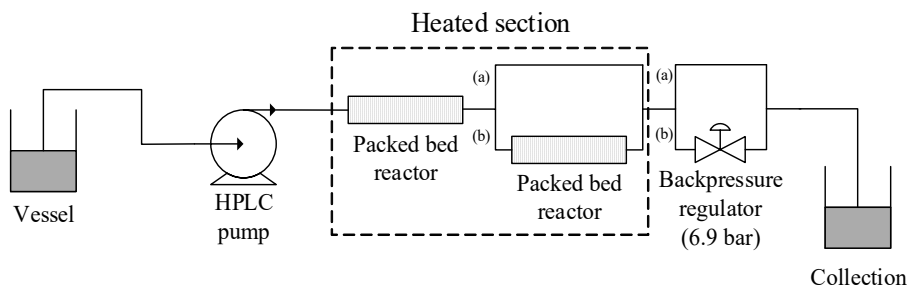


Figure 3.3. Schematic overview of the packed bed set-up, with (a) and (b) representing two different options used

In a typical potassium carbonate–packed bed experiment, a mixture of K_2CO_3 and 1 mm borosilicate glass beads is prepared in a mass ratio of 1:1.4. The inert glass beads are used to prevent the K_2CO_3 crystals to compress to an impermeable layer ($\Delta p > 100$ bar). The packed bed reactor is filled with the prepared mixture (1.73 g, $\epsilon_{\text{sol}} = 0.45$), connected to the described set-up and wetted with pure solvent before use. In a vessel, phenol (1.18 g, 12.5 mmol), allyl bromide (3.02 g, 25 mmol) and the internal standard for HPLC analysis benzonitrile (0.258 g, 2.5 mmol) are dissolved in 25 ml methyl ethyl ketone (MEK) as solvent. This solution is introduced in the set-up with the HPLC pump at 5.1 ml/h (space time = 10 min).

In a typical Amberlyst A26 (mesh size 16-45) packed bed experiment, the ion exchange resin is first treated before use. The resin (20 g) is washed with subsequently 2 times 20 ml H_2O and 2 times 20 ml MEK. The resin is then mixed with 40 ml of MEK in a closed vessel and shaken for 24 hours, to remove all water from the resin pores. The resin is then decanted and dried at room temperature for 24 hours. The packed bed reactor is filled with dry resin which is then swollen with the solvent MEK by flooding the reactor vertically using the HPLC pump at 30 ml/h. The reactor is then sealed at both sides and ready for use in the same manner as in a K_2CO_3 experiment. After an experiment, the bed is regenerated to the OH^- form by letting an aqueous 1M NaOH solution flow over the bed for 1 hour at 30 ml/h. The resin is returned to the MEK-swollen form by flowing pure MEK over the bed at 30 ml/h for 20 minutes.

3.2.3 Other experiments

Acid-base liquid-liquid extraction and acid absorption

In order to perform the L-L acid-base extraction on a mixture obtained after the nucleophilic substitution reaction, HCl (37%) is diluted with H_2O to a concentration of 2 M. Then, 40 ml of mixture to be extracted is mixed with 40 ml of the HCl solution in a separating funnel. The funnel

is shaken for 5 minutes and then left for settling for at least 12 hours. The aqueous and organic phases are thereafter separately collected. The extent of extraction has been checked by means of acidity measurement and detection of DBU by HPLC.

To achieve acid absorption by use of the weak basic ion exchange resin Amberlyst A21, the resin (20 g) is first washed with 2 times 20 ml H₂O and subsequently dried at 100 °C for at least 12 hours. The dried resin is added to 40 ml of n-butanol, left for at least 12 hours and decanted. An excess (10 g) of ion exchange resin is added to 20 ml of solution where acid needs to be absorbed. The mixture is shaken for at least 12 hours and decanted. The extent of acid absorption is tested by acidity measurement.

General reactant information, analytical procedures and batch nucleophilic substitution

See supplementary material

3.3 Results and Discussion

3.3.1 Orthogonality of product and auxiliary materials between the two reactions

As described in section 3.1, the starting point of the present research is the low selectivity of the optimized Claisen rearrangement when connected directly to the optimized nucleophilic substitution reaction. The resulting mixture contains the target product, 2-allyl phenol, along with a number of different by-products, and auxiliary materials such as the base. This likely causes the incompatibility between the two reactions.

We decided to check experimentally whether this is true or not. Before doing that, one needs to be aware about the various side reactions possible in the thermal Claisen rearrangement in flow. Razzaq *et al.* have identified those by-products and their proposed reaction pathway; see Supplementary Material [18]. The three main types of by-products are phenol resulting from an O-deallylation, E/Z 2-(prop-1-enyl)phenol resulting from allylic double bond migration and 2-methylbenzofurans from cyclization. The amount of the components formed depends on the reaction conditions.

It can be expected that acids or bases can play a role to activate such reactions. Therefore, the Claisen rearrangement has been performed with and without manually added DBU, the base used in the nucleophilic substitution reaction. As demonstrated in Figure 3.4, the reaction without DBU gave an excellent yield (X=99%, S=95%), while the reaction with added DBU had a selectivity of only 35%. Therefore, this is a component which is not orthogonal to the Claisen rearrangement.

Additionally, the Claisen rearrangement has been performed with the manually added reagents from the nucleophilic substitution, namely phenol and allyl bromide. The resulting HPLC chromatogram is shown in Figure 3.4c. While the reaction has a selectivity similar to the reaction

with DBU ($S=25\%$), there is a shift in the distribution of by-products. While DBU predominantly gave rise to by-products 1 and 2, the reaction with allyl bromide gave increased amounts of phenol and by-products 3 and 4. Furthermore, upon relieving pressure of the stream, large amounts of gas left the system along with the liquid phase. This gas is expected to be a gaseous pyrolysis product of allyl bromide which dissolves in the liquid under high pressures. One of the possible pyrolysis products is propene [36]. Another possible product is HBr; this leads to the hypothesis that an acid might especially induce the O-deallylation and either the cyclization reactions or double bond migration, while a base assists mainly the other side reaction.

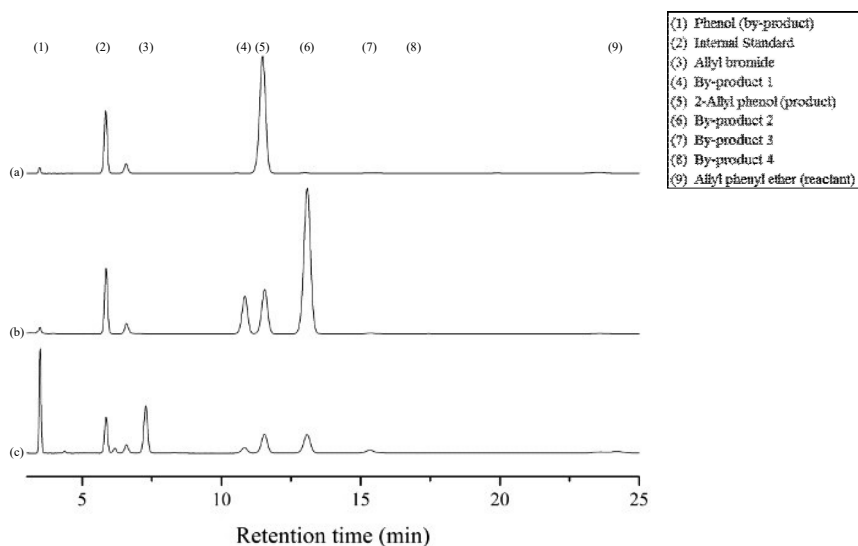


Figure 3.4. HPLC chromatograms of Claisen rearrangement with 0.5 M allyl phenyl ether; (a) no additions (b) with 2 eq. DBU (c) with 1.2 eq. allyl bromide and 0.2 eq. phenol

While the formed by-products have not been identified in the present study, it can be predicted from [18] that by-product 1 and 2 are Z/E 2-(prop-1-enyl)phenol, correspondingly. Also, by product 3 and 4 correspond to 2-methyl-2,3-dihydrobenzofuran and 2-methylbenzofuran, respectively [18].

3.3.2 Homogeneous base removal

The results reported in section 3.3.1 lead to the conclusion that both allyl bromide and the base DBU cause various side reactions at the conditions of the Claisen rearrangement. In order to improve the selectivity, the presence of both components needs to be minimized before performing the second reaction. The most straightforward approach is simply to remove the

harmful components (DBU and allyl bromide) of resulting mixture from the nucleophilic substitution reaction before entering into the Claisen rearrangement.

3.3.3 Liquid-liquid extraction and acid absorption

Initially, the resulting mixture of the nucleophilic substitution reaction has been extracted with an aqueous HCl solution. The DBU is expected to react with the HCl and migrates to the aqueous phase, removing it from the organic phase. However, upon performing the Claisen rearrangement with the extracted mixture, the selectivity of the reaction surprisingly has dropped to 5%, which is lower than without any treatment. It was found that the reason for this even lower selectivity simply is that during the extraction, the desired result of all DBU migrating to the aqueous phase was not achieved. Instead, DBU was present in both the aqueous and the organic phase, while both phases became highly acidic. It is expected that both HCl and the formed ion pair $\text{DBU-H}^+\text{Cl}^-$ interact with the polar, protic solvent *n*-butanol, resulting in a high solubility in both phases. In the Claisen rearrangement afterwards, HCl is likely to cause side reactions, leading to the very low selectivity observed.

For these reasons, an acid-base extraction by itself is not sufficient to increase the selectivity. Therefore, a method has been searched to remove the acid which is present after the extraction. In this case, $\text{DBU-H}^+\text{Cl}^-$ ion pairs still remain, but the solution being pH-neutral is expected to increase the selectivity of the Claisen rearrangement. The method used to remove the HCl is by using the weak base ion exchange resin Amberlyst A21.

The mixture obtained after extraction has been exposed to an excess of ion exchange resin in batch. As expected, the solution was pH-neutral after the treatment. The Claisen rearrangement with this mixture gave an improved selectivity ($S=85\%$ at a conversion of 93%, compared to 65% without treatment, see Figure 3.5).

When this method is to be utilized in a continuous production, the liquid-liquid extraction can be performed in a continuous manner with e.g. the combination of a capillary slug flow followed by a membrane phase separator. The ion exchange resin can be utilized continuously in a parallel packed bed operation. In one column, the stream from the extraction is exposed to the ion exchanger for acid removal. Since the ion exchanger's functional groups are consumed in this process, a second column is necessary to simultaneously regenerate the consumed ion exchanger with an NaOH solution and a third one to flush the remaining NaOH before use. This system is then switched at the moment that acid is about to break through the end of the first column, see Figure 3.6.

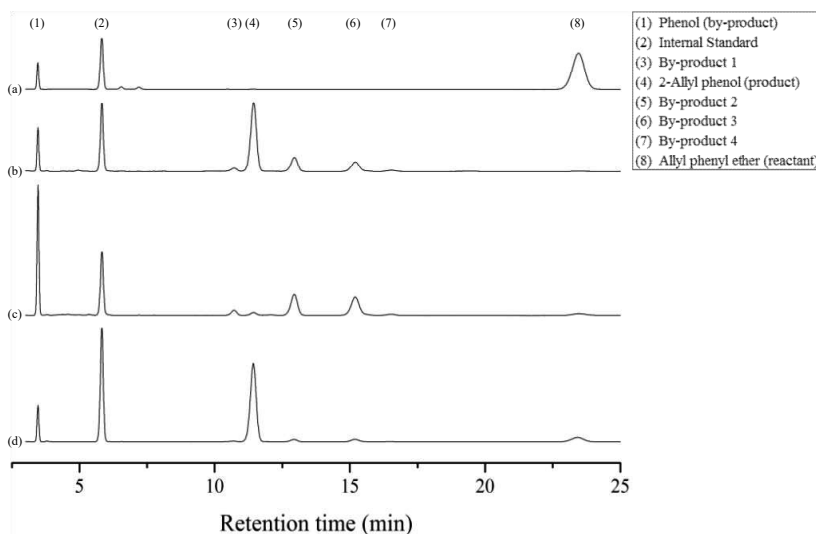


Figure 3.5. HPLC chromatograms of the mixture after (a) S_N2 (Williamson ether synthesis of phenol to allyl phenyl ether) (b) S_N2 and Claisen rearrangement (no treatment, $S=65\%$) (c) S_N2 , extraction and Claisen rearrangement ($S=5\%$) (d) S_N2 , extraction, acid removal and Claisen rearrangement ($S=85\%$)

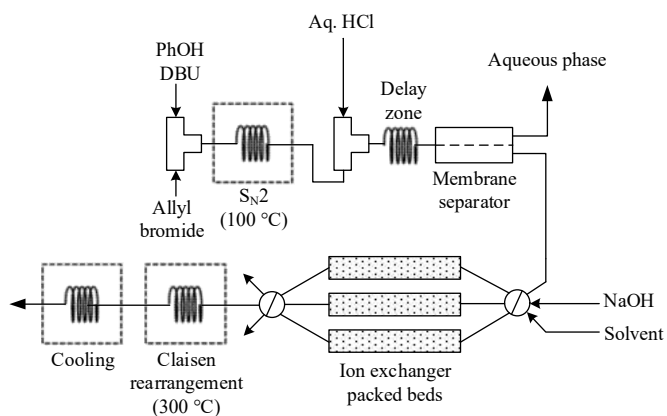


Figure 3.6. Proposed process utilizing continuous L-L extraction and acid absorption using weak basic ion exchange resin (Amberlyst A21) parallel packed beds

We like to give one remark to the envisaged productivity of the plant as shown in Figure 3.6. The current laboratory set-up gives 0.90 g/h final product (assuming 85% total yield). This amounts to 21.6 g/d (24h) and 6.5 kg/a (300 d). A productivity goal may be based on the needs of the pharma or flavor & fragrance industry for which Claisen rearrangement routes have been

described in literature [20]. Then a kilo-lab in industry might be the target, i.e. kg-scale per day. Thus, a productivity increase by a factor of about 46 is needed to match 1 kg/d. By a small increase in diameter, e.g., a factor of 10 in terms of productivity should be achievable still for just one tube. Moreover, a concentration increase could serve for the rest of the productivity increase needed (or a further smart scaling-up). Finally, we consider a parallel operation of 10 tubes as realistic. The first microreactor-based production plant of the Merck Company (Darmstadt/Germany) used 5 micromixer-tubes in parallel [37]. Amberlyst A21 has a capacity of 4.6 eq/kg_{H₂O-swollen resin} and one equivalent can facilitate the removal of 1 mole of HCl. We assumed a concentration of 0.75M acid to remove (our base case). Thus, if we consider the scale-up factor of 46, this amounts to 13.0 moles (for one day) acid and 2.76 kg of Amberlyst A21 resin.

The mini-fixed bed reactor used in this chapter is a tube of inner diameter of 4.6 mm and length of 10.3 cm (volume 1.69 ml) filled with 700 mg solvent-swollen polymeric material weight. A daily exchange and regeneration of such a fixed bed is assumed. Extrapolating that to 2.76 kg resin size, the following fixed-bed tube dimensions result, as given in Figure 3.6: 3 tubes of 7.5 cm diameter and 148.8 cm length (1 used, 2 in stand-by/refreshment/flushing); single bed volume being 6574 ml.

It is obvious that, in terms of tube diameter and volume, the reaction section and Amberlyst separation section have a misfit. That likely will have consequence on flow distribution (channeling) and residence times consequently. A fast recharging of the Amberlyst ion exchanger, e.g. hourly, is needed which then consequently will reduce the corresponding tube diameter and volume.

A better fit can be reached by more frequent exchange and reloading of the resin fixed beds than daily, e.g. every hour. Using the 3-tube approach, 2.65 cm diameter and 49.5 cm length are the right dimensions (1 used, 1 stand-by and 1 for regeneration); single bed volume being 273 ml with residence time of 11 min. The new dimensioning based on hourly recharging results in a better fit of dimensions and thus assumed compatibility of flow operations. To give an idea about true production scale, e.g., one of our industrial pharma partners uses 1000 l resin with a reaction mixture flow rate of 2500 l/h and regeneration times of 3-4 hours [38].

Details on solvent selection can be found in the Supplementary Material.

3.3.4 Heterogeneous base

Since resolution to the selectivity issue failed when utilizing a homogeneous base, it might be a more promising method to use a heterogeneous base. Then, the advantage is that there is no need to remove the base in the next step. Therefore, two different solid bases have been investigated - potassium carbonate (K₂CO₃) and the strong base ion exchange resin Amberlyst A26. The investigated solid-liquid continuous reaction system in both cases is a milli-packed bed

reactor. In all experiments, MEK has been used as solvent for its assumed suitability for the reaction and its immiscibility with water.

Potassium carbonate

Potassium carbonate is the preferred base of choice in laboratory synthesis when performing nucleophilic substitution reactions. Commonly, it is stirred to form a suspension, where the K_2CO_3 transforms after the S_N2 reaction into the (also insoluble) salt KBr, H_2O and CO_2 .

A complete filling of the milli-packed bed with the small, poly-shaped K_2CO_3 crystals is not advised. This leads to the packing of the reactor rapidly forming an impermeable solid cake with a pressure drop of over 100 bars. Therefore, K_2CO_3 has been mixed with inert glass beads with a size of 1 mm, in a mass ratio of K_2CO_3 and glass beads of 1:1.4.

The milli-packed bed reactor set-up has been used at a temperature of 60 °C, with a space time of 10 minutes. The yield of allyl phenyl ether quickly rises to a value of 25%, which is maintained for approximately 5 space times (see Figure 3.7). However, the K_2CO_3 in this reaction is not a catalyst but a reagent. Therefore, after some time, the decreasing amount of base present leads to a lower yield and recharging is advised. Since the original yield of 25% is not deemed high enough to be usable, the temperature has been increased to 120 °C, with the use of a backpressure of 6.9 bar to prevent solvent evaporation. This leads to a significantly higher maximal yield of 90%, which is even higher than for using a homogeneous base. However, since the consumption rate of the base is also higher, the yield rapidly decreases during operation time.

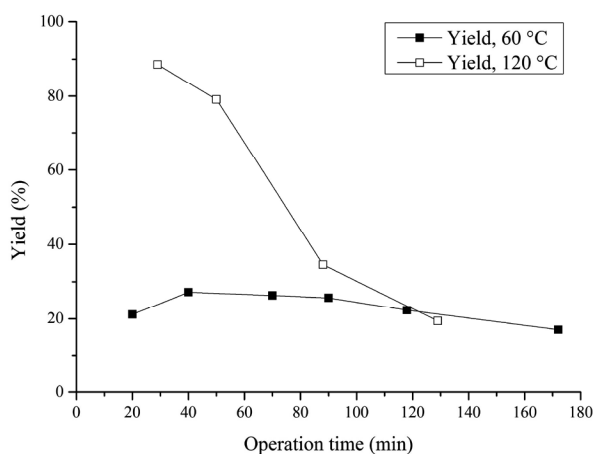


Figure 3.7. Yield of allyl phenyl ether plotted against operation time using a milli-packed bed reactor filled with K_2CO_3 , $\tau=10$ min (a) 60 °C (b) 120 °C

In order to attempt to increase the operational timeframe at a constant high yield, a lower reagent concentration (0.1 M instead of 0.5M) has been used at 120 °C. However, due to the

second order rate law of the reaction, the rate is significantly decreased and as the conversion also, leading to a maximum yield of 40%. For this reason, a concentration of 0.5 M has been maintained, while utilizing two identical packed beds in series. The amount of available base is now effectively doubled. Additionally, allyl bromide is now used as limiting reactant at 0.5 M, instead of phenol, which is now used in 2 equivalents with respect to allyl bromide. This way, the amount of allyl bromide present in the resulting mixture can be minimized, since allyl bromide also causes problems in the Claisen rearrangement. It can be seen that while the outlet concentration of allyl bromide is initially low, it quickly rises despite the larger amount of base used (see Figure 3.8).

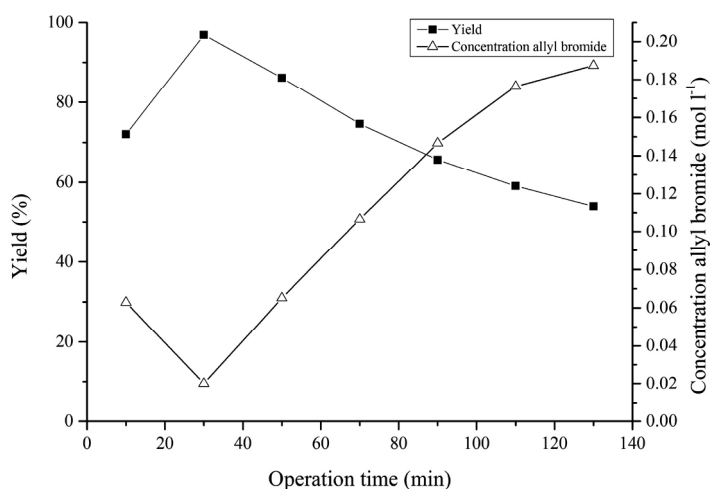


Figure 3.8. Yield of allyl phenyl ether and outlet concentration of allyl bromide plotted against operation time using two milli-packed bed reactors filled with K_2CO_3 , ($\tau_s=20$ min, $T=120$ °C), Allyl bromide (0.5 M) is the limiting reactant. $n_{\text{allyl bromide},0} : n_{\text{phenol},0} = 1:2$

In order to simulate the outcome of the Claisen rearrangement when connected directly to the packed bed reactor, samples have been collected for the first 80 operation minutes, leading to a concentration of allyl bromide of 0.065 and an average yield of 88%. With this mixture, a Claisen rearrangement has been performed using a space time of 6 minutes, to compensate for the different thermal expansion of the solvent MEK. The Claisen rearrangement has in this case only a conversion of 62% and a selectivity of 62%. This indicates that even small amounts of allyl bromide cause significant issues, possibly in the form of catalytic activity of HBr, a possible decomposition product.

From the obtained results, it can be concluded that in order to use potassium carbonate as a base in a milli-packed bed reactor, virtually all allyl bromide needs to be reacted to obtain a good overall multistep synthesis. A high excess of K_2CO_3 is needed, so a large packed bed reactor is required. To overcome this, two beds are required, where one bed is utilized until the outlet concentration of allyl bromide remains below a specified value, while the other bed is being refilled with new, unused base, see Figure 3.9. Advantages of this method include the fact that there is no base present at all in the final product stream of the two-step synthesis, which can significantly increase the ease of recovery of the pure product. A significant drawback is that after a packed bed has been consumed, it has to be opened, emptied, cleaned and refilled with fresh base, which increases the manual labor required for the process.

There are two options to minimize the allyl bromide concentration, as it is required for the Claisen rearrangement. Firstly, allyl bromide can be used as limiting reactant instead of phenol. In this case, the packed beds should be sufficiently large to obtain a complete conversion of allyl bromide for a larger timeframe. This brings the advantage that no intermediate work-up is required after the nucleophilic substitution reaction. The downside of this is that the phenol, not allyl bromide, is often the building block in the two-step synthesis and it may already have functionalized groups from earlier synthesis steps. The other option is, while leaving phenol as limiting reactant, removing allyl bromide through a single stage micro distillation.

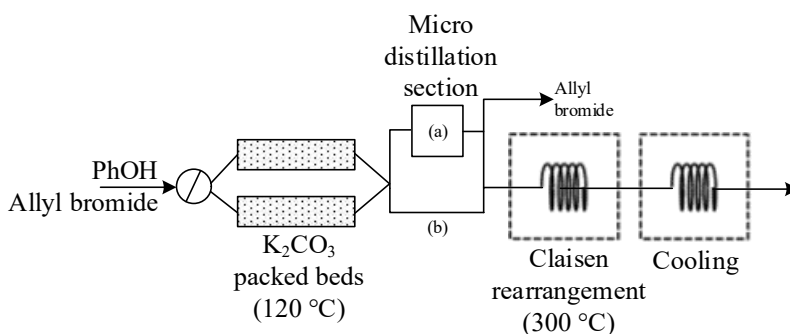


Figure 3.9. Proposed production set-up using the base K_2CO_3 in a milli-packed bed, where one bed is in use while the other bed is refilled with fresh base, while (a) and (b) represent different options

Strong base ion exchange resin

As an alternative for using K_2CO_3 as a base, the strong base ion exchange resin Amberlyst A26 has additionally been tested. This resin is sold in either uniform or non-uniform spheres, which are much more suitable for use as a packing than K_2CO_3 crystals.

Initially, a batch experiment has been performed with an excess of Amberlyst A26. From this experiment, it appeared that the nucleophilic substitution reaction proceed with significant

degree of conversion in the temperature range of 20-60 °C, meaning that the resin is basic enough to deprotonate phenol. A noteworthy result is that while the target allyl phenyl ether was gradually formed, all phenol already disappeared from the solution after 15 min. This leads to the assumption that the deprotonation of phenol is very fast and does not need to be accompanied by a simultaneous reaction with allyl bromide.

Experiments were performed with phenol and allyl bromide flowing through the Amberlyst A26 resin milli-packed bed reactor at 60 °C with a space time of 10 minutes (see Figure 3.10). The highest yield obtained was 70%, which subsequently decreased again due to consumption of the resin's functional groups. It can be noted that both substrates, phenol and allyl bromide are consumed more than allyl phenyl ether is formed, leading to the assumption that a part of the resin's functional groups is used for allyl bromide decomposition. This leads to a short operational timeframe at high yield.

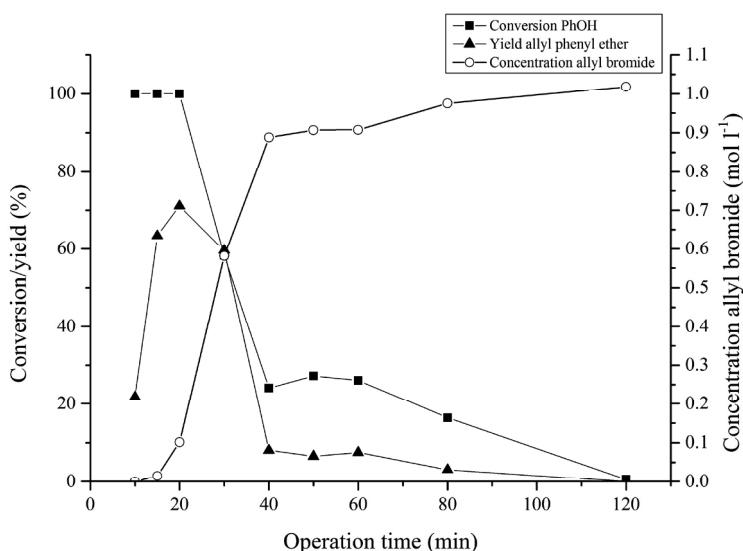


Figure 3.10. Concentration, conversion or yield of phenol, allyl bromide and allyl phenyl ether plotted against operation time using a packed bed filled with Amberlyst A26 at 60 °C at a space time of 10 minutes

In order to utilize the ion exchange resin's potential for creating an immobilized form of deprotonated phenol, phenol is first fed to the bed, after which allyl bromide is fed to the phenolate saturated bed. The predicted deprotonation and the desired reaction do occur, but are accompanied with severe tailing effects due to smaller amounts of active resin (see Figure 3.11). Additionally, phenol is leaving the reactor during the second step, which could either indicate leaching of phenol, possibly from re-protonation of phenol due to allyl bromide decomposition, or solvated phenol still being present from the previous step. In the second step

there is, again, a small window of time at which the yield is high and the allyl bromide concentration low.

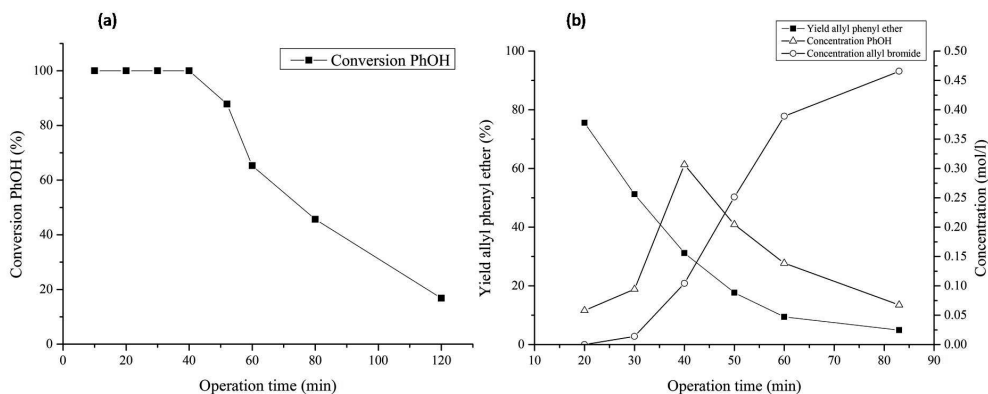


Figure 3.11. Outlet concentration, conversion or yield or conversions when using a packed bed filled with Amberlyst A26 at 60 °C with a space time of 10 minutes, (a) entering only phenol (b) subsequently entering only allyl bromide

A proposed design for a production process is given in Figure 3.12. This process utilizes the separate deprotonation of phenol and reaction with allyl bromide. As just reported, this sequence gave severe tailing effects leading to large unusable timeframes. It is, however, believed that a large increase of ion exchange resin could lead to a significantly enlarged operational timeframe in which allyl phenyl ether can be obtained without any allyl bromide present. This resulting mixture can then be immediately connected to the Claisen rearrangement, which is expected to give a high selectivity. In the proposed design, five packed beds are necessary. In the first packed bed, phenol is deprotonated. In the second one, the residual phenol is washed out, while in the third one the actual nucleophilic reaction with allyl bromide occurs. Then, the resin is regenerated with NaOH, forming NaBr as waste, and in the last bed the remaining NaOH is washed out. The concept of this design can be introduced with simulated moving bed.

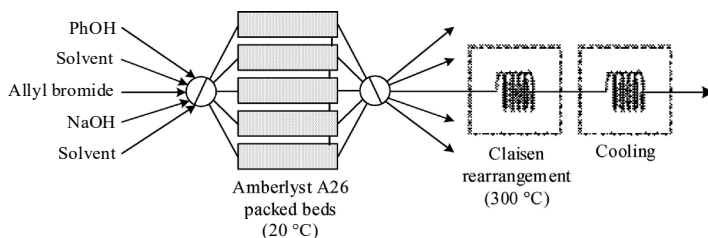


Figure 3.12. Proposed production design utilizing Amberlyst A26 as base in packed beds in series, utilizing the following sequence: phenol deprotonation, flushing, S_N2 with allyl bromide, regeneration and flushing

Compared to utilizing K_2CO_3 , the Amberlyst A26 method sacrifices compactness and simplicity. More parallel packed beds and streams are needed and larger required reactor volumes are anticipated, since the volumetric capacity of Amberlyst A26 is lower than that of K_2CO_3 (approx. 3.5 times as low). In return, the process is more streamlined, since all packed beds can remain stationary and do not need to be opened. Instead, the resin can be used numerous times due to its capability to be regenerated, while K_2CO_3 is constantly consumed permanently. Additionally, the separate introduction of phenol and allyl bromide potentially increases the efficiency in both reactants.

Alike for Amberlyst A21 fixed beds, we like to give once more a forecast to the envisaged productivity of such plants as given in Figure 3.12. The productivity target is the same which is 1 kg/d. Further details are given in the former discussion and apply here as well.

Amberlyst A26 has a capacity of $1.32 \text{ eq/kg}_{\text{H}_2\text{O-swollen resin}}$ and one equivalent can facilitate the conversion of 1 mole of phenol. We assumed a concentration of 0.5M (our base case). Thus, in one day 8.67 moles of phenol would be processed. This amounts to 6.6 kg of Amberlyst A26 resin. Yet, the experiments showed that the reaction rate will drop, if not an excess of resin is used. With some assumptions, not quoted in detail here, a resin of 7.2 kg is needed.

The Amberlyst A26 mini-fixed bed reactor used in this chapter is a tube with an inner diameter of 4.6 mm and length of 10.3 cm (volume 1.69 ml) filled with 700 mg solvent-swollen polymeric material weight. A daily exchange and regeneration of such fixed bed is assumed. Extrapolating that to 7.2 kg resin weight, the following fixed-bed tube dimensions result, as given in Figure 3.12: 5 tubes of 9.9 cm diameter and 223.8 cm length (2 used, 3 in stand-by/regeneration); single bed volume being 17.3 l. Assuming a 4 mm-diameter reaction tube for the kilo-lab processing, this would mean almost two orders of magnitude difference in diameter to the resin tube for the first case. That is not realizable in practice. Therefore, a more frequent exchange and reloading of the resin fixed beds than daily is mandatory, e.g. every hour. In this case, a single bed will be sized 3.4 cm in diameter and 77.6 cm in length, giving a bed volume of 0.7 l with a residence time of 30 min. As for the Amberlyst A21 case, it is possibly doable, however with no ideal fit. To give an idea about the true production scale and that our assumptions are not far from reality, e.g., one of our industrial pharma partners uses 1000 l resin with a mixture reaction flow rate of 2500 l/h and regeneration times of 3-4 hours [38].

3.3.5 Dilution

One of the most direct ways to improve the selectivity of the 2-step synthesis of 2-allylphenol is to simply use the inherent reaction kinetics of the occurring reactions. According to [6], the Claisen rearrangement obeys first order reaction kinetics, so the conversion after a given reaction time is not sensitive to the absolute concentration. However, the various side reactions are all

caused by components other than allyl phenyl ether, meaning that they are likely to obey second order reaction kinetics. Therefore, these reactions are expected to be relatively faster at high absolute reagent concentrations. This means that upon dilution the mixture obtained by the nucleophilic substitution reaction, the conversion will remain high while the selectivity increases.

The effect of dilution of the mixture on the selectivity of the Claisen rearrangement has been investigated. The results are shown in Figure 3.13. Note that in all experiments, the sample of the nucleophilic substitution is collected, mixed and separately used as input for the Claisen rearrangement. A clear positive effect of diluting on the selectivity can be observed. Selectivities as high as 95% have been reached at a dilution of allyl phenyl ether from 0.5 M to 0.035 M. This selectivity is equal to the selectivity in the single step Claisen rearrangement.

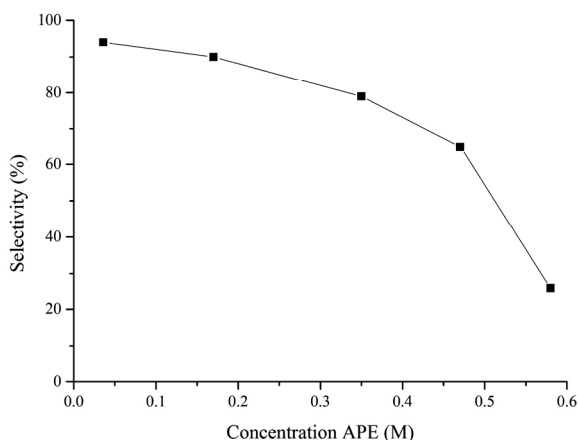


Figure 3.13. Effect of dilution of the nucleophilic substitution mixture on the Claisen rearrangement selectivity

However, operation at low concentration is not good for the nucleophilic substitution reaction, which obeys second order kinetics [39]. Therefore, the reaction rate of the nucleophilic substitution reaction greatly decreases upon dilution. This leads to the conclusion that dilution has to occur after the nucleophilic substitution reaction performed at high concentration. When this is translated to a production operation, this leads to a proposed set-up as depicted in Figure 3.14. After the nucleophilic substitution reaction, a T-junction or micromixer is introduced, depending on rate of mixing. Afterwards, a delay is needed for mixing before entering the Claisen rearrangement reaction zone.

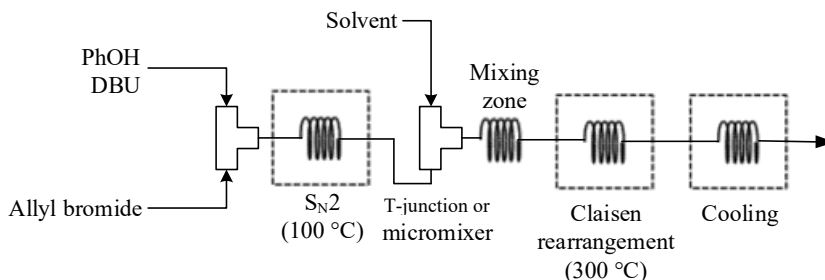


Figure 3.14. Schematic production operation for 2-allylphenol utilizing dilution for higher selectivity

The volumetric throughput of the second reaction zone depends on the degree of dilution. To maintain the same space time required for the Claisen rearrangement, a larger reactor is needed at higher degrees of dilutions. Two different approaches can be taken when designing the production set-up. From an atom efficiency point of view, the highest dilution possible would be optimal. Yet, this compromises volumetric reactor efficiency. Different reactor efficiencies are given in Figure 3.15. There is an optimum around a concentration of 0.35 M , where the selectivity of the Claisen rearrangement is 79%. By diluting further, the reactor volume increase is limiting the reactor productivity.

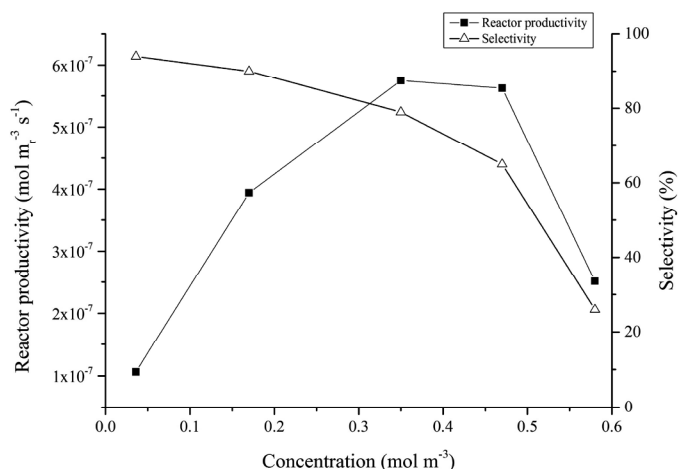


Figure 3.15. Volumetric reactor productivity plot for different Claisen rearrangement concentrations

The approach of diluting the reaction mixture after the nucleophilic substitution reaction has several advantages and drawbacks. The main advantage of this method is its relative simplicity: no intermediate unit operations other than diluting are necessary, while the yield performance of the two-step synthesis approaches the theoretically optimal value of the two reactions performed separately. One main drawback is that by diluting to low concentrations, the inherent

potential for miniaturization that microreactor technology possesses is ignored [15]. Kobayashi *et al.* reported that the Claisen rearrangement in micro-flow can even be performed solvent free [10] and consequently this is among the preferred novel process windows recommendations [14, 16]. Instead, large reactor volumes undermine the principle idea of process intensification ('shrink plants' [40]). Also, large quantities of solvent are opposed to the fundamental principles in Green Chemistry and Green Engineering. Finally, another drawback is that the product, 2-allylphenol, is not obtained in the pure form but in a diluted state, mixed with several other components like DBU, allyl bromide and phenol.

Yet, in absolute terms we dilute "just" by a factor of 6 and gain a reactor productivity increase more than 3, as it is evident from Figure 3.15. In view of the disadvantages of the packed-bed related approaches, the dilution option seems to be a straight-forward and also a promising one.

3.3.6 Orthogonality check via photo-Claisen rearrangement approach

Another proposed solution to overcome limitations due to missing orthogonality of combined nucleophilic substitution -Claisen rearrangement is that instead of applying thermal approach of the Claisen rearrangement in micro-flow, conduct a photo-Claisen rearrangement. With this way the effect of heat on DBU or allyl bromide in Claisen rearrangement step is diminished and the irradiated light selectively converts only the allyl phenyl ether. In chapter 4 we make for our photo micro-flow approach an orthogonality check and compare with the results of the thermal Claisen rearrangement path.

3.4 Conclusions

In the present work, the selectivity issue of the two-step synthesis of phenol to 2-allylphenol in flow is addressed. One major orthogonality lack is reagent compatibility based, i.e. products, reactants and auxiliary agents from the first reaction cause side reactions in the second step. Details on the exact agents involved and their impact have been revealed showing that total exclusion and not just their minimization is the dictate. The second major orthogonality problem is kinetically based. The first bimolecular reaction is best boosted under high concentrations and gives then high yields. On the contrary, the Claisen rearrangement as a unimolecular reaction obeys best selectivity at low allyl phenyl ether concentration.

Five alternative approaches to these issues have been considered, of which four are regarded as viable.

Firstly, an acid-base extraction is performed after the nucleophilic substitution reaction. However, the acid remains in the organic phase after extraction and is not compatible with the Claisen rearrangement. Therefore, this process variant had to be rejected and it was aimed at corrections. Acid removal was found to be possible via the weak base Amberlyst A21 ion

exchange resin using two parallel packed beds. A disadvantage was that not the highest possible selectivity can be achieved and an increased operation complexity is demanded.

Accordingly, the use of heterogeneous bases has been investigated since these do not interfere with the Claisen rearrangement. Both K_2CO_3 and the strong basic ion exchange resin Amberlyst A26 have shown to be suitable for this purpose. The use of K_2CO_3 gives a larger volumetric base capacity, but the base is permanently consumed, while the ion exchange resin can be re-used numerous times. Additionally, the use of K_2CO_3 requires high temperatures while the ion exchange resin performs well at room temperature.

Finally, dilution the reaction mixture of the nucleophilic substitution reaction before the Claisen rearrangement was performed, for above given reaction kinetics arguments. While this approach is the most promising one, it is in contradiction to principal concepts in process intensification, green chemistry and green engineering.

In a wider perspective, these severe orthogonality issues of a supposed-to-be-simple connection of two flow reactions underlines that the term Flow Chemistry truly denotes more than 'Chemistry in Flow'.

For all the approaches, production-targeted process schemes were given and discussed in detail. For the examples of the Amberlyst A21 and A26 resins, a rough-cut dimensioning of the respective fixed-bed resin tubes was made based on a final production of 1 kg/d Claisen product, i.e. sufficient for a pharma kilo lab. Based on daily recharging, the resin material is accordingly large in weight and volume, i.e. on the kilogram and liter-scale. As the nucleophilic substitution is performed under intensified conditions and high concentration, the reaction volume is much smaller. Therefore, initially there is a misfit of the flow reactor and flow resin packed bed which is not allowing a proper connection. This poses the demand for an hourly recharging, which then shrinks the resin bed volumes accordingly. Therefore, the whole investigation shows the general need for intensification of the downstream processes after reaction and even more when considering cascaded flow processes.

Figure 3.1 gives an overview about the advantages and drawbacks of all four possible options.

As often, it is not possible to consider one option as optimal, but rather by weighing of process features, a multi-criteria decision is to be taken.

At first glance when yield (here: 38%) is considered as critical factor, the use of heterogeneous base, K_2CO_3 , is the worst option. Dilution allows a boost in reactor productivity. Using ion exchange resins Amberlyst A21 and A26 increases the complexity in setup design, but allow reaching high yield. A26 needs higher volumes of the packed bed than A21, yet A21 has more complex process scheme. Finally, A21-operation has higher yield.

Table 3.1. Comparison of the proposed synthesis resolutions on various aspects

	Acid-base extraction and acid absorption	S _N 2: K ₂ CO ₃ packed bed	S _N 2: Amberlyst A26 packed bed	Dilution before Claisen rearrangement
Claisen rearrangement yield %	79%	38% [*]	70%	79% ^{**}
Ease of operation	-	-	+/-	++
Volumetric efficiency	+	+/-	-	--
Energy consumption	-	--	++	--
Chemicals requirement	-	+	-	--
Steady operation	+/-	--	+/-	++
Additional research needed	+	-	-	++

3.5 Acknowledgment

We kindly acknowledge the European Research Council for the Advanced Grant on "Novel Process Windows—Boosted Micro Process Technology" No 267443.

3.6 References

- [1] L. Claisen, Über Umlagerung von Phenol-allyläthern in C-Allyl-phenole, *Ber. Dtsch. Chem. Ges.* 45(1912) 3157–3166.
- [2] L. Claisen and O. Eisleb, Über die Umlagerung von Phenolallyläthern in die isomeren Allylphenole, *Liebigs Ann. Chem.* 401, (1913) 21–119.
- [3] A. M. M. Castro, Claisen Rearrangement over the Past Nine Decades, *Chem. Rev.* 104 (2004) 2939–3002.
- [4] F. W. Schuler, G.W. Murphy, The Kinetics of the Rearrangement of Vinyl Allyl Ether, *J. Am. Chem. Soc.* 72 (1950) 3155–3159.
- [5] J. Rehbein, M. Hiersemann, Claisen Rearrangement of Aliphatic Allyl Vinyl Ethers from 1912 to 2012: 100 Years of Electrophilic Catalysis, *Synthesis*, 45 (2013) 1121–1159.
- [6] M. Hiersemann, U. Nubbemeyer, *The Claisen Rearrangement. Methods and Applications*, Wiley-VCH, Weinheim, 2007.
- [7] K. Mikami, K. Akiyama, in *The Claisen Rearrangement. Methods and Applications*, (Ed.: M. Hiersemann, U. Nubbemeyer), Wiley-VCH, Weinheim, 2007, 25–44.
- [8] H. Ito, T. Taguchi, Asymmetric Claisen rearrangements, *Chem. Soc. Rev.* 28 (1999) 43–50.
- [9] For a selection of reviews which deal with micro process technologies and flow chemistry: (a) R. L. Hartman, J. P. McMullen, K. F. Jensen, Deciding Whether To Go with the Flow: Evaluating the Merits of Flow Reactors for Synthesis, *Angew. Chem. Int. Ed.* 50 (2011) 7502–7519; (b) J. Wegner, S. Ceylan, A. Kirschning, Ten key issues in modern flow chemistry, *Chem. Commun.* 47 (2011) 4583–4592; (c) T. N. Glasnov, C. O. Kappe, *J. Heterocycl. Chem.*, 2011, 48, 11–30; (d) D. Webb, T. F. Jamison, Continuous flow multi-step organic synthesis, *Chem. Sci.* 1 (2010) 675–680; (e) A. Cukalovic, J.-C. M. R. Monbaliu, C. V. Stevens, Microreactor Technology as an Efficient Tool for Multicomponent Reactions, *Top. Heterocycl. Chem.* 23 (2010) 161–198; (f) C. G. Frost, L. Mutton, Heterogeneous catalytic synthesis using microreactor technology, *Green Chem.* 12 (2010) 1687–1703; (g) R. L. Hartman, K. F. Jensen, Microchemical systems for continuous-flow synthesis, *Lab Chip.* 9 (2009) 2495–2507; (h) K. Geyer, T. Gustafsson, P. H. Seeberger, Developing Continuous-Flow Microreactors as Tools for Synthetic Chemists, *Synlett.* (2009) 2382–2391; (i) S. V. Ley, I. R. Baxendale, The Changing Face of Organic Synthesis, *Chimia*, 62 (2008) 162–168; (k) B. P. Mason, K. E. Price, J. L. Steinbacher, A. R. Bogdan, D. T. McQuade, Greener Approaches to Organic Synthesis Using Microreactor Technology, *Chem. Rev.* 107 (2007) 2300–2318; (m) K. Jaehnisch, V. Hessel, H. Loewe, M. Baerns, Chemistry in Microstructured Reactors, *Angew. Chem. Int. Ed.* 43 (2004) 406–446; (n) V. Hessel, H. Loewe, Microchemical Engineering: Components, Plant Concepts User Acceptance – Part I, *Chem. Eng. Technol.* 26 (2003) 13–24; (p) V. Hessel, H. Loewe, Microchemical Engineering: Components, Plant Concepts, User Acceptance – Part II, *Chem. Eng. Technol.* 26 (2003) 391–408; (q) K. F. Jensen, Microreaction engineering — is small better?, *Chem. Eng. Sci.* 56 (2001) 293–303; (r) K. F. Jensen, Microchemical systems: Status, challenges, and opportunities, *AIChE J.* 45 (1999) 2051–2054; (r) E. Shahbazali, V. Hessel, T. Noël, Q. Wang, Metallic nanoparticles made in flow and their catalytic

- applications in organic synthesis, *Nanotechnology Reviews*. 3 (2013) 65-86; (t) T. Noël, S. L. Bochwald, Cross-coupling in flow, *Chem. Soc. Rev.* 40 (2011) 5010-5029.
- [10] H. Kobayashi, B. Driessen, D. J. G. P. van Osch, A. Talla, S. Ookawara, T. Noel, V. Hessel, The impact of Novel Process Windows on the Claisen rearrangement, *Tetrahedron* 69 (2013) 2885-2890.
- [11] M. Sato, N. Otabe, T. Tuji, K. Matsushima, H. Kawanami, M. Chatterjee, T. Yokoyama, Y. Ikushima, T. M. Suzuki, Highly-selective and high-speed induced with subcritical water microreaction in the absence of catalyst, *Green Chem.* 11 (2009) 763-766.
- [12] L. Kong, Q. Lin, X. Lv, Y. Yang, Y. Jia, Y. Zhou, Efficient Claisen rearrangement of allyl *para*-substituted phenyl ethers using microreactors, *Green Chem.* 11 (2009) 1108-1111.
- [13] H. Maeda, S. Nashihara, H. Mukae, Y. Yoshimi, K. Mizuno, Improved efficiency and product selectivity in the photo-Claisen-type rearrangement of an aryl naphthylmethyl ether using a microreactor/flow system, *Res. Chem. Intermed.* 39 (2013) 301-310.
- [14] V. Hessel, I. Vural-Gursel, Q. Wang, T. Noel, J. Lang, Potential analysis of smart flow processing and micro process technology for fastening process development - Use of chemistry and process design as intensification fields, *Chem. Eng. Technol.* 35 (2012) 1184-1204.
- [15] V. Hessel, Novel Process Windows – Gate to Maximizing Process Intensification via Flow Chemistry, *Chem. Eng. Technol.* 32 (2009) 1655-1681.
- [16] V. Hessel, B. Cortese, M. H. J. M. de Croon, Novel process windows – Concept, proposition and evaluation methodology, and intensified superheated processing, *Chem. Eng. Sci.* 66 (2011) 1426-1448.
- [17] V. Hessel, D. Kralisch, N. Kockmann, T. Noël, Q. Wang, Novel Process Windows for Enabling, Accelerating, and Uplifting Flow Chemistry, *ChemSusChem*. 6 (2013) 746-789.
- [18] T. Razzaq, T.N. Glasnov, C.O. Kappe, Continuous-Flow Microreactor Chemistry under High-Temperature/Pressure Conditions, *Eur. J. Org. Chem.* 9 (2009) 1321-1325.
- [19] H. Kawanami, M. Sato, M. Chatterjee, N. Otabe, T. Tuji, Y. Ikushima, T. Ishizaka, T. Yokoyama, T. M. Suzuki, Highly selective non-catalytic Claisen rearrangement in a high-pressure and high-temperature water microreaction system, *Chem. Eng. J.* 167 (2011) 572-577.
- [20] M. Damm, T. N. Glasnov, C. O. Kappe, Translating high-temperature microwave chemistry to scalable continuous flow processes, *Org. Proc. Res. Dev.* 14 (2010) 215-224.
- [21] S. Ceylan, C. Friese, C. Lammel, K. Mazac, A. Kirschning, Inductive heating for organic synthesis by using functionalized magnetic nanoparticles inside microreactors, *Angew. Chem. Int. Ed.* 47 (2008) 8950-8953.
- [22] S.C. Stouten, T. Noël, Q. Wang, V. Hessel, A View Through Novel Process Windows, *Austr. J. Chem.* 66 (2013) 121-130.
- [23] V. Hessel, D. Kralisch, N. Kockmann, Novel Process Windows: Innovative Gates to Intensified and Sustainable Chemical Processes, Wiley-VCH, Weinheim, 2015

- [24] (a) S. Zelentsov, V. Hessel, E. Shahbazali, T. Noël, The Claisen rearrangement – Part 1 : mechanisms and transition states, revisited with quantum mechanical calculations and ultrashort pulse spectroscopy, *ChemBioEng Review*. 1 (2014) 230-240. (b) V. Hessel, E. Shahbazali, T. Noël, S. Zelentsov, The Claisen rearrangement - part 2: impact factor analysis of the Claisen rearrangement, in batch and in flow, *ChemBioEng Reviews*. 1 (2015) 244-261.
- [25] a) For metabolic pathways: (a) J. M. Berg, J. L. Tymoczko, L. Stryer, *Biochemistry* sixth ed. New York: W H Freeman, 2007; (b) G.F. Cahill, Fuel Metabolism in Starvation, *Annual Review of Nutrition*. 26 (2006) 1–22; (c) A. Iyer, D. P. Fairlie, J. B. Prins, B. D. Hammock, L. Brown, Inflammatory lipid mediators in adipocyte function and obesity, *Nature Reviews Endocrinology*. 6 (2010) 71–82; (d) W.G. Kaelin, C.B. Thompson, Q&A: Cancer: Clues from cell metabolism, *Nature*. 465 (2010) 562–564; (e) I.F. Kodde, J. van der Stok, R. T. Smolenski, J. W. de Jong, Metabolic and genetic regulation of cardiac energy substrate preference, *Comparative Biochemistry and Physiology - Part A: Molecular & Integrative Physiology*. 146 (2007) 26–39; b) For signaling pathways: (f) B. D. Gomperts, P. E. R. Tatham, I. M. Kamer, *Signal transduction*, Amsterdam, Elsevier Academic Press. 2004 (g) P.W. Jungham, Y. Nakano, C. Seger, Mechanisms and functions of Hedgehog signalling across the metazoan, *Nature Reviews Genetics*. 12 (2011) 393-406.
- [26] (a) C. A. Denard, J. F. Hartwig, H. Zhao, Multistep One-Pot Reactions Combining Biocatalysts and Chemical Catalysts for Asymmetric Synthesis, *ACS Catal*. 3 (2013) 2856-2864; (b) H. Gröger, W. Hummel Combining the 'two worlds' of chemocatalysis and biocatalysis towards multi-step one-pot processes in aqueous media, *Curr. Opin. Chem. Biol.* 19 (2014) 171-179; (c) H. Gröger, W. Hummel in: *Chemoenzymatic Multistep One-Pot Processes*, in: S. Riva, W. D. Fessner (Eds.), *Cascade Biocatalysis*, Wiley-VCH, Weinheim, 2014, pp. 427-456; (d) A. L. E. Larsson, B. A. Persson, J. E. Bäckvall, Enzymatische Racematspaltung von Alkoholen gekoppelt mit Ruthenium-katalysierter Racemisierung des Substrat-Alkohols, *Angew Chem*. 109 (1997) 1256-1258; (e) A. Boffi, S. Cacchi, P. Ceci, R. Cirilli, G. Fabrizi, A. Prastaro, S. Niembro, A. Shafir, A. Vallribera, The Heck Reaction of Allylic Alcohols Catalyzed by Palladium Nanoparticles in Water: Chemoenzymatic Synthesis of (R)-(-)-Rhododendrol, *ChemCatChem*, 3 (2010) 347-353; (f) D. A. Denard, H. Huang, M. J. Bartlett, L. Lu, Y. Tan, H. Zhao, J. F. Hartwig, Cooperative Tandem Catalysis by an Organometallic Complex and a Metalloenzyme, *Angew Chem. Int. Ed.* 53 (2014) 465-469; (g) H. Gröger, Hydroxy Functionalization of Non-Activated C-H and C=C Bonds: New Perspectives for the Synthesis of Alcohols through Biocatalytic Processes, *Angew. Chem. Int. Ed.* 53 (2014) 3067-3069; (h) M. Heidlindemann, G. Rulli, A. Berkessel, W. Hummel, H. Gröger, Combination of Asymmetric Organo- and Biocatalytic Reactions in Organic Media Using Immobilized Catalysts in Different Compartments, *ACS Catal*. 4 (2014) 1099-1103; (i) E. Burda, W. Hummel, H. Gröger, Modular Chemoenzymatic One-Pot Syntheses in Aqueous Media: Combination of a Palladium-Catalyzed Cross-Coupling with an Asymmetric Biotransformation, *Angew. Chem. Int. Ed.* 47 (2008) 9551-9554.
- [27] J. I. Yoshida, *Flash Chemistry: Fast Organic Synthesis in Microsystems*, Wiley-Blackwell, 2008.
- [28] J. I. Yoshida, A. Nagaki, T. Yamada, *Flash Chemistry: Fast Chemical Synthesis by Using Microreactors*, *Chemistry - A European Journal*, 14 (2008) 7450-7459.

- [29] A. Nagaki, K. Imai, H. Kim, J. I. Yoshida, Flash synthesis of TAC-101 and its analogues from 1,3,5-tribromobenzene using integrated flow microreactor systems, *RSC Adv.* 1 (2011) 758-760.
- [30] A. Nagaki, D. Ichinari, J.-i. Yoshida, Three-component coupling based on flash chemistry. Carbolithiation of benzyne with functionalized aryllithiums followed by reactions with electrophiles, *J. Am. Chem. Soc.* 136 (2014) 12245-12248.
- [31] C.F. Carter, H. Lange, D. Sakai, I.R. Baxendale, S.V. Ley, Diastereoselective Chain-Elongation reactions using microreactors for applications in complex molecule assembly, *Chemistry - European J.* 17 (2011) 3398-3405.
- [32] H. Lange, C. F. Carter, M. D. Hopkin, A. Burke, J. G. Goode, I. R. Baxendale, S. V. Ley, A breakthrough method for the accurate addition of reagents in multi-step segmented flow processing, *Chem. Sci.* 2 (2011) 765-769.
- [33] C. J. Smith, N. Nikbin, S. V. Ley, H. Lange, I. R. Baxendale, A fully automated, multistep flow synthesis of 5-amino-4-cyano-1,2,3-triazoles, *Org. Biomol. Chem.* 9 (2011) 1938-1947.
- [34] J.C. Pastre, D.L. Browne, S.V. Ley, Flow chemistry syntheses of natural products, *Chem. Soc. Rev.* 42 (2013) 8849-8869
- [35] W. N. White, D. Gwynn, R. Schlitt, C. Girard, and W. Fife, The *ortho*-Claisen Rearrangement. I. The effect of substituents on the rearrangement of allyl *p*-*x*-phenyl ethers, *J. Am. Chem. Soc.* 80, (1958) 3271-3277.
- [36] C. H. Bamford, C. F. H. Tipper, *Decomposition and isomerization of organic compounds*, Elsevier Publishing Company, Amsterdam, 1972.
- [37] W. Ehrfeld, V. Hessel, H. Löwe, *Microreactors: New Technology for Modern Chemistry*, Wiley-VCH, Weinheim, 2000.
- [38] Personal information from industry partner who prefers not to be named.
- [39] R. Bruckner, *Advanced Organic Chemistry: Reaction Mechanisms*, Harcourt/Academic Press, San Diego, 2002.
- [40] (a) J. R. Burns, J. N. Jamil, C. Ramshaw, *Chem. Eng. Sci.* 55 (2000) 2401-2415; (b) D. Reay, C. Ramshaw, A. Harvey, *Process Intensification – Engineering for Efficiency, Sustainability and Flexibility* Elsevier, Oxford, 2008;

3.7 Supplementary Material

The micro-flow set up used in this chapter is presented in Figure S3.1

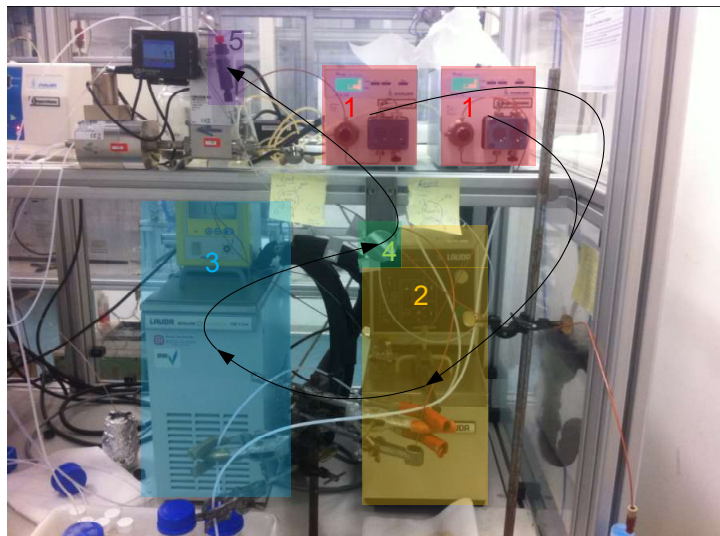


Figure S3.1. Micro-flow set-up. 1: HPLC pumps, 2: heating bath, 3: cooling bath, 4: sampling valve, 5: back pressure regulator

S1. General reagent information

The supplier of used chemicals and additional information is given in Table S3.1. All chemicals are used as received, except for Amberlyst A21 and Amberlyst A26. These procedures are described earlier in this section.

Table S3.1: Supplier and additional details of used chemicals

Chemical	Supplier	Additional information
2-Allyl phenol	Sigma-Aldrich	98%
Acetonitrile	VWR	HiPerSolv Chromanorm
Aliquat 336	Sigma-Aldrich	-
Allyl Bromide	Acros	Stabilized, 99%
Allyl phenyl ether	Sigma-Aldrich	99%
Amberlyst A21	Sigma-Aldrich	Free base
Amberlyst A26	Sigma-Aldrich	OH-form
Benzonitrile	Merck	For synthesis
DBU (1,8-diazabicycloundec-7-ene)	Merck	For synthesis
Formic acid	Merck	For synthesis
Hydrochloric acid	Sigma-Aldrich	ACS reagent, 37%
Methyl ethyl ketone (MEK)	VWR	AnalaR Normapur
n-Butanol	Sigma-Aldrich	Chromasolv Plus
Potassium carbonate (K ₂ CO ₃)	Sigma-Aldrich	Food grade
Sodium hydroxide	Sigma-Aldrich	98.5%, microprills

S2. Analytical procedures for Claisen rearrangement and nucleophilic substitution experiment

A sample is taken with the sample loop after 4 space times to ensure steady state operation. The 100 μl of sample taken is diluted in 1400 μl acetonitrile. Subsequently, 100 μl of this mixture is taken and diluted in 1400 μl acetonitrile, to yield a target analyte concentration of approx. 2 mM for HPLC analysis.

S3.1. Batch nucleophilic substitution reaction

In a batchwise nucleophilic substitution reaction to test different solvents, phenol (0.47 g, 5 mmol) and benzonitrile (0.103 g, 1 mmol) are added to the used solvent. DBU (1.52 g, 10 mmol) is slowly added at 0 °C. The mixture is diluted with the solvent until 10 ml. At the start of the reaction, allyl bromide (1.12 g, 10 mmol) is slowly added at 0 °C. This mixture is then heated stepwise to 50 °C in 2 hours and left at 50 °C for 1 hour with a reflux cooler.

In a batchwise experiment to test different bases, phenol (0.24 g, 2.5 mmol) and benzonitrile (0.05 g, 0.5 mmol) are diluted in the solvent MEK until 5 ml. To this mixture, the base to be tested (5 mmol) is added. At the start of the experiment, allyl bromide (0.60 g, 5 mmol) is added, after which the mixture is heated to 70 °C in a sealed stirred vessel. The mixture is left for 4.5 hours at 70 °C and cooled to note the visual results.

S3.2. Amberlyst A26 characterization

The density of the Amberlyst A26 beads without void space has been determined by adding a known mass (1.98 g) of MEK-swollen resin to pure solvent MEK (5 ml) in a measuring cylinder and noting the read volume before and after adding the resin. This leads to an estimated density of 1040 kg m^{-3} .

The capacity of Amberlyst A26 has been measured by adding an excess of NaCl (3 g) to a known amount of water-swollen resin (3 g) in water (25 ml). The mixture has been stirred for 30 minutes. The resin exchanges OH^- by Cl^- , forming NaOH in the aqueous solution. The mixture is filtered and the residue is washed with water (20 ml). The amount of formed NaOH has been determined by means of titration with a 0.2 M aqueous HCl solution, using methyl-red as indicator. This leads to an estimated capacity of 1.32 equivalents per kg of H_2O -swollen resin.

S3.3. Analysis for batch reactions

Samples collected from the various experiments are analyzed using the HPLC internal standard method, with benzonitrile as internal standard in a 1:5 molar ratio with the limiting reactant. A Shimadzu Prominence HPLC system has been used with a GraceSmart RP 18 5u column (150 mm), using a flow of 0.75 ml/min H_2O with 1 vol.% formic acid and 0.25 ml/min acetonitrile. A Shimadzu SPD-M20A diode array detector has been used at 215 nm with a bandwidth of 4 nm. All measured samples had an approximate analyte concentration of 2 mM with an injection volume of 1 μl .

For pH measurement of an aqueous mixture, a 4-color pH indicator strip has been used. For acidity measurements of organic mixtures, the 4-color indicator strip was first wetted with H_2O before measurement of the mixture.

S4. Solvent selection

The reason that acid needs to be removed after the extraction is the interaction of the acid with the polar protic solvent, n-butanol. Experiments have indicated that when performing the same extraction with an apolar aprotic organic solvent like toluene, all DBU migrates to the aqueous phase and the resulting organic phase is pH-neutral. Therefore, if n-butanol is switched for such a solvent, the acid-base extraction would fully reach its target and the Claisen rearrangement could be performed directly after the extraction.

In order to select which solvent is suitable for this purpose, a small list of possible alternatives has been made (Table S3.2). These solvents follow the criteria that it needs to be aprotic and immiscible with water for the extraction. From these solvents, a selection is made based on a number of factors.

Table S3.2: list of potential solvents for two-step synthesis, of which all are aprotic and immiscible with water, sorted by polarity; relative density equals density at given conditions divided by normal liquid density

Solvent	Polarity[S1] (water=100, n-butanol=60)	Relative density (300 °C, 69 bar)
Toluene	9.9	0.60
Diethyl ether	11.7	0.20
Ethyl acetate	23	0.29
Isobutyl acetate	24.1	0.54
Chloroform	25.9	0.16
Methyl isobutyl ketone (MIBK)	27	0.60
Cyclohexanone	28	0.67
Dichloromethane (DCM)	30.9	0.11
1,2-Dichloroethane	32.7	0.35
Methyl ethyl ketone (MEK)	32.7	0.30

Based on several criteria, every solvent in this selection has been examined for potential suitability. Firstly, since the thermal expansion at the conditions of the Claisen rearrangement heavily influences the actual reaction time, a high relative density at the given conditions is favorable for the Claisen rearrangement. Furthermore, as described in section 2.1.1, a more polar solvent is advantageous for the Claisen rearrangement reaction rate. However, a more apolar solvent increases the reaction rate of the nucleophilic substitution. Therefore, a single solvent will always show a compromise between boosting the rate of both reactions.

One of the reasons to perform the two-step synthesis in micro-flow is that the reaction can be performed more green, with potentially high intensification, low energy consumptions and absence of catalyst. However, chlorinated solvents are generally not a preferred green solvent choice due to their toxic nature [S1]. Therefore, in this selection, chlorinated solvents (chloroform, DCM, 1,2-dichloroethane) have been omitted, since their use compromises the potentially green character of the synthesis.

Additionally, the selected solvent should be stable at the harsh conditions used in the synthesis, which includes the use of a strong base and high pressure and temperature. Esters (ethyl acetate, isobutyl acetate) are likely [S2] to participate in thermal decomposition, transesterification with phenol or hydrolysis in the presence of water at these conditions, and are therefore not deemed suitable.

Finally, it is important that all reactants remain dissolved during the reaction, since precipitation in a microchannel can cause clogging, which hinders the operation of the reaction. Since ionic species are involved in the nucleophilic substitution reaction, a highly apolar solvent is likely to be unable to dissolve these species. To investigate which solvents show this behavior, the reaction has been performed in batch in various solvents. From these experiments, it appeared that the solvents toluene, diethyl ether and methyl isobutyl ketone show precipitation during the reaction, meaning that they are too apolar, while methyl ethyl ketone (MEK) and cyclohexanone remained transparent.

Maintaining these criteria, the only solvents deemed suitable from the selection are methyl ethyl ketone (MEK) and cyclohexanone. To investigate the reactivity in the new solvent, the nucleophilic substitution reaction has been conducted in flow in the same manner as in the original reaction, but now with MEK as solvent. However, even though theoretically, this solvent leads to a higher reaction rate, the yield of allyl phenyl ether obtained is merely 40%, as opposed to 80% when using n-butanol. This yield is independent on space time from 1-8 minutes.

In order to investigate this unexpected behavior, the nucleophilic substitution has been performed at a fixed space time of 4 minutes, while varying the temperature from 20 to 120 °C. The obtained results are shown in Figure S3.2. It appears that the obtained yield increases with increasing temperature, but this rise staggers when the outlet concentration of allyl bromide becomes low. From this, it can be deduced that the final obtained yield is in fact not limited by the reaction rate of the nucleophilic substitution reaction, but by the concentration of allyl bromide. The nucleophilic substitution reaction obeys a second order rate law, so the rate will rapidly become low when the concentration of allyl bromide drops. Since allyl bromide is added in 2 equivalents to 1 eq phenol, it is concluded that allyl bromide acts as a reagent in a reaction besides the nucleophilic substitution reaction. Even though the product(s) of this reaction have not been detected in HPLC, this reaction is expected to be the base-induced decomposition of allyl bromide. This reaction may yield allene, HBr, propene and benzene [S3]. The fact that the final yield slightly drops at even higher temperatures, indicates that the decomposition reaction is relatively favored slightly more at higher temperatures.

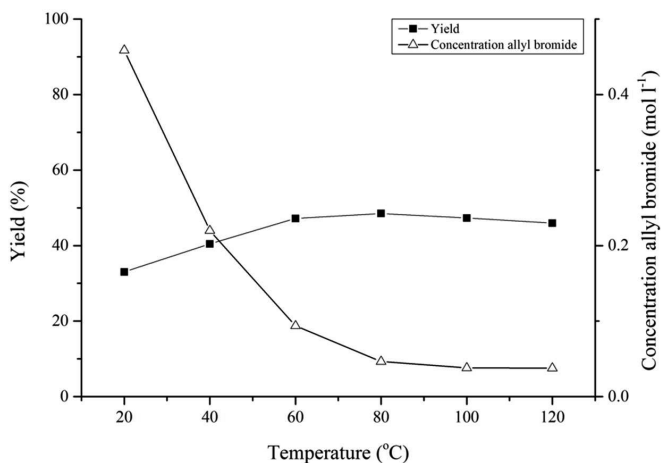


Figure S3.2. Yield and outlet concentration of allyl bromide of S_N2 reaction in flow with MEK as solvent, as a function of temperature, at a space time of 4 minutes

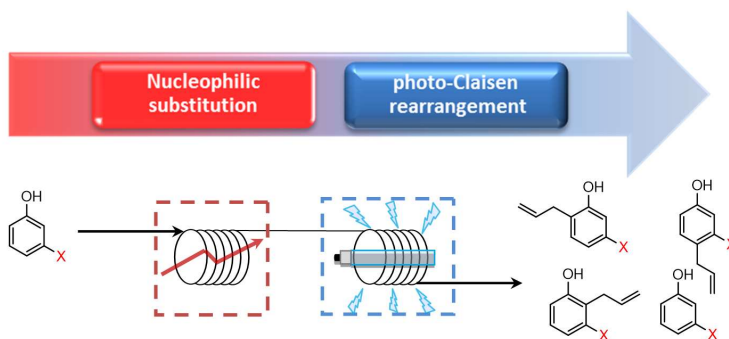
It is observed that using the polar aprotic solvent MEK results in a significantly lower yield of allyl phenyl ether than using n-butanol, which is already reached after 1 minute of space time. This leads to the conclusion that while the new solvent may indeed increase the rate of the nucleophilic substitution reaction, it increases the rate of the decomposition reaction even more, leading to higher allyl bromide consumption. The higher allyl bromide consumption, paired with the second order reaction kinetics of the nucleophilic substitution, leads to a lower final yield of allyl phenyl ether when the allyl bromide is consumed. Similar results have been obtained using cyclohexanone as solvent. In order to perform the two-step synthesis with intermediate extraction successfully, the yield of the nucleophilic substitution reaction in the new solvent first needs to be improved.

S5. References

- [S1] I. M. Smallwood, *Handbook of organic solvent properties*, Arnold, London, Sydney, Auckland, 1996.
- [S2] M. B. Smith and J. March, *March's Advanced Organic Chemistry: Reactions, Mechanisms and Structure*, John Wiley & Sons, Inc., New York, 2007.
- [S3] C. H. Bamford and C. F. H. Tipper, *Decomposition and Isomerization of Organic Compounds*, Elsevier Publishing Company, Amsterdam, 1972.

CHAPTER 4

Photo-Claisen Rearrangement of Allyl Phenyl Ether in Micro-Flow: Influence of Phenyl Core Substituents and Vision on Orthogonality



This chapter is based on:

Shahbazali, E., Noël, T., Hessel, V., *J. Flow Chem.* 2016, 6(3), 252–259

Abstract

We converted diverse commercial meta-substituted phenols to the allyl-substituted precursors via nucleophilic substitution using batch technology to allow processing these in micro-flow by means of the photo-Claisen rearrangement. The latter process is investigated on its own, as reported in detail below, and also prepares the ground for a fully continuous two-step micro-flow synthesis, as outlined in chapter 3. It is known that batch processing of electronically deactivated phenols (e.g. bearing a cyano or nitro group) have a several orders of magnitude lower reactivity than their parental counterparts [1]. Therefore, we here explore if the high quantum yield of micro-flow, yet at a very short residence time, is sufficient to activate the deactivated molecules. In addition, the realization of a true orthogonal two-step flow synthesis can open the door to a large synthetic scope of our approach and possibly overcome limitations due to missing orthogonality of our previously reported thermal approach of combined nucleophilic substitution-Claisen rearrangement in micro-flow. Consequently, we make for our photo micro-flow approach an orthogonality check, as previously reported for the thermal approach, and compare both.

To get a broader picture, we have investigated some major parametric sensitivities such as the irradiation intensity, the choice of solvent, the reactant concentration, and most notably the influence of the substitution pattern. The irradiation intensity was varied by increasing the distance between a lamp and the micro-flow capillary. In addition, the normal photo-Claisen micro-flow process (at room temperature) is compared to a high-temperature photo-Claisen micro-flow process, to check the potential of such novel process window [2]. This is difficult to realize in batch, as the combination of strong UV irradiation and high temperature causes a high hazard potential. Yet, under micro-flow this can be safely handled.

4.1 Introduction

The Claisen rearrangement, which is the [3,3]-sigmatropic rearrangement of allyl phenyl ethers, makes a valuable synthetic transformation for organic chemistry [3]–[5]. The thermal Claisen rearrangement requires high temperatures in order to result in sufficient conversion.

In the last decade, microreactor technology has revealed a promising potential for many synthetic applications and has even been applied on an industrial scale [6], [7]. Microreactor technology has been proven to be beneficial for the Claisen rearrangement [8]–[11].

Previously, we reported on the combination of a nucleophilic substitution to the thermal-Claisen rearrangement in micro-flow, i.e. a continuous micro-flow two-step synthesis [12] (see also chapter 3). In the first step thereof, phenol and allyl bromide yield phenyl allyl ether which is then in a second step and directly converted by the thermal Claisen rearrangement. Targeting synthetic scope, the motivation was to show that in this way many substituted phenyl allyl ethers may be derived from respectively substituted phenols. Yet, as reported, just combining the individual micro-flow syntheses was by no means sufficient, which is surprising. Rather, both syntheses lacked considerably in orthogonality. This was partly due to the remaining base DBU, which acts as catalyst for the allyl group substitution, and caused cleavage of the Claisen products to the phenol starting material. Unexpected was that the allyl bromide had a similar strong effect. At the high temperatures used in the thermal Claisen rearrangement, which are typically set even higher in micro-flow [13], [14], the allyl bromide decomposes to give propene and HBr. HBr can lead to the same decomposition rate of the Claisen product as the acid does. As a consequence, we have discussed several continuous acid or base removal techniques based on extraction and adsorption. We discussed all the advantages and disadvantages. Finally, the preference was given by using Amberlyst A21 and A26 ion exchanger in a packed bed configuration, see chapter 3, section 3.3.3.

Moreover, microreactors have received a lot of attention in photochemical applications since they are capable of improving some issues related to the batch photochemistry [15], [16]. In essence, the narrowness of the microreactor channels enables a better exposure of the reaction mixture to the irradiated light and avoids the undesired warming up of the reaction solutions. A larger amount of reactant molecules is excited under a more defined experimental protocol and, therefore, the reaction is expedited.

The photo-Claisen rearrangement can be connected to a nucleophilic substitution, which introduces the allyl group into various phenol derivatives. Here, the main advantage is the possibility to generate *para*-substituted products besides the *ortho*-substitution pattern and also, parental phenol (for details on mechanism of photo-Claisen rearrangement, one is referred to [17]–[20]). Yet, it should be noted as well that this generates an extra separation issue. In

addition, it might be anticipated that the orthogonal fit between the two reaction steps might be better, as the photo-Claisen reaction is performed at normal temperature so that (at least) the allyl bromide decomposition should be reduced to a large extent or becomes even absent.

With such motivation on an enlarged synthetic scope and improved orthogonality, we aim to develop a micro-flow protocol for the photo-Claisen rearrangement.

4.2 Results and discussion

4.2.1 Parametric sensitivities of the photo-Claisen rearrangement of allyl phenyl ether in micro-flow

It is known from literature that the photo-Claisen rearrangement of allyl phenyl ether works well under given conditions in batch. Therefore, we started our parametric investigation with the unsubstituted precursor (also because this molecule is commercially available, whereas we needed to synthesize the substituted molecules before the photo chemical experiments).

Flow process development - isomer distribution/phenol content and conversion/yield

In a typical batch experiment documented in literature, the relative product distribution after the photoreaction of allyl phenyl ether is reported as (mole %) 21% (*ortho*, 2-), 31% (*para*, 4-), and 48% (phenol) in hexane and 42% (*ortho*, 2-), 42% (*para*, 4-), and 16% (phenol) in MeOH (Irradiation time= 4h) [17]. Irradiation was conducted to about 30% conversion [17][18]. In an own batch experiment, after 5hr irradiation in 1-butanol (10 ml solution), no product was detected, while in photo micro-flow we achieved (mole %) 30% (*ortho*), 30% (*para*), and 21% (phenol) and therefore, could reach similar performance in batch mentioned above.

5-70 h irradiation time is quite common for batch-type photo Claisen experiments [18]. Therefore, in our batch experiments we applied 5 h, while the photo micro-flow process was most often finished in less than 8 min. This is due to the much smaller dimensions of the capillary providing a high transmittance throughout the reaction volume and thus ensuring high light efficiency. It is also beneficial to give a comparison of results for the different lamp power (watt). Three more batch experiments, with different lamp power, found in literature have been listed in Table 4.1. According to the results, it can be concluded that lamp with a lower power gives a lower conversion. For instance, the experiment with 10 W-low pressure mercury lamp gives 31.4% conversion in 24 hr. On the other hand, the experiment with 15 W-low pressure mercury lamp gives higher conversion, 74% in 32 hrs. Although in the second experiment the reaction time increases by 25%, the conversion rises 2.3 times. It should be mentioned that the lamp power is not the only parameter which controls the conversion. Yet it is one of the key parameters. Besides the lamp power, one should consider the effect of other parameter such as concentration, volume of the solution, and solvent. In this research we aimed to use the low

power lamp and instead improving the other influential parameters. Also, Sugimoto *et al.* [21] has thoroughly studied the application of the Barton reaction in microreactors and the effect of different light sources. These authors showed that in their case, a UV-LED lamp (1.7 W) is more efficient than a 300 W Hg lamp.

Table 4.1. Comparison of the conversion of photo-Claisen rearrangement of allyl phenyl ether for different light source wattage in alcohol as solvent in batch system [18].

UV lamp	Time (hr)	Solvent	Concentration (M)	Conversion (%)	Reference
10 W-low pressure-mercury	24	2-Propanol	0.05	31.4	[19]
15 W-low pressure-mercury	32	2-Propanol	0.03	74	[20]
450-medium pressure-mercury	No time mentioned	Methanol	0.01	10-20	[1]
10 W-low pressure-amalgam	5	1-Butanol	0.01	0	Our own experiment

The photo micro-flow synthesis avoids the formation of migration of the double bond of the allyl group to give E/Z 2-(prop-1-enyl)phenols which was reported for the corresponding thermal (high-T) micro-flow synthesis of allyl phenyl ether, especially at temperatures above 300°C [14]. These substances can undergo ring closure to give 3-dihydro-2-methylbenzo[b]furan and 2-methylbenzo[b]furan as further byproducts of the thermal process which we did not observe. The latter effect was remarkably dependent on the solvent in the thermal process, with alkanolic solvents giving the cleanest process.

Solvent effect

One of the key parameters both for the thermal and photo-Claisen rearrangement is the solvent used. Proper selection of a solvent is a key issue. Basic needs are to ensure that all reactants are completely soluble (which is particularly relevant for micro-flow synthesis), the solvent is transparent to the desired wavelength, and the solvent should not suppress the photochemical process. We have already shown that for the thermal Claisen micro-flow process variant the performance varies largely with the solvent chosen. Even in the class of alkanol, considerable differences were found for different alkyl chain lengths, yet also even when comparing 1- and 2-alkanol isomers.

Since Hughes *et al.* [22] state that increasing polarity causes an increase in reaction rate for the photo-Claisen process, we would like to continue this investigation with alkanols as solvents of

the choice. The explanation for the acceleration is that the transition state is more polar than the initial reagent so that it has more stabilization by interaction with the solvents. As a consequence ΔG^\ddagger decreases and the reaction rate increases. Besides polarity, hydrogen bond formation is responsible for the acceleration of the Claisen rearrangement [23][24][25]. Also several other references report that polar solvents accelerate the Claisen rearrangement [26]–[28].

It is further known that the primary products of the photo-Claisen rearrangement in protic (alcoholic) solvents are 2- and 4-allyl phenol, in an almost comparable ratio; while 3-allyl phenol is formed in a very small amount [29]. So, sufficient access to the desired *para*-product (4-allyl phenol) is given.

Table 4.2 shows that there is hardly any difference in the ultraviolet transmission (at various relevant wavelengths) and cut-off wavelengths of the majorly used alcohols. They have similar optical properties as given for the non-polar heptane solvent [30].

Table 4.2. Ultraviolet transmission at diverse wavelengths and cut-off wavelengths of the majorly used alcohols and compared to the non-polar solvent heptane [30].

Solvent	%T	%T	%T	T=10%
	254 nm	313 nm	366 nm	at λ (nm)
Heptane	100	100	100	197
Methanol	100	100	100	205
Ethanol	98	100	100	205
2-propanol	98	100	100	205

Figure 4.1 compares the yield of the photo-flow product *ortho*-allyl phenol in methanol, 2-propanol, 1-butanol, and heptane. Later, we will comment on the formation of *para*-allyl phenol and phenol, yet here the focus is on the *ortho*-product which is formed as the largest fraction. It is evident that the alcohols as polar protic solvents enhance the conversion as compared to the non-polar heptane benchmark. This is in line with the observation that 1',1'-dimethylallyl phenyl ether has a quantum yield of disappearance of 0.75 in *i*-propanol, whereas this value is 0.55 for cyclohexane [31]. Also, the conversion obtained by irradiation of diphenyl ether in methanol is 67%; however, the conversion drops significantly to 18% in *n*-hexane [34]. This effect has been justified in terms of stabilization of the intermediate cyclohexadienones by hydrogen bonding. Another possibility could be that the C–O cleavage in the excited singlet state is assisted by the presence of protic solvents [32].

1-butanol gives the best performance, followed by 2-propanol and methanol. The hydrogen bonding and polarity relate to the pK_a value [33], [34]. Yet, the reaction sequence does not follow the line of pK_a values: pK_a (methanol): 15.3, pK_a (2-propanol): 17.1, pK_a (1-butanol): 16.1, for comparison pK_a (water): 15.7. Thus, the result is depending on other parameters as well.

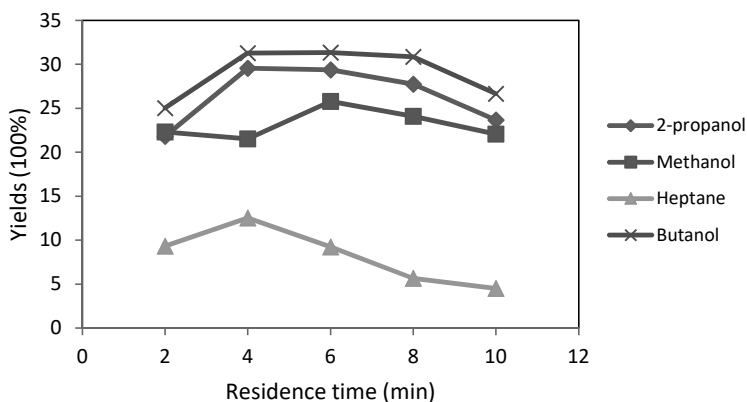


Figure 4.1. Photo-Claisen rearrangement of allyl phenyl ether. Yield of *ortho*-allyl phenol for some relevant alkanolic solvents and heptane (for comparison) versus residence time (concentration of allyl phenyl ether: 0.01 M), at $T = 295$ K.

Moreover, it can be clearly seen that 2 min are not long enough to ensure best yield under the given conditions. Rather from 4 min onwards a stable yield is achieved. Irradiation above 8 min leads to a decrease in yield, probably by decomposition of the Claisen product into phenol. This happens already on a shorter time-scale for the heptane solvent. It was therefore concluded to the performance the most of the experiments reported here at the longest residence time (8 min) which allowed for high yields. In this sense, it was aimed to ensure that also the less reactive substrates can show some yield under photo-flow irradiation.

Concentration effect

The concentration of reactants can have an impact on kinetics and overall productivity. In a photo process, an increase of the concentration of absorbing reactants decreases the radiation intensity. Also, photo-irradiation hardly penetrates deeper than 1 mm in a flask, and provides a major argument to use micro-flow conditions throughout the capillary (100–1000 μm). This ensures that irradiation is present and can activate the photoreaction in micro-flow [35]. Due to this, micro-flow is able to operate at higher concentrations than in batch and therefore has potential to achieve high space-time yields.

The radiation transport is a complicated process which is affected by the source of light, as well as the configuration of the photoreactor [36]. The Bouguer–Lambert–Beer equation (see Equation 4.1) can be applied to single-phase (homogeneous) photochemical reactions.

$$T = \frac{I}{I_0} = 10^{-\epsilon lc} \quad (4.1)$$

where, ε is the molar extinction coefficient, c is the concentration of the absorbing species, and l is the optical path length of the light.

In order to achieve maximum effectiveness of the photons and therefore higher productivity, the distance between the lamp and capillary reactor was decreased as much as possible by winding the capillary around the cylindrical UV lamp. In this way, it was aimed to minimize the absorption of the radiation when passing through the air separating the lamp and microcapillary. Major contributions in lowering UV transmittance through air are caused by the presence of water vapor, global warming gases, and dust particles [37].

Figure 4.2 shows the yield obtained for various concentrations of allyl phenyl ether, ranging from 0.001 to 0.4 M.

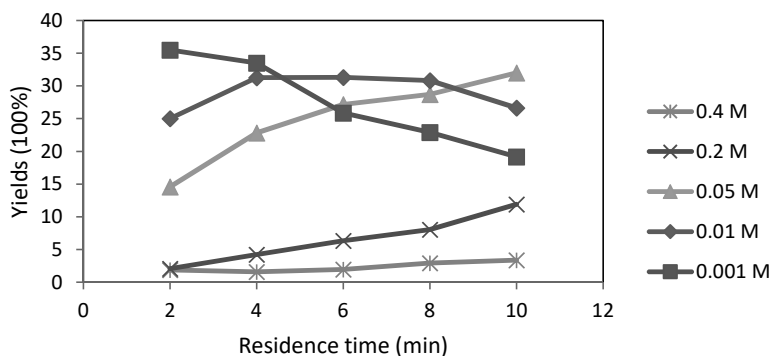


Figure 4.2. Photo-Claisen rearrangement of allyl phenyl ether. Yield of *ortho*-allyl phenol versus residence time for different concentration of allyl phenyl ether.

It is evident that up to a concentration of 0.05 M good performance is achieved. However, photoreaction at the lowest concentration is finished already after 2 min and longer residence times show reduced yield by photodegradation of the product. Operation at highest concentration (0.2 and 0.4 M) needs higher residence times and is incomplete in the time frame observed here.

The value of 0.05 M is nearby what is commonly used for preparative photolysis. For example, 0.0625 M (500 mg of substrate in 56 mL of ethanol) meta-methoxy phenyl allyl ether was converted in a preparative manner [38]. To ensure the light transmittance, petri dishes were used as flat reaction cells. Typical analytical photoreaction experiments are performed at lower concentrations, e.g. at 0.0001 M in water for the above given case [38]. Galindo reports use of concentrations from 0.01 M to 0.4 M in his photochemistry overview (Table A.1. in [18]).

Distance from light source

The lamp used in the experiments reported here has a power of 10 W (providing a UV intensity of 21-24 microwatt/cm²). This is at the lower edge of lamps used in literature for UV photochemistry. Galindo reports in his overview the use of 6 W-lp-quartz to 450 W-mp lamps (lp: low pressure; mp: medium pressure) [18].

Even though, it was observed above that, for the given low distance between reaction capillary and UV lamp, the energy of the UV light might be so high that it may cause degradation of the starting compound. This effect was noted at a long residence time. Therefore, an experiment was performed with increased distance between the capillary and the light source (see Figure 4.3) and thus allowing absorption of the UV light by air. 2 cm distance was given throughout the entire lamp perimeter.

The yield performance with 0 and 2 cm distance are very different, respectively. In case of tight contact, a decline of yield with residence time is observed for the reason given, whereas the reaction with capillary and lamp in a distance shows increasing yields. It is worth mentioning that the surface temperature of this uv lamp was measured after 30 minutes being in use and it did not exceed 35 °C. Therefore, adjusting the distance between capillary reactor and light source is a means to fine-tune the photo process.

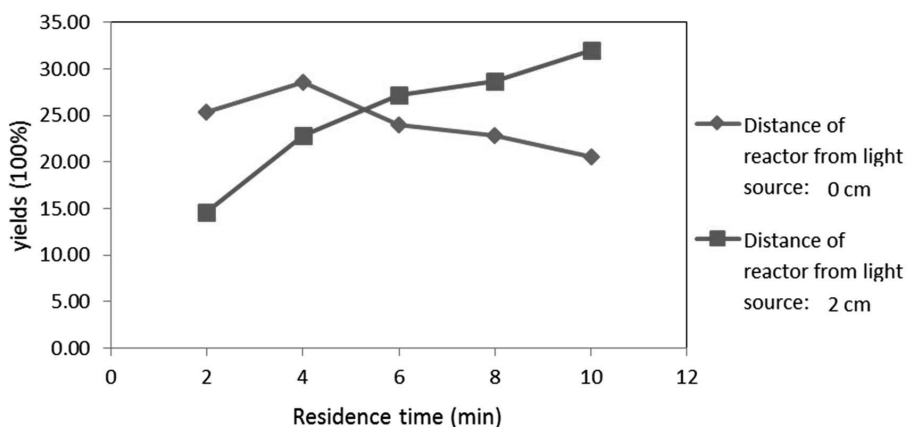


Figure 4.3. Photo-Claisen rearrangement of allyl phenyl ether. Yield of *ortho*-allyl phenol for 0.05 M allyl phenyl ether for two different distances of the reaction capillary from light source, being 0 cm and 2 cm.

4.2.2 Orthogonality – Process simplification when connecting to a prior nucleophilic substitution

According to the results reported in chapter 3, when the thermal-Claisen rearrangement was connected to the nucleophilic substitution reaction in flow, the presence of allyl bromide and the base DBU used, were negatively affecting the final product distributions and lowering considerably the product yield. This asks for continuous-flow separation which make the process complex, as reported earlier [12]. We aim here correspondingly for process simplification. Therefore, as described in the introduction, one of the goals of this work is to check the orthogonality when the photo-Claisen rearrangement is coupled with the nucleophilic substitution reaction. In order to study this, photo-Claisen rearrangement of allyl phenyl ether has been performed by manually adding allyl bromide and DBU. The results are compared with the photo-Claisen rearrangement of allyl phenyl ether without any addition.

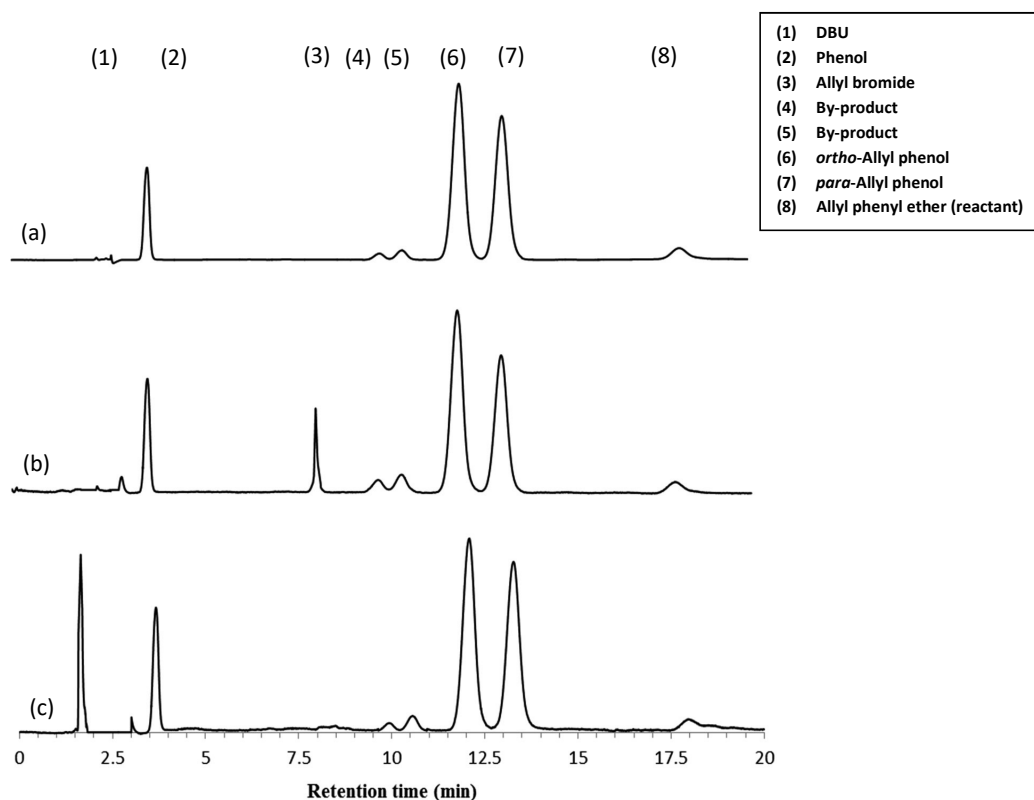


Figure 4.4. HPLC chromatograms of photo-Claisen rearrangement with 0.01 M allyl phenyl ether; (a) no additions (b) with 1 eq. allyl bromide (c) with 1 eq. DBU (residence time=6 min).

Figure 4.4 shows the resulting HPLC chromatograms of the above-mentioned experiments for a residence time of 6 min. As seen in Figure 4.4 (a), the main products of photo-Claisen rearrangements are phenol and *ortho* as well as *para*-allyl phenol. Increasing the residence time may increase the possibility of secondary reactions or polymerization [11]. Thus, with the residence time higher than 6 mins, some other byproducts could be formed.

Also, comparing Figure 4.4 (a),(b) and (c) it can be seen that the presence of allyl bromide and DBU do not influence the photo-Claisen rearrangement; it does not lead to the formation of new products or affects the product selectivity.

This result is fundamentally different to the respective HPLC chromatograms of thermal-Claisen rearrangement as reported in [12]. In the thermal case, the product peak almost vanished and the chromatograms showed several new peaks due to the formation of side and decomposition products. Therefore, the same reaction can be tuned orthogonal or non-orthogonal by choice of the activation mode.

4.2.3 Meta-substituent effect on *para*- to *ortho*-isomer distribution for the photo-Claisen Rearrangement of allyl phenyl ether in micro-flow

White *et al.* [39] presented that electron-donating groups and polar solvents accelerate the reaction rate of the thermal Claisen rearrangement. The substituent effects are related to intramolecular forces while the solvation effects are correlated to intermolecular forces.

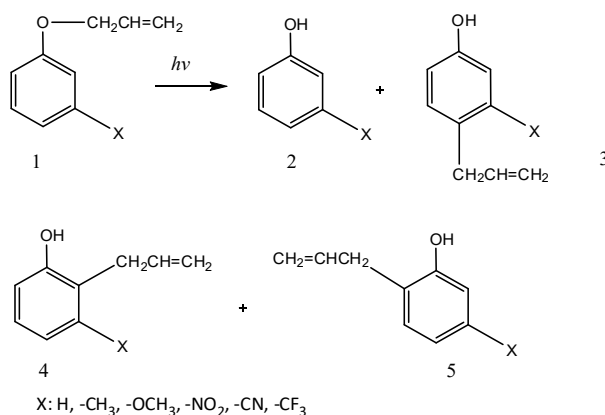
Pincock *et al.* [1], [40] reported also that substituent effects on the rates are significant, and that the reaction rate of ethers with electron-donating groups (methoxy, methyl) is higher than ethers with electron-withdrawing groups (trifluoromethyl, cyano). The values are consistent with the change in bond dissociation energy (BDE) relative to phenol which is σ^+ ; $\rho=+28.1$ ($r=0.990$) for ΔB_{DE} (kJ/mol) for both *para*- and meta-substituted compounds. This means that the bond is weakened by the electron-donating groups (ΔB_{DE} : -22 kJ/mol for 4-methoxy), while it is reinforced by the electron-withdrawing groups (ΔB_{DE} : +18 kJ/mol for 4-cyano). The reason behind this is not clearly mentioned; more precisely, there is an ambiguity as to which effect - changes in stability of the substituted phenols or changes in the stability of the substituted phenoxy radicals - is decisive. Although there is a controversy on this topic, the latest argumentations strongly support the latter factor. This effect may prevail over the other more typical substituent effects (electron density changes on excitation, resonance, induction, etc.) for the σ bond cleavage reactions of phenolic ethers because it is mostly large for XC_6H_4Y-Z cases when $Y=O$ and $Z=H$ or C . For other cases where $Y=C$ and $X=H, C,$ or halogen, the substituent has small influence on the BDE which seems to be ruled out by the other effects of the substituent. The electronic effects are found similar in MeOH and cyclohexane [31], [32].

The absolute differences in reactivity are huge and can span several orders of magnitude. For example, reaction rate coefficients measured in methanol for 4-OCH₃ and 4-CH₃ were almost the

same, being 5.3×10^9 and $5.1 \times 10^9 (s^{-1})$, respectively [1]. They are almost double as compared to the reaction rate of the unsubstituted molecule which was found to be $2.5 \times 10^9 (s^{-1})$. The latter still is more than 10 times higher of a deactivated molecule (cyano group, $0.16 \times 10^9 (s^{-1})$). The use of different solvents can shift the relative sequence of reactivities, as e.g. found when taking cyclohexane instead of methanol.

4.2.4 Substitution effects in photo micro-flow

To investigate the above mentioned effect for the photo-Claisen rearrangement in micro-flow, allyl aryl ethers with different relevant meta-substitution groups ($X=H, CH_3, OCH_3, CF_3$, and Cl) were synthesized from the corresponding phenols (see Scheme 4.1, Table 4.3). This was achieved by reaction with allyl bromide using potassium carbonate in dry acetone [40]–[43]. In line with above given result for the parental compound with $X=H$ and as expected from literature, the major products for $X=H, CH_3, OCH_3$, and CF_3 , are the corresponding phenols (2) and the rearranged allyl substituted phenols 2-allyl-3- X (4), 2-allyl-5- X (5), and 4-allyl-3- X (3), see Table 3.



Scheme 4.1. Possible main products in the photo-Claisen rearrangement of 3-substituted allyl phenyl ethers in micro-flow.

Table 4.3. Product distribution ($\times 100$) for the photo-Claisen rearrangement of diverse 3-substituted allyl phenyl ethers at a residence time=8 min in micro-flow. Tight configuration (0 cm distance between the reaction capillary and the lamp).

Compound	Solvent	Product 2	Product 3	Product 4+5
X:H	1-Butanol	21	30	30
X:-CH ₃	1-Butanol	15	35	42
X:-OCH ₃	1-Butanol	13	19	53
X:-CF ₃	1-Butanol	-	34	48

If we consider the yields given in Table 4.3 to qualitatively correlate to the rate constants (although this cannot be strict as probably an excess of residence time was given for some of the runs), it can be concluded that the photochemical Claisen rearrangement shows the same trend in substituent dependence as reported above for the thermal one. We therefore propose that changes in BDEs may have as well a major effect on the photochemical rate constants.

The 3-cyano and 3-nitro compounds are not listed in Table 4.3, because no product was formed in the 'distant' reactor configuration (distance from light source = 2 cm) at 15 min residence time. However, in the 'tight' process variant (distance from light source = 0 cm) and 100 min residence time, the 3-cyano compound reacted to give phenol (10%) as the main product and 9% of unknown products. According to the literature [1] 3-cyano compound is photochemically very unreactive and even after the prolonged reaction time, some conversion happened but the product mixtures are very complicated and could not be characterized. Even under such forced conditions, the 3-nitro compound reacted not at all.

4.2.5 Substitution effects in photo batch as comparison

Table 4.4 shows the results of the respective batch experiments reported by Pincock *et al.* [1]. The total amount of all yields, which were obtained at low conversions (10-20%), were normalized to 100%. There is no report on the reaction time of these batch results, yet the first guess is that the batch residence time is much longer than the micro-flow reaction time. Also, since the batch results have been normalized, it is only possible to compare the product distribution in batch with the micro-flow results. Although there is no general trend, it seems that, in batch, the product distribution is higher for some of the 4-allyl and 5-allyl phenols and the phenol share is much lower in batch. This could be the case since these yields were taken at low conversions, and the results may change at higher conversions due to over-irradiation [18].

Table 4.4. Product distribution (×100) for the photo-Claisen rearrangement of diverse 3-substituted allyl phenyl ethers in batch. Please note that the given values are not yields, but mole fractions normalized by the sum of all yields. Note that the real yields will be much lower, as conversion was 10-20% [1].

Compound	Solvent	Product 2	Product 3	Product 4+5
X:H	Methanol	4	46	50
X:-CH ₃	Methanol	8	25	68
X:-OCH ₃	Methanol	8	40	52
X:-CF ₃	Methanol	3	32	65

4.2.6 High-temperature photo micro-flow

Photoreactions are known to heat up bigger vessels through their thermal radiation. Often, hazardous intermediates are accumulated in photoreactions such as singlet oxygen or peroxides.

Therefore, the use of high temperatures is commonly not advised for safety reasons. Microreactors allow safe handling at even such conditions and therefore allow exploration of high-T photo micro-flow as novel process window.

There are reasons to do so. Schubnell *et al.* [44] explored the possibility of performing photochemistry at a high temperature for the conversion of solar energy into chemicals using ZnO as solid photocatalyst. Temperature changes the photocharacteristics quite remarkably. The luminescence intensity decreases with increasing temperature because of vibrational level population which leads to a red shift of the spectra. The luminescence spectra also broaden with increasing temperature due to increased phonon populations. In the UV-photo synthesis of vitamin D₃, the provitamin 7-dehydrocholesterol is reacted via singlet state irradiation to the previtamin intermediate. By virtue of a temperature pathway this is then transferred to vitamin D₃ [45], yet in competition with photo-induced equilibrium reactions to the side products tachysterol and lumisterol (which in turn can also be converted to vitamin D₃) [46], [47]. For our case, the Claisen rearrangement, motivation also might be that we simply like to omit the cooling-down step needed after the 100°C hot nucleophilic substitution for reasons of process simplicity and energy efficiency. That might be especially desirable in case, another high-temperature processing follows the Claisen rearrangement (making up a three-step flow synthesis). In a way, this means ensuring orthogonality in the combined process protocols.

Considering the above, and with the process window opened by our microreactor processing, the high-T photo micro-flow process variant of the Claisen rearrangement of allyl phenyl ether was investigated. The temperature could be set maximally to 78°C and that reaction performance was compared to room-temperature photo micro-flow operation (see Table 4.5). While the 3-meta 4-allyl phenol (product 3) is formed in a similar amount, the relative amount of *ortho*-products (3-meta 2-allyl phenol and 3-meta 6-allyl phenol; product 4+5) is much lower at the high temperature. The 3-meta phenol yield (product 2) is accordingly higher. Thus, the thermal pathway results in increased product degradation. A possible explanation could be that by giving more energy in the form of thermal energy (in addition to the photo energy), the intersystem crossing takes place to create a triple radical pair, where the radical can escape from the solvent cage and generate more phenol.

Table 4.5. High-T photo micro-flow process variant of the Claisen rearrangement of 3-methyl allyl phenyl ether ('tight' configuration) in 1-butanol, residence time= 8 min.

	Product 2	Product 3	Product 4+5
Photo-Claisen at 20°C	15	35	42
Photo-Claisen at 78°C	29	34	29

It can be concluded that, while not finding better product-related performance, a still sufficient performance is given (which may be optimized), whenever other urgent issues (e.g. orthogonality-driven) would demand a high-temperature operation.

4.3 Conclusions

A micro-flow route was developed for the photo-Claisen rearrangement of allyl phenyl ether as a parental compound and various 3-substituted allyl phenyl ethers. This was done with the vision to continue the continuous two-step micro-flow synthesis reported in chapter 3. Two measures reported here can contribute to an increasing molecular diversity: first is the use of 3-substituted phenols as precursors and the second refers to the possibility to achieve the 4-allyl product, besides the two 2-allyl products. The latter (*para*-substitution) is unique to the photo pathway, whereas the thermal rearrangement is known to provide only the *ortho*-pattern. Yet, in the photo pathway, the products are formed as well and a part of the product is decomposed to the phenol starting material.

To give a complete process window view, some relevant parametric sensitivities could be tackled. The superiority of using alcoholic solvents could be shown, with 1-butanol being the best one. As shown before, by many other photo micro-flow processes, the reaction time could be dramatically reduced from several hours to 8 min and less. Moreover, it could be shown that operation at preparatively relevant high concentrations could be achieved. Yet, the offset in the given timeframe was at about 0.05M. As third parameter, the distance between the reaction capillary and the UV-lamp was varied, from tight contact (0 cm) to some distance (2 cm). In this way, the UV intensity can be adjusted to the reaction needs. For slow reactions and less reactive substrates, the tight contact mode can intensify the reaction (to higher conversion and conversion rates), while the distant mode allows to avoid an overdosis of photons for reactive conditions and substrates. The latter can then decrease the undesired photodegradation. Finally, a high-temperature photo micro-flow process was investigated to combine two activation means and constituting a novel process window, enabled by micro-flow. Yet, this did not improve the reaction performance, but rather led to more photodegradation.

4.4 Acknowledgment

We kindly acknowledge the European Research Council for the Advanced Grant on “Novel Process Windows—Boosted Micro Process Technology” No 267443.

4.5 References

- [1] A. L. Pincock, J. A. Pincock, and R. Stefanova, "Substituent effects on the rate constants for the photo-claisen rearrangement of allyl aryl ethers," *J. Am. Chem. Soc.*, vol. 124, no. 33, pp. 9768–9778, 2002.
- [2] V. Hessel, D. Kralisch, N. Kockmann, T. Noël, and Q. Wang, "Novel process windows for enabling, accelerating, and uplifting flow chemistry," *ChemSusChem*, vol. 6, no. 5, pp. 746–789, 2013.
- [3] M. B. Smith and J. March, *March's Advanced Organic Chemistry: Reactions, Mechanisms, and Structure: Sixth Edition*, vol. 9780471720. John Wiley and Sons, 2006.
- [4] S. Zelentsov, V. Hessel, E. Shahbazali, and T. Noël, "The Claisen Rearrangement – Part 1: Mechanisms and Transition States, Revisited with Quantum Mechanical Calculations and Ultrashort Pulse Spectroscopy," *ChemBioEng Rev.*, vol. 1, no. 5, pp. 230–240, 2014.
- [5] V. Hessel, E. Shahbazali, T. Noël, and S. Zelentsov, "The Claisen Rearrangement – Part 2: Impact Factor Analysis of the Claisen Rearrangement, in Batch and in Flow," *ChemBioEng Rev.*, vol. 1, no. 6, pp. 244–261, 2014.
- [6] V. Hessel and H. Löwe, "Microchemical Engineering: Components, Plant Concepts User Acceptance – Part I," *Chem. Eng. Technol.*, vol. 26, no. 1, pp. 13–24, 2003.
- [7] V. Hessel and H. Löwe, "Microchemical engineering: Components, plant concepts, user acceptance - Part II," *Chem. Eng. Technol.*, vol. 26, no. 4, pp. 391–408, 2003.
- [8] H. Kobayashi, B. Driessen, D. J. G. P. van Osch, A. Talla, S. Ookawara, T. Noël, and V. Hessel, "The impact of Novel Process Windows on the Claisen rearrangement," *Tetrahedron*, vol. 69, no. 14, pp. 2885–2890, 2013.
- [9] M. Sato, N. Otabe, T. Tuji, K. Matsushima, H. Kawanami, M. Chatterjee, T. Yokoyama, Y. Ikushima, and T. M. Suzuki, "Highly-selective and high-speed Claisen rearrangement induced with subcritical water microreaction in the absence of catalyst," *Green Chem.*, vol. 11, no. 6, p. 763, 2009.
- [10] L. Kong, Q. Lin, X. Lv, Y. Yang, Y. Jia, and Y. Zhou, "Efficient Claisen rearrangement of allyl $para$ -substituted phenyl ethers using microreactors," *Green Chem.*, vol. 11, no. 8, pp. 1108–1111, 2009.
- [11] H. Maeda, S. Nashihara, H. Mukae, Y. Yoshimi, and K. Mizuno, "Improved efficiency and product selectivity in the photo-Claisen-type rearrangement of an aryl naphthylmethyl ether using a microreactor/flow system," *Res. Chem. Intermed.*, vol. 39, no. 1, pp. 301–310, 2013.
- [12] E. Shahbazali, M. Spapens, H. Kobayashi, S. Ookawara, T. Noël, and V. Hessel, "Connected nucleophilic substitution-Claisen rearrangement in flow – Analysis for kilo-lab process solutions with orthogonality," *Chem. Eng. J.*, vol. 281, pp. 144–154, 2015.
- [13] T. Razzaq and C. O. Kappe, "Continuous flow organic synthesis under high-temperature/pressure conditions," *Chem. An Asian J.*, vol. 5, no. 6, pp. 1274–1289, Jun. 2010.
- [14] T. Razzaq, T. N. Glasnov, and C. O. Kappe, "Accessing novel process windows in a high-temperature/pressure capillary flow reactor," *Chem. Eng. Technol.*, vol. 32, no. 11, pp. 1702–1716, 2009.
- [15] D. Cambié, C. Bottecchia, N. J. W. Straathof, V. Hessel, and T. Noël, "Applications of Continuous-Flow Photochemistry in Organic Synthesis, Material Science, and Water Treatment," *Chem. Rev.*, DOI: 10.1021/acs.chemrev.5b00707
- [16] J. P. Knowles, L. D. Elliott, and K. I. Booker-Milburn, "Flow photochemistry: Old light through new

windows," *Beilstein J. Org. Chem.*, vol. 8, pp. 2025–2052, 2012.

- [17] K. Pitchumani, M. Warriar, and V. Ramamurthy, "Remarkable Product Selectivity During Photo-Fries and Photo-Claisen Rearrangements within Zeolites," *J. Am. Chem. Soc.*, vol. 118, no. 39, pp. 9428–9429, 1996.
- [18] F. Galindo, "The photochemical rearrangement of aromatic ethers: A review of the Photo-Claisen reaction," *Journal of Photochemistry and Photobiology C: Photochemistry Reviews*, vol. 6, no. 2–3, pp. 123–138, 2005.
- [19] G. Koga, N. Kikuchi, and N. Koga, "Photo-Claisen Rearrangement. The Photochemical Rearrangement of Allyl Phenyl Ethers," *Bull. Chem. Soc. Jpn.*, vol. 41, no. 3, pp. 745–746, 1968.
- [20] H. R. Waespe, H. Heimgartner, H. Schmid, H. J. Hansen, H. Paul, and H. Fischer, "Photoreactions. Part 55. The photochemistry of allyl aryl ethers," *Helv. Chim. Acta*, vol. 61, no. 1, pp. 401–429, 1978.
- [21] A. Sugimoto, T. Fukuyama, Y. Sumino, M. Takagi, and I. Ryu, "Microflow photo-radical reaction using a compact light source: application to the Barton reaction leading to a key intermediate for myricic acid A," *Tetrahedron*, vol. 65, no. 8, pp. 1593–1598, 2009.
- [22] E. D. Hughes and C. K. Ingold, "55. Mechanism of substitution at a saturated carbon atom. Part IV. A discussion of constitutional and solvent effects on the mechanism, kinetics, velocity, and orientation of substitution," *J. Chem. Soc.*, p. 244, 1935.
- [23] A. Lee, J. D. Stewart, J. Clardy, and B. Ganem, "New insight into the catalytic mechanism of chorismate mutases from structural studies," *Chemistry and Biology*, vol. 2, no. 4, pp. 195–203, 1995.
- [24] C. Uyeda and E. N. Jacobsen, "Enantioselective Claisen rearrangements with a hydrogen-bond donor catalyst," *J. Am. Chem. Soc.*, vol. 130, no. 29, pp. 9228–9229, 2008.
- [25] Y. Huang, A. K. Unni, A. N. Thadani, and V. H. Rawal, "Hydrogen bonding: single enantiomers from a chiral-alcohol catalyst," *Nature*, vol. 424, no. 6945, p. 146, 2003.
- [26] J. S. Lindsey and R. W. Wagner, "Investigation of the synthesis of *ortho*-substituted tetraphenylporphyrins," *J. Org. Chem.*, vol. 54, no. 4, pp. 828–836, 1989.
- [27] D. L. Severance and W. L. Jorgensen, "Effects of hydration on the Claisen rearrangement of allyl vinyl ether from computer simulations," *J. Am. Chem. Soc.*, vol. 114, no. 27, pp. 10966–10968, 1992.
- [28] M. M. Davidson, I. H. Hillier, R. J. Hall, and N. A. Burton, "Effect of Solvent on the Claisen Rearrangement of Allyl Vinyl Ether Using *ab initio* Continuum Methods," *J. Am. Chem. Soc.*, vol. 116, no. 20, pp. 9294–9297, 1994.
- [29] E. Brandes, P. A. Grieco, and J. J. Gajewski, "Effect of polar solvents on the rates of Claisen rearrangements: assessment of ionic character," *J. Org. Chem.*, vol. 54, no. 3, pp. 515–516, 1989.
- [30] C. Reichardt and T. Welton, *Solvents and Solvent Effects in Organic Chemistry: Fourth Edition*. 2010.
- [31] F. A. Carroll and G. S. Hammond, "Mechanisms of photochemical reactions in solution. LXXII. Electronic pathways in the photodissociation of 3-methyl-1-phenoxybut-2-ene," *J. Am. Chem. Soc.*, vol. 94, no. 20, pp. 7151–7152, Oct. 1972.
- [32] N. Haga* and Hiroaki Takayanagi, "Mechanisms of the Photochemical Rearrangement of Diphenyl Ethers," *J. Org. Chem.*, vol. 61, no. 2, pp. 735–745, 1996.
- [33] D. H. Ripin and D. A. Evans, "pKa table." [Online]. Available:
http://evans.rc.fas.harvard.edu/pdf/evans_pKa_table.pdf.

- [34] PKa, [Online]. Available: <https://pubchem.ncbi.nlm.nih.gov/compound/1-butanol#section=Odor-Threshold>.
- [35] E. E. Coyle and M. Oelgemöller, "Micro-photochemistry: photochemistry in microstructured reactors. The new photochemistry of the future?," *Photochem. Photobiol. Sci.*, vol. 7, no. 11, p. 1313, 2008.
- [36] Y. Su, N. J. W. Straathof, V. Hessel, and T. Noël, "Photochemical Transformations Accelerated in Continuous-Flow Reactors: Basic Concepts and Applications," *Chem. – A Eur. J.*, vol. 20, no. 34, pp. 10562–10589, 2014.
- [37] M. M. Makogon, Y. N. Ponomarev, and B. A. Tikhomirov, "The problem of water vapor absorption in the UV spectral range," *Atmos. Ocean. Opt.*, vol. 26, no. 1, pp. 45–49, 2013.
- [38] M. S. Syamala and V. Ramamurthy, "Modification of photochemical reactivity by cyclodextrin complexation: selectivity in photo-claisen rearrangement," *Tetrahedron*, vol. 44, no. 23, pp. 7223–7233, 1988.
- [39] W. N. White and E. F. Wolfarth, "ortho-Claisen rearrangement. IX. Effect of solvent on the substituent effect," *J. Org. Chem.*, vol. 35, no. 10, p. 3585, 1970.
- [40] C. M. Gonzalez and J. A. Pincock, "Substituent effects, Arrhenius activation parameters, and rate constants for the photo-Claisen rearrangement of allyl aryl ethers," vol. 690, pp. 686–690, 2008.
- [41] F. C. Gozzo, S. A. Fernandes, D. C. Rodrigues, M. N. Eberlin, and A. J. Marsaioli, "Regioselectivity in aromatic Claisen rearrangements," *J. Org. Chem.*, vol. 68, no. 14, pp. 5493–5499, 2003.
- [42] I. A. Sayyed, V. V. Thakur, M. D. Nikalje, G. K. Dewkar, S. P. Kotkar, and A. Sudalai, "Asymmetric synthesis of aryloxypropanolamines via OsO₄-catalyzed asymmetric dihydroxylation," *Tetrahedron*, vol. 61, no. 11, pp. 2831–2838, 2005.
- [43] X. Han and D. W. Armstrong, "Using geminal dicationic ionic liquids as solvents for high-temperature organic reactions.," *Org. Lett.*, vol. 7, no. 19, pp. 4205–8, Sep. 2005.
- [44] M. Schubnell, I. Kamber, and P. Beaud, "Photochemistry at high temperatures -- potential of ZnO as a high temperature photocatalyst," *Appl. Phys. A*, vol. 64, no. 1, pp. 109–113, 1996.
- [45] S. Fuse, N. Tanabe, M. Yoshida, H. Yoshida, T. Doi, and T. Takahashi, "Continuous-flow synthesis of vitamin D₃," *Chem. Commun.*, vol. 46, no. 46, pp. 8722–8724, 2010.
- [46] N. Gottfried, W. Kaiser, M. Braun, W. Fuss, and K. L. Kompa, "Ultrafast electrocyclic ring opening in previtamin D photochemistry," *Chem. Phys. Lett.*, vol. 110, no. 4, pp. 335–339, Oct. 1984.
- [47] F. A. Carey and R. J. Sundberg, *Advanced Organic Chemistry Part A: Structure and Mechanisms*. 2007.

4.6 Supplementary Material

Experimental

S.1. General reagent information

Allyl phenyl ether, 1-butanol, 2-propanol, methanol, heptane, 3-methoxyphenol, 3-methyl phenol, 3-cyanophenol, 3-nitrophenol, 1,3 dinitrobenzene were purchased from the Aldrich chemical company and used as received. For the flow experiment, solutions were prepared in volumetric flasks.

S.2. Experimental section

In order to perform the photo-Claisen rearrangement in flow, a microfluidic setup was assembled as shown in Figure S.4.1. The photo-microreaction system consists of a capillary tube of 5 m length and 0.5 mm internal diameter (volume of ≈ 1 ml) which is made of fluorinated ethylene propylene (FEP 1548; Upchurch Scientific). This capillary is wound around a cylindrical UV light source placed inside a closed oven. The sample solutions were introduced in the photo-microreactor by using an HPLC pump (Knauer, Smartline 1050). Irradiation was carried out using a low-pressure amalgam lamp (TS23-212; Dinies Technologies GmbH). Directly after exiting the photo-microreactor, the product samples were collected into vials. The samples were analyzed with HPLC-UV for quantification by applying the internal standard method. Each data point in the plot constitutes the average of two samples.

The samples obtained from the photo-Claisen rearrangement of the 3-substituted allyl phenyl ethers were analyzed with HPLC-UV. In order to identify the HPLC peaks, thermal-Claisen rearrangement of the same compounds was performed [12] and analyzed with HPLC-UV; also one sample of the thermal-Claisen rearrangement of 3-methyl allyl phenyl ether was analyzed via NMR. Then, the thermal-Claisen results were compared with the photo-Claisen results. From literature and the NMR results, it is known that the product of thermal Claisen rearrangement of 3-substituted allyl phenyl ethers are 3-substituted 2-allyl phenol and 3-substituted 6-allyl phenol; product 4+5 [41]. By comparing the HPLC results of thermal-Claisen with photo-Claisen, the *para*-product (3-substituted 4-allyl phenol, product 3) was also identified, along with the other two *ortho*-products.

S.3. General analysis information

The samples were analyzed via ^1H NMR and HPLC. Nuclear magnetic resonance spectra were recorded on a Varian 400 MHz or 500 MHz instruments. All ^1H NMR are reported in δ units, parts per million (ppm), and were measured relative to the signal for tetramethylsilane (0 ppm) in the deuterated solvent, unless otherwise stated.

HPLC analyses were performed on Shimadzu UFLC XR (205 nm) using a GraceSmart RP 18 5u column (150 mm, 4.2 mm). 1,3 dinitrobenzene was used as an internal standard to carry out HPLC quantification in Claisen rearrangement of allyl phenyl ether.

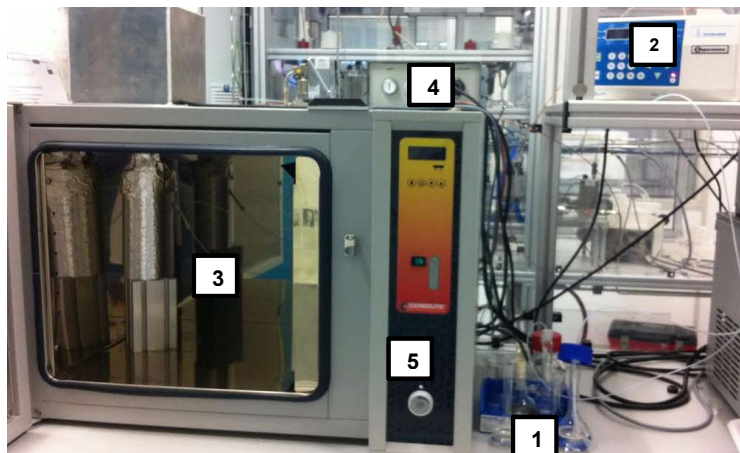


Figure S4.1. Microfluidic setup utilized for Claisen Rearrangement 1-Inlet and outlet of the microreactor 2-HPLC pump 3-Light source surrounded with microreactor, covered with aluminum sheet 4-light source power supply 5-Micro-photoreactor safety oven.

S.4. Synthesis of 3-substituted allyl phenyl ethers

A mixture of one of the phenols (10 mmol), allyl bromide (12 mmol) and anhydrous K_2CO_3 (15 mmol) in dry acetone (20 mL) was refluxed under N_2 (reactions monitored by TLC). After completion of the reaction (10-20 h) the reaction mixture was cooled to room temperature, filtered through sintered funnel and the filtrate was evaporated to remove the acetone. The residue was purified by column chromatography using petroleum ether/EtOAc as eluent to yield pure 3-substituted allyl phenyl ethers in an average yield of 90% [40] [41] [42] [43].

3-methyl allyl phenyl ether (1-allyloxy-3-methyl-benzene): 1H NMR (400 MHz, $CDCl_3$) δ ppm 7.14 (t, ArH, 1H), 6.75 (dt, $J=8.0, 1.9$ Hz, ArH, 1H), 6.72 (t, ArH, 1H), 6.70 (dt, $J=8.0, 1.9$ Hz, ArH, 1H), 5.91-6.15 (m, CH=C, 1H), 5.40 (dq, $J=17.4, 1.6, 1.6, 1.8$ Hz C=CH₂, 1H), 5.28 (dq, $J=10.6, 1.5, 1.5, 1.4$ Hz, C=CH₂, 1H), 4.51 (dt, $J=5.3, 1.5, 1.5$ Hz, CH₂, 2H), 2.30(s, CH₃, 3H)

3-methoxy allyl phenyl ether (1-allyloxy-3-methoxy-benzene): 1H NMR (400 MHz, $CDCl_3$) δ ppm 7.15 (t, ArH, 1H), 6.45-6.64 (m, ArH, 3H), 5.92-6.18 (m, CH=C, 1H), 5.42 (dq, $J=17.4, 1.7, 1.7, 1.8$ Hz C=CH₂, 1H), 5.29 (dq, $J=10.4, 1.5, 1.5, 1.4$ Hz, C=CH₂, 1H), 4.52 (dt, $J=5.3, 1.5, 1.5$ Hz, CH₂, 2H), 3.79 (s, CH₃, 3H)

3-trifluoromethyl allyl phenyl ether (1-allyloxy-3-trifluoromethyl-benzene): 1H NMR (400 MHz, $CDCl_3$) δ ppm 7.38 (t, ArH, 1H), 7.22 (d, $J=8.0$ Hz, ArH, 1H), 7.16 (s, ArH, 1H), 7.09 (dd, $J=4.4, 8.1$ Hz, ArH, 1H), 5.98-6.09 (m, CH=C), 5.44 (dq, $J=17.4, 1.6, 1.6, 1.8$ Hz, C=CH₂, 1H), 5.32 (dq, $J=10.4, 1.5, 1.5, 1.4$ Hz, C=CH₂, 1H), 4.60 (m, CH₂, 2H)

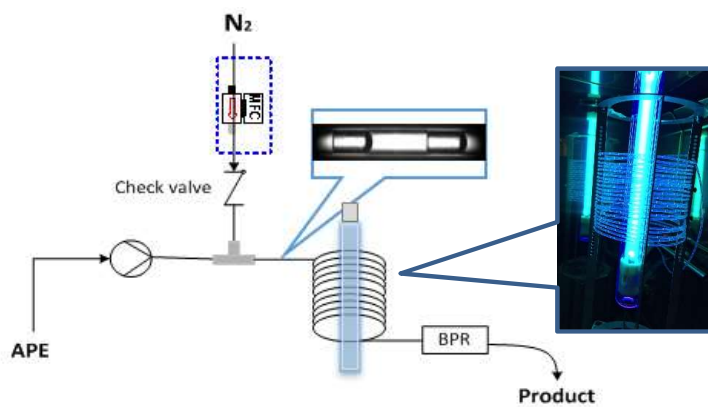
3-nitroallyl phenyl ether (1-allyloxy-3-nitro-benzene): ^1H NMR (400 MHz, CDCl_3) δ ppm 7.78-7.81 (m, ArH, 1H), 7.75 (t, ArH, 1H), 7.43 (t, ArH, 1H), 7.25 (d, $J=16.5$, Hz, ArH, 1H), 6.0-6.10 (m, CH=C), 5.45 (dd, $J=17.1$, 1.4 Hz, C=CH₂, 1H), 5.35 (dd, $J=10.5$, 1.2 Hz, C=CH₂, 1H), 4.63 (d, $J=5.5$ Hz, CH₂, 2H)

3-cyano allyl phenyl ether (1-allyloxy-3-cyano-benzene): ^1H NMR (400 MHz, CDCl_3) δ ppm 7.36 (t, ArH, 1H), 7.24 (dt, $J=7.6$, 1.2, 1.2 Hz, ArH, 1H), 7.10-7.18 (m, ArH, 2H), 5.96-6.09 (m, CH=C, 1H), 5.42 (dq, $J=17.3$, 1.6, 1.6, 1.5 Hz C=CH₂, 1H), 5.33 (dq, $J=10.6$, 1.4, 1.4, 1.4 Hz, C=CH₂, 1H), 4.56 (dt, $J=5.2$, 1.5, 1.5 Hz, CH₂, 2H)

2-allyl-3-methylphenol and 2-allyl-5-methylphenol: ^1H NMR (500 MHz, $(\text{CD}_3)_2\text{SO}$) δ ppm 6.91 (d, $J=8.0$ Hz, ArH, 1H), 6.89 (d, $J=7.7$ Hz, ArH, 1H), 6.61 (d, $J=0.6$ Hz, ArH, 1H), 6.6 (d, $J=8.1$ Hz, ArH, 1H), 6.54 (d, $J=7.6$ Hz, ArH, 2H), 6.51–6.56 (m, ArH, 1H), 5.88–6.02 (m, CH=C, 2H), 5.78–5.91 (m, CH=C, 2H), 4.85–5.06 (m, C=CH₂, 4H), 3.30–3.34 (m, CH₂, 2H), 3.29 (s, OH, 1H), 3.28 (s, OH, 1H), 3.23 (d, $J=6.7$ Hz, CH₂, 2H), 2.19 (s, CH₃, 3H), 2.18 (s, CH₃, 3H)

CHAPTER 5

UV-Photo-Flow Intensification - Taylor Flow for Enhancing Photo-Microreactors



This chapter is based on:

Shahbazali, E., Su, Y., Noël, T., Hessel, V. To be submitted to Chem. Eng. J.

Abstract

Recently, microreactors have received a lot of attention in photochemical applications since they are capable to improve some issues related to the batch photochemistry. In essence, the narrowness of the microreactor channels enables a better exposure of the reaction mixture to the irradiated light. However, flow chemistry is commonly sustainable when being operated at high concentration or even solvent-free. In such highly intensified process window, the same limitations can occur as for batch reactions. Yet, there is a new solution, which is presented in this chapter. Under high concentration, a photochemical reaction may occur only down to a certain layer depth even in a microchannel. Therefore the reaction is then photon transfer limited. It was shown for liquid-liquid micro-flow at the example of the Paternò-Büchi reaction that an intensification (at high concentration) can be achieved as compared to single flow. This is explained by an effect of the small liquid layer which interstices at the interface gas bubble and microcapillary wall [1]. The experiments of this chapter confirm and considerably extend this investigation, as given in the main body text and Conclusions. Essential new elements are the use of gas-liquid segmented flow (Taylor flow), the joint creation of a thin liquid layer around the gas bubble and the usage of a recirculation vortex in the liquid slugs, and light confinement effect. In this chapter, the possibility of performing the photo-Claisen rearrangement at high concentration under Taylor flow conditions by applying an inert immiscible phase (N_2 or water) is investigated. The results are compared with those of single-phase flow. Moreover, the three mentioned effects of Taylor flow on the performance of the photoreaction are studied. Finally, in order to enhance the mixing in the liquid slug, a new microreactor configuration, micro coiled flow inverter (MCFI) is tested. The results showed by applying photo MCFI, allyl phenyl ether (APE) conversion could be increased by at least 1.5 times or more.

5.1 Introduction

Organic photochemistry utilizes light as an efficient source of energy that is considered green, traceless, and is therefore a sustainable “reagent”. In the past decades, photoreactions especially photocatalytic reactions have received a lot attention due to new discoveries towards transition metal complexes or organic dyes [2]–[5]. These new discoveries are impressive since they allow scientists to take advantage of visible light that is an abundant source of energy [2], [4], [6], [7]. In photochemistry the most important driving force is photon absorption. According to the Bouguer–Lambert–Beer law [8] absorption reduces by increasing the optical path length and the concentration of the absorbing species. Therefore, it is not unexpected that organic photoreactions have been limited to lab-scale only. The attenuation consequence of photon transport, burdens the common scalability (dimension expanding approach) for the photoreactors. On the other hand, in larger scale reactors, increasing the irradiation time would result in over irradiation of the reaction mixture and consequently decomposition or formation of byproducts.

Recently, microreactors have become popular in photochemical applications since they are capable of improving some of the unsolved issues related to the batch photochemistry [9]–[13].

In essence, the narrowness of the microreactor channels enables a better exposure of the reaction mixture to the irradiated light. A larger amount of reactant molecules is excited and therefore the reaction proceeds in much reduced irradiation time. Reduction in irradiation time, suppresses the formation of potential by products and therefore boosts the productivity. Recently, many examples of efficient photoreactions have been published [10], [12]–[15]. Also, some efforts have been made to scale-up the photo-microreactors including numbering up of the parallel microreactors [11].

However, flow chemistry is commonly sustainable when being operated at highest possible concentration or even solvent-free. In such a highly intensified process window, the same limitations can occur as for batch reactions as expected from Bouguer–Lambert–Beer law. Yet, there is a novel solution to this, using segmented flow conditions. In general, segmented flow (also known slug flow or Taylor flow) condition is applied for heterogeneous reactions where two or three phases are involved [16]–[21]. Oelgemöller *et al.* reported on the efficiency of photoreactions using segmented flow applying a gaseous reagent in a column reactor [18]. They performed the photooxygenation of 1,5-dihydroxynaphthalene, furfural, α -terpinene, and citronellol with singlet oxygen sensitized by rose bengal in a glass tubular reactor. Under the segmented flow condition, a higher efficiency of photooxygenation by using oxygen bubble flow was observed. It was concluded that a segmented flow pattern permitted for improved mass transfer within a thin layer of the continuous phase (liquid) along the side of the gas bubble [22]. This can be scaled down to the microreactor level. Recently, Kakiuchi *et al.* reported on the

Paternò-Büchi photoreaction in a microreactor under slug flow conditions by using organic and aqueous slug. It was shown that by using the slug flow mode, the productivity increased remarkably [1].

Under the highest possible concentration, a photochemical reaction may occur only down to a certain layer depth even in a microchannel and is therefore transfer limited. Gas-liquid segmented flow (Taylor flow) might overcome this due to the paper of Cambié *et al.* [23]:

- Creation of a thin liquid film around the gas bubble, which reduces the penetration depth of the light. Therefore, it might be possible to go for higher concentrated solutions in photo microreactors.
- The recirculation vortex caused in the liquid slugs creates mixing down to the molecular level, which leads to a constant renewal of reactant concentration to maximally profit from the photons entering only part of the microchannels.
- The light confinement effect resulted from the refractive index difference between the continuous phase and the dispersed phase inside the reaction medium [1].

Gas-liquid (Taylor flow) is greener than slug flow, since air is used which can be easily separated, while the water phase can get contaminated with reaction impurities and constitutes a notable element in lowering the process mass index (PMI) which is an essential parameter to judge on the greenness of the reaction. Also, air is much easier separated from the liquid reaction phase (release to atmosphere) than it is for a water/organic separation, which needs a more complex membrane separation, which hardly works at 100% separation efficiency in one step.

In this chapter, it is aimed to investigate all three effects of Taylor flow in a photo-microreactor. As a proof-of-concept, the photo-Claisen rearrangement of allyl phenyl ether (APE) was chosen to be performed in a micro reactor (the reactions are shown in Figure 5.1). Previously, we have reported the photo-Claisen rearrangement of APE in single-phase flow [12]. A much higher conversion of 0.1 M APE was achieved in a microreactor than in batch mode, yet, there are some limitations for higher reactant concentrations even in a microreactor. Therefore, higher concentrations are tested under Taylor flow conditions. And also, two different reactor configurations were applied to compare the mixing effect in the slug phases.

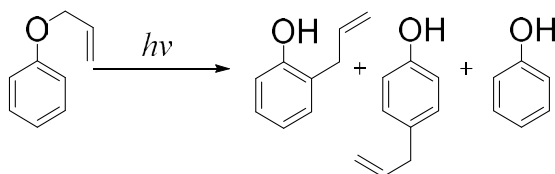


Figure 5.1. Photo-Claisen rearrangement path of Allyl phenyl ether (APE)

5.2 Experimental section

5.2.1 General Taylor flow experiments

In order to carry out the photo-Claisen rearrangement in gas-liquid segmented flow, a microfluidic setup was assembled as shown in Figure 5.2. The reactant solutions were introduced in the photo-microreactor by using an HPLC pump (Knauer, Azura P4.1S) and mixed with nitrogen stream using a T-mixer (1/16", PEEK, P-712, IDEX-Health & Science). The gas flow is supplied from a nitrogen source. A mass flow controller (MFC) was installed after nitrogen source to control the gas flow rate. Before the T-mixer a check valve (CV-3500 micro volume inline- IDEX Health & Science) was added to prevent any back flow of liquid towards the gas MFC. The check valve with a minimum internal volume was selected in order to prevent gas flow disturbance. Between the check valve and the T-mixer a transparent FEP tubing of (ID 0.25 mm, length of 10 cm) was installed in order to verify visually whether any liquid ever was moving towards the check valve and also to keep the gas flow rate more homogeneous. After the T-mixer, the liquid slugs and gas bubbles were created and sent into the photoreactor which consists of a capillary tube (FEP 1548, ID 0.02", 5 m length) wound on a capillary tower around a cylindrical UV light source (TS23-212; Dinies Technologies GmbH). A back pressure regulator of 75 psi (P-786 IDEX-Health & Science) was applied at the end of the setup before sampling in order to keep the Taylor flow behaviour inside the microreactor more homogenous. Directly after leaving the photo-microreactor, the product samples were collected into vials. The samples were analyzed with HPLC-UV for quantification by applying the internal standard method. Each data point in the plot constitutes the average of two samples.

The liquid flow rate and gas flow rate were ranging from 0-1 ml/min. For each set of experiments of gas-liquid, the flow rate of liquid was set and kept at a certain value (ranging 0.05, 0.1, or 0.2 ml/min) and the gas flow rate was varied ranging from 0-1 ml/min, according to the required mean irradiation time.

In experiments that used aqueous solutions as the dispersed phase instead of N₂, the aqueous solution was introduced by using a syringe pump into the T-mixer.

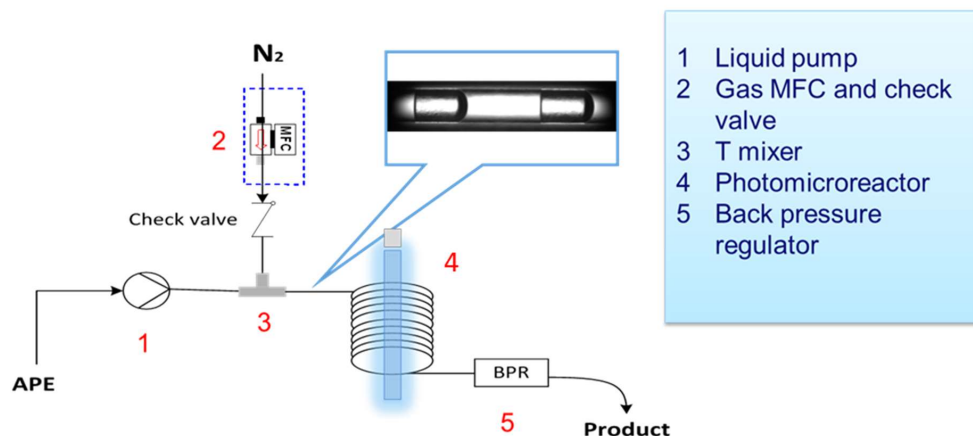


Figure 5.2. Schematic representation of the photo-microreactor assembly for the photo-Claisen rearrangement of APE in 1-butanol under a Taylor flow pattern by using nitrogen as a dispersed phase.

5.2.2 Taylor flow experiments in MCFI

An almost similar experimental set-up was used for Taylor flow experiments in micro coiled flow inverter (MCFI). The only difference is the photo-microreactor. The photo-microreactor consists of a capillary tube (FEP 1548, ID 0.02", 1.25 m length) that is coiled on each side of the MCFI and at a 90° bended to the adjacent side. Each side of MCFI is approximately 3 cm. In order to keep consistency in the experiments, the MCFI is located vertically (that each side has equal distance to the lamp) in parallel to the lamp. The distance between the MCFI and the lamp is 2.5 cm.

5.3 Results and Discussion

5.3.1 Concentration effect on Photo-Claisen Rearrangement

As it was explained in section 5.1, the starting point of this research was the observation of the low conversion of the photoreaction at high reactant concentrations in microreactors (here FEP tubing). In order to observe the photoreaction efficiency in a microreactor. The photo-Claisen rearrangement of allyl phenyl ether (APE) was carried out in a microreactor at various irradiation times for three different initial concentrations, 0.01 molar, 0.1 molar, and 0.5 molar. The results are presented in Figure 5.3. According to the results, at the lowest concentration, 0.01 molar, after 8 minutes, full conversion is reached. At 0.1 molar, after 8 min. 80% of APE is converted. However, at the highest concentration, 0.5 molar, even after 8 min of irradiation time, not more than 20% of conversion has been observed. Therefore, the results indicated that as expected the photoreaction at a higher concentration of the reactant even in a microreactor is not fully

converted. This can be explained by the Bouguer–Lambert–Beer law that is introduced in chapter one, Equation 1.1.

$$A = -\log_{10}T = \log_{10} \frac{I_0}{I} = \epsilon cl \quad (5.1)$$

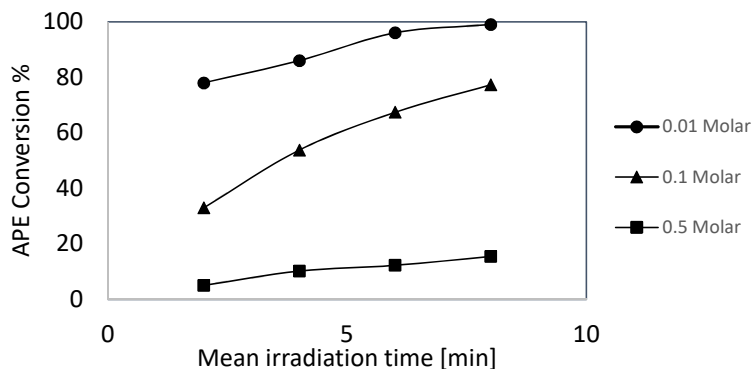


Figure 5.3. APE conversion versus irradiation time for 0.01, 0.1, and 0.5M APE at room temperature

As explained earlier in chapter 1, transmittance (T) is reduced by increasing the reactant concentration (c) or the path length (l) of light propagation. To elaborate more, the effect of characteristic dimensions of photoreactors on light absorption is illustrated in Figure 5.4 by measuring the transmittance spectrum of different concentrations of APE in 1-butanol as a solvent at 254 nm.

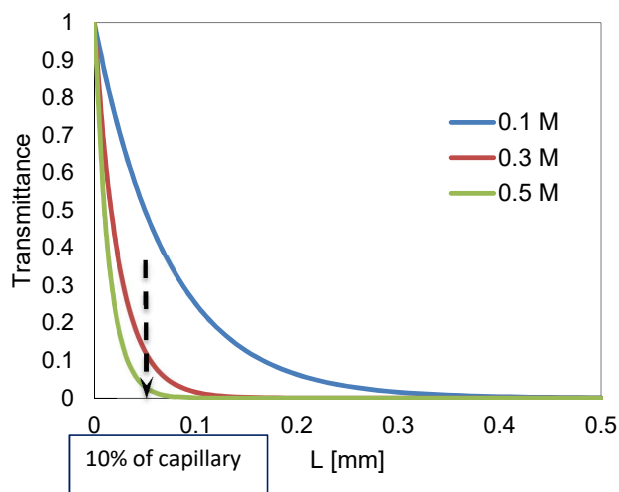


Figure 5.4. Transmission spectrum of APE in 1-butanol at 254 nm for 0.1, 0.3, and 0.5 M

Transmittance is calculated according to the Bouguer–Lambert–Beer law. First the molar extinction coefficient (ϵ) at 254 nm was determined and according to that the transmittance for different concentrations of APE in 1-butanol is depicted. As it can be seen, the light intensity is reduced rapidly as the penetration path of the light is increasing. And this is more noticeable for higher reactant concentrations. For instance, results indicate that for 0.5 M APE, light transmittance reaches to less than 0.05 by the first 0.05 mm of the light penetration depth. In other words, if a capillary tube with ID of 0.5 mm is considered, more than 95 % of the light is absorbed by the liquid mixture within the first 10% of the tube diameter and the light intensity promptly reduced towards the center of the capillary tube. Therefore, the share of the propagating light for the remained 90% of the tube diameter is only 5 %.

5.3.2 Introducing the Taylor flow Concept into Photoreaction

Two-phase flow patterns are typically applied in microreactors, i.e., Taylor flow (also known as segmented or slug flow) and annular flow. Taylor flow is considered by liquid slugs (continuous phase) and elongated bubbles of an immiscible phase (e.g., gas or liquid). Toroidal vortices are made in both phases which create mixing zones (Figure 5.5). Depending on the wettability of the liquid phase and the reactor surface, a thin liquid film might be created around the bubble which detaches the bubble from the reactor wall. The hydrophilic nature of the continuous phase and the reactor wall material plays the most important role to determine whether the dispersed phase (gas phase) is disjoined from the wall with the liquid phase [24]. According to the literature [25], in microreactors the thickness of this liquid film is around 5-20% of the reactor internal diameter. This film receives the highest intensity of the photons, therefore it is expected that the rate of the photoreaction within the liquid film is quite high. The recirculation vortex caused in the liquid slugs creates mixing down to the molecular level not only in the liquid slug but also within the liquid film, which leads to a constant renewal of reactant concentration, which leads to a maximum profit of the photons entering only part of the microchannels. Another effect caused by the segmented flow is the light confinement effect within the liquid phase (continuous phase). This effect is elaborated in section 5.3.3.

In order to study the Taylor flow effect on a photoreaction, the photo-Claisen rearrangement of APE in 1-butanol with various gas flow rates (N_2) in a microreactor is considered and the results are presented in Figure 5.6. Since the FEP tubing and organic phase (1-butanol) are both hydrophobic, it is considered that there is a liquid layer formed around the gas bubbles. Three sets of experiments were carried out for constant liquid flow rates of 0.05-0.1-0.2 ml/min, in such a way that in each set, the liquid flow rate was kept constant and the gas flow rate was varied from 0.1-1 ml/min. A blank experiment of only liquid flow without gas flow (single-phase flow) was also conducted to compare the results with those of the Taylor flow experiments. The mean

irradiation time of the liquid mixture inside the microreactor, τ_m is calculated according to Equation 5.2 [26], [27].

$$\tau_m = \frac{V}{\bar{Q}} \quad (5.2)$$

Where, V and \bar{Q} are the photo-microreactor volume and the overall flow rate. The average overall flow is defined as

$$\bar{Q} = \frac{Q_g + Q_l}{2} \quad (5.3)$$

Q_g and Q_l are the gas flow rate and liquid flow rate, respectively.

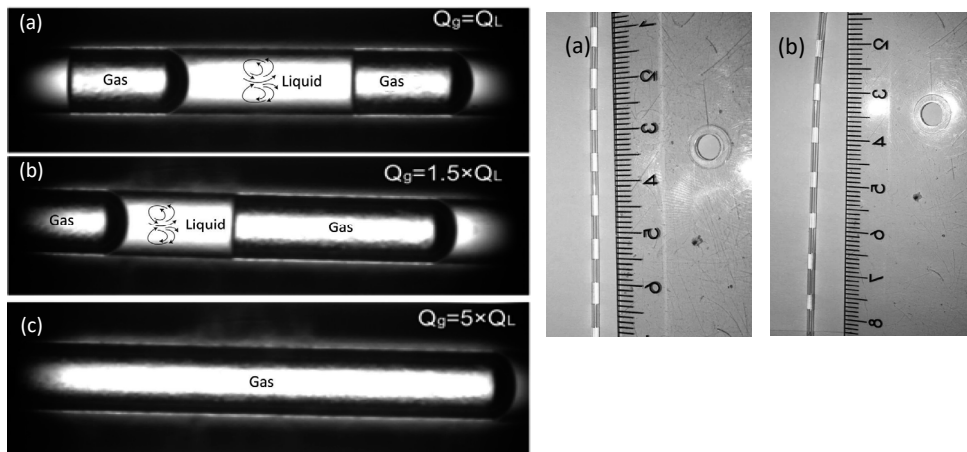


Figure 5.5. Liquid slug and gas bubble created under Taylor flow regime in a microreactor with different gas to liquid flow rates, (a) $Q_g/Q_l=1$, (b) $Q_g/Q_l=1.5$ and (c): $Q_g/Q_l=5$, (Images are captured using a Redlake Motion Pro X-4 high speed camera)

In Figure 5.6 (a), the conversion of APE (0.1 M) is plotted versus the mean irradiation time for different gas and liquid flow rates. The results are compared with those of single-phase flow. For each set of data points where the liquid flow rate is constant, increasing the gas flow rate leads to a decrease of the mean irradiation time. For instance, the data points with $\tau_m=6.6$ min has lower gas flow rate than the data point with $\tau_m=1.5$ min. As demonstrated by Figure 5.6 (a) the experiment with no gas flow (only single-phase flow) gives a lower conversion at any mean irradiation time ranging from 0-8 min as compared with data points in which Taylor flow has been applied.

Furthermore, for each set of data points for which the liquid flow rate is constant, the conversion of APE increases by increasing the mean irradiation time. This is quite obvious, since the reacting

molecules are exposed to the irradiated photons for a longer time. By increasing the gas flow rate or liquid flow rate, the average overall flow rate of the liquid mixture in the reactor would be higher and consequently the average exposure time is reduced. The increase in conversion in lower τ_m is negligible. However, by further increase in τ_m , the APE conversion tends to increase at faster and goes up to 80 %. Nevertheless, the first set of data points with $Q_l=0.05$ ml/min has a smoother deviation in the conversion versus τ_m and it has higher conversion for each value of irradiation time, compared to the rest of data points. In addition, if the conversion of the data points at different τ_m is compared, the data points with $Q_l=0.05$ ml/min reach the highest values.

Considering the $\frac{Q_g}{Q_l}$ ratio, for instance, at $\tau_m=2$ min, this ratio for the data point with $Q_l=0.05$ ml/min is equal to 9, while for the data point with $Q_l=0.2$ ml/min, this ratio is equal to 1.5.

As the ratio of the gas flow rate to liquid flow rate (while keeping τ_m constant) increases, the length of the gas bubble becomes larger than the size of the liquid slug. Therefore, by expanding the gas bubble, the liquid film around it also becomes longer and with an even larger gas flow rate, at a certain point the flow pattern tends to behave similar to the annular flow. In annular flow, either there is no liquid slug or the amount of liquid slug is very low compared to the gas bubble. Therefore, most of the liquid is carried through the reactor via the liquid film around the gas. As stated earlier, the liquid film receives the most intensive amount of photons. Therefore, it is expected that in this type of flow the conversion in liquid phase is higher than when the ratio of gas flow to liquid flow rate is low or comparable and the flow pattern is closer to Taylor flow rather than annular flow.

To understand the effect of the feed concentration, the same experiments with the similar amount of gas and liquid flow rate have been repeated for 0.5 M of APE and the results are presented in Figure 5.6 (b). Similar to the case with 0.1 M of APE (Fig 5.6 (a)), the APE conversion obtained with single-phase flow is less than for the cases where Taylor flow was applied. Likewise, the data points with $Q_l=0.05$ ml/min, gives a higher conversion compared to the rest. With single-phase flow after 8 min, 20 % conversion is reached, whereas with $Q_l=0.05$ ml/min, after 2 min, already the double amount, 40% of conversion is achieved.

An interesting question is if selectivity changes under new photo-irradiation conditions and at higher conversion (as this is commonly observed. Actually, both the Paternò-Büchi reaction [1] and the photo-Claisen rearrangement are good candidates for it. The first gives rise to regio-, stereo- and site selectivity. Indeed a sharp transition from low to high diastereoselectivity was observed in batch operation [28]. This indicates a distinct switch from singlet to triplet photocycloaddition with different selectivity controlling mechanisms, i.e. what could be termed a novel process windows (NPW).

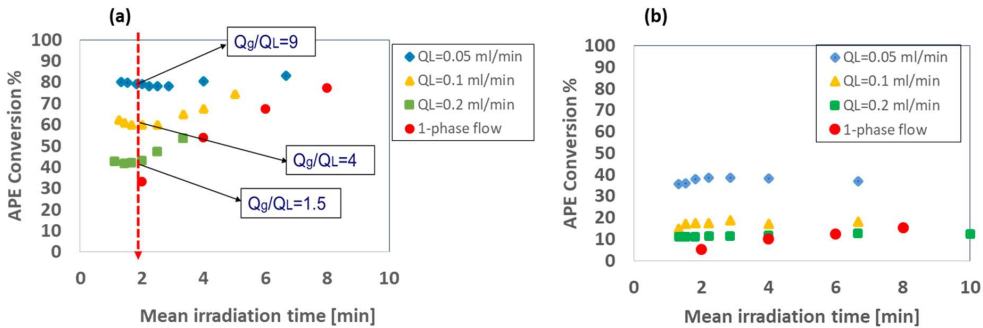


Figure 5.6. APE conversion versus mean irradiation time under Taylor flow conversion and single-phase flow for two APE concentration, (a) 0.1 M APE and (b) 0.5 M APE at room temperature

The photo Claisen rearrangement gives also rise to stereoisomerism and selectivity issue. Two different isomers are formed and phenol as side product.

Yet, the [1] study did not investigate the change of selectivity with increased conversion. Also this study was limited in the determination of selectivity, as the pure isomer compounds were not at hand to allow a calibration and exact quantitative comparison. Yet, what can be stated by comparison of the HPLC spectra under two-phase and one-phase flow conditions that the respective ratios of the peak areas of the two main isomers are practically the same as is the ratio of phenol peak area. Thus, there is a hint for an unchanged selectivity with the conversion boost, and deeper investigations would be desired which re-confirm and deepen that effect.

5.3.3 Light confinement effect in Taylor flow

Maximizing the Taylor flow effect-using refractive index transition at phase interfaces as mirror

Light refraction, caused because of two different phases (or medium), can lead to more light confinement inside the reactor. In order to understand it better, one should compare single-phase flow with segmented flow. In both cases light beams enter the reactor from all angles and since these two cases together are compared, only the differences are considered. Therefore, the light refraction caused by the reactor material is not considered.

If the angle of incidence of the propagating light is larger than a particular angle (critical angle) with respect to the vector normal to the interfacial surface of the media, total internal reflection occurs (Figure 5.7). The critical angle is the angle at which a light beam which strikes the interface with that angle is reflected with 90 degrees, see Figure 5.7 (2). The critical angle is given by Snell's law [29]:

$$n_1 \cdot \sin \theta_1 = n_2 \cdot \sin \theta_2 \quad (5.4)$$

In order to find the critical angle θ_c , it is considered that $\theta_2 = 90$, $\sin 90=1$, therefore

$$\sin \theta_c = \frac{n_2}{n_1} \quad (5.5)$$

For instance, it is considered 1-butanol is medium 1 and nitrogen is medium 2 and their refractive indexes (n) are 1.403 and 1.0003 at $\lambda=589$ nm, respectively [30]. The critical angle for the aforementioned phases is $\theta_c = \sin^{-1} \frac{1}{1.403} = 45.46^\circ$.

Any light beam with an incident angle larger than 45.46° will be totally internally reflected (see Figure 5.7 (3), which means these beams will be confined in the reaction mixture. Comparing this situation with the case that water is used instead of nitrogen the critical angle comes out to be (n_{water} is 1.33 [30]) $\theta_c = \sin^{-1} \frac{1.33}{1.403} = 71.43^\circ$. Since this critical angle is larger than that of the earlier case, the number of beams that are confined inside the reactor is less.

Therefore, it is concluded that applying gas (N_2) instead of water leads to more light confinement and hence nitrogen is more favorable than water.

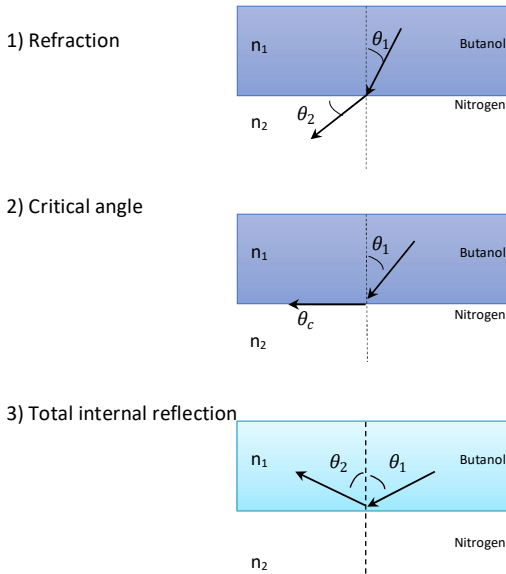


Figure 5.7. Schematic overview of (1) light refraction, (b) critical angle and (c) total internal reflection between two medium of n_1 : 1-butanol and n_2 : N_2

The Taylor micro-flow comprises a gas-liquid interface which causes refraction of the photons entering the microcapillary. Those photons might be lost for the reaction which can be minimized

by a smart reactor engineering. A maximization of photo efficiency has been reported when using a highly reflective aluminum mirrored cylinder in a photo micro-flow reactor [31].

The same mirror effect, reported for reducing losses outside the capillary, can be achieved inside the capillary by fine-tuning the optical properties of gas-liquid interfaces of Taylor micro-flow. In other words, by smartly choosing the continuous and disperse phase in a way that getting more benefits from light confinement effects under Taylor flow condition, it is possible to capture more photons. Aqueous glucose solutions are known to have a higher refraction index as compared to water (1.330 at 589.29 nm) from 1.3477 (10% aqueous glucose solution) to 1.418 (50% aqueous glucose solution) [30].

In order to understand the influence of light confinement on Taylor flow, the photo-Claisen rearrangement experiments were carried out at 0.1 M APE in 1-butanol, considering five cases in which in the first one N₂ was used and in the other 4 experiments, water with different percentages of glucose as the second phase were used. The second phase characteristics including the glucose (%), n and θ_c are presented in Table 5.1. The flow rate of the continuous phase (the slug) considered to be 0.1 ml/min for all the experiments.

Table 5.1. R_f and θ_c of the 2nd phase with respect to 1-butanol at $\lambda=589$ nm [30]

Entry	Second phase (bubble)	Refractive index (n)	θ_c°
1	Nitrogen	1.000	45.46
2	Water	1.333	71.82
3	Water-glucose 10%	1.347	73.757
4	Water-glucose 30%	1.384	80.56
5	Water-glucose 50%	1.418	No internal reflection

Figure 5.8 depicts the results obtained from the aforementioned experiments. In order to minimize the solubility of the organic phase in water, saturated water with 1-butanol was utilized. Solubility of 1-butanol in pure water at room temperature and pressure is 7.7 g/L [32].

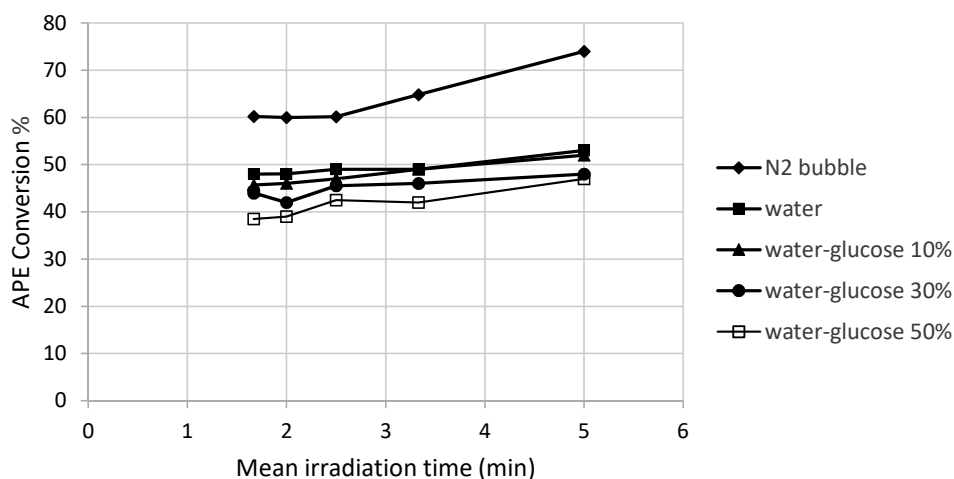


Figure 5.8 APE conversion vs τ_m applying Taylor flow pattern by using different second phase at constant $Q_l=0.1$ ml/min. $[APE]=0.1M$ at room temperature

The results collected in Figure 5.8 as expected clearly show that the APE conversion has the highest value for any τ_m applying N_2 as the second phase having the lowest refractive index as compared to pure water and water with different amount of glucose. Also, water-glucose 50% with the highest refractive index gives the lowest APE conversion. Therefore, it is concluded that applying gas (N_2) instead of water leads to higher conversions than water or aqueous glucose solutions. These results are in line with light confinement effect in Taylor flow. Gas bubbles that have a lower refractive index than liquid droplets can confine more photons inside the reactor and this results in higher reaction conversion.

5.3.4 Taylor flow in MCFI

In contrast to a horizontal or vertical tubular microreactor, the curved microreactor, especially micro coiled flow inverter (MCFI) is known to enhance mixing [33]–[37]. The curved micro channel creates a directional change in the flow advection which causes the unusual advection and augments phase interaction to enhance gas bubble or liquid slug break-up [34]. In MCFI the helical coils of equal lengths are bended at 90° as shown in Figure 5.9 (a). MCFI improves mixing as well and provides a narrow residence time distribution [38], which are mostly due to the reorientation of centrifugal force after each 90° bend. One important factor in MCFI is curvature diameter, D_c , that optimally should be equal to 10 times of capillary diameter, d_h , Equation 5.6 [33].

$$D_c = 10 \times d_h \quad (5.6)$$

The helically curved inverted flow adds a new effect to literature or at least confirms one so far only speculated about. So far, the photo intensification achieved in Taylor flow in a micro-flow reactor, achieved for the Paternò-Büchi reaction, has been solely discussed as an effect of the small liquid layer which interstices at the interface gas bubble and microcapillary wall [22]. This has been thought as the actual reaction volume and the intensification is then due to a reduction of the photo-diffusion path down to 5% and lower. Yet, Taylor flows are known for their intense circulation patterns which cause convection as a mixing mechanism. For a fast photoreaction, a situation may arise where the time constant of reactant delivery to the microcapillary is larger than the time constant of the intrinsic reaction rate, which points to diffusion limitation and to operation at which the observed reaction rates does not obey intrinsic kinetics. Fast convection can constantly refresh the reactant surface layer and therefore eliminate such transfer limitation. In a situation where both the thin-layer and convection photo intensification is present, a way to show that each of those effects are effective is to further intensify them by a method which is known to do so and which is supposed to work only for one of the mechanisms. The use of MCFI and its convection intensification has been deeply investigated previously in our group for liquid-liquid (segmented) micro-flows [35]–[37].

Any effect of a coiled inverted micro-flow would be seen as a sign that convection adds to the thin-layer effect in the photo intensification possible through Taylor flows. An additional effect of the use of helically inverted flows is that they were found to be stable and effective up to a milli-flow scale for liquid-liquid flows. This means that scale-up can be achieved by simple capillary diameter increase and avoiding complex numbering-up strategies and their malfunctions of multi-phase flows.

Assuming that both liquid film thickness and convection play a role in the photo intensification, question is how to control it in order to maximize it. A detailed control can easily fill a whole thesis on its own. Manifold theoretical and experimental relations for the liquid film thickness are at hand; both of Taylor flow or slug flow [25], [39].

In similar manifold manner, the convection inside liquid slug is experimentally and theoretically been described [25], [39].

Such subtle optimization was far out of the scope of this research. Yet, what could be added to literature [1], is that Taylor flow provides a powerful option for photo intensification, and at least convection plays a major role here. This has been confirmed in a semi-quantitative manner by Guenther *et al.* via fluorescence imaging of the mass flows associated.

A similar pragmatic (=without quantitative justification) use of gas-liquid (Taylor) aside liquid-liquid flow showed that this can make a notable difference in product performance [40].

Sebastian *et al.* [41] demonstrated that Taylor flow yielded the smaller and more uniform nanoparticles, and it was explained by the convection effect.

In order to investigate the effect of using MCFI on Taylor flow, photo-Claisen rearrangement of 0.5 M APE in Taylor flow mode were performed, applying two different reactor configurations. The first applied configuration was the so-called capillary tower and the second one is MCFI.

The microreactor diameter is 0.5 mm. Therefore the D_c in MCFI should be equal to 5 mm.

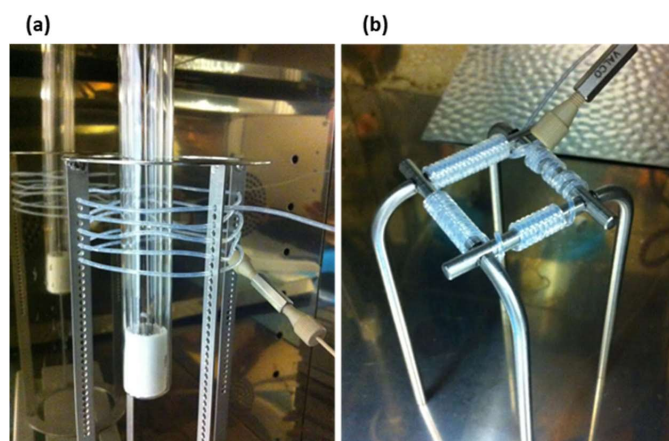


Figure 5.9. Schematic representation of the photo-microreactor by using two configurations: (1) capillary tower, (2) MCFI configuration

The capillary tower diameter (7 cm) compared to the capillary tube diameter (0.5 mm) is quite high, therefore, the curvature effect in capillary tower is negligible in comparison with MCFI (Figure 5.9). As stated before, the experiments were carried out using two phase flow pattern (gas-liquid) and the liquid flow rates were kept constant at 0.1 ml/min. MCFI is supposed to improve mixing behavior mostly in the slugs, therefore in order to weigh the impact of using MCFI in a photoreaction, it was decided to carry out the experiments in the slug flow regime rather than annular flow.

Figure 5.10 presents the results of the APE conversion against the mean irradiation time in the reactors applying Taylor flow carried out in a capillary tower (design 1) and a MCFI (design 2). According to the results, overall, the APE conversion obtained in the MCFI is higher than in the capillary tower configuration. For instance, at $\tau_m=2.8$ min, MCFI design offers 26% conversion while the capillary tower design gives only 18% conversion. Therefore, it can be concluded that applying MCFI with Taylor flow pattern enhance the conversion as compared to the design with less curvature characteristics.

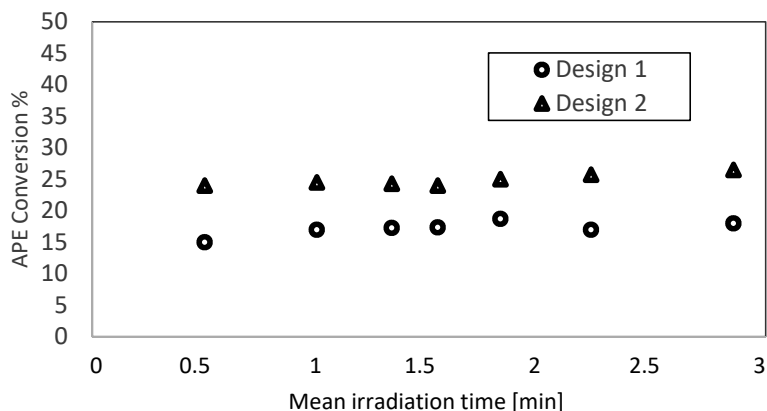


Figure 5.10. APE conversion vs τ_m applying Taylor flow pattern in MCFI (design 2) and capillary tower (design 1) at constant $Q_l=0.1$ ml/min. [APE] = 0.5M

5.4 Conclusion

The segmented flow concept is likely to facilitate the reaction at a higher reactant concentration. We can get higher conversions in smaller exposure times. According to the Lambert-Beer law, a higher concentration leads to lower radiation transmittance. In photochemistry not only the concentration, but also light penetration depth is important. Light penetration in single-phase (liquid) flow is limited to the outer layer close to the reactor wall, while with the segmented flow a more efficient irradiation could be reached. Another important factor is light confinement caused by a difference in refractive indices of the phases in the microreactor. In this chapter, three effects of Taylor flow in photo-microreactor have been studied. This was done by carrying out the photo-Claisen rearrangement of APE in a micro reactor under Taylor flow conditions by applying a chemically inert and immiscible phase, N_2 or aqueous glucose solutions.

Firstly, according to the experimental results, APE conversion under Taylor flow conditions especially at low irradiation times, gives a much higher value than the value obtained at single-phase flow conditions. Also, it has been shown that in the Taylor flow mode, the gas flow to liquid flow rate ratio plays an important role. By increasing this ratio while keeping the irradiation time (τ_m) constant, the APE conversion boosts.

As the ratio of the gas flow rate to liquid flow rate (while keeping τ_m constant) increases, the flow pattern tends to behave similar to the annular flow. In annular flow, the liquid flows inside the reactor as a film around the gas bubbles. The thickness of this film is 5-20% of the reactor diameter and receives the most intensive amount of photons. Therefore, under annular flow conditions the conversion is higher than when the flow pattern is closer to the slug flow. This

effect shows its importance for higher concentration. For instance, for APE 0.5 M, after 2 min irradiation time under Taylor flow condition ($Q_l/Q_g=10$) almost 40% conversion could be obtained while in single-phase flow after 8 min of irradiation time hardly 20% conversion was achievable.

Moreover, it was shown that the light confinement effect can lead to higher APE conversions. This was revealed by performing experiments under Taylor flow conditions and varying the dispersed phase from N_2 to water with different amount of glucose (with different refractive indices). The results indicated that the medium with lower refractive index (N_2) results in much light confinement and therefore to higher APE conversions than for a medium with a higher refractive index (matter with 50% glucose).

Finally, in order to enhance the mixing in the liquid slug, a novel microreactor configuration, MCFI, was tested. The results demonstrate that upon applying a micro coiled flow inverter (MCFI), the APE conversion could be boosted to at least 1.5 time more compared to the capillary tower design (Figure 5.10). This could be due to the better mixing in MCFI which results from the reorientation of centrifugal force after each 90° bend.

It is worth mentioning that, one should notice by applying Taylor flow conditions in photoreactions the conversion increases considerably. However, the throughput of the reactor reduces. This reduction of throughput is because of the lower liquid flow rate as compared to single-phase flow. Nevertheless, with a lower throughput, higher conversions are obtained which is vital. For instance, in some pharmaceutical fields where the active reagent is quite unstable and requires fast conversion. Fast conversion can also avoid unwanted by products that can be formed with longer exposure times. Also, with the Taylor flow concept, smaller amounts of solvent would be used as compared to single-phase flow that is towards the direction of more green chemistry.

At the start of the thesis, the photo intensification by liquid-liquid micro-flow was known as compared to single flow, given at the example of the Paternò-Büchi reaction. This is explained by an effect of the small liquid layer which interstices at the interface gas bubble and microcapillary wall [22]. This investigation

- Confirmed that claim at another common example of a photoreaction
- Extends this investigation, to the use of gas-liquid segmented flow (Taylor flow)
- Thereby allowing a more facile phase separation and a greener reaction (e.g. evidenced by a higher process mass index; being virtually the same as for the single-phase reaction)
- Gives evidence for the intensification being caused by joint creation of a thin liquid layer around the gas bubble and the usage of a recirculation vortex in the liquid slugs, while [22] only discusses the first.

- Uses a tailoring of the refraction index by adding a second liquid phase to improve the utilization of the photons which enter and to decrease the losses by diffraction ('internal mirroring')
- Introduces the use of coiled inverted micro-flow as a further intensification option and explains that through the increased effect of convection.
- Gives a hint that the selectivity between the isomers is not changed, while [22] does not discuss the selectivity issue.

5.5 References

- [1] M. Nakano, Y. Nishiyama, H. Tanimoto, T. Morimoto, and K. Kakiuchi, "Remarkable Improvement of Organic Photoreaction Efficiency in the Flow Microreactor by the Slug Flow Condition Using Water," *Org. Process Res. Dev.*, 2016.
- [2] D. M. Schultz and T. P. Yoon, "Solar synthesis: Prospects in visible light photocatalysis," *Science*. 2014.
- [3] J. Xuan and W. J. Xiao, "Visible-light photoredox catalysis," *Angewandte Chemie - International Edition*. 2012.
- [4] C. K. Prier, D. A. Rankic, and D. W. C. MacMillan, "Visible Light Photoredox Catalysis with Transition Metal Complexes: Applications in Organic Synthesis," *Chem. Rev.*, 2013.
- [5] R. A. Angnes, Z. Li, C. R. D. Correia, and G. B. Hammond, "Recent synthetic additions to the visible light photoredox catalysis toolbox," *Organic and Biomolecular Chemistry*. 2015.
- [6] T. P. Yoon, M. A. Ischay, and J. Du, "Visible light photocatalysis as a greener approach to photochemical synthesis," *Nat. Chem.*, 2010.
- [7] J. Xuan, X.-D. Jia, L.-P. Jiang, E. S. Abdel-Halim, and J.-J. Zhu, "Gold nanoparticle-assembled capsules and their application as hydrogen peroxide biosensor based on hemoglobin.," *Bioelectrochemistry Amsterdam Netherlands*, vol. 84, pp. 32–7, 2012.
- [8] H.-H. Perkampus, *UV-VIS Spectroscopy and Its Applications*. 1992.
- [9] J. P. Knowles, L. D. Elliott, and K. I. Booker-Milburn, "Flow photochemistry: Old light through new windows," *Beilstein Journal of Organic Chemistry*, vol. 8. pp. 2025–2052, 2012.
- [10] D. Cambié, C. Bottecchia, N. J. W. Straathof, V. Hessel, and T. Noël, "Applications of Continuous-Flow Photochemistry in Organic Synthesis, Material Science, and Water Treatment," *Chem. Rev.*
- [11] Y. Su, K. Kuijpers, V. Hessel, and T. Noël, "A convenient numbering-up strategy for the scale-up of gas–liquid photoredox catalysis in flow," *React. Chem. Eng.*, vol. 1, no. 1, pp. 73–81, 2016.
- [12] E. Shahbazali, T. Noel, and H. Volker, "Photo-claisen rearrangement of allyl phenyl ether in micro-flow: influence of phenyl core substituents and vision on orthogonality," *J. Flow Chem.*, vol. 6, no. 3, pp. 252–259, 2016.
- [13] Y. Matsushita *et al.*, "Recent progress on photoreactions in microreactors," *Pure Appl. Chem.*, 2007.
- [14] E. E. Coyle and M. Oelgemöller, "Micro-photochemistry: Photochemistry in microstructured reactors. The new photochemistry of the future?," *Photochemical and Photobiological Sciences*. 2008.
- [15] Y. Su, N. J. W. Straathof, V. Hessel, and T. Noël, "Photochemical transformations accelerated in continuous-flow reactors: Basic concepts and applications," *Chemistry - A European Journal*, vol. 20, no. 34. pp. 10562–10589, 2014.
- [16] R. C. R. Wootton, R. Fortt, and A. J. De Mello, "A microfabricated nanoreactor for safe, continuous generation and use of singlet oxygen," *Org. Process Res. Dev.*, 2002.
- [17] F. Lévesque and P. H. Seeberger, "Highly efficient continuous flow reactions using singlet oxygen as a 'Green' reagent," *Org. Lett.*, 2011.
- [18] A. Yavorsky, O. Shvydkiv, C. Limburg, K. Nolan, Y. M. C. Delauré, and M. Oelgemöller, "Photooxygenations in a bubble column reactor," *Green Chem.*, 2012.

- [19] F. Lévesque and P. H. Seeberger, "Continuous-flow synthesis of the anti-malaria drug artemisinin," *Angew. Chemie - Int. Ed.*, 2012.
- [20] C. J. Mallia and I. R. Baxendale, "The Use of Gases in Flow Synthesis," *Organic Process Research and Development*. 2016.
- [21] T. Noël and V. Hessel, "Membrane microreactors: Gas-liquid reactions made easy," *ChemSusChem*, 2013.
- [22] A. Yavorsky, O. Shvydkiv, N. Hoffmann, K. Nolan, and M. Oelgemöller, "Parallel microflow photochemistry: Process optimization, scale-up, and library synthesis," *Org. Lett.*, 2012.
- [23] D. Cambié, C. Bottecchia, N. J. W. Straathof, V. Hessel, and T. Noël, "Applications of Continuous-Flow Photochemistry in Organic Synthesis, Material Science, and Water Treatment," *Chemical Reviews*, vol. 116, no. 17. pp. 10276–10341, 2016.
- [24] V. S. Ajaev and G. M. Homsy, "MODELING SHAPES AND DYNAMICS OF CONFINED BUBBLES," *Annu. Rev. Fluid Mech.*, 2006.
- [25] P. Angeli and A. Gavriilidis, "Hydrodynamics of Taylor flow in small channels: A review," in *Proceedings of the Institution of Mechanical Engineers, Part C: Journal of Mechanical Engineering Science*, 2008.
- [26] K. Wang, L. Li, P. Xie, and G. Luo, "Liquid-liquid microflow reaction engineering," *Reaction Chemistry and Engineering*. 2017.
- [27] K. Wang and G. Luo, "Microflow extraction: A review of recent development," *Chem. Eng. Sci.*, 2017.
- [28] S. Bondock, "Mechanism and Synthetic Use of Paternò-Büchi Reactions: Spin-Mapping and Photo-Aldol Reactions," Universität zu Köln, 2003.
- [29] R. L. Sutherland, "Handbook of Nonlinear Optics," *Opt. Eng.*, 1997.
- [30] D. R. Lide, "CRC Handbook of Chemistry and Physics, 84th Edition, 2003-2004," *Handb. Chem. Phys.*, 2003.
- [31] B. Shen, M. W. Bedore, A. Sniady, and T. F. Jamison, "Continuous flow photocatalysis enhanced using an aluminum mirror: Rapid and selective synthesis of 2'-deoxy and 2',3'-dideoxynucleosides," *Chem. Commun.*, 2012.
- [32] I. M. Roberts, "Iso-butanol saturated water: A simple procedure for increasing staining intensity of resin sections for light and electron microscopy," *J. Microsc.*, 2002.
- [33] J. Singh, N. Kockmann, and K. D. P. Nigam, "Novel three-dimensional microfluidic device for process intensification," *Chem. Eng. Process. Process Intensif.*, 2014.
- [34] D. M. Kirpalani, T. Patel, P. Mehrani, and A. Macchi, "Experimental analysis of the unit cell approach for two-phase flow dynamics in curved flow channels," *Int. J. Heat Mass Transf.*, 2008.
- [35] P. Rojahn, V. Hessel, K. D. P. Nigam, and F. Schael, "Applicability of the axial dispersion model to coiled flow inverters containing single liquid phase and segmented liquid-liquid flows," *Chem. Eng. Sci.*, 2018.
- [36] I. Vural Gürsel *et al.*, "Utilization of milli-scale coiled flow inverter in combination with phase separator for continuous flow liquid-liquid extraction processes," *Chem. Eng. J.*, 2016.
- [37] S. K. Kurt, I. Vural Gürsel, V. Hessel, K. D. P. Nigam, and N. Kockmann, "Liquid-liquid extraction system with microstructured coiled flow inverter and other capillary setups for single-stage extraction

applications," *Chem. Eng. J.*, 2016.

- [38] A. K. Saxena and K. D. P. Nigam, "Coiled configuration for flow inversion and its effect on residence time distribution," *AIChE J.*, 1984.
- [39] M. Mac Giolla Eain, V. Egan, and J. Punch, "Film thickness measurements in liquid-liquid slug flow regimes," *Int. J. Heat Fluid Flow*, 2013.
- [40] A. Günther, S. A. Khan, M. Thalmann, F. Trachsel, and K. F. Jensen, "Transport and reaction in microscale segmented gas-liquid flow," *Lab Chip*, 2004.
- [41] V. Sebastian Cabeza, S. Kuhn, A. A. Kulkarni, and K. F. Jensen, "Size-controlled flow synthesis of gold nanoparticles using a segmented flow microfluidic platform," *Langmuir*, 2012.

5.6 Supplementary Material

S.1. General reagent information

Allyl phenyl ether, 1-butanol, D-(+)-glucose were purchased from Sigma-Aldrich chemical company and used as received. For the flow experiment, solutions were prepared in volumetric flasks. The solvent purity were all according to HPLC grade (>95%). Ultrapure water (HPLC grade, 18.2 M Ω at 25°C) was used.

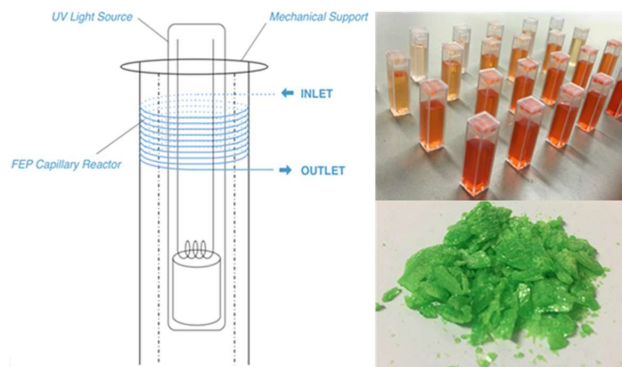
S.2. General analysis information

The samples were analyzed via HPLC. HPLC analyses were performed on Shimadzu UFLCXR (205 nm) using a GraceSmart RP 18 5u column (150 mm, 4.2 mm). 1,3 dinitrobenzene was used as an internal standard to carry out HPLC quantification in Claisen rearrangement of allyl phenyl ether.

The samples related to transmittance diagram were analyzed by making use of a UV/VIS spectrophotometer (Shimadzu UV-2501PC Spectrophotometer).

CHAPTER 6

UV-Photo Flow: Photostatistics-Actinometry Measurements in Flow



Abstract

The rescaling of reactors from conventional batch processes towards micrometer dimensions has proven to be beneficial in the field of organic chemistry. In the case of photochemical reactions, the reduced dimensions allow an increase in the efficiency of light penetration which eventually will influence the overall efficiency of the process. Although the characteristics of microreactors for photo-conversions are well known and reported, the quantification of reaction quantum yields is still a challenging topic.

Three different configurations of the micro reactor with respect to the light source, were considered (being applied in the work reported in this thesis). The capillary tower, Coil Flow Inversion (CFI) and the wound microreactor around the UV-lamp are characterized as these were irradiated by a monochromatic UV light source. Determination of photon fluxes (einstein s^{-1}) was carried out by making use of chemical ferrioxalate actinometry where the actinometer conversion with respect to the light absorption is evaluated. It has been found that the photon flux increases as follows;

$$\langle q_{p,\lambda} \rangle_{\text{capil.}} = 5.7 \times 10^{-9} \text{einstein} \cdot \text{s}^{-1} \leq \langle q_{p,\lambda} \rangle_{\text{CFI}} = 6.2 \times 10^{-9} \text{einstein} \cdot \text{s}^{-1} \\ < \langle q_{p,\lambda} \rangle_{\text{around The Lamp}} = 19 \times 10^{-9} \text{einstein} \cdot \text{s}^{-1}$$

As the photon flux is connected to the system setup, the overall reaction quantum yield of any other reaction can be calculated. The performance of each configuration in terms of photon flux efficiency was tested by determination of the photon flux. According to the results where reactor is wound around the lamp shows the highest amount of photon flux. Comparing CFI with the capillary tower, as a consequence of the intensified mixing pattern, slightly higher photon flux has been observed for the CFI as compared with the capillary tower.

6.1 Introduction

Using photons as reaction stimuli opens up a new world of complex structures[1] which can be challenging to be obtained by conventional thermal conditions. Despite this, industry has not embraced these principles yet, mainly because of the low light efficiency of the traditional batch reactors. Also, in these batch processes, due to the large reaction volume involved, intensive mixing and heating are necessary in order to reach perfect mixing. Additionally, handling large volumes of solvents/mixtures makes severe safety regulations. These operations/regulations are time consuming and will increase the processing time.

As an alternative, the use of microreactor technology overcomes many of these obstacles. To accelerate the industrial application of photochemical reactions carried out in flow, the understanding of photochemical reaction mechanisms, the emission spectrum of the light source and the photon flux absorbed by the reaction mixture are required. This could help to realize reproducible operation and reliability of the photoreactions in continuous mode [2].

The combination of photochemical reactions and micro-flow technology has been widely investigated [1], [3]–[7]. The micro-dimensions will ensure efficient light penetration, even for concentrated solutions. With that, one of the major drawbacks of traditional photo-induced processes can be overcome. In these conditions, the radiative and convective transfer phenomena are essential and have to be with the reaction kinetics.

In order to be able to compare different experimental setups, to optimize reaction conditions or to model the reactor system, it is necessary to determine the interaction between the light source and the reactor. A criterion used for this purpose can be expressed as the amount of photons received by the capillary reactor, also known as the photon flux (einstein s^{-1}). Estimations of this parameter can be done by modelling [8] or from characteristics of the light source [9]. Since the photon flux is not only depending on the light source, but also on the configuration of the microreactor with respect to the lamp and the optical properties of the reactor material, an alternative method is required for accurate determination of the photon flux. In traditional batch photo-reactors, this can be done by using radiometers [10]. As the dimensions of microsystems prohibit the usage of these, it is advised to make use of chemical actinometers to determine photon fluxes.

This chapter aims at establishing a procedure for actinometric measurements in a micro-flow system. In a first step, the emission spectrum of the light source is measured and characterized. Various configurations of the microreactors that are applied in the work reported in this thesis are considered and corresponding photon fluxes are determined. Also, the conversion of the actinometer as a function of residence time is evaluated.

6.2 Theoretical description

6.2.1 Actinometry: Concept & experimental setup

The predominant challenge in photochemistry is the determination of the reaction quantum yield. This parameter is defined as the number of molecules that undergoes a certain event per photon absorbed in the system [11]:

The quantum yield denotes the ratio between the number of molecules converted or formed and the number of absorbed photons of a certain wavelength in the same period of time.

$$\varphi_{\lambda} = \frac{\text{amount of molecules (moles) converted or formed}}{\text{amount of photons (einstein) of radiation absorbed}} \quad (6.1)$$

The Equation 6.1 shows that in case one molecule is generated from the absorption of one photon, the quantum yield will be equal to unity. Quantum yield values often differ from one. Values much larger than one reflect the occurrence of a chain reaction. On the other hand, values smaller than one indicate a non-chain mechanism. Intrinsically the rate of photochemical reactions is affected by the intensity of the light source. Quantification of the intensity, expressed as the number of photons per unit of time, can be accomplished by making use of actinometers.

The numerator in the expression of quantum yield is being determined by standard analytical techniques that evaluate the conversion of the starting reagent. By applying actinometers, it is possible to gain knowledge about the number of active photons in a reaction system.

Chemical actinometers undergo photo-induced reactions where the conversion is directly correlated to the number of photons absorbed. The important feature in these methods lies in the accurate knowledge of the quantum yield of the actinometer considered. This provides an approach to determine the number of photons absorbed in the system, a parameter also known as the photon flux (einstein s⁻¹).

The requirements for a chemical actinometer are defined by IUPAC [11] as:

- The system considered should be simple and well-studied
- The photo reaction must be reproducible under well-defined and easily controllable conditions
- Accurate knowledge of quantum yields for a large number of wavelengths
- Preferably applicable in a wide spectral range and wavelength independent quantum yields in that range
- Thermal stability of the components to avoid dark reactions
- Simple analytical procedures
- The system should show large sensitivity
- Handling the system and the evaluation of the photon flux should be simple and straightforward

- The actinometer should easily be synthesized and purified, preferably be commercially available

Data concerning the available actinometer systems are accessible in literature [11]. The majority of actinometers are available in the liquid state. And amongst them, only some of them are well established and are applied for several years. A list of these well-established actinometers is shown in Table 6.1.

As mentioned earlier, the parameter of interest whilst doing these experiments is the photon flux, expressed in units einstein per second. This is a property correlated to a specific reaction system (position of the reactor compared to the lamp) and is fixed for any other photochemical reaction taking place in the same system. Subsequently, it is feasible to determine the quantum yield of the photoreaction of interest, since both the conversion of the initial compound as well as the photon flux are known.

Table 6.1. Overview of well-established actinometers [12]

	Name	Wavelength range (nm)
<i>Gas - phase</i>	Dinitrogen oxide	147 – 210
	Hydrogen bromide	170 – 255
	photolysis	
	Acetone photolysis	250 – 320
	Pentane-3-one	250 – 320
<i>Liquid - phase</i>	photolysis	
	<i>cis</i> -Cyclooctene	185
	Ethanol photolysis	185
	Uranyl oxalate	200 – 500
	Uridine	216 – 280
	photohydration	
	Azobenzene	230 – 460
Potassium ferrioxalate	254 – 500	

The most widely used and accepted chemical actinometer is potassium ferrioxalate, which is also known as the Hatchard and Parker actinometer [13] and often being referred to as ferrioxalate (FeOx). As stated in Table 6.1, the absorption range stretches out from the middle ultra violet region up to approximately halfway the visible spectrum. Part of this spectrum is given in Figure 6.16.1. As a consequence of the absorption range and the sensitivity of the actinometer, all ambient daylight and room lightning should be excluded in order to detect only photons originating from the light source. This requirement is fulfilled when working in a darkroom with the use of a desk lamp covered with UV-protection foil, so that $\lambda \geq 500\text{nm}$, for photons emitted by the desk lamp.

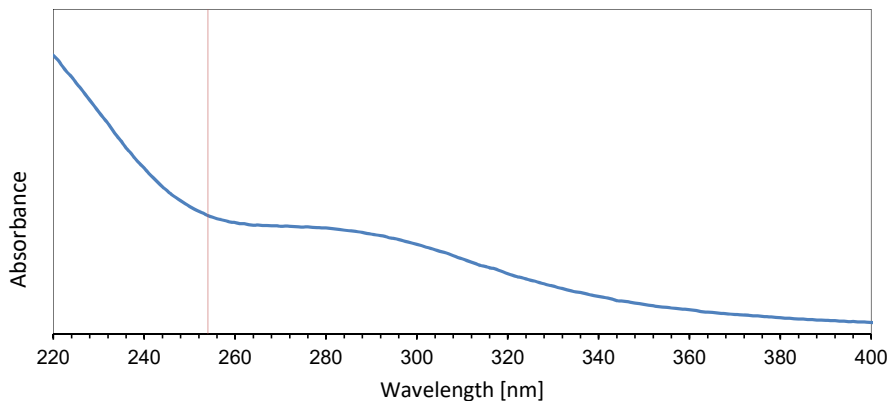
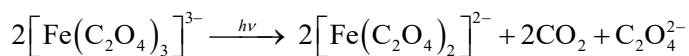


Figure 6.1. Absorption spectrum of the ferrioxalate actinometer in 0.2N H₂SO₄ at 254nm. $\epsilon_{\text{Fe(III)}-254\text{nm}} = 3698 \text{ M}^{-1}\text{cm}^{-1}$

Under the influence of incident light, the ferrioxalate actinometer undergoes a redox reaction where the ferric ions in solution will be reduced to ferrous ions. Simultaneously, one oxalate ligand undergoes an oxidation to form carbon dioxide. The overall reaction is represented in Scheme 6.1.



Scheme 6.1. Reduction of ferrioxalate with the production of ferrous ions

As the incident photons are used as reagents, exposing the actinometer longer to these photons will increase the conversion of iron(III) to iron(II). Conversion not only depends on the amount of photons absorbed but also on the initial concentration of the actinometer, as well as on the quantum yield. For many years, the quantum yield of the actinometer was assumed to be 1.25 [11], [13]. But in the recent couple of years, radiometers have become more accurate and higher values have been reported, i.e. 1.40 [14]. The value chosen here is based on the one reported most recently in literature; 1.38 [15].

In order to determine the photon flux by using ferrioxalate actinometer, the time dependent conversion of iron(III) is evaluated. This conversion is assessed by complexation of the generated iron(II) with a ligand added as 1,10-phenanthroline to the system after irradiation. This iron-phenanthroline complex, known as ferroin, is quantified by measuring its absorption using UV/VIS spectroscopy. Figure 6.2 clearly shows that the maximum absorption peak of this complex lies at wavelengths considerably larger than those where the reduction of iron takes place.

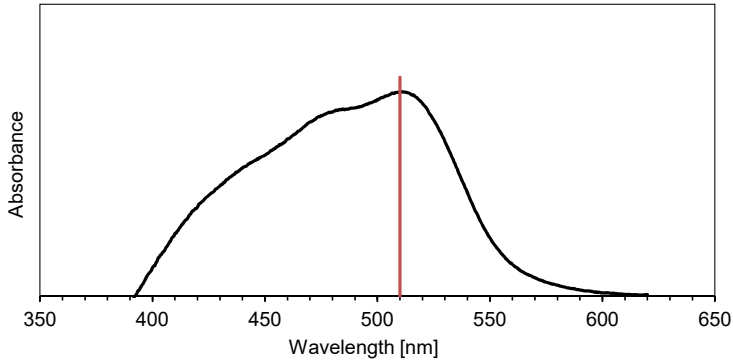
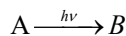


Figure 6.2. Absorption spectrum for ferrioxalate with a maximal absorption at 510nm with $\varepsilon_{\text{Fe(II)}-510} = 11639 \text{ M}^{-1}\text{cm}^{-1}$

Besides these features, the use of this actinometer has a few complications. The actinometer on itself suffers from a low solubility in water and from the precipitation of ferrous oxalate after irradiation. Additionally, the conversion also involves the production of carbon dioxide gas bubbles. When these complications play a significant role, the hydrodynamics in the system will be disturbed and eventually will lead to clogging of the reactor. This should be avoided, especially when working with micro-scale reactors. Therefore, the ferrioxalate actinometer as well as the consecutive complexation of Fe (II) with 1,10-phenanthroline should be operated at low conversions.

6.2.2 Theoretical description photon flux

The photoreduction reaction of the actinometer represented in Scheme 6.1 can be summarized as



The concentration of component B will be measured by using UV/VIS spectrophotometry. The absorption at $\lambda=510 \text{ nm}$ will be linked to the conversion of this reaction. After calibration of the spectrophotometer, concentration of the Fe(II) phenanthroline complex (component B) is determined by using the Lambert-Beer law.

$$C_{\text{Fe(II)}} = A_{510\text{nm}} \frac{1}{\varepsilon_{\lambda} l} \quad (6.2)$$

The conversion is defined as

$$X = \frac{C_{\text{Fe(II)}}}{C_{\text{Fe(III)}}^0} = \frac{1}{C_{\text{Fe(III)}}^0} A_{510\text{nm}} \frac{1}{\varepsilon_{\lambda} l} \quad (6.3)$$

Here, l is the optical path length and ε_λ is the Napierian molar absorption coefficient ($\text{Lmol}^{-1}\text{cm}^{-1}$) of compound A (refer to Equation 6.6).

The mass balance of component A (ferrioxalate) over a slice of a tubular reactor with plug flow, Equation 6.4, associates the conversion of component A directly to the quantum yield (mol einstein^{-1}) of the reaction and at the same time to the mean absorbed photon flux density, $\langle L_{p,\lambda}^a \rangle$, ($\text{einstein m}^{-3}\text{s}^{-1}$). Both parameters being dependent on the considered wavelength, λ .

$$-\frac{dC_A}{d\tau} = \varphi_\lambda \langle L_{p,\lambda}^a \rangle \quad (6.4)$$

Where

$$\langle L_{p,\lambda}^a \rangle = \frac{\langle q_{p,\lambda} \rangle}{V_r} f_\lambda \quad (6.5)$$

The mean photon flux density can be correlated to the photon flux, $q_{p,\lambda}$, by normalization with the reactor volume, V_r . Additionally, a correction has to be included in this expression since only a fraction of the light will be absorbed. This absorbed fraction, f_λ is given in expression 6.7 and follows from the Lambert-Beer law, Equation 6.6.

$$A = \varepsilon_\lambda C_A l \quad (6.6)$$

$$f_\lambda = 1 - e^{-A} = 1 - e^{-\varepsilon_\lambda C_A l} \quad (6.7)$$

where A_e is defined as the Napierian absorbance.

Substitution of the Equations 6.5 and 6.7 into the general mass balance of the model, equation 6.4, results in:

$$-\frac{dC_A}{dt} = \varphi_\lambda \langle L_{p,\lambda}^a \rangle = \varphi_\lambda \frac{\langle q_{p,\lambda} \rangle}{V_r} f_\lambda = \varphi_\lambda \frac{\langle q_{p,\lambda} \rangle}{V_r} (1 - e^{-\varepsilon_\lambda C_A l}) \quad (6.8)$$

After rearrangement and addition of the boundary conditions, the following integral is defined

$$\int_{C_A^0}^{C_A} \frac{dC_A}{1 - e^{-\varepsilon_\lambda C_A l}} = \varphi_\lambda \frac{\langle q_{p,\lambda} \rangle}{V_r} \int_0^\tau d\tau \quad (6.9)$$

After solving the integral and substitution for the conversion, Equation 6.9 is formulated as:

$$\left(\varphi_\lambda \frac{\langle q_{p,\lambda} \rangle}{V_r} \right) \tau = C_A^0 X + \frac{1}{\varepsilon_\lambda l} \ln \left[\frac{1 - e^{-\varepsilon_\lambda C_A^0 l}}{1 - e^{-\varepsilon_\lambda C_A^0 (1-X) l}} \right] \quad (6.10)$$

and

$$C_A = C_A^0 (1 - X) \quad (6.11)$$

The Lambert-Beer law directly shows its benefits with the use of microreactors. The law gives a direct relation of the absorbance with the concentration and the optical pathway (Equation 6.6).

In case the reaction conditions require high concentrations of a compound, the effective absorption can be established by the use of small (micro-level) reaction pathways. The small dimensions ensure a better penetration depth perpendicular to flow, i.e. in the radial direction of the capillary.

6.3 Experimental section

6.3.1 Reactor configurations

There are three configurationally different continuous flow microreactors used in the work reported in this thesis. All of them include the winding of a capillary around a mechanical support. The first one is being characterized as a capillary tower (CT) (Figure (left)) and has been used in several studies before. This model includes the single pass winding around a mechanic support. A photograph of this system is shown in Figure (right). The light source is placed in the middle of this structure in a way that the entire reactor is directly exposed to direct incident light. This configuration is the mostly-used reactor set-up in this thesis.

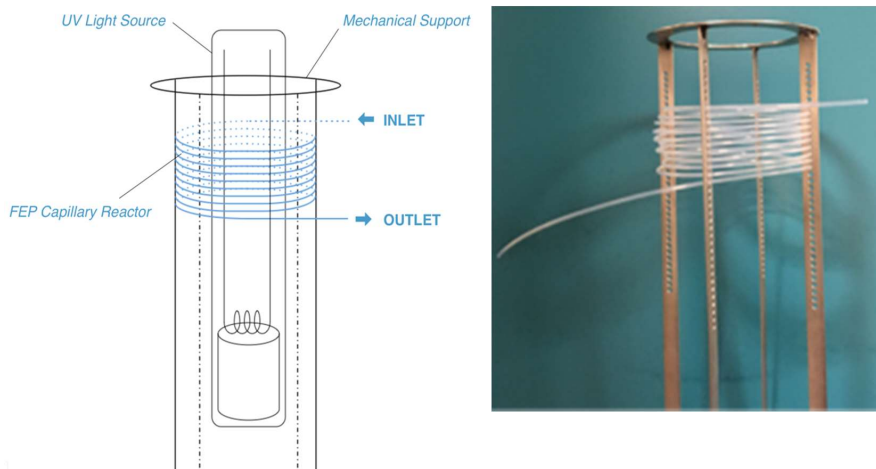


Figure 6.3. Reactor configuration where the picture on the left hand side is a schematic representation of the capillary tower consisting and designating the various components. The picture on the right hand side represents the actual capillary reactor wound around a mechanical support.

The second configuration of interest relies on a tighter winding of the capillary reactor around a square support, creating a coil flow inverter (CFI) (Figure). The loops considered will have a

reduced diameter, as compared to the capillary tower. Subsequently, the cubic nature of the support will initiate directional changes of 90° . The combination of these features results in improved mixing of the solution passing the system. This configuration has been applied in chapter 5.

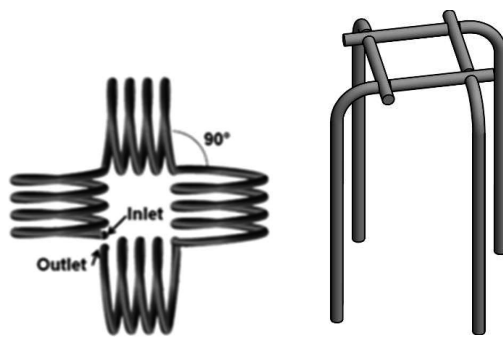


Figure 6.4. Model of the coil flow inverter reactor configuration. Reprinted with permission from Parida *et al.*[16]. Copyright © 2014 American Chemical Society.

The last considered configuration is the capillary tube wound directly on the wall of the UV-lamp. This configuration has been tested in chapter 4.

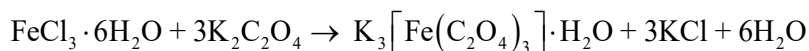
Due to the sensitivity of the system towards light and the aim to obtain accurate and reliable results, additional requirements are set. As daylight and lighting are present in an everyday laboratory environment, the setup has been moved to a darkroom. The addition of a safety light is mandatory in order to be able to perform the experiments. Preferentially, the emission spectrum of this safety lamp lies beyond the absorption spectrum of the actinometer. To ensure this, an ordinary desk lamp is covered with UV protection foil (Kapton® K6338A – Lohmann Technologies) so that emission lies above 500nm. It is important for the operator to shield the UV-lamp as it may cause health issues. This has been done by covering up the system with thick black paper.

6.3.2 Actinometer Synthesis

The active complex is obtained by synthesizing the corresponding ferrioxalate crystals, as shown in Scheme 6.2. Hereby 50 – 60g (~ 0.3-0.36 mole) of potassium oxalate is dissolved in purified water. At the same time, in another beaker, around 25g (~ 0.09-0.1 mole) of Iron (III) chloride Hexahydrate is dissolved in purified water. As the stoichiometry represents, one mole-equivalent

of iron chloride is used with 3 mole-equivalents of potassium oxalate. In order to increase the solubility of the compounds, both mixtures were heated on a hotplate.

As soon as all components are dissolved, the two solutions are carefully mixed and removed from the heat source in order to cool to room temperature. Additional cooling resulted from placing the mixture in an ice bath for 15min. In this way, a precipitate is formed and crystals are able to be formed and allowed to grow. The ions formed during synthesis can disturb the photoreaction in the reactor and therefore influence the outcome. By recrystallizing (using water as solvent) the crystals, impurities are reduced.



Scheme 6.2. Reaction representation of the formation of the photoactive potassium ferrioxalate actinometer using iron(III)chloride Hexahydrate and potassium oxalate

After three times recrystallization, the formed crystals were filtered and washed with cold water. Where after, they were left to dry overnight in an oven at 50°C. Once the crystals are dry, they are kept in vials all together and shielded from direct light.

The actinometer solution is prepared by dissolving the appropriate amount of crystals in 0.1M H₂SO₄. These solutions shielded for any light by covering them up with alumina foil.

General reagent information, Post-irradiation treatment, Continuous flow system, Characterization:
See supplementary material

6.4 Results & discussion

6.4.1 Ferrioxalate synthesis

Potassium ferrioxalate is produced as reported in the experimental section. The final form of these crystals is presented in Figure6.5.



Figure 6.5. The green ferrioxalate crystals as obtained after synthesis and three times recrystallization.

6.4.2 Light source

The selection of ferrioxalate as the actinometer applied in this system relies on its activity in the UV-region[17] as indicated in Table 6.1. The emission spectrum of the UV-lamp, is presented in Figure6.6.

The peaks in this spectrum correspond to the radiant transitions within mercury[18]. Although, this shows that the lamp should be interpreted as a polychromatic source, the main peak around 254nm is the only one of interest. The consideration was made to eliminate all photons with wavelengths higher than 400nm. However, due to limited transmission and geometrical challenges, this has been renounced. In further experiments and calculations, the lamp considered to be a monochromatic source.

An additional light source, safety lamp is present in the darkroom. Its emission spectrum only starts around 550nm and higher; it will not interfere with the photons originating from the main light source.

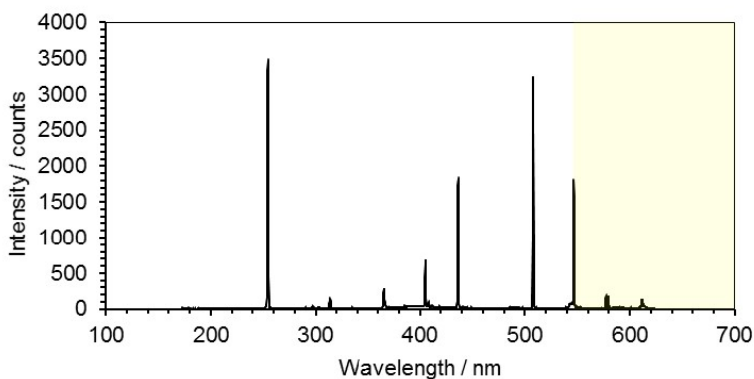


Figure 6.6. Emission spectrum (black) of the 3.5W germicidal UV-source. The light yellow area indicates the emission range of the safety lamp.

6.4.3 Results & discussion for the three configurations

Capillary Tower

The first case considers the reactor wound around the mechanical support. Within the range of 1.25 and 2.25 seconds residence time, conversion of ferrioxalate is linearly increasing. In order to evaluate the stability/reproducibility of the system, multiple experiments, from the same FeOx-stock solution, were done over a timespan of several days. Absorption values for the ferrioxalate complex were converted to Fe(III)-conversions by using Equation 6.3. The results are given in Figure 6.7. Figure 6.7 (a) and show an excellent reproducibility. Note that the error bars in the plot are

within the size of the markers. In contrast to what literature reports, the experiments didn't show deviations from earlier results due to reaction of the stock solution. Furthermore, the conversions in this region meet the requirement by exceeding 10% conversion.

This reproducibility is considered to be applicable for all the discussed configurations of the microreactor with respect to the lamp.

The determination of the photon flux for the conversion values presented in Figure 6.7 (b), is given by Equation 6.10.

Photon flux received can then be calculated by plotting the whole right hand side of equation 6.10 against the residence time. From the slope of Figure 6.7 (b), photon flux can be determined.

$$\left(\varphi_{\lambda} \frac{\langle q_{p,\lambda} \rangle}{V_r} \right) \tau = C_A^0 X + \frac{1}{\varepsilon_{\lambda} l} \ln \left[\frac{1 - e^{-\varepsilon_{\lambda} C_A^0 l}}{1 - e^{-\varepsilon_{\lambda} C_A^0 (1-X) l}} \right] \quad (6.10)$$

$$\langle q_{p,\lambda} \rangle = \frac{3.24 \times 10^{-5} \text{ mol}_{pr} \cdot \text{s}^{-1} \cdot \text{L}^{-1} \times 2.5 \times 10^{-4} \text{ L}}{1.38 \text{ mol}_{pr} \cdot \text{einstein}^{-1}} \approx 5.7 \times 10^{-9} \text{ einstein} \cdot \text{s}^{-1}$$

where subscript "Pr" refers to products

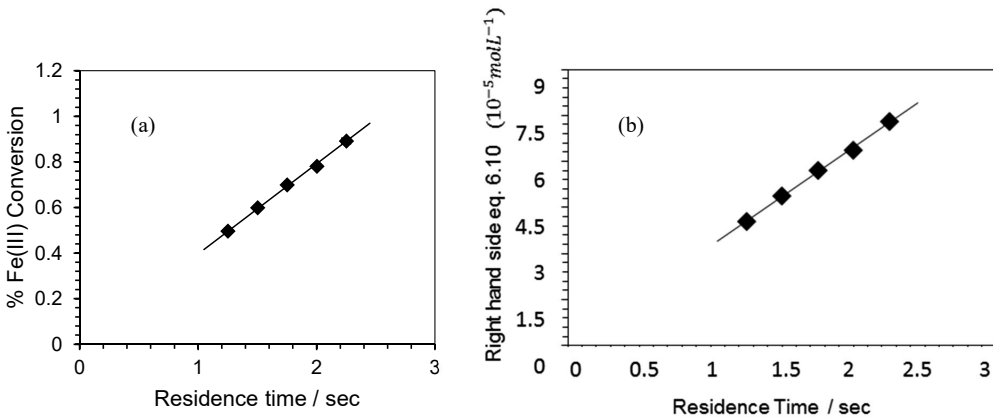


Figure 6.71. (a) Conversion of Fe(III) to Fe(II) as a function of residence time. The two parameters show off a linear dependency. $C_{\text{FeOx}}^0 \approx 5 \times 10^{-3} \text{ M}$, $R^2 = 0.99$ (b) Plotting of the right hand side of equation 6.10 against their corresponding residence time. $R^2 = 0.99$, $Y = 3.24 \times 10^{-5} X$

By repeating the experiment for multiple times, with the same initial FeOx-solution and determining the value of the received photon flux, eventually, it is possible to report an average value for the photon flux. It is given by the dotted line in Figure 6.8.

$$\langle q_{p,\lambda} \rangle = (5.78 \pm 0.08) \times 10^{-9} \text{ einstein} \cdot \text{s}^{-1}$$

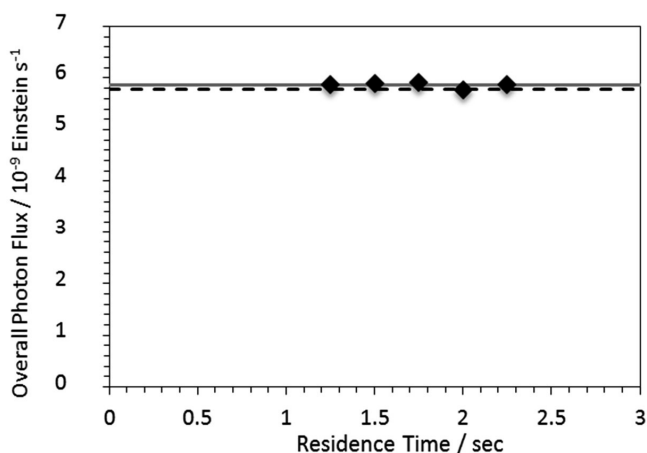


Figure 6.8. The individual conversions per residence time give an alternative way of calculating the photon flux. The full grey line is the average calculated by the individual points. As for the data points, these are calculated from the slopes when the right hand side of equation 6.10 is plotted against the residence time. The dotted black line is the average pulled through these latter points.

An alternative route, but based on the same equation, can generate comparable photon flux values. This is proposed by considering several experiments with the same residence time range. These residence times, together with the corresponding conversion are substituted in equation 6.10 which will end up giving a value for the photon flux for that specific residence time. So when this method is applied on the identical experiments as before, an average photon flux per residence time can be reported which are indicated as data points in Figure 6.8. The grey line in the same figure gives the average over these values. In the continuing discussion, this is appointed as the overall photon flux.

The error range on these data points is so minimal that they fall within the symbol. Eventually, the average of these photon fluxes is labelled as the photon flux, see Table 6.2.

Table 6.2. The average photon fluxes based on residence time

τ [s]	$\langle q_{p,\lambda} \rangle$ [10^{-9} <i>einstein</i> . s^{-1}]
1.25	5.87
1.5	5.78
1.75	5.92
2	5.91
2.25	5.87

According to the Lambert-Beer law, optimal absorption conditions can be quantified by changing the initial ferrioxalate concentration. Therefore, the amount of light absorbed will change with

the concentration as it is assumed that the light source is a constant emitter during all experiments.

This concept was investigated and the outcome is given in Figure 6.9.

Over the considered concentration range, the photon flux does not change significantly. For some of the results larger variations are observed, which can be assigned to the sensitivity of the actinometer itself. Based on these arguments, the indicated concentration range around 5×10^{-3} mol/L is considered as being optimal.

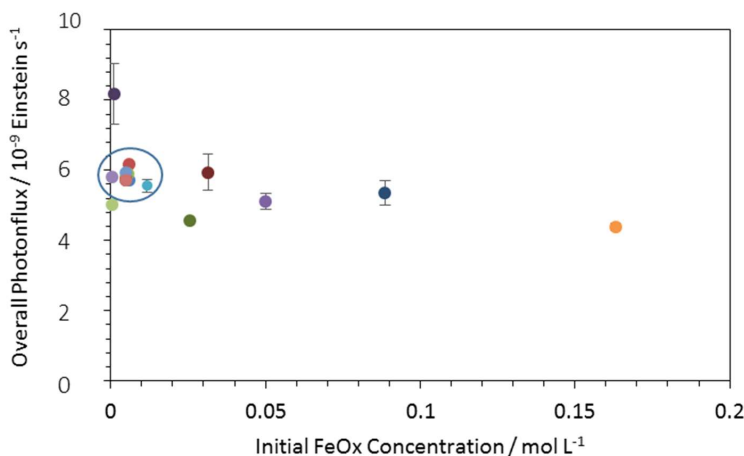


Figure 6.9. Average photon flux related to the initial actinometer concentration. The circled area is of interest due to its stability and the reduced amount of ferrioxalate used.

Coil Flow Inverter (CFI)

A coil flow inverter is wound around a cubic mechanical support. The diameters of the loops will in this case be smaller compared to the ones in the capillary tower. This increases the centrifugal forces of the solution in the reactor. Additionally, passing from one side of the cubic support to the other, a 90° switch of direction of the reactor is made. Both effects will contribute to improve mixing features in these types of reactors.

The conversion of Fe(III) is evaluated as a function of the residence time for a single-liquid phase. Considered residence times range from 1.20 – 20 sec. Given by Figure 6.1026.10 (a), a linear relation between the two parameters is only observed for residence times up to about 4 seconds.

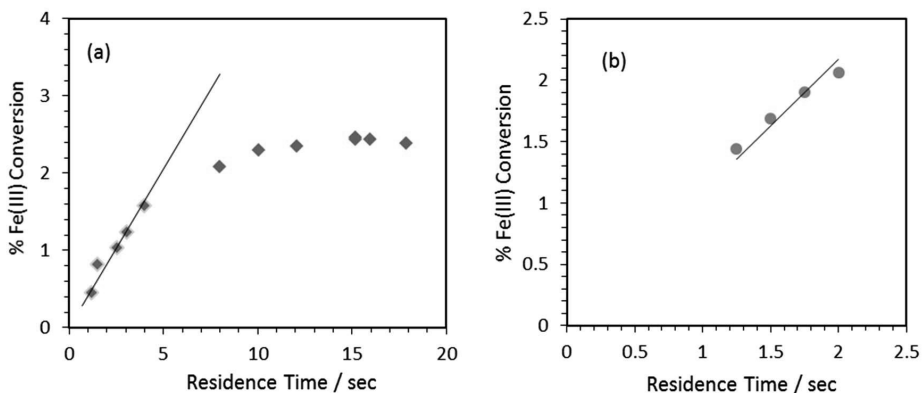


Figure 6.102. Ferrioxalate actinometry for an initial ferrioxalate concentration of 0.005 M. Due to the high rate of incident photons, the conversion is only linear in the first few seconds. (a) CFI, (b) reactor on the lamp

Similarly by plotting the right hand side of equation 6.10 versus residence time, an estimation of the photon flux can be made and is equal to $6.2 \times 10^{-9} \text{einstein } s^{-1}$.

Microreactor wound on the UV-lamp

Similar to the two aforementioned experiments done in previous configurations, the actinometry experiment carried out this time in the reactor wound directly on the UV-light wall. The results of Fe(III) conversion are presented in Figure 6.10 (b). In the same way as explained before, the Photon flux can be determined and is equal to $1.9 \times 10^{-8} \text{einstein } s^{-1}$

6.4.4 Comparison between the different configurations of the microreactor with respect to the lamp

In order to observe the benefits for a system, a comparison between all three microreactor configurations is made. The comparison of the mutual iron(III) conversion, indicated in Figure 6.1136.11, for all three systems, gives a first indication for the trend of the photon flux. The values for these fluxes have been calculated earlier and are summarized as

$$\langle q_{p,\lambda} \rangle_{\text{Capil.}} = 5.7 \times 10^{-9} \text{einstein} \cdot s^{-1} \leq \langle q_{p,\lambda} \rangle_{\text{CFI}} = 6.2 \times 10^{-9} \text{einstein} \cdot s^{-1} < \langle q_{p,\lambda} \rangle_{\text{On The Lamp.}} \\ = 19 \times 10^{-9} \text{einstein} \cdot s^{-1}$$

The different configurations of the microreactor with respect to the lamp give rise to different mixing features where the capillary tower is the base case and expected to have lowest photon flux. The CFI benefits from two phenomena to improve mixing behavior, but the highest photon flux is observed for when the reactor is positioned on the wall. Direct illumination, without too

many losses, is the system that absorbs the most photons. The difference between the capillary tower and the CFI is hardly significant.

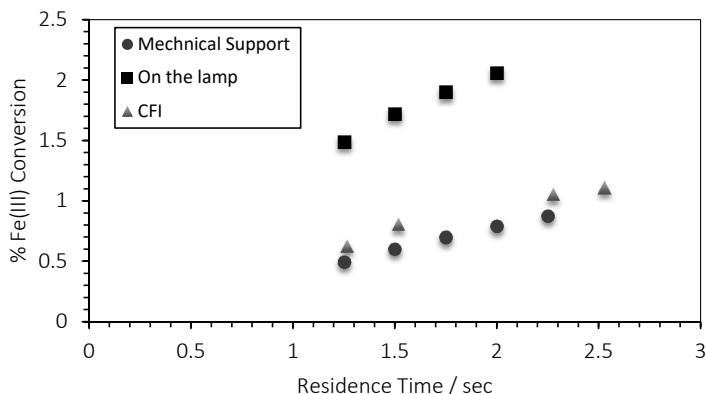


Figure 6.113. Iron(III) conversion for each system, gives an indication for the photon flux trend.

6.5 Conclusions

In this chapter a procedure for photon flux measurements, by means of actinometry experiments using ferrioxalate in microcapillary reactors, has been developed. This method describes the reduction of Fe(III) to Fe(II) under influence of UV-light at 254nm. We are only interested in measuring the amount of photons absorbed in the reactor and originating from the considered source. According to the sensitivity of the ferrioxalate towards light, special precautions have been considered in order to obtain verifiable and reproducible results. Because of these points, the experiments were performed in a darkroom to avoid any light interfering with the system. It has been demonstrated several times by experiments that the results are reproducible.

The determination of photon fluxes have been considered for configurationally different systems, including a capillary tower, placing the reactor directly on the lamp and a coil flow inverter. The first step included the determination of photon fluxes for a single-phase liquid system, for all three of the configurations. The high intensity UV-light source will have some consequence for the reaction itself. In order to stay under the earlier stated 10% conversion limit for the ferrioxalate, low residence times are required. These are established by applying high flow rates that could only be obtained by high-pressure pumps.

A summary of calculated photon fluxes is given in the table below, for the different configurations of the microreactor with respect to the lamp. The highest photon flux belongs to where the reactor is placed on the lamp. Also, it is worth mentioning that in order to be in the linear region

of Fe(III) conversion, even higher flow rates (and therefore low residence times) should be considered. Our equipment at this point was not able to reach residence times lower than 1 sec.

	Capillary Tower	CFI	Reactor on the lamp
Photon flux (einstein s ⁻¹)	5.7×10^{-9}	6×10^{-9}	19×10^{-9}

According to the results the different configurations of the microreactor with respect to the lamp are ranked by the amount of photons absorbed

Reactor on the lamp > CFI ≥ capillary tower

CFI seems to show slightly enhanced photon fluxes compared to the capillary tower. However the difference is not significant.

6.6 References

- [1] D. Cambié, C. Bottecchia, N. J. W. Straathof, V. Hessel, and T. Noël, "Applications of Continuous-Flow Photochemistry in Organic Synthesis, Material Science, and Water Treatment," *Chem. Rev.*, vol. 116, no. 17, pp. 10276–10341, Sep. 2016.
- [2] C. C. Le *et al.*, "A General Small-Scale Reactor to Enable Standardization and Acceleration of Photocatalytic Reactions," *ACS Cent. Sci.*, 2017.
- [3] H. V., "Novel Process Windows – Gate to Maximizing Process Intensification via Flow Chemistry," *Chem. Eng. Technol.*, vol. 32, no. 11, pp. 1655–1681, Oct. 2009.
- [4] V. Hessel, B. Cortese, and M. H. J. M. de Croon, "Novel process windows – Concept, proposition and evaluation methodology, and intensified superheated processing," *Chem. Eng. Sci.*, vol. 66, no. 7, pp. 1426–1448, 2011.
- [5] R. T., G. T. N., and K. C. O., "Accessing Novel Process Windows in a High-Temperature/Pressure Capillary Flow Reactor," *Chem. Eng. Technol.*, vol. 32, no. 11, pp. 1702–1716, Oct. 2009.
- [6] J. Jovanovic, "Liquid-liquid microreactors for phase transfer catalysis," Technische Universiteit Eindhoven, 2011.
- [7] J. P. Knowles, L. D. Elliott, and K. I. Booker-Milburn, "Flow photochemistry: Old light through new windows," *Beilstein J. Org. Chem*, vol. 8, pp. 2025–2052, 2012.
- [8] T. Aillet, K. Loubiere, O. Dechy-Cabaret, and L. Prat, "Photochemical synthesis of a 'cage' compound in a microreactor: Rigorous comparison with a batch photoreactor," *Chem. Eng. Process. Process Intensif.*, vol. 64, pp. 38–47, 2013.
- [9] O. Shvydkiv *et al.*, "Microphotochemistry: a Reactor Comparison Study Using the Photosensitized Addition of Isopropanol to Furanones as a Model Reaction.," *Photochem. Photobiol. Sci.*, vol. 10, no. 10, pp. 1399–1404, 2011.
- [10] M. Li, Z. Qiang, J. R. Bolton, J. Qu, and W. Li, "A Mini-Fluidic UV Photoreaction System for Bench-Scale Photochemical Studies," *Environ. Sci. Technol. Lett.*, vol. 2, no. 10, pp. 297–301, Oct. 2015.
- [11] H. J. Kuhn, S. E. Braslavsky, and R. Schmidt, "Chemical actinometry (IUPAC Technical Report)," *Pure Appl. Chem.*, 2004.
- [12] H. J. Kuhn, S. E. Braslavsky, and A. R. Schmidt, "CHEMICAL ACTINOMETRY (IUPAC Technical Report)," *Pure Appl. Chem. J. R. Bolt. (Canada)South Africa) G. A. Argüello (Argentina), T. D. Z. Atvars*, vol. 76, no. 12, pp. 2105–2146, 2004.
- [13] C. A. Hatchard, C. G.; Parker, "A new sensitive chemical actinometer - II. Potassium ferrioxalate as a standard chemical actinometer," *Proc. R. Soc. London. Ser. A. Math. Phys. Sci.*, vol. 235, no. 1203, p. 518 LP-536, Jun. 1956.
- [14] S. Goldstein and J. Rabani, "The ferrioxalate and iodide–iodate actinometers in the UV region," *J. Photochem. Photobiol. A Chem.*, vol. 193, no. 1, pp. 50–55, 2008.
- [15] J. R. Bolton, M. I. Stefan, P.-S. Shaw, and K. R. Lykke, "Determination of the quantum yields of the potassium ferrioxalate and potassium iodide–iodate actinometers and a method for the calibration of radiometer detectors," *J. Photochem. Photobiol. A Chem.*, vol. 222, no. 1, pp. 166–169, 2011.
- [16] D. Parida *et al.*, "Coil Flow Inversion as a Route To Control Polymerization in Microreactors," *Macromolecules*, vol. 47, no. 10, pp. 3282–3287, May 2014.

- [17] T. Oppenländer, *Photochemical Purification of Water and Air: Advanced Oxidation Processes (AOPs) - Principles, Reaction Mechanisms, Reactor Concepts. Chapter 6 Properties, Reactivity and Photochemistry of Auxiliary Chemicals*. Wiley, 2007.
- [18] W. Heering, "UV-sources - Basics, Properties and Applications," *Int. Ultrav. Assoc.*, vol. 6, no. 4, pp. 7–13, 2004.

6.7 Supplementary Material

S1. General reagent information

The chemicals used throughout the experiments are listed in Table and are used without further purification.

Winding 1.25m transparent[14], [15] polymeric tubing around the considered supports shapes the reactor systems. The tubing was a FEP - *Fluorinated Ethylene Propylene* - capillary (IDEX Health & Science) with an internal diameter of 508 μ m and with an outer diameter of 1.6 mm. This results in an internal volume of 0.25mL.

Table S6.1. General reagent information

Chemical	CAS-number	Supplier	Process
di-Potassium oxalate, Monohydrate	6487 – 48 – 5	Merck	ACTINOMETRY
Iron (III) chloride, Hexahydrate	10025 – 77 – 1	Acros Organics	
Sulfuric acid (95.0 – 98.0%)	7664 – 93 – 9	Sigma - Aldrich	
1,10 phenanthroline	66 – 71 – 7	Sigma - Aldrich	
Sodium acetate, Trihydrate	6131 – 90 – 4	Merck	

S.2 Light Source

The used light source is an immersion amalgam lamp (TS12-212, Sadechaf Curing & Bonding). The lamp has an UV capacity of 3.5W.

S.3 Post-irradiation treatment

After reaction, a sample (100 μ L) is taken and is subjected to a post-irradiation treatment. This includes the addition of 1mL water, 1mL of the chelating agent and 1mL buffer solution. The iron(II) in solution forms a complex upon addition of 0.1(w/v)% 1,10-phenanthroline. Where 0.1 g of the substance is diluted to 100mL by water and stored in the dark. Additionally, 1mL of a 1M sodium acetate/0.1M sulfuric acid

buffer is added. To prepare this mixture, 68g of sodium acetate is dissolved in 100mL of a 0.5M sulfuric acid stock solution and further diluted to 500mL with water.

S.4 Continuous flow system

A flowchart of the system is given in Figure S6.1 which starts from the loading of the actinometer solution in a 6mL stainless steel syringe pump (Chemyx, Nexus 6000). The syringe is connected to the reactor by using PEEK (*Polyether Ether Ketone*) connections.

Relatively high flow rates are used in order to ensure a low conversion of the actinometer. Typical flow rates, and corresponding residence times, are given in

$$\tau = \frac{V_r}{Q_L} \quad (\text{S6.1})$$

Table S6.22.

The residence times in this case are calculated by the ratio of the irradiated volume in the reactor, V_r , and the flow rate, Q_L .

$$\tau = \frac{V_r}{Q_L} \quad (\text{S6.1})$$

Table S6.2. Overview of the liquid flow rates

Flow rate (ml min ⁻¹)	Residence time (sec)
5.00	3
5.45	2.75
6.00	2.50
6.67	2.25
7.50	2
8.57	1.75
10.00	1.50
12.00	1.25
12.71	1.18

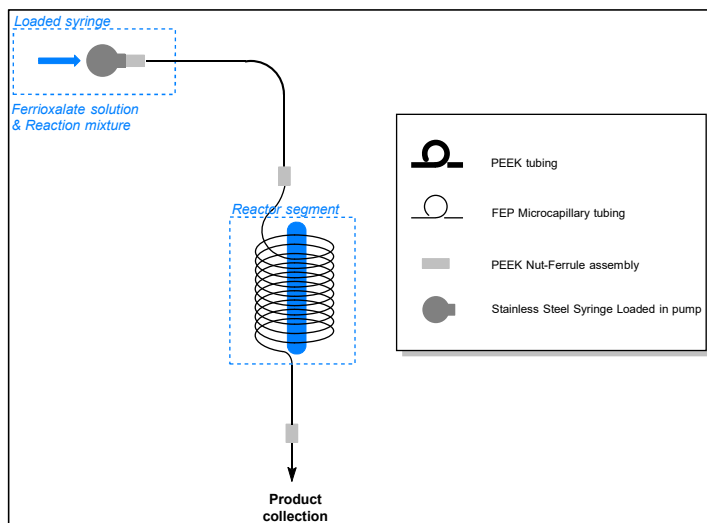


Figure S6.1. Flowchart of the micro-flow system

S.5 Characterization

Actinometer solution

In order to determine the conversion of the actinometer, the iron(II) concentration will be evaluated. This is done by post-irradiation treatment of the collected sample. To a 100 μ L sample, 1mL water, 1mL buffer and 1mL phenanthroline solution was added in a polystyrene cuvette. The cuvette was sealed with a cap and wrapped in alumina foil to be shielded from light. After 45min the complexation of iron(II) with the ligand to form a ferroin complex was completed. The samples are analyzed by making use of a UV/VIS spectrophotometer (Shimadzu UV-2501PC Spectrophotometer), leading to a series of samples as represented in Figure .2.

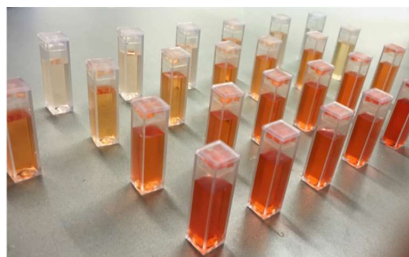
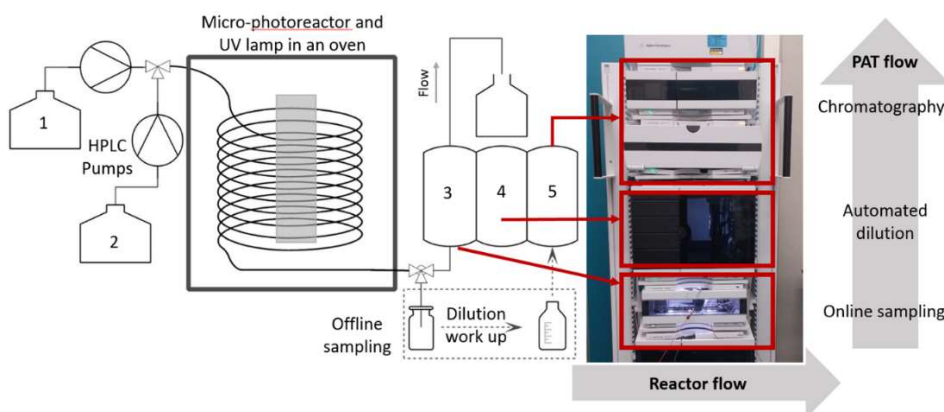


Figure S6.2. Samples after post-irradiation treatment. The shades of red indicate the amount of ferroin present.

The measuring range of the spectrophotometer was set from 390 – 600 nm, a sample interval of 0.1nm and a medium exposure time. The concentration of iron(II) can be determined by evaluation of the absorption at the maximum peak at 510nm, the dilution factor and the molar absorption coefficient of the ferriox complex ($11\,639\text{ M}^{-1}\text{ cm}$, determined via calibration).

CHAPTER 7

UV-Photo-Flow on-line Analytics - Coupled UHPLC and Potential for Design of Experiments



This chapter is based on:

Shahbazali, E., Escribà-Gelonch, M., Honing, M., T., Hessel, V., *Tetrahedron*. 2016, 74(25), 3143–3151

Abstract

Process intensification commonly enables reaction acceleration, i.e. very short processing times. The coupling of flow chemistry and continuous online analytics is described. The low volumes typical for micro-flow pose challenges for sampling operations in analytics. In this chapter, a very fast process is combined with a modified ultra-high-performance liquid chromatography (UHPLC) system allowing for very fast sampling and analysis. Low-volume online sampling is introduced here for UHPLC analysis of the photo-Claisen rearrangement in micro-flow. Chances and challenges are critically reviewed, including the reproducibility and robustness of the sampling. Furthermore, the ability and speed of the chosen set-up in order to capture process changes and adjust the process parameters properly is investigated. With the applied online sampling system, it was possible to perform, almost unattended and spending 12 times less sampling volume, a full factorial analysis of all relevant reaction conditions (243 experiments) in three days. Assuming a systematic difference compared to manual sampling and dilution of $0.5\% \pm 1.4$, online sampling avoids random errors due to automation.

7.1 Introduction

Over the last 20 years, continuous micro-flow reactions have become an eminent topic in process design[1]. The enhanced process control given through miniaturization results in many benefits such as higher yields, less waste, and improved sustainability [2]. More far fetching, flow chemistry makes meanwhile possible the development of multi-step end-to-end platforms which deliver the product from raw materials (up to the pill in pharmaceutical manufacturing) in one continuous run. The need to keep control of such cascaded processing has paved the way for finding a suited analytical technology and fast detection which finally demand for process automation[3], reducing the human operator interaction to check a software interface[4]–[8]. Nowadays the goal for multi-step processes is to be fully telescoped and managed by a single researcher. Therefore, continuous automated reaction monitoring can enhance the reliability and the quality of the final product, reducing labour and costs[9]. In-time analytics are usually classified depending on where and how the sampling operation is carried out as: offline, atline, online and inline[10].

Offline sampling in batch processing has some drawbacks even when its single steps are as fast as continuous micro-flow. First, the reaction outcome is often superimposed products by mass and heat transfer and even dependent on the location of sampling in the vessel, which is termed heterogeneity here. Therefore, in order to get the complete view, a large sample volume has to be taken at different points in the vessel. Complex statistical strategies are used in quality control of industrial chemical production[11]. In addition, the heterogeneity of batch processes might cause higher errors or higher deviations between samples, and therefore lower confidence. These drawbacks are partially overcome sampling (offline) in continuous flow due to the (spatial and timely) homogeneity of sample qualities within the microcapillary. Thus a lower amount of sampling and samples is needed. Nevertheless, offline sampling still do not solve (i) the need for a minimum sampling volume to allow the, also longer, manual work-up, (ii) the possibility to damage or contaminate the sample during the operation, especially with air-/light-sensitive or short lifetime compounds, and subsequently (iii) the chance of errors. Here, inline/online analysis becomes a viable solution.

Intensified continuous flow provides order-of-magnitude shorter residence times[12]–[14] and essentially needs ultrafast sampling operating with lower volumes and without interruption. For the intensified flow chemistry, the frequency of sampling and the time for analysis simply has to be faster than the time needed for completion of reaction and changing to the next process condition. Accordingly, online and inline analysis is preferred over atline and offline, and even those need to be speed up as given in this chapter. An automation of online sampling also allows for the use of the precise volume needed, avoiding the unprecise manual sampling, which tends to increase the sampling volume in order to ensure enough quantity. In addition, automation also

reduces random errors derived by manual operations, which take also more time to be carried out.

Recognizing the ambition of the United States Food and Drug (FDA) to establish continuous processing in pharmaceutical manufacturing by 2026[15] and our previous flow chemistry research[16]–[18], the application of Process Analytical Technology (PAT)[19], [20] to flow chemistry is a major future goal relevant to the innovation of this chapter. Here, real-time information accessibility has proven to enhance process control by reducing the timeline of the measurements, with the possibility to correct any leverage or malfunction in-time avoiding losses of chemicals. This creates a vast amount of data which typically demands for some extra data processing strategy. Established are multi-factorial mathematical analysis, statistical evaluations, model predictions, and algorithms like the Nelder-Mead simplex optimization algorithm[21]. Common to all is to aim to optimize the pattern recognition of the variables or to improve even in two-dimensional fashion (e.g. temperature and reaction time). The traditional one-factor-at-a-time sometimes is not effective in explaining the interactions between factors[22], [23].

Coupling PAT systems to processes would avoid sample transfer and therefore their possible deterioration. In order to allow adequate monitoring and efficient reaction control, the sampling time and subsequent analysis has to be very short compared to the overall reaction time. In this connection, some analytical techniques are preferred, such as near infrared (NIR)[24]–[26], Raman[27], Mid-IR[28], acoustic emission signals[29], X-ray absorption spectroscopy[30] and nuclear magnetic resonance[31], [32] because of their analytical speed, non-contact spectroscopic analysis as well as their condition of not destructive methods. As an example, IR spectroscopy is commonly used for the determination of physical factors such as moisture[33], crystalline polymorphism[34], particle size[35], and density[36].

Nonetheless, the development of PAT for monitoring of micro-flow chemistry has not largely reported. One reason might be the small volumes of chemicals in the micro-channels which pose a need for miniaturized versions of conventional analytical instruments[37]. Some analytical techniques, which include sampling, fulfil that criterion such as Raman[38], liquid chromatography[39], or capillary electrophoresis[40], [41]. However, for small molecule analysis, high-performance liquid chromatography (HPLC) is commonly preferred and is quasi the unique method used for process monitoring applications in micro-channels offline. HPLC coupled to microreactors have been applied for the synthesis of, e.g., cycloadducts[42], pyrazoles[43] and ciprofloxacin analogues[44]. Flow automation has also reached continuous multistep systems[45]. The work of Kock *et al.* [46] shows one issue to be solved around automated flow operation. 51 samples (0.2 mg solution) collection needed as much as 5.6 h sampling time. Also, the length of the chromatographic methods still is a main problem for the use HPLC for online

micro-flow process monitoring[47]. Other issues are the analysis costs[37], as well as the long equilibration times when non-isocratic conditions are used[40].

Yet, with the already proven ultra-high-performance liquid chromatography (UHPLC) conditions, analysis times are shortened significantly. Together with micro column approaches, low sample volumes are feasible, allowing fast sequential experiments, and also novel process time windows. As an example, it allows to operate free of constraints by heat transfer limitations, much different from batch experiments[48]. Indeed since recently there is evidence for advanced process control with the goal of fast kinetic screening[49]–[53], biological analysis[54]–[56] and mechanistic studies[28], [57] under stable, well reproducible reaction conditions. The combination of flow chemistry and online monitoring gives also the chance for non-stop UHPLC continuous analytics, when spectroscopic online analytic sources, e.g. FTIR or NMR, are not suitable for specific products. As an example, online UHPLC coupled with a Teflon/FEP-capillary-based flow microreactor has been reported as especially effective for the analysis of non-volatile organic molecules because of the rapid separation achieved[58]. However and as outlined above, the sampling step of UHPLC remains an issue, because of the small volumes supplied by the small channels. Attiya *et al.* [59] and Lin *et al.* [60] reported in 2001 the first approaches to online sampling using micro-channels, but both applied to electrophoresis. Schlund *et al.* [61] reported in 2007 the first continuous sampling applied to HPLC based on a double-T junction emulating an HPLC injector loop. Also, fraction collectors have been used for sampling operation in microchannels[46]. Therefore, the next step in micro-flow based reaction development should be to determine the optimal operating speed, as suggested by FDA[62].

In this chapter, the combination of flow chemistry with a modified UHPLC system allowing rather fast online sampling is discussed. As a proof-of-concept, this configuration was tested in combination with a photo-Claisen rearrangement reaction. We previously reported the thermal-Claisen rearrangement of allyl phenyl ether (APE) to *ortho*-allyl phenol achieving process intensification[63] without the need of a catalyst. Latter an intensification of micro-flow route for photo-Claisen rearrangement was also reported[64]. The photo pathway gave *para*-substituted isomer besides the *ortho*-substituted given by thermal process. The latter opened the chance of a new radicalary unexplored path. Therefore, the photo-reaction path used in this study and given in Figure 7.1, offers still an attractive way for research in an automated fashion. Here, after carrying out the reaction in the capillary photoreactor, samples are automatically taken and subsequently analysed using short timing enabled by the modified UHPLC system coupled to the setup. The different residence times for the different operations, the number of samples, the process simplification and the process automation are parameters taken into account.

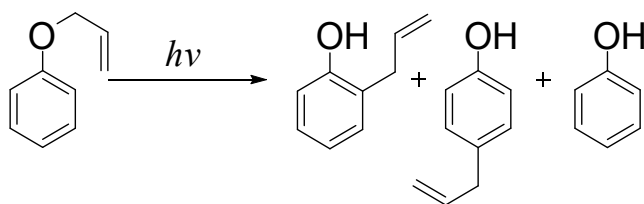
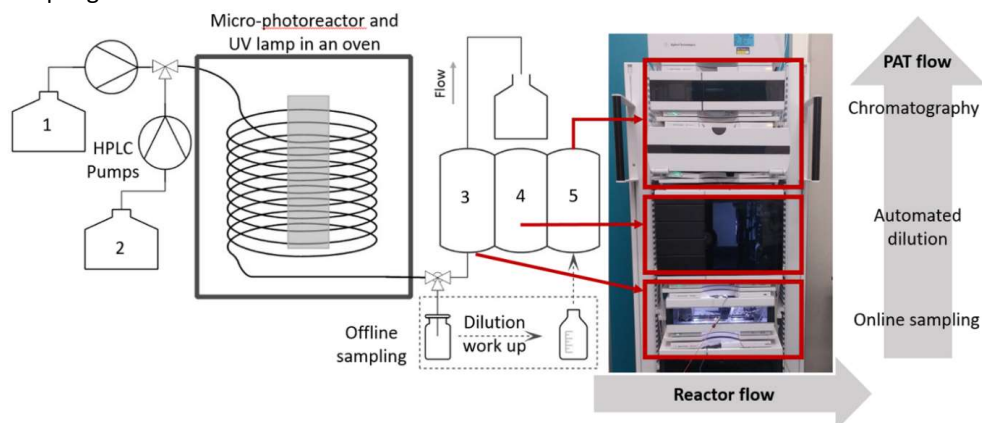


Figure 7.1. Photo-Claisen rearrangement path used in online sampling.

7.2 Experimental Part

7.2.1 Experimental setup

Microchannel experiments have been performed using the reactor set-up depicted in Scheme 7.1. The setup is composed of two HPLC pumps (Knauer Azura P4.1S). The first feeds a 0.5 M stock solution of APE (Sigma Aldrich 99%, 16.77 g, 12.5 mmol) in 250 mL n-butanol (Sigma Aldrich). The second feeds pure n-butanol and is used to arrange, in-flow and in one run, the experiments carried out using 0.1 M and 0.05 M concentration. A T-mixer (Valco) is subsequently used for this purpose. The flow-rate is adjusted accordingly to achieve reaction times of 2, 5 and 8 minutes respectively. Inside an oven, a low-pressure amalgam UV-lamp with distinctive peak at 254 nm (TS23-212; Dinies Technologies GmbH) is installed, and 5 m (approx. 1 mL equivalent volume) UV-transparent fluorinated ethylene propylene capillary tubing (FEP 1548, 0.5 mm ID; Upchurch Scientific) is wound on a metallic tower around the cylindrical shaped lamp. Accordingly, the tubing is properly connected to the T-mixer in the inlet and to the sampling unit in the outlet of the oven. Just before online UHPLC connection, a T-piece (IDEX) allows for offline sampling.



Scheme 7.1. Photo-Claisen rearrangement setup coupled to offline and online sampling. 1: Stock solution of alkyl phenyl ether in n-butanol. 2: n-butanol. 3: online autosampling. 4: Automated dilution. 5: UHPLC analyzer.

7.2.2 Experimental conditions of sampling and chromatographic separation.

Allyl phenyl ether, 1-butanol, formic acid, acetonitrile, and 1,3-dinitrobenzene were purchased from Aldrich chemical company and used as received. The solvents purity were all according to HPLC grade of Sigma-Aldrich solvents (>99.5). The online UHPLC system was based on an Agilent 1290 Infinity II LC system (Scheme 7.1) consisting of a binary pump, an autosampler, a thermostated column compartment and a diode array detector equipped with a 10 mm Max-Light Cartridge Cell. Analytical isocratic separation was achieved with an Agilent ZORBAX Eclipse Plus C18 UHPLC column (2.1×50mm, 1.8µm) and applying a mixture of 0.1% formic acid in water and acetonitrile (55/45; v/v) as the mobile phase. The detection was carried out with a UV-visible diode array detector at 270 nm, and data processing performed with the Agilent OpenLAB ChemStation software. The analytical setup was linked to the flow reactor by means of an “in-house” modified autosampler (an item of a patent application) encompassing a series of multi-port valves allowing the direct sampling from the outlet of the flow reactor. The sampling cycle was programmed to perform a system purge, sampling and dilution followed by separation and detection. A total of 40 µL sample was trapped before being dilute with acetonitrile to a total volume of 100 µL. An aliquote of 1 µL was subsequently injected onto the analytical column.

7.3 Results and Discussion

7.3.1 Online sampling and analytic time distribution

The first goal was to investigate three experimental parameters with certain discrete values for the photo-Claisen reaction as fast as possible using the online UHPLC-UV analyser, i.e. to show minimal analysis time demands and to benchmark this to any combination of conventional and micro-flow processing with conventional analytics. These three parameters were considered: temperature (T), concentration (c) and reaction time (t). Concerning temperature, the values were 21 °C, 35 °C and 50 °C, for concentration 0.05 M, 0.1 M and 0.5 M, and for reaction times were 2 min, 5 min and 8 min. Each operation was timed using a chronometer.

7.3.2 Timing of sampling, analysis, and settling time for next experiment

Figure 7.2 gives the time distribution for testing three flow rates at one temperature and one concentration, here referred as one cycle. In this Figure, the fragment striped refers to the settling and stabilization time (here, three residence times were taken). Also the dead time refers to the delay of setting the conditions in flow. Despite of the advantages of flow chemistry in terms of heat and mass transfer, the existence of such dead time frames suggest that flow chemistry could not be fast enough in this case. After setting them three online samples were taken, all of them with the same protocol. In total, the sampling operation (including sampling and automatic work-up) lasted 7 min. After sampling, a new flow rate was set. During the stabilization time, the

UHPLC analysed automatically all samples and the results were taken before the new sampling (Figure 7.3). In addition, during the next sampling operation, the results of the previous samples were processed by the user (Figure 7.3). As a consequence, 9 samples in 3 different conditions were taken, analysed in parallel and the results were processed. The online test speed then was set at 72 min/cycle. It is relevant to note that the time for sampling and analysis was usually shorter than the time for setting new conditions. Then this ultrafast procedure becomes faster than continuous flow intensification. In addition, the researcher only needed to set the conditions and get the results, which reduced drastically the random error derived of manual operation. Thus, three flow rates were triple tested largely automated in somewhat more than one hour ten minutes. In this way, for each of the 3 flow rates, 3 temperatures and 3 concentrations (9 cycles) were tested in just a bit more than 10 hours in the same day. Thus, the parametric variations sum up to $3 \times 3 \times 3 = 27$ measurements. As all of them were repeated three times, 81 samples were achieved in one run and one day. The same set of experiments was carried out in 3 different days, during which 27 conditions were three times tested and 243 samples were taken, analysed and the results were processed.

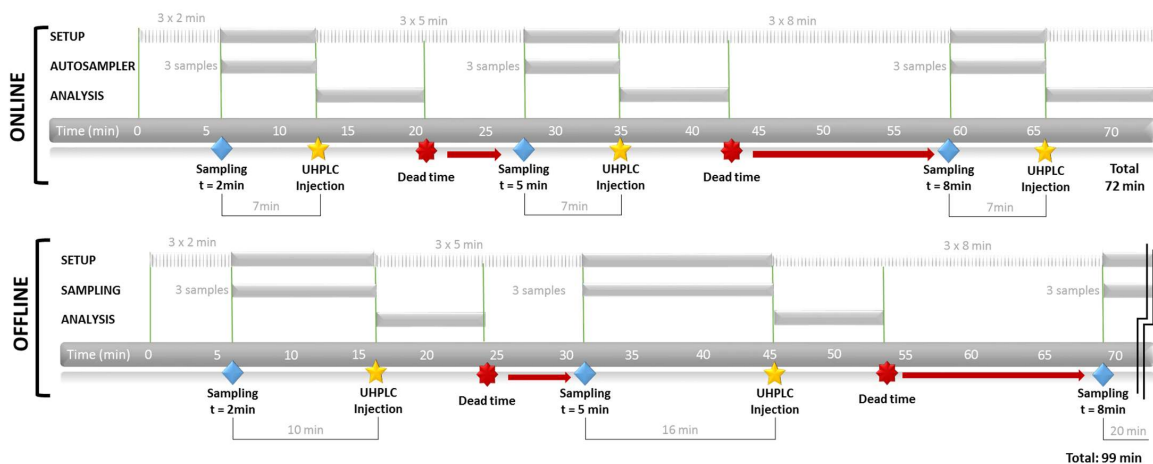


Figure 7.2. Timeline for sequentially testing 3 flow rates at the same temperature and concentration. Online sampling allowed for, 9 samples (taken and analyzed) in 72 min. Offline sampling needed around 30 min more. The fragment striped refers to the time needed to set and stabilize the new conditions (3 residence times).

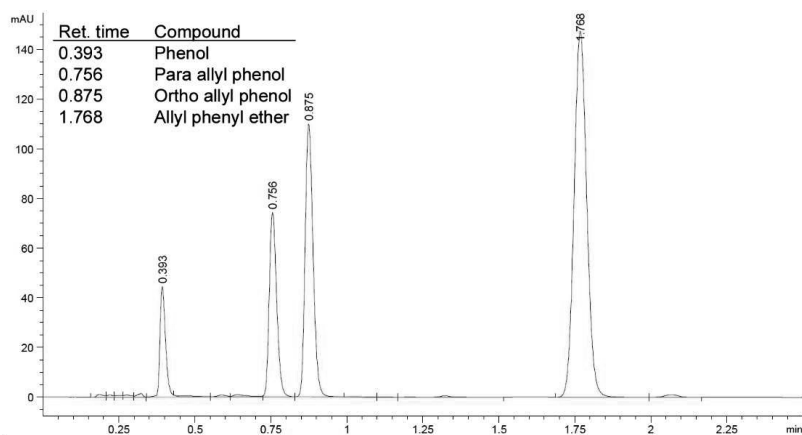


Figure 7.3. Online sample chromatogram of 0.05 M APE, using 2 min reaction time at 21 °C.

7.3.3 Sampling volume

The same set of experiments was carried out offline. Here both sampling and dilutions were performed manually. The sampling time was set according to the reactor flow-rate in order to achieve 0.5 ml sample. An important point to highlight is the fact that this sampling volume means almost the half of the volume of the whole capillary microreactor. In addition, online sampling needed 12 times less volume to perform the same experiments, as shown in Figure 7.4, which is more suitable for low volumes used in flow chemistry. Therefore for 2, 5 and 8 min residence time, 1 min/sample 3 min/sample and 4.25 min/sample were needed respectively. Therefore, in Figure 7.5 it is noted that the difference between online and offline sampling increases when the flow rate in the reactor decreases, because of the time needed offline to get 0.5 mL of sample even with low flow rates. The subsequent work-up of three samples in order to get the final injection vials was set in 6 min. This operation is reduced drastically online in terms of time, avoiding also random errors. Overall, offline sampling operation and work-up needed 10 min, 16 min and 20 min for 2, 5 and 8 min reaction time respectively for each sample. Figure 7.2 shows the compared timeline online/offline for each cycle of experiments. The difference in time was set to almost half an hour for each cycle, which means online sampling delivered 4.5 hours less, therefore in overall, online experiments saved 40 % time.

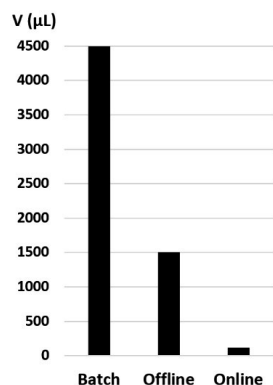


Figure 7.4. Comparative between the needed volumes for every set of 3 samples.

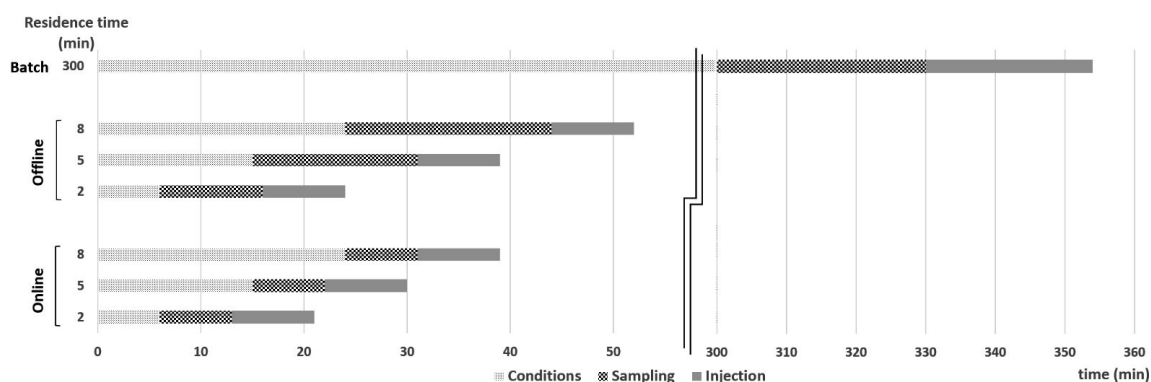


Figure 7.5. Comparison between sampling procedures for a single set of 3 samples at low, medium and high residence times, equivalent to high, medium and low flow rates respectively.

7.3.4 Sampling reliability and robustness

Table 7.1 shows the average values, their standard deviation and their variation coefficient (VC) of each set of experiments performed in the 3 days. The repeatability is characterized by the VC and found in all cases to be below 3 % using low and medium concentrations. Nevertheless, when increasing the concentration, the variability was found to be higher, especially in low residence times. This finding could be explained by (i) the viscosity of the final solution at high concentration (viscosity of just *n*-butanol is rather high: 2.6 mPa·s at 25 °C)[65], which can modify the rheology and the hydrodynamics making difficult to achieve a homogeneous sampling at the same drawing speed. Furthermore, (ii) the precision could be compromised because of solubility constraints due to the incomplete reaction of precipitated *ortho*-allylphenol. In fact, it was observed that at high concentrations the solution sometimes became not fully homogeneous because of the close solubility limit. This could be a limitation for representative sampling, since an online particulate

matter of 40 μL might be not sufficient compared to 0.5 mL in offline sampling. The viscosity- and solubility-related explanation is in line with the finding that the repeatability is improved with an increase of temperature.

Table 7.1. Average values of three repeated measurements of photo-Claisen reaction conversions obtained at three different days. (VC = variation coefficient)

Concentration (M)→			0,05			0,1			0,5		
Da y	T (°C)	t (min)	Conversio n (%)	Std. Dev.	% VC	Conversio n (%)	Std. Dev.	% VC	Conversio n (%)	Std. Dev.	% VC
I	21	2	49.7 ± 0.77 2	2	30.4 ± 0.91 6	3	6.0 ± 1.56 5	26			
		5	82.5 ± 0.22 8	0	55.5 ± 0.56 3	1	15.7 ± 1.26 7	8			
		8	94.5 ± 0.04 7	0	72.4 ± 0.32 1	0	23.1 ± 0.22 7	1			
	35	2	51.0 ± 0.40 9	1	31.9 ± 0.10 2	0	8.8 ± 1.56 1	18			
		5	83.4 ± 0.16 7	0	57.0 ± 0.02 5	0	20.0 ± 1.36 1	7			
		8	94.6 ± 0.02 7	0	74.4 ± 0.09 6	0	27.6 ± 1.11 8	4			
	50	2	59.9 ± 0.61 1	1	39.0 ± 0.02 5	0	9.5 ± 0.42 8	4			
		5	89.2 ± 0.42 2	0	71.0 ± 0.01 5	0	22.0 ± 0.07 1	0			
		8	94.0 ± 0.20 3	0	85.9 ± 0.01 5	0	32.0 ± 0.04 1	0			
II	21	2	42.5 ± 0.30 3	1	31.0 ± 0.04 0	0	7.3 ± 1.04 2	14			
		5	72.5 ± 0.71 0	1	50.5 ± 0.30 5	1	13.8 ± 0.33 5	2			
		8	87.6 ± 0.19 0	0	69.0 ± 0.23 8	0	19.3 ± 0.69 7	4			
	35	2	43.0 ± 0.46 3	1	30.0 ± 0.07 0	0	5.1 ± 1.81 1	36			

		5	72.6 ± 0.36 9	1	55.0 ± 0.02 6	0	13.8 ± 1.25 0	9
		8	87.8 ± 0.27 0	0	70.6 ± 0.54 4	1	23.0 ± 0.67 3	3
	50	2	65.0 ± 0.02 7	0	38.6 ± 0.71 7	2	10.0 ± 0.46 3	5
		5	91.0 ± 0.04 4	0	68.1 ± 0.04 0	0	19.9 ± 0.25 0	1
		8	95.5 ± 0.01 6	0	83.0 ± 0.05 3	0	30.0 ± 0.03 4	0
III	21	2	46.1 ± 1.45 4	3	33.2 ± 0.61 4	2	6.3 ± 1.39 9	22
		5	77.9 ± 0.37 7	0	56.0 ± 0.09 3	0	17.1 ± 0.96 2	6
		8	91.5 ± 0.03 8	0	74.0 ± 0.09 1	0	23.6 ± 1.17 1	5
	35	2	45.0 ± 0.41 7	1	29.8 ± 0.81 7	3	7.2 ± 1.79 7	25
		5	76.8 ± 0.03 7	0	56.5 ± 0.68 4	1	18.7 ± 0.93 3	5
		8	90.9 ± 0.16 2	0	73.1 ± 0.09 1	0	23.9 ± 0.05 4	0
50	2	58.0 ± 0.11 8	0	38.1 ± 0.22 0	1	11.0 ± 0.30 3	3	
	5	86.7 ± 0.18 7	0	68.0 ± 0.21 8	0	22.0 ± 0.10 5	0	
	8	97.5 ± 0.10 3	0	85.5 ± 0.23 5	0	33.5 ± 0.03 6	0	

Table 7.2 summarizes the reproducibility of these results. The term reproducibility is used, as the same experiment carried out under the same conditions but at different days. Then, Table 7.2 gives the deviation between the mean values of the same three reproducible experiments carried out in different days. The majority of the VC values are below 10 %, except the ones at higher concentration. Rheological and solubility issues may explain these results as described above.

Table 7.2. Averages of three repeated measurements of photo-Claisen reaction conversions obtained at different days.

Concentration (M) →		0.05			0.1			0.5		
T (°C)	t (min)	Conversion (%)	Std. Dev.	%VC	Conversion (%)	Std. Dev.	%VC	Conversion (%)	Std. Dev.	%VC
21	2	46.1 ± 3.602	8	31.5 ± 1.477	5	6.6 ± 0.690	10			
	5	77.6 ± 5.006	6	54.0 ± 3.070	6	15.6 ± 1.633	10			
	8	91.2 ± 3.480	4	71.8 ± 2.577	4	22.0 ± 2.388	11			
35	2	46.4 ± 4.166	9	30.6 ± 1.178	4	7.0 ± 1.868	26			
	5	77.6 ± 5.479	7	56.1 ± 1.032	2	17.5 ± 3.258	19			
	8	91.1 ± 3.376	4	72.7 ± 1.880	3	24.8 ± 2.441	10			
50	2	60.9 ± 3.618	6	38.6 ± 0.454	1	10.2 ± 0.752	7			
	5	89.0 ± 2.136	2	69.0 ± 1.718	2	21.3 ± 1.209	6			
	8	95.6 ± 1.741	2	84.8 ± 1.568	2	31.8 ± 1.743	5			

7.3.5 Analysis of the confidence in the results obtained

As described above, simultaneously to the online sampling, conventional samples in 5 mL vials (VWR International) were taken in parallel for each set of conditions. These samples were manually diluted and injected in the same UHPLC using the conventional procedure of injection from vials. These results were used to compare offline sampling and sample preparation with online sampling. Hence, each online average and deviation value was opposed to the corresponding offline average and deviation value. The subtraction of these paired results generated a new variable defined as $W = \text{online} - \text{offline}$. Statistical procedures were used to study this new variable using Statgraphics Centurion VII. In ideal conditions, the average of this variable should be 0 with 0 deviation, which means that the result obtained by online would be exactly the same, as the corresponding offline sample. Figure 7.6 shows the frequency histogram of W , where a Gauss bell shows a slight tendency of a leverage in the 0 value of W . Figure 7.7 shows the normal test which suggests that the values of W can be represented by a normal distribution at 95 % of confidence level. The latter is relevant in order to carry out further hypothesis tests and set the interval of confidence of W .

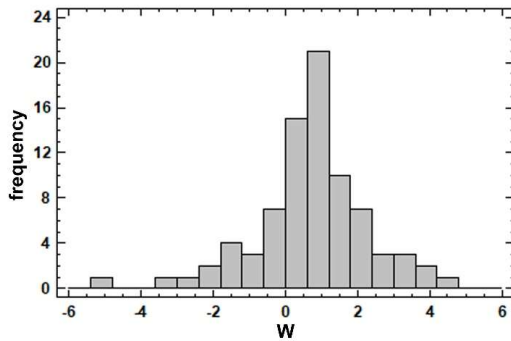


Figure 7.6. Frequency histogram of variable W

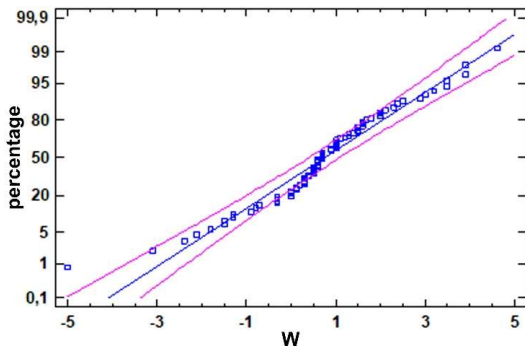


Figure 7.7. Normality test for W

In a context of normality, a hypothesis test was performed in order to determine if it could statistically be accepted that the average of W is zero, and therefore the results online are as reliable as offline. The null hypothesis of the T-test was subsequently: average equal to 0, giving an alternative hypothesis of non-equality. Unfortunately, this test was rejected with 95 % confidence level, concluding that the average of W is not 0, and therefore a systematic leverage has to be accepted. In order to delimit this leverage, a new test was performed based on the distribution of W showed in Figure 7.6. The assumption that the average value equals 0.5 was checked. As a result, the P-value of this test was 0.0677836 which is above the significance level of 0.05. Hence, in these conditions the null hypothesis cannot be rejected at the 95 % confidence level. Therefore, it can be accepted that the average value of W is +0.5, which means that the systematic difference for the online sampling compared to manual sampling and dilution is +0.5 %.

In order to set the interval of confidence of W, a new hypothesis test was performed to fix the standard deviation. In this case a Chi-squared test[66] was performed. Considering Figure 7.6, the null hypothesis was set to be equal to 1.4 versus the alternative hypothesis of different. This

test gave a P-value of 0.138879, above the significance level of 0.05. Hence the value of 1.4 can be accepted as the standard deviation of W at the 95 % confidence level. Therefore, it can be concluded the variable W is normally distributed and has an average of 0.5 with a standard deviation of 1.4. Transferring this conclusion to the sampling, the online sampling gives 0.5 % higher conversion \pm 1.4 % compared to offline sampling.

7.3.6 Statistical approach of the Photo-Claisen reaction parameters

Taking advantage of the experiments carried out, an additional study of the effect of the reaction conditions in the conversion of the photo-Claisen reaction was performed, using one of the sets of online experiments which corresponds to almost one day working. In this connection, a balanced completely randomized design was performed using the 3 levels of each factor (T, c and t) as described above. All data were analysed using generalized linear model (PROC GLM) of SAS (V9.0, SAS Institute Inc., Cary, NC, USA)[67]. The significance of the analysis of variance was set at 0.05 and a Duncan's multiple comparison test was added[68]. Table 7.3 (up) shows the significance of the model and Table 7.3 (down) shows the analysis of variance (ANOVA) derived from the statistical analysis. Here, the F-statistic refers to a ratio of two variances: variation between sample means and variation within the samples. Thus, higher dispersion gives higher F value, which means that concentration gives more variability on the APE conversion than reaction time and temperature.

7

Table 7.3. Significance of the GLM model (up) and the ANOVA derived of this analysis (down).

Source	DF	Sum of Squares	Mean Square	F Value	Pr > F
Model	26	66792.62840	2568.94725	360.28	<.0001
Error	54	385.04667	7.13049		
Corrected Total	80	67177.67506			

Source	DF	Type I /III SS	Mean Square	F Value	Pr > F
T	2	1477.26247	738.63123	103.59	<.0001
C	2	46782.28469	23391.14235	3280.44	<.0001
T * C	4	120.27457	30.06864	4.22	0.0048
t	2	16290.81654	8145.40827	1142.33	<.0001
T * t	4	14.45383	3.61346	0.51	0.7309
C * t	4	1928.20049	482.05012	67.60	<.0001

Source	DF	Type I /III SS	Mean Square	F Value	Pr > F
T * c * t	8	179.33580	22.41698	3.14	0.0054

Table 7.3 shows that all single variables: T, c and t have significant ($P < 0.001$) differences in their levels. Therefore, the APE conversion of the photo-Claisen reaction is different at different concentrations, different temperatures and different residence times. Nevertheless, apparently the interaction T * t is not significant, which means that the variability of the conversion when using different residence times is statistically the same when using different temperatures. Hence, parallel lines are expected in the T * t interaction plot (Figure 7.8). In this plot, the 21 °C and 35 °C lines are close to each other, which can be correlated with a statistically identical behaviour related to the conversion. The latter is confirmed by the Duncan's test (Table 7.4), which means that the same conversion profile is obtained by operating at 21 °C and at 35 °C. In the light of these results, it can be concluded that maximal APE conversion of the photo-Claisen reaction is achieved at high temperature (50 °C), low concentration (0.05 M) and long residence time (8 min). This is also shown on the 3D plot in Figure 7.9.

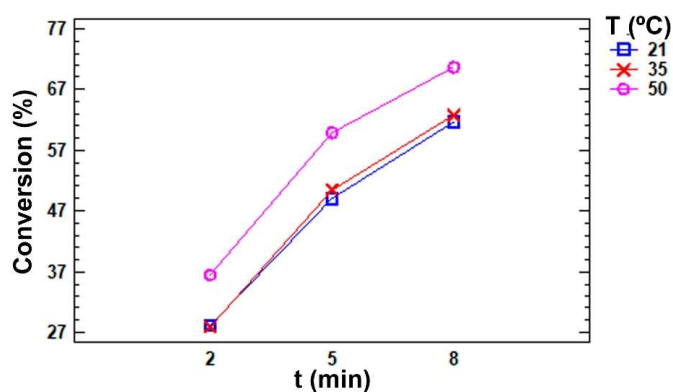


Figure 7.8. Interaction plot of residence time (t) and temperature (T) using 0.05 M concentration.

Table 7.4. Duncan's test for the temperature, concentration and residence time (means with the same letter are not significantly different).

Groupin g	Conv. (%)	N	T (°C)	Grouping	Conv. (%)	N	c (M)	Grouping	Conv. (%)	N	t (min)
A	55.7074	27	50	A	75.0630	27	0.05	A	65.1000	27	8
B	47.0852	27	35	B	56.5778	27	0.1	B	53.0926	27	5
B	46.2667	27	21	C	17.4185	27	0.5	C	30.8667	27	2

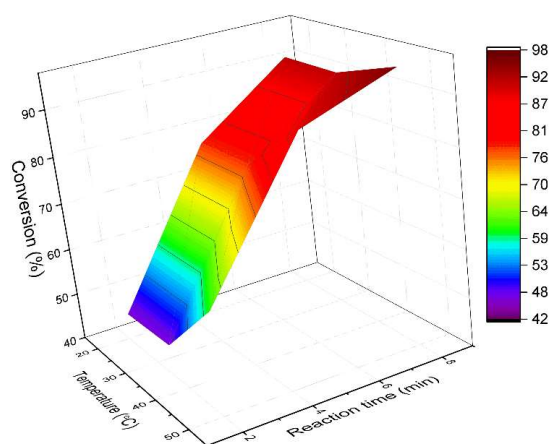


Figure 7.9. Effect on conversion of the interaction of residence time (t) and Temperature (T) using 0.05M concentration.

7.4 Conclusions

In this chapter, a novel analytical approach in online sampling, separation and detection successfully applied for the monitoring of a photo induced Claisen rearrangement reaction in micro-flow channels is described. It allowed the low volume and high speed sampling while maintaining very good repeatability and reproducibility of both the separation and detection of all reaction products. The developed analytical set-up avoids the complex sampling strategies of batch operation, as well as reduces drastically the manual work-up timing as well as the sampling volume. The increased sampling speed, allowed the screening of up to 27 process conditions in 24 hours; due to 3 times repetition, 81 samples were taken. In average, one sampling (at coupled continuous micro-flow reaction) took less than 7 min. This fact becomes relevant compared to

offline sampling especially in low flow rates. Testing reproducibility via comparing tests at 3 different days, all in all 243 samples were collected online, analysed and processed under almost automatized conditions. The results were enabled due to the speed of both online sampling and online UHPLC analysis. As the latter is established, it can be concluded that very fast online sampling opens the door for further intensification analysis for flow chemistry. Here the automatic online sampling was 40 % faster than offline sampling, keeping the same repeatability and robustness, and using more than 12 times less sample volume than used offline. Therefore, in the studied case, assuming a known systematic difference of $0.5 \% \pm 1.4$ compared to offline sampling and analysis, online analysis can be taken with the same reliability, avoiding the difficult to balance random errors. In addition, the photo-Claisen reaction conditions in terms of conversion were monitored and successfully optimized at 50 °C, 0.05 M and 8 min with the results obtained in just three working days.

7.5 Acknowledgements

The authors acknowledge Ms. Bettina Schuhn, Mr. Thomas Ortmann and Dr. Thomas Glauner (Agilent Technologies) for supporting the modification of the UHPLC system for online sampling. This project was funded by the Horizon 2020: Marie Skłodowska-Curie Individual Fellowship awarded by Dr. Marc Escribà Gelonch under grant agreement number 659233.

7.6 References

- [1] M. B. Plutschack, B. Us Pieber, K. Gilmore, and P. H. Seeberger, "The Hitchhiker's Guide to Flow Chemistry," *Chem. Rev.*, 2017.
- [2] B. P. Mason, K. E. Price, J. L. Steinbacher, A. R. Bogdan, and D. T. McQuade, "Greener Approaches to Organic Synthesis Using Microreactor Technology," *Chem. Rev.*, vol. 107, no. 6, pp. 2300–2318, Jun. 2007.
- [3] S. V. Ley, D. E. Fitzpatrick, R. J. Ingham, and R. M. Myers, "Organic Synthesis: March of the Machines," *Angew. Chemie Int. Ed.*, vol. 54, no. 11, pp. 3449–3464, Jan. 2015.
- [4] V. Sans and L. Cronin, "Towards dial-a-molecule by integrating continuous flow, analytics and self-optimisation," *Chem. Soc. Rev.*, vol. 45, no. 8, pp. 2032–2043, 2016.
- [5] B. J. Reizman, Y.-M. Wang, S. L. Buchwald, and K. F. Jensen, "Suzuki-Miyaura cross-coupling optimization enabled by automated feedback," *React. Chem. Eng.*, vol. 1, no. 6, pp. 658–666, 2016.
- [6] J. P. McMullen, M. T. Stone, S. L. Buchwald, and K. F. Jensen, "An Integrated Microreactor System for Self-Optimization of a Heck Reaction: From Micro- to Mesoscale Flow Systems," *Angew. Chemie Int. Ed.*, vol. 49, no. 39, pp. 7076–7080, Aug. 2010.
- [7] V. Sans, L. Porwol, V. Dragone, and L. Cronin, "A self optimizing synthetic organic reactor system using real-time in-line NMR spectroscopy," *Chem. Sci.*, vol. 6, no. 2, pp. 1258–1264, 2015.
- [8] S. A. P. and S. Nagl, "Microfluidic platforms employing integrated fluorescent or luminescent chemical sensors: a review of methods, scope and applications," *Methods Appl. Fluoresc.*, vol. 3, no. 3, p. 34003, 2015.
- [9] R. Carlson, "Preface to the first edition," in *Design and optimization in organic synthesis*, vol. 24, R. Carlson and J. E. B. T.-D. H. in S. and T. Carlson, Eds. Elsevier, 2005, pp. xi–xiii.
- [10] M. Clemens, H. Sonja, and K. Stefan, "Stopping the Babylonian Confusion: An Updated Nomenclature for Process Analyzers in PAT Applications," *Chemie Ing. Tech.*, vol. 88, no. 6, pp. 694–697, May 2016.
- [11] NIST, "Process or Product Monitoring and Control," in *NIST/SEMATECH e-handbook of statistical methods*, 2012.
- [12] V. Hessel, I. Vural Gürsel, Q. Wang, T. Noël, and J. Lang, "Potential Analysis of Smart Flow Processing and Micro Process Technology for Fastening Process Development: Use of Chemistry and Process Design as Intensification Fields," *Chem. Eng. Technol.*, vol. 35, no. 7, pp. 1184–1204, Jun. 2012.
- [13] V. Hessel, "Novel Process Windows – Gate to Maximizing Process Intensification via Flow Chemistry," *Chem. Eng. Technol.*, vol. 32, no. 11, pp. 1655–1681, Oct. 2009.
- [14] V. Hessel, D. Kralisch, N. Kockmann, T. Noël, and Q. Wang, "Novel Process Windows for Enabling, Accelerating, and Uplifting Flow Chemistry," *ChemSusChem*, vol. 6, no. 5, pp. 746–789, Apr. 2013.
- [15] FDA, "Pharmaceutical CGMPs for the 21st Century—a risk-based approach Final Report," 2004.
- [16] M. Escriba, V. Hessel, S. Rothstock, J. Eras, R. Canela, and P. Lob, "Applying a continuous capillary-based process to the synthesis of 3-chloro-2-hydroxypropyl pivaloate," *Green Chem.*, vol. 13, no. 7, pp. 1799–1805, 2011.
- [17] S. Borukhova, T. Noel, B. Metten, E. de Vos, and V. Hessel, "From alcohol to 1,2,3-triazole via a multi-step continuous-flow synthesis of a rufinamide precursor," *Green Chem.*, vol. 18, no. 18, pp. 4947–

- 4953, 2016.
- [18] B. Svetlana, N. Timothy, and H. Volker, "Continuous-Flow Multistep Synthesis of Cinnarizine, Cyclizine, and a Buclizine Derivative from Bulk Alcohols," *ChemSusChem*, vol. 9, no. 1, pp. 67–74, Dec. 2015.
- [19] "Database of ICH Guidelines, Compilation prepared by International Conference on Harmonisation of Technical Requirements for Registration of Pharmaceuticals for Human Use (ICH)."
- [20] FDA, "Database of FDA Guidance for Industry, Compilation prepared by Food and Drug Administration."
- [21] K. F. McMullen, Jonathan P. Jensen, "AN INTELLIGENT MICROREACTOR SYSTEM FOR REAL-TIME OPTIMIZATION OF A CHEMICAL REACTION," in *Twelfth International Conference on Miniaturized Systems for Chemistry and Life Sciences*, 2008, pp. 1907–1909.
- [22] D. C. Montgomery, *Design and Analysis of Experiments*. New York: John Wiley, 2001.
- [23] W. Huyer Neumaier, Arnold, "Stable Noisy Optimization by Branch and Fit," *ACM Trans. Math. Softw.*, vol. 35, no. 2, pp. 1–25, 2008.
- [24] R. Tanaka, N. TAKAHASHI, Y. NAKAMURA, Y. HATTORI, K. ASHIZAWA, and M. Otsuka, *In-line and Real-time Monitoring of Resonant Acoustic Mixing by Near-infrared Spectroscopy Combined with Chemometric Technology for Process Analytical Technology Applications in Pharmaceutical Powder Blending Systems*, vol. 33. 2017.
- [25] Y. Roggo, P. Chalus, L. Maurer, C. Lema-Martinez, A. Edmond, and N. Jent, "A review of near infrared spectroscopy and chemometrics in pharmaceutical technologies," *J. Pharm. Biomed. Anal.*, vol. 44, no. 3, pp. 683–700, 2007.
- [26] W. Ferstl, T. Klahn, W. Scheikert, G. Billeb, M. Schwarzer, and S. Loebbecke, "Inline Analysis in Microreaction Technology: A Suitable Tool for Process Screening and Optimization," *Chem. Eng. Technol.*, vol. 30, no. 3, pp. 370–378, Feb. 2007.
- [27] D. S. Hausman, R. T. Cambron, and A. Sakr, "Application of Raman spectroscopy for on-line monitoring of low dose blend uniformity," *Int. J. Pharm.*, vol. 298, no. 1, pp. 80–90, 2005.
- [28] T. M. Floyd, M. A. Schmidt, and K. F. Jensen, "Silicon Micromixers with Infrared Detection for Studies of Liquid-Phase Reactions," *Ind. Eng. Chem. Res.*, vol. 44, no. 8, pp. 2351–2358, Apr. 2005.
- [29] Y. Hu, L. Wang, X. Huang, X. Qian, L. Gao, and Y. Yan, "On-line Sizing of Pneumatically Conveyed Particles Through Acoustic Emission Detection and Signal Analysis," *IEEE Trans. Instrum. Meas.*, vol. 64, no. 5, pp. 1100–1109, 2015.
- [30] S. Hübner *et al.*, "An Ozonolysis–Reduction Sequence for the Synthesis of Pharmaceutical Intermediates in Microstructured Devices," *Org. Process Res. Dev.*, vol. 13, no. 5, pp. 952–960, Sep. 2009.
- [31] S. Araneda, J.F.; Boehringer, T.; Rehm, T.; Riegel, in *254th ACS National Meeting & Exposition*, 2017.
- [32] Y. Maguire, I. L. Chuang, S. Zhang, and N. Gershenfeld, "Ultra-small-sample molecular structure detection using microslot waveguide nuclear spin resonance," *Proc. Natl. Acad. Sci.*, vol. 104, no. 22, p. 9198 LP-9203, May 2007.
- [33] M. Otsuka, A. Koyama, and Y. Hattori, "Real-time release monitoring for water content and mean particle size of granules in lab-sized fluid-bed granulator by near-infrared spectroscopy," *RSC Adv.*, vol. 4, no. 34, pp. 17461–17468, 2014.

- [34] K. Kamada *et al.*, "Characterization and monitoring of pseudo-polymorphs in manufacturing process by NIR," *Int. J. Pharm.*, vol. 368, no. 1, pp. 103–108, 2009.
- [35] M. Tanabe, H. Otsuka, K. Otsuka, "Theoretical analysis of tablet hardness prediction using chemoinformetric near-infrared spectroscopy," *Anal. Sci.*, vol. 23, no. 7, pp. 857–862, 2007.
- [36] M. Otsuka, "Comparative particle size determination of phenacetin bulk powder by using Kubelka–Munk theory and principal component regression analysis based on near-infrared spectroscopy," *Powder Technol.*, vol. 141, no. 3, pp. 244–250, 2004.
- [37] M. V. Koch *et al.*, "Selected Developments in Micro-analytical Technology," in *Micro Instrumentation: For High Throughput Experimentation and Process Intensification-a Tool for PAT*, Wiley-VCH Verlag GmbH &, 2007, pp. 209–313.
- [38] B. Marquardt, "Application of on-line raman spectroscopy to characterize and optimize a continuous microreactor," in *Micro Instrumentation*, Weinheim, Germany: Wiley-VCH Verlag GmbH &, 2007.
- [39] C. J. Malherbe, D. de Beer, and E. Joubert, "Development of On-Line High Performance Liquid Chromatography (HPLC)-Biochemical Detection Methods as Tools in the Identification of Bioactives," *International Journal of Molecular Sciences*, vol. 13, no. 3, 2012.
- [40] J. P. McMullen and K. F. Jensen, "Integrated Microreactors for Reaction Automation: New Approaches to Reaction Development," *Annu. Rev. Anal. Chem.*, vol. 3, no. 1, pp. 19–42, Jun. 2010.
- [41] J. W. Albrecht, J. El-Ali, and K. F. Jensen, "Cascaded Free-Flow Isoelectric Focusing for Improved Focusing Speed and Resolution," *Anal. Chem.*, vol. 79, no. 24, pp. 9364–9371, Dec. 2007.
- [42] M. Fernandez-Suarez, S. Y. F. Wong, and B. H. Warrington, "Synthesis of a three-member array of cycloadducts in a glass microchip under pressure driven flow," *Lab Chip*, vol. 2, no. 3, pp. 170–174, 2002.
- [43] E. Garcia-Egido, V. Spikmans, S. Y. F. Wong, and B. H. Warrington, "Synthesis and analysis of combinatorial libraries performed in an automated micro reactor system," *Lab Chip*, vol. 3, no. 2, pp. 73–76, 2003.
- [44] S. Thomas, K. Daniel, and J. Gerhard, "Synthesis of a Library of Ciprofloxacin Analogues By Means of Sequential Organic Synthesis in Microreactors," *QSAR Comb. Sci.*, vol. 24, no. 6, pp. 758–768, Aug. 2005.
- [45] C. M. Griffiths-Jones *et al.*, "Fully Automated Flow-Through Synthesis of Secondary Sulfonamides in a Binary Reactor System," *J. Comb. Chem.*, vol. 9, no. 3, pp. 422–430, May 2007.
- [46] K. Koch, B. J. A. van Weerdenburg, J. M. M. Verkade, P. J. Nieuwland, F. P. J. T. Rutjes, and J. C. M. van Hest, "Optimizing the Deprotection of the Amine Protecting p-Methoxyphenyl Group in an Automated Microreactor Platform," *Org. Process Res. Dev.*, vol. 13, no. 5, pp. 1003–1006, Sep. 2009.
- [47] C.-Y. Shih, Y. Chen, J. Xie, Q. He, and Y.-C. Tai, "On-chip temperature gradient interaction chromatography," *J. Chromatogr. A*, vol. 1111, no. 2, pp. 272–278, 2006.
- [48] J. P. McMullen and K. F. Jensen, "An Automated Microfluidic System for Online Optimization in Chemical Synthesis," *Org. Process Res. Dev.*, vol. 14, no. 5, pp. 1169–1176, Sep. 2010.
- [49] H. J. J., Z. Neomy, R. Maarten, and J. Tanja, "The Kinetics of n-Butyl Acrylate Radical Polymerization Revealed in a Single Experiment by Real Time On-line Mass Spectrometry Monitoring," *Macromol. React. Eng.*, vol. 11, no. 4, p. 1700016, May 2017.
- [50] M. Edward R., M. Joseph R., Z. Nikolay, B. Stephen L., and J. Klavs F., "Accelerating Reactions with

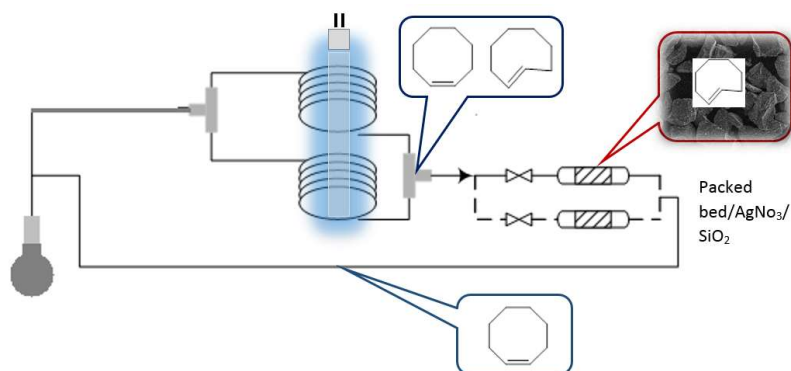
- Microreactors at Elevated Temperatures and Pressures: Profiling Aminocarbonylation Reactions," *Angew. Chemie Int. Ed.*, vol. 46, no. 10, pp. 1734–1737, Feb. 2007.
- [51] D. M. Ratner, E. R. Murphy, M. Jhunjunwala, D. A. Snyder, K. F. Jensen, and P. H. Seeberger, "Microreactor-based reaction optimization in organic chemistry-glycosylation as a challenge," *Chem. Commun.*, no. 5, pp. 578–580, 2005.
- [52] S. Tadepalli, R. Halder, and A. Lawal, "Catalytic hydrogenation of o-nitroanisole in a microreactor: Reactor performance and kinetic studies," *Chem. Eng. Sci.*, vol. 62, no. 10, pp. 2663–2678, 2007.
- [53] D. J. Quiram *et al.*, "Integrated Microreactor System for Gas-Phase Catalytic Reactions. 3. Microreactor System Design and System Automation," *Ind. Eng. Chem. Res.*, vol. 46, no. 25, pp. 8319–8335, Dec. 2007.
- [54] J. El-Ali, P. K. Sorger, and K. F. Jensen, "Cells on chips," *Nature*, vol. 442, p. 403, Jul. 2006.
- [55] D. Gerber, S. J. Maerkl, and S. R. Quake, "An in vitro microfluidic approach to generating protein-interaction networks," *Nat. Methods*, vol. 6, p. 71, Dec. 2008.
- [56] S. Monpichar *et al.*, "Analysis of Protein–Protein Interactions by Using Droplet-Based Microfluidics," *ChemBioChem*, vol. 10, no. 10, pp. 1605–1611, Jun. 2009.
- [57] S. K. Ajmera, C. Delattre, M. A. Schmidt, and K. F. Jensen, "Microfabricated Differential Reactor for Heterogeneous Gas Phase Catalyst Testing," *J. Catal.*, vol. 209, no. 2, pp. 401–412, 2002.
- [58] H. Fang, Q. Xiao, F. Wu, P. E. Floreancig, and S. G. Weber, "Rapid Catalyst Screening by a Continuous-Flow Microreactor Interfaced with Ultra-High-Pressure Liquid Chromatography," *J. Org. Chem.*, vol. 75, no. 16, pp. 5619–5626, Aug. 2010.
- [59] A. Said *et al.*, "Design of an interface to allow microfluidic electrophoresis chips to drink from the fire hose of the external environment," *Electrophoresis*, vol. 22, no. 2, pp. 318–327, Jan. 2001.
- [60] Y.-H. Lin, G.-B. Lee, C.-W. Li, G.-R. Huang, and S.-H. Chen, "Flow-through sampling for electrophoresis-based microfluidic chips using hydrodynamic pumping," *J. Chromatogr. A*, vol. 937, no. 1, pp. 115–125, 2001.
- [61] M. Schlund, S. E. Gilbert, S. Schnydrig, and P. Renaud, "Continuous sampling and analysis by on-chip liquid/solid chromatography," *Sensors Actuators B Chem.*, vol. 123, no. 2, pp. 1133–1141, 2007.
- [62] L. X. Yu, "Pharmaceutical Quality by Design: Product and Process Development, Understanding, and Control," *Pharm. Res.*, vol. 25, no. 4, pp. 781–791, 2008.
- [63] E. Shahbazali, M. Spapens, H. Kobayashi, S. Ookawara, T. Noel, and V. Hessel, "Connected nucleophilic substitution-Claisen rearrangement in flow -analysis for kilo-lab process solutions with orthogonality," *Chem. Eng. J.*, vol. 281, pp. 144–154, 2015.
- [64] E. Shahbazali, T. Noël, and V. Hessel, "Photo-Claisen Rearrangement of allyl phenyl ether in microflow: influence of phenyl core substituents and vision on orthogonality," *J. Flow Chem.*, vol. 6, no. 3, pp. 252–259, 2016.
- [65] BASF, "n-Butanol," 2014. [Online]. Available: <http://www.solvents.basf.com/portal/streamer?fid=278912>.
- [66] K. Pearson, "X. On the criterion that a given system of deviations from the probable in the case of a correlated system of variables is such that it can be reasonably supposed to have arisen from random sampling," *London, Edinburgh, Dublin Philos. Mag. J. Sci.*, vol. 50, no. 302, pp. 157–175, Jul. 1900.

[67] SAS institute, "Base SAS 9.2 Procedures Guide, Statistical Procedures," 2009.

[68] D. B. Duncan, "Multiple Range and Multiple F Tests," *Biometrics*, vol. 11, no. 1, pp. 1–42, 1955.

CHAPTER 8

UV-Photo-Flow Application- Isomerization of *cis*-Cyclooctene to *trans*-Cyclooctene



This chapter is based on:

Shahbazali, E., Billaud, E. M. F., Meuldijk, J., Bormans, G., Noël, T., Hessel, V., *Ind. Eng. Chem. Res.* (2018), submitted.

Abstract

Liquid-phase adsorption has hardly been established in micro-flow, although this constitutes an industrially vital method for product separation. A micro-flow UV-photoisomerization process converts *cis*-cyclooctene partly into *trans*-cyclooctene, leaving an isomeric mixture. *Trans*-cyclooctene adsorption and thus separation was achieved in a fixed-bed micro-flow reactor, packed with $\text{AgNO}_3/\text{SiO}_2$ powder, while the *cis*-isomer stays in the flow. The closed-loop recycling-flow has been presented as systemic approach to enrich the *trans*-cyclooctene from its *cis*-isomer. In-flow adsorption in recycling-mode has hardly been reported so that a full theoretical study has been conducted. This insight is used to evaluate three process design options to reach an optimum yield of *trans*-cyclooctene. These differ firstly in the variation of the individual residence times in the reactor and separator, the additional process option of refreshing the adsorption column under use, and the periodicity of the recycle flow.

8.1 Introduction

In cancer discovery research, radiolabeled monoclonal antibodies directed against tumor-associated antigens have been developed as promising vectors to visualize or to treat tumors, mostly owing to their high affinity and specificity [1], [2]. Since antibodies have a long biological half-life, it takes a long time (in the order of days) to clear the antibodies from plasma. The half-life of radionuclides that are used to radiolabel antibodies should be sufficiently long (>12h) to allow clearance of the radiolabeled antibody from plasma prior to acquire high signal-to-noise ratio tumor PET images. The use of long lived radionuclides (e.g. ^{64}Cu , ^{124}I , ^{89}Zr) will however result in prolonged exposure to radiation and a high absorbed radiation dose. Fluorine-18 (F-18) is the most frequently used radionuclide for positron-emission tomography (PET) [3]–[5] radioisotopes due to its favorable physical properties (e.g. half-life of 109.8 min) [6].

Application of short-lived F-18 for *in vivo* visualization of antibodies can be achieved by pretargeting approaches based on high yield *in vivo* click reaction using e.g. ^{18}F -labeled *trans*-cyclooctene (TCO) or tetrazine derivatives [7]. This reaction strategy has been used for both *in vitro* and *in vivo* applications [5], [8], [9].

Trans-cyclooctene has a high reactivity due to the release of high strain energy upon the click reaction providing a well-defined chiral structure which makes it interesting for stereocontrolled synthesis. Therefore, radiolabeled TCOs are good candidates for bio-orthogonal chemistry [10].

There are many routes to synthesize a *trans*-cyclooctene. A common and elegant way is the photoisomerization of *cis* to *trans*-cyclooctene [11]. Yet, the photoisomerization is not irreversible and thus removal of the *trans*-isomer from the equilibrium *cis* and *trans* mixture is required to shift the equilibrium. Fox *et al.* have proposed an elegant procedure for the photochemical synthesis of TCO [12]. In this method, TCO was produced via photoisomerisation of *cis*-cyclooctene by exposure to UV light (254 nm) in a batch vessel. The reaction mixture was continuously passed through a bed of silver nitrate impregnated on silica gel. Subsequently, the TCO is selectively retained by silver nitrate and the remaining *cis*-cyclooctene-containing solution is recycled to the photochemistry batch vessel. This is a very unique method yet the total yield was 66% and the total reaction time was relatively long, i.e. 12 hrs.

Recently, the sustainable production of active pharmaceuticals and excipients in a has received a lot of attention [13]. Novel bioprocesses, continuous-flow processing, process integration and intensification and green chemistry are the main assets of sustainable processes. Flow chemistry, especially micro-flow technology, is a high potential platform in terms of equipment size reduction, energy efficiency, and reduced solvent usage to achieve process intensification and thereby performing more sustainable processes in fine chemistry [14], [15].

More specifically, for photochemical reactions, microreactors have several advantages compared to batch processes such as improved photon transport, energy efficiency and better mixing [16]–[18]. The constricted diameter of the microreactors (shorter photon diffusion pathway) allows better use of the irradiated light efficiently reducing the total exposure time, which leads to shorter reaction time and possibly reduced byproduct formation [19], [20].

Beyond microfabricated channels, and microcapillaries, mini-scale packed-bed reactors allow to form micro-flow in their void spaces. Indeed, enhanced reaction rates, higher conversions and selectivities were found as well and can be attributed to the reduced mass-transfer limitations [21], [22]. This, in combination with the high surface-to-volume ratio, makes the packed-bed reactor suited for performing biphasic reactions in multiple-repeated reentrance-flow mode or for heterogeneous catalytic reactions [23]. Adsorption (and desorption) is an essential step in heterogeneous catalysis. Hernández Carucci *et al.* proposed a model based on the competitive adsorption of ethylene and molecular oxygen over a silver surface of microchannels at 260 °C as part of a precise kinetic model for the ethylene oxide formation [24].

Accordingly, it stands to reason that sole adsorption processes (without catalysis) might be intensified in micro-flow. Microspheres have been reported and termed as adsorption ‘microreactors’ and indeed use the same transfer intensification by size reduction [25]. Rutin-Cr(III) loaded alginate microspheres were designed to reduce Cr(VI) to Cr(III) through adsorption and recover it. Yet, true micro(channel)reactors and micro-flow packed bed reactors have been hardly applied for adsorption so far.

Recently, we reported on the combination of a nucleophilic substitution to the thermal-Claisen rearrangement and also to photo-Claisen rearrangement in micro-flow [26], [27]. The motivation was to integrate two processes and to address the resulted challenging issues towards orthogonality. Also, here, we would like to design and integrate two processes, photoreaction and adsorption, yet with more in depth theoretical study for each process.

Therefore, the aim of this study is to develop a photo micro-flow process for the photochemical isomerization of *cis*-cyclooctene to TCO and its subsequent in-flow separation to isolate isomerically pure TCO derivatives. Such a compact integration of small devices fed with minute volumes provides opportunities for synergism between reaction and separation, which is a means of process intensification and was termed process-design intensification [28] as one arms of novel process windows [29]–[31].

More specifically, we focus in this work on the experimental procedures (batch as well as flow) for the photoisomerisation, and the design and operation of the adsorption column. Furthermore, the theoretical concepts behind these operations are explained and relevant

models for both sections are developed. Finally, the results of the experiments and theoretical modeling are presented and discussed.

8.2 Continuous Flow Setup

The experimental setup used for micro-flow based photoisomerization and in-flow separation process is presented in Figure 8.1. The solution is pumped from the inlet solution vessel using an HPLC pump (Knauer Azura P4.1S). The outlet stream from the pump is fed to FEP (fluorinated ethylenepropylene copolymer, IDEX 1548 L) capillary tubular reactor (ID 0.02", OD 1/16", length 5 m) which is wound around a cylindrical UV light source placed inside a closed oven. Irradiation is carried out using a low-pressure amalgam lamp (TS23-212; Dinies Technologies GmbH). The outlet then flows to the packed bed. The packed bed (stainless steel, ID 4.5 mm, L 25 mm) is packed with 200-220 mg of AgNO_3 impregnated silica gel (as packing or adsorbent) with a mesh size of 230+ (Sigma-Aldrich). The AgNO_3 /silica particles are mixed with 1 mm borosilicate glass beads in a mass ratio 1.66:1 and then introduced to the packed bed with a funnel. The inert glass beads are applied to prevent particle agglomeration which results in channeling of the flow inside the packed bed (for more information on micropacked beds and the assembling process, we refer to [32]–[34]).



Figure 8.1. Micro-flow setup for photoisomerization and in-flow separation process

The inlet and outlet of the packed bed have attached separately two frits with a pore size of 10 μm to keep the packing material inside the reactor. The outlet of the packed bed is recycled to the inlet solution vessel through a 0.2 m long FEP capillary tube. Samples are collected exactly before the recycle stream enters the inlet solution vessel. The inlet solution vessel is stirred with a magnetic stirrer bar to ensure a uniform concentration in the vessel. In a general micro-flow based photoisomerization and an in-flow separation experiment, *cis*-cyclooctene (0.06 g, 0.55

mmol), methyl benzoate as a singlet sensitizer (0.136 g, 1mmol) and n-dodecane as the internal standard for GC analysis (0.017g, 0.1 mmol) are dissolved in 25 ml n-hexane (with 1% diethyl ether) as solvent and mixed in the same vessel (volumetric flask of 50 ml) and from this vessel the solution is pumped to the flow setup. For more information regarding other experiments carried out in flow or batch, it is referred to supplementary material.

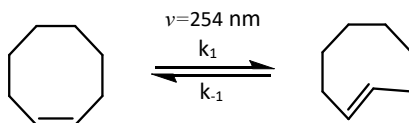
8.3 Theoretical study

8.3.1 Photoisomerization of *cis* to *trans*-cyclooctene

It is known from the literature [11], [35], [36] that the photoisomerization of *cis* to *trans*-cyclooctene is an equilibrium reaction. However, we could not find an in depth kinetic study about this photoisomerization. To investigate the kinetics of the equilibrium reactions, the conversion time histories have been monitored. The results reveal the existence of equilibrium between the *cis* and *trans*-isomers.

8.3.2 Kinetics of the photoisomerization

When it is assumed that intrinsic kinetics is obeyed and that the photoreaction follows the first order kinetics, the photoisomerization of *cis*-cyclooctene to *trans*-cyclooctene is represented in scheme 8.1:



Scheme 8.1. Photo isomerisation of *trans* from *cis*-cyclooctene

For a first order reversible reaction [37], the concentration of the *cis*-cyclooctene C_{cis} as a function of time obeys Equation 8.1. For a batch process, the conversion time histories have been monitored:

$$\frac{C_{cis}(\tau)}{C_{cis}(0)} = \left[\frac{1}{k_1 + k_{-1}} (k_1 e^{-\tau(k_1+k_{-1})} + k_{-1}) \right] \quad (8.1)$$

In this equation $C_{cis}(0)$ represents the concentration of *cis* at the start of reaction. See supplementary material S1 for the derivation.

8.3.3 Adsorption Isotherm

An experimental adsorption isotherm correlates the adsorbed amount of the adsorbate (*trans*-cyclooctene) onto the adsorbent (AgNO₃) with the concentration of the adsorbate in solution at equilibrium at a fixed temperature.

8.3.4 Langmuir isotherm

The Langmuir isotherm is one of the adsorption models that describe physisorption of neutral molecules onto adsorption sites [38], [39]. Based on the Langmuir model assumption, adsorption takes place on homogeneously distributed adsorbent sites by monolayer adsorption.

The nonlinearized Langmuir equation is expressed as:

$$q_{Be} = \frac{bq_{max}C_{Be}}{1 + bC_{Be}} \quad (8.2)$$

where q_{Be} (mg/g) is the amount of TCO adsorbed by AgNO₃ at equilibrium, q_{max} (mg/g) represents the maximum adsorption capacity, C_{Be} (g/dm³) is the equilibrium concentration of the adsorbate in solution, and b (dm³/mg) is a constant that amongst others is related to the heat of adsorption.

Moreover, Equation 8.2 can be expressed as Equation 8.3.

$$\frac{C_{Be}}{q_{Be}} = \frac{C_{Be}}{q_{max}} + \frac{1}{q_{max}b} \quad (8.3)$$

Plotting $\frac{C_{Be}}{q_{Be}}$ against C_{Be} , allows the calculation of the parameters, b and q_{max} .

8.3.5 Packed bed Modeling

In order to predict the dynamic behavior of the adsorption column, a mass balance over the liquid phase of an infinitesimal sized slice of the packed bed leads with perfect radial mixing and negligible pressure drop to Equation 8.4, see [40]–[42].

$$D_{ax} \frac{\partial^2 C_i}{\partial Z^2} - v \frac{\partial C_i}{\partial Z} - \frac{1 - \varepsilon_b}{\varepsilon_b} N_i = \frac{\partial C_i}{\partial t} \quad (8.4)$$

In Equation 8.4 C_i , D_{ax} , v , ε_b , and N_i are the concentration of TCO in the liquid phase, the axial dispersion coefficient, the interstitial liquid velocity, the bed porosity, and the mass transfer rate into the particle per unit volume of the particle phase, respectively. The first and second term in Equation 8.4 stand for the dispersive transport and the convective transport in the column, respectively. The third term represents the mass transfer between liquid phase and adsorbent.

The last term is related to accumulation of the adsorbate. This model is based on the following assumptions: isothermal adsorption and spherical adsorbent particles packed uniformly in the bed.

As it was stated, N_i is the mass transfer rate between solid and fluid phase and can be represented as [40]–[42]:

$$N_i = \rho_p \frac{\partial q_i}{\partial t} \quad (8.5)$$

$q_i \left[\frac{\text{mol}}{\text{kg}_s} \right]$ is the concentration of TCO on the adsorbent surface and $\rho_p \left[\frac{\text{kg}_s}{\text{dm}^3} \right]$ is the adsorbent particle density. In order to define $\frac{\partial q_i}{\partial t}$ mathematically, it is important to know whether the mass transfer resistance or the intrinsic adsorption kinetics dominates the adsorption rate.

8.3.6 Mass transfer resistance and intrinsic adsorption rate

A useful approach to investigate and to compare the mass transfer resistance with the kinetic resistance is by comparing $\frac{1}{k_c \cdot a}$ with $\frac{1}{k_{ads}}$, i.e. the time constant for mass transfer and adsorption, respectively. Since the diameter of adsorbent particle is small, 60 microns, and the AgNO_3 layer thickness is much smaller than the silica particle diameter, the internal mass transport through the pores of the adsorbent has been neglected (For more information see supplementary material, S2). Therefore, the mass transfer resistance calculation is only based on the external mass transfer from the bulk fluid to the adsorbent surface.

In order to determine k_c first the Reynolds number based on the particle diameter, Re , should be investigated. The calculated Reynolds number, Re , in our system is smaller than 2. From the literature [43] for low Re number, the Sherwood number can be defined as

$$Sh = \frac{k_c d_p}{D} = \frac{\phi_s}{6(1 - \varepsilon_b)\xi} \frac{u d_p}{D} \quad (8.6)$$

where ϕ_s , u , d_p , ξ , and D represent particle sphericity factor, the superficial liquid velocity, the particle diameter, the channeling factor and the diffusion coefficient of TCO in the solvent. In the Equation 8.6, it is assumed that particles are spherical; so $\phi_s = 1$. Unfortunately, the ξ value cannot be estimated exactly. However, in literature [43] the value of ξ has been predicted to be in the range of 1-10. Here the worst case value, $\xi=10$ (the case that gives highest mass transfer resistance) has been considered.

D is estimated on the basis of values in the similar systems[44]. As the fluid phase is very diluted, parameters such as density and viscosity are approximated based on solvent characteristics (n-hexane) at 25°C.

On the other hand, in order to determine $\frac{1}{k_{ads}}$ which has the dimension of time, an adsorption experiment can be performed in batch in a way that mass transfer resistance is eliminated as much as possible. By this experiment, the time to reach 50% of the equilibrium adsorption ($t_{1/2,ads}$) is calculated which can be considered to be $\frac{1}{k_{ads}}$. Lastly, k_{ov} is calculated according to:

$$\frac{1}{k_{ov}} = \frac{1}{k_{ads}} + \frac{1}{k_c \cdot a} \quad (8.7)$$

In the mentioned experiment (adsorption of TCO on AgNO_3) the batch vessel was well stirred so it is assumed that there is no external mass transfer limitation (more details on the experiment can be found in experimental section). Adsorption is an equilibrium process. According to the results, by plotting TCO concentration versus time it is possible to record $t_{1/2,ads}$.

8.3.7 Breakthrough curve prediction

The common available models in reported literature for breakthrough curve prediction are divided into two main categories based on the existence of a mass transfer resistance between the adsorbent particles and fluid phase or local adsorption assumption between adsorbent particle and bulk phase, i.e. by using intrinsic adsorption kinetics [45].

Local adsorption model-local equilibrium theory

Local adsorption theory is divided into two sets of models depending on the rate of adsorption-local equilibrium theory and local kinetic theory [45], [46].

Local equilibrium theory is based on the existence of equilibrium between adsorbate and fluid concentration, and how fast the equilibrium is reached in each stage in the packed bed column.

Thus $\frac{\partial q_i}{\partial t}$ is defined by using the Langmuir isotherm as follows:

$$\frac{\partial q_i}{\partial t} = \frac{\partial q_i}{\partial C_i} \times \frac{\partial C_i}{\partial t} \quad (8.8)$$

and

$$\frac{\partial q_i}{\partial C_i} = \frac{q_{max} b}{(1 + bC_i)^2} \quad (8.9)$$

where q_{max} and b are from Langmuir isotherm model, see Equation. 8.2.

The local kinetic theory is based on a non-equilibrium adsorption reaction. It is expressed based on the rate of adsorption and desorption of the adsorbate on the surface of adsorbent particles.

In this work an equilibrium surface reaction is governing, so the only model that has been applied is the local equilibrium theory. For the local kinetic theory, see the related literature [45], [46].

Therefore, Equation 8.4 becomes

$$D_{ax} \frac{\partial^2 C_i}{\partial z^2} - v \frac{\partial C_i}{\partial z} = \left[1 + \rho_p \frac{(1 - \varepsilon_b)}{\varepsilon_b} \times \frac{q_{max} b}{(1 + b C_i)^2} \right] \frac{\partial C_i}{\partial t} \quad (8.10)$$

For the model calculations the partial differential equation (8.10) has to be solved. Equation 8.10, is discretized using finite differences and solved using MATLAB® with implicit PDEPE solvers.

The initial condition is a packed bed filled with solvent. Then, at the inlet of the column a step change is applied. The applied boundary conditions are of Danckwert's type conditions [47] and used at the inlet ($z=0$) and at the outlet ($z=L$) of the column (Equation 8.11).

$$\frac{\partial C_i}{\partial z} \Big|_{z=0} = \frac{v}{D_{ax}} (C_i - C_{i,feed}); \quad \frac{\partial C_i}{\partial z} \Big|_{z=L} = 0 \quad (3.11)$$

The initial conditions are given by Equation 8.12

$$C_i(z, t = 0) = 0 \quad (3.12)$$

8.3.8 Modeling the combination of the photo-microreactor and the adsorption column

In this section it is aimed to predict the *cis*-cyclooctene conversion when there is a continuous closed system of the photo-microreactor with an integrated adsorption column and recycling the unreacted *cis*-isomer to the reactor feed solution (Figure 8.2). In order to mathematically model the system, two control volumes are selected: the photo-microreactor and the packed bed (1), and the stirred vessel with solution to be fed to the photoreactor (2).

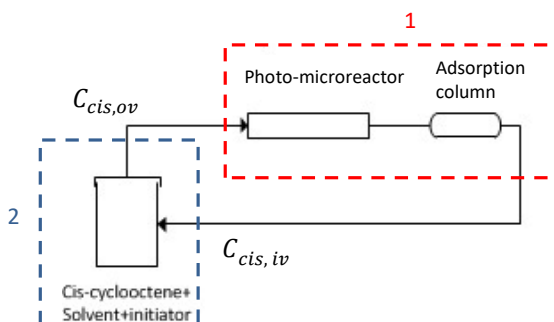


Figure 8.2. Schematic overview of the complete photo-microreactor and the adsorption system control volumes; (1): photo-microreactor and packed bed, (2): inlet vessel with reactor feed solution

The rate of photoisomerization of the *cis*-isomer into the *trans*-isomer has been given in the previous section (3.1). It is assumed that the amount of the *cis*-isomer adsorbed in the packed bed is negligible. Therefore, for the first control volume and a single pass of the flow, if $C_t = \frac{n_{cis}}{V}$, where n_{cis} denotes the molar amount of the *cis*-isomer in the inlet vessel and V the volume of the photo-microreactor, the rate equation becomes (only if the outlet concentration of the *trans*-isomer from the packed bed is zero):

$$-\frac{dC_{cis}}{dt} = (k_1 + k_{-1}) \times C_{cis} - k_{-1} \times \frac{n_{cis}}{V} \quad (8.13)$$

In order to model the second control volume, a mass balance is set up over the inlet vessel, see Equation 8.14. The inlet vessel is assumed to be ideally mixed.

$$[n_{cis}]_{t+\Delta t} - [n_{cis}]_t = Q \times C_{cis,iv} \times \Delta t - Q \times \frac{n_{cis}}{V} \times \Delta t \quad (8.14)$$

where Q and $C_{cis,iv}$ stand respectively for the total volumetric flow rate and the *cis* concentration at the inlet of the vessel. Division the right and left hand side of Equation 8.14 by Δt and taking the limit $\Delta t \rightarrow 0$, leads to:

$$\frac{dn_{cis}}{dt} + \frac{Q}{V}n_{cis} = Q \times C_{cis,iv} \quad (8.15)$$

Equation 8.15 expresses the change in the amount of *cis*-isomer with respect to time. The concentration of *cis*-isomer at the outlet of the first control volume, (i.e. the outlet of the packed bed for *trans*-isomer adsorption) is equal to the concentration of the *cis*-isomer at the inlet of control volume 2, (i.e. the vessel with the reactor feed solution) $C_{cis,iv} = C_{cis}$.

Equation 8.13 and 8.15 are first order ordinary differential equations (ODEs) which are solved simultaneously by employing numerical methods (in MATLAB®) whereby the final concentration of *cis*-isomer or the final conversion of the *cis*-isomer with respect to time is obtained. The initial values for numerically solving Equation 8.13 and 8.15 are $C_{cis} = C_0$ and $n_{cis} = \frac{C_0}{V}$, where C_0 is the initial concentration of the *cis*-isomer in the reactor feed vessel.

8.4 Results and Discussion

8.4.1 Kinetic study of photoisomerisation

The photoisomerization of *cis*-cyclooctene into *trans*-cyclooctene has been investigated in detail in photo-microreactor. In order to determine the optimal reaction condition, the photoisomerisation was performed at various residence times (for more details see experimental

section in supplementary material). The results are presented in Figure 8.3. Figure 8.3 shows that conversion is limited by equilibrium to approximately 28%.

k_1 and k_{-1} determination

The experimental data points in Figure 8.3 have been fitted to Equation 8.1. A regression analysis is carried out in MATLAB® (see Figure 8.3). k_1 and k_{-1} at 23°C are calculated to be 0.45 and 1.23 (1/min), respectively. For 23°C the equilibrium constant is $K = \left(\frac{C_{trans}}{C_{cis}}\right)_{eq} = \frac{k_1}{k_{-1}} = 0.36$.

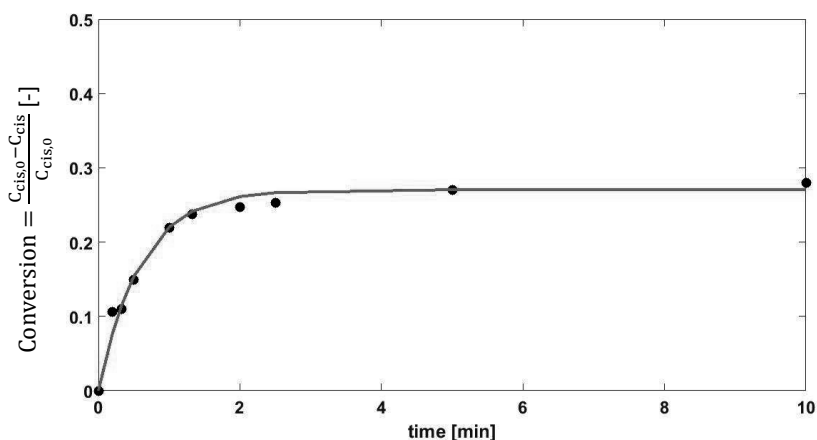


Figure 8.3. Results of regression analysis for calculating k_1 and k_{-1} . $X_{eq}=0.28$ at 23°C, (●): experimental points; calculated line with Equation 8.1 and $k_1=0.45$ (1/min) and $k_{-1}= 1.23$ (1/min).

8.4.2 Adsorption isotherm

As stated before, the experimental adsorption isotherms represent the balance between adsorbent and adsorbate at equilibrium conditions. Figure 8.4 shows the adsorption isotherm for *trans*-cyclooctene on $\text{AgNO}_3/\text{silica}$ at 23°C. Provided that the adsorption isotherm obeys the Langmuir isotherm type, $\frac{C_{B_e}}{q_B}$ versus C_{B_e} should represent a linear behavior. Furthermore, $\frac{C_{B_e}}{q_B}$ versus C_{B_e} has been plotted, from which it can be observed that $\frac{C_{B_e}}{q_B}$ is a linear function of C_{B_e} . The results indicate that the adsorption of TCO on AgNO_3 obeys the Langmuir isotherm model and the highest adsorption capacity was recorded at 43.089 mg/g at initial concentration of 5.85 g/dm³.

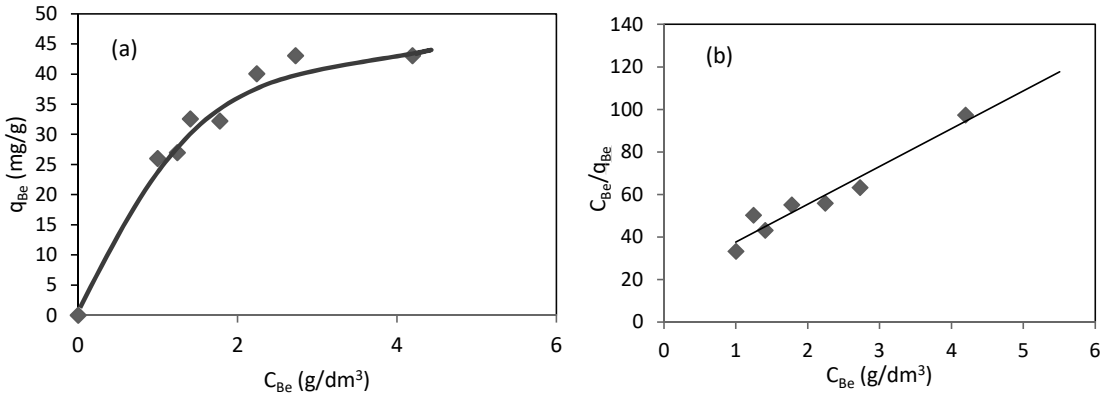


Figure 8.4. Adsorption isotherm of *trans*-cyclooctene on the AgNO₃/SiO₂ at 23°C, $W_{AgNO_3}=0.175$ g, $\frac{C_{Be}}{q_{Be}} = 17.515C_{Be} + 20.529, R^2 = 0.965$; (a) nonlinearized form and (b) linearized form (Equation 8.3), for calculated parameters b and $q_{B_{max}}$, see Table 8.1

Accordingly, the Langmuir model parameters, b and $q_{B_{max}}$, have been calculated see Table 8.1.

Table 8.1. Langmuir isotherm parameter b and $q_{B_{max}}$ for TCO adsorption on AgNO₃/silica at 296.15 K

$b = 0.85$ (dm ³ /g _{trans})	$q_{B_{max}} = 57.1 \times 10^{-3}$ (g _{trans} /g _{AgNO₃})
---	--

8.4.3 Adsorption kinetics

Adsorption kinetics of TCO on to AgNO₃/silica was studied by performing an experiment in batch. In that experiment a known amount of AgNO₃/silica, (0.175g) was suspended in the solution of TCO, $C_0=8.06$ g/dm³ in n-hexane. The time history of the liquid concentration of TCO was recorded, see Figure 8.5. In order to prevent any external mass transfer limitation, the suspension was stirred intensively. The experimental data were analyzed using (pseudo-)first-order and (pseudo-)second-order kinetics [48]–[52], see Equation 8.16 and 8.18, respectively:

$$\frac{dq_t}{dt} = k(q_{max} - q_t)^n \quad (8.16)$$

$n=1$ for (pseudo-)first-order and $n=2$ for (pseudo-)second-order

$$\ln \frac{(q_{Be} - q_{B_t})}{q_{Be}} = -k't \quad (8.17)$$

$$\frac{1}{q_{B_t}} = \frac{1}{k'' q_{B_e}^2 \cdot t} + \frac{1}{q_{B_e}} \quad (8.18)$$

Where k' (min^{-1}) is the rate constant for the (pseudo-)first-order and k'' ($\text{g mg}^{-1} \text{min}^{-1}$) is the rate constant for the (pseudo-)second-order kinetic models. q_{B_e} and q_{B_t} are the amount of the *trans*-isomer adsorbed per gram AgNO_3 at equilibrium and at time t , respectively. The constants can be calculated from the intercepts and slopes of the linear plots of $\ln(q_{B_e} - q_{B_t})$ versus t and t/q_{B_t} versus t , respectively (Figure 8.5).

Figure 8.5a shows that adsorption of *trans*-cyclooctene proceeds rapidly during the first 30s and becomes almost constant after 1 min. The adsorption rate constants and linear regression values are collected in Table 8.2. The results in Figure 8.5 and Table 8.2 reveal that adsorption obeys a (pseudo-)second order rate law. Also the experimentally observed value of q_{B_e} is equal to $44.3 \times 10^{-3} \text{ g}_{\text{trans}}/\text{g}_{\text{AgNO}_3}$ and it can be easily observed that it is very close to q_{B_e} calculated from pseudo-second order kinetic model This fact suggests that the adsorption rate of *trans*-cyclooctene is dependent on the adsorption site availability on AgNO_3 rather than the *trans*-cyclooctene concentration in solution [53], [54]. Initially, there are many adsorption sites are available, however with the prolonging time the sites have been occupied, hence, limited free sites for molecule to be adsorbed on [53], [55].

Table 8.2. Pseudo-second-order rate constant for adsorption of TCO onto AgNO_3 at 23°C

Models	Model parameters	R ²
(pseudo-)first-order	$q_{B_e} = 15.87 \text{ mg/g}$	0.69
	$k' = 8.8 \times 10^{-3} \text{ min}^{-1}$	
(pseudo-)second-order	$q_{B_e} = 44.25 \text{ mg/g}$	0.9924
	$k'' = 0.51 \times 10^{-3} \text{ g}_{\text{AgNO}_3} \text{ mg}^{-1}_{\text{trans}} \text{ min}^{-1}$	

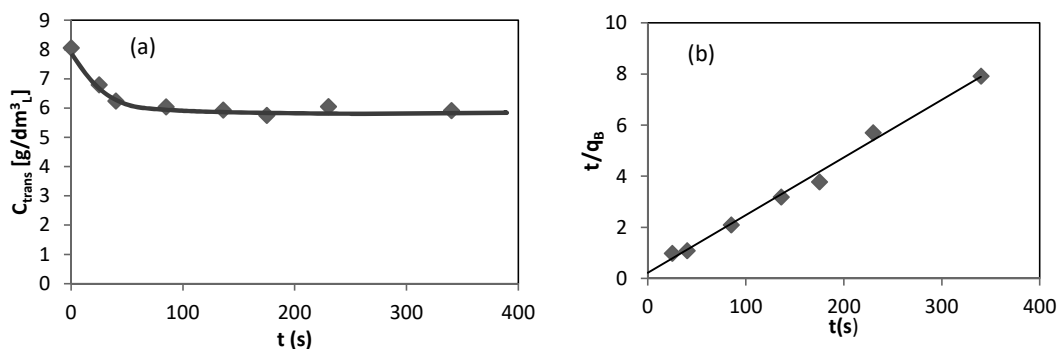


Figure 8.5. (a) Liquid phase concentration of *trans*-cyclooctene in a stirred vessel with a suspension of $\text{AgNO}_3/\text{SiO}_2$ in *n*-hexane (1% diethyl ether) $W_{\text{AgNO}_3/\text{SiO}_2}=0.175 \text{ g}$, $C_0=8.06 \text{ g/dm}^3$ at 23°C , (b) (pseudo-)second-order kinetics for adsorption of *trans*-cyclooctene onto $\text{AgNO}_3/\text{SiO}_2$

8.4.4 Packed bed

Breakthrough model validation

In order to validate the model (see Equation 8.8-8.12), the obtained results from the adsorption breakthrough curve model are compared with the experimental results, see Figure 8.6. The calculated breakthrough curve agrees reasonably well with the experimentally observed curve. The proposed breakthrough curve model is able to predict the saturation time, t_s , of the adsorption column. t_s is the time at which $\frac{C_{trans}}{C_{tran}} = 0.05$.

8.4.5 Process design for integration of a photo-microreactor and adsorption for the isomerization of *cis*-cyclooctene in to *trans*-cyclooctene

After optimizing each sub process, i.e. photoisomerisation and adsorption, in this section, the process configuration for photoisomerisation of *cis* into *trans*-cyclooctene is presented for three different cases. These three cases were experimentally tested. The model for the adsorption column that was presented earlier in this chapter, can be used to estimate saturation time and the operational parameters such as the temperature for the adsorption of *trans*-cyclooctene. Later in the text the validity of the model as described in section 3.3 is confirmed with the experimental results.

Solvent selection

The selection of a proper solvent is crucial in any (photo)chemical reaction. Here, this is even more significant as the solvent should play a role in different process steps. First, it should be able to solubilize the cyclooctene (both *cis*- and *trans*-) and the sensitizer. Also, the solvent has to be transparent at the required wavelength, 245 nm. On the other hand, it should not dissolve the packing powders ($\text{AgNO}_3/\text{silica}$). If AgNO_3 dissolves, the *trans*-complex will not be collected

in packed bed and there is no separation of the *trans*-isomer from the *cis*-isomer. This means that there is no equilibrium shift in the direction of the *trans*-isomer. Considering the features mentioned, n-hexane or cyclohexane seem to be proper choices. Cyclohexane has a higher boiling point than n-hexane. Since to desorb *trans*-cyclooctene from $\text{AgNO}_3/\text{SiO}_2$ there is an elution step needed which is not included in this process design. Therefore, as the solvent of this process, n-hexane is preferred. Also, in order to increase the solubility of *cis* and *trans*-cyclooctene 1% of diethyl ether is added. It is worth mentioning that diethyl ether dissolves AgNO_3 , so it is recommended not to increase the ratio of diethyl ether to n-hexane to more than 5:95 (volume ratio).

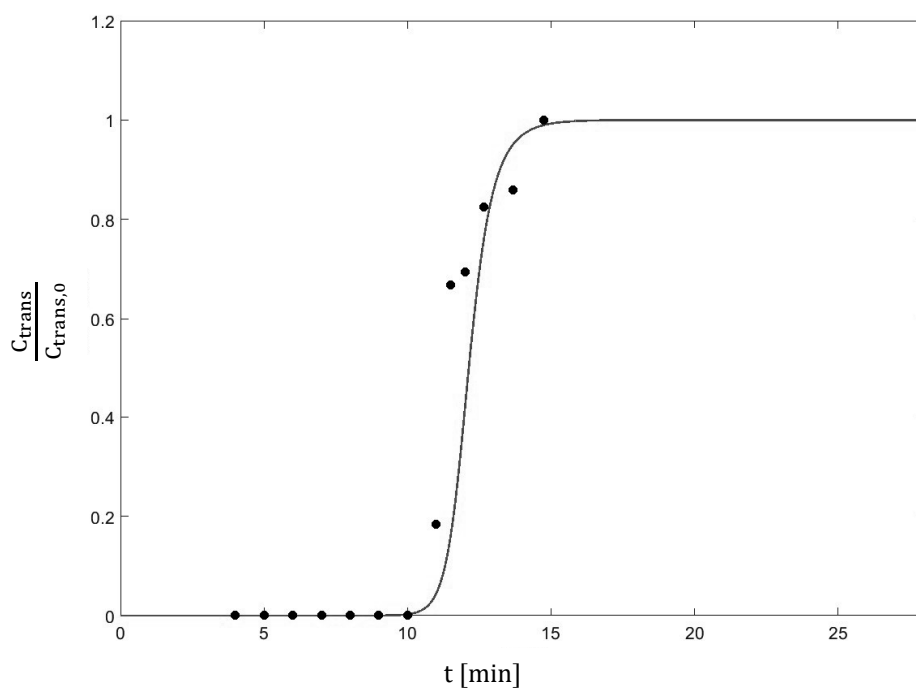


Figure 8.6. Calculated and experimental breakthrough curve at 23°C, $W_{\text{AgNO}_3}=0.2$ g, volumetric flow rate= 1 ml/min, $C_{\text{trans}0}=1.99$ gr/dm³

8.4.6 Process configurations

Case (a). This case concerns the basic continuous flow setup in which a photo-microreactor of 5 m length and an adsorption column of 5 cm length packed with $\text{AgNO}_3/\text{SiO}_2$ powders are used (Figure 8.7a). The flow rate is set to 0.2 ml/min. As reported earlier in section 2.4, in all cases the outlet flow from the packed bed is recycled to the vessel with the reactor feed solution.

Case (b). Since, our system is a closed-loop recycle flow system, it is important that as soon as photoreaction takes place the molecules are transferred to the separation unit and from there quickly recycled to the feed vessel. Therefore, the key in this design (case (b)) is to reduce the residence time of the flowing fluid in the connecting tubes and parts between the feed vessel, the photo-microreactor(s) and the packed bed.

In this case, we applied the concept of symmetrical flow splitting by using a T-micromixer placed in reverse mode to act as flow splitter in a bifurcate fashion the feed flow rate is directed towards two photo-microreactors of 5 m length which are wound around one UV light and placed in parallel (Figure 8.7b). With this design, it is possible to double the main flowrate while keeping the residence time in the photo-microreactor the same as in case (a).

Therefore, the total flow rate is raised to 0.4 ml/min which speeds up the flow in connecting parts, and by symmetrical flow splitting, the flow rate is kept 0.2 ml/min in each photo-microreactor.

Case (c). This case is similar to the case (b). Again, two parallel photo-microreactors are used. But, the main difference is that in this configuration more than one packed bed, each with a length of 2.5 cm, are installed in parallel, see Figure 8.7c. This adds the function of refreshing the adsorption column under use, by switching between two columns set in parallel – one for the closed-loop flow and the other in a wait position, being re-activated. Such an integrated flow configuration for purification following micro-flow reaction was already proposed by us in the first chapter, using a fixed-bed column packed with Amberlyst resin for an ion-exchange based purification of the product mixture [26].

In the operational mode, the parallel packed beds are connected to the photoreactor by a switching valve. While one packed bed is in use to adsorb the *trans*-isomer, the other is in the waiting mode. As soon as the first column reaches saturation, the flow is switched to pass through a fresh packed bed. Based on the amount of the inlet *cis*-cyclooctene, in this case, three parallel packed beds are used. Also, the flow rate is increased to 0.66 ml/min.

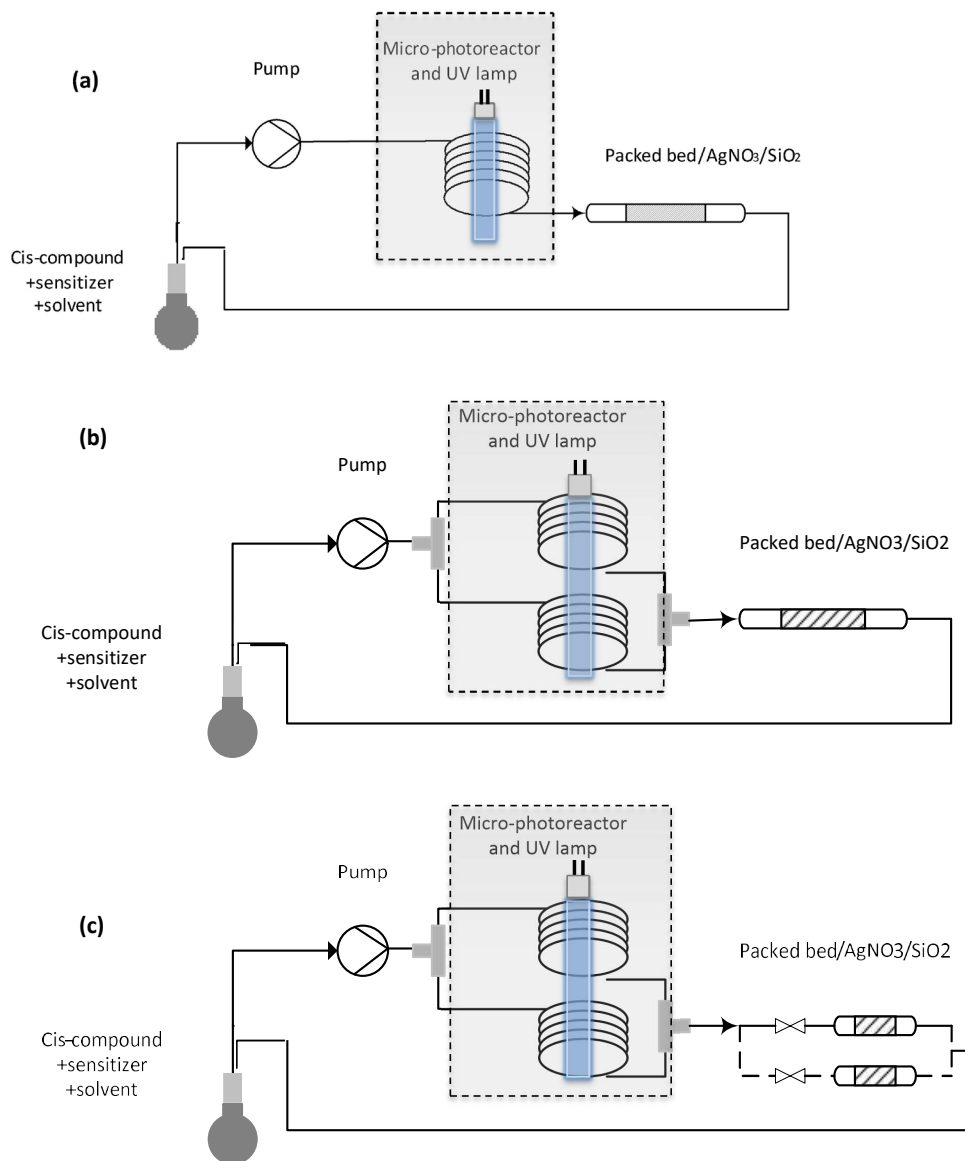


Figure 8.7. Three different process configuration for photoisomerisation of *cis* to *trans*-cyclooctene. case (a), case (b), case (c).

8.4.7 Validation of the model in the combination of photo-microreactor and adsorption column

The results in Figure 8.8 demonstrate that the conversion of *cis*-cyclooctene as a function of the process time obtained from solving the model discussed in section 3.3. This model has been solved and sketched for different total flow rates and compared with each experimental case. Here, time is the total operational time.

In case (a) after 400 min almost 70% conversion is achieved. This time is the total required time of operation since this is a closed-loop system operating in a recycling mode. In the case (b), as stated earlier the total flow rate is doubled to 0.4 ml/min, while the residence time in each photoreactor is the same as in case (a). Figure 8.8b shows that there is a small deviation between the results of the model calculations and the experimental results. Besides, upon increasing the total operational time, the deviation increases and at some point the experimental results tend to reach a plateau earlier than with the predicted model. Since the total flow rate is doubled, the flow rate inside the packed bed is also doubled. Therefore, the packed bed reaches saturation earlier in case (b) than in case (a). With prolonging time, the packed bed becomes saturated with TCO and TCO molecules are not adsorbed anymore and recycled in the system which also affects the photoreaction process to reach equilibrium faster. As a result, the total conversion of *cis*-cyclooctene is not improved anymore and therefore the experimental points tend to reach a plateau and deviate from the model.

In case (c), there is less deviation between the experimental points and the results of the model calculations (Figure 8.8c). The first switching towards a fresh packed bed was at 75 min operational time and the second switch was at 180 min. As indicated in Figure 8.8c, after 50 min the packed bed tends to reach saturation. Therefore there is a plateau before the fresh packed bed was in use (75 min) which explains the small deviation between the experimental results and the results of model calculations. Also, it is important to note that this is a closed system and the concentration of the *cis*-isomer is getting less with respect to the operational time. Therefore, the first packed bed is saturated in less time than the ones used later, so as time increases the packed bed saturation time also increase due to the smaller concentration of *cis*-isomer in the flowing fluid. In case (c) 90% conversion is achieved after 250 min.

According to the results, case (c) shows a massive improvement compared to the first two cases. Primarily, using the packed bed with smaller volume gives the chance to quicker recycle the *cis*-isomer. This results in an improvement of the total conversion at any certain time. Also, changing the packed bed as soon as it reaches its saturation point, improves the process performance in terms of an increasing rate of production of the *trans*-isomer. Table 8.3 summarizes the performance of the different design cases. To give better comparison, we calculate the total conversion divided by the total time of operation for each case which can be correlated to the

overall reaction rate of the closed-loop system. As it is expected this number is much higher in case (c), 0.36 (min^{-1}) compared to the case (a) and (b), which are 0.175 and 0.2 (min^{-1}), respectively.

Table 8.3. Summary of different configuration's performance

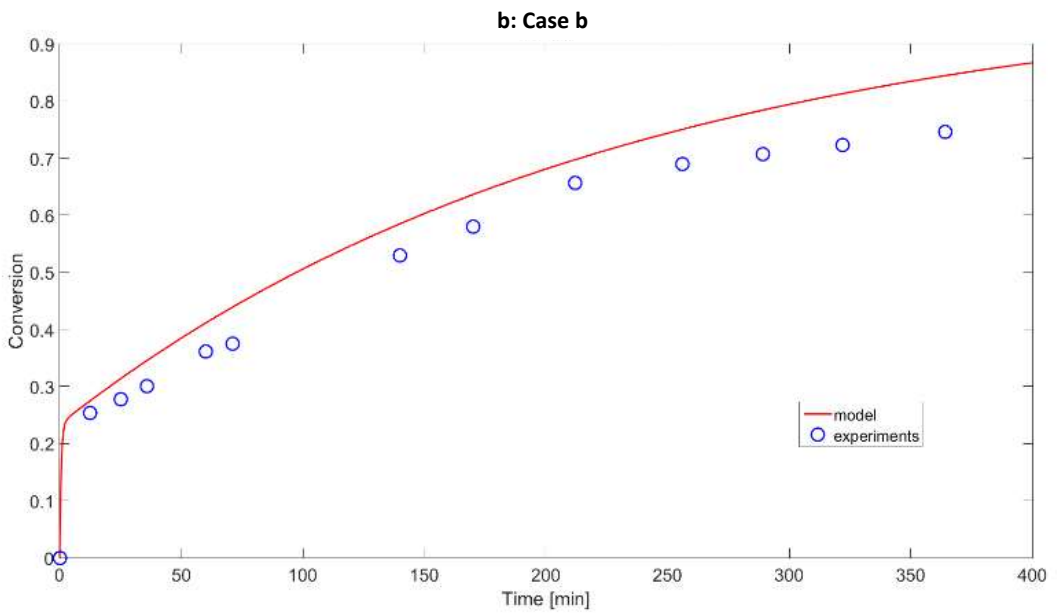
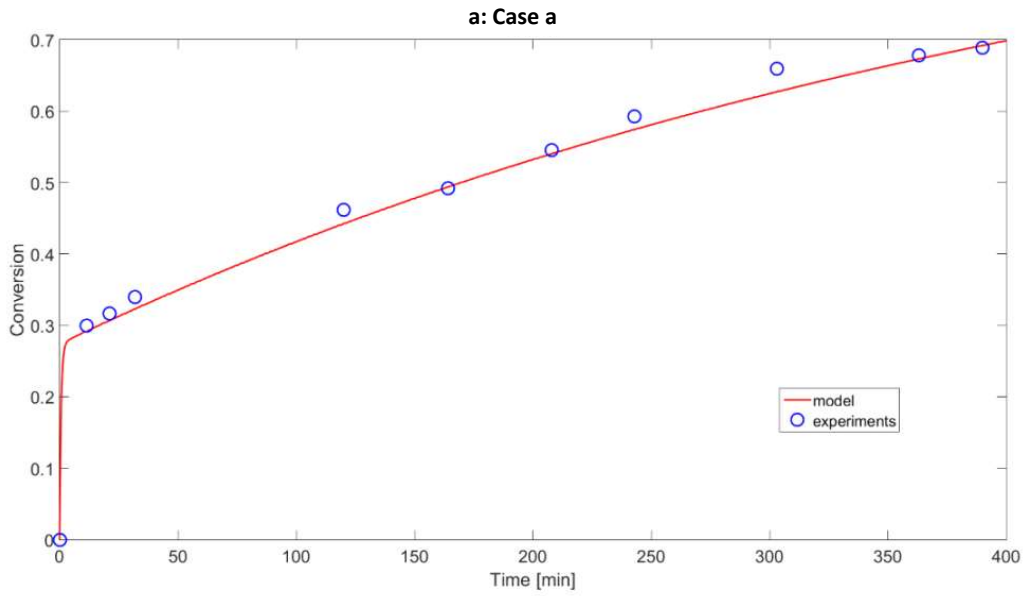
	Total flow rate (ml/min)	Time of operation (min)	Total conversion (%)	Conv./time of operation (min^{-1})
Case (a)	0.2	400	70	0.175
Case (b)	0.4	365	75	0.2
Case (c)	0.66	250	90	0.36

It is worth mentioning that the outcome of this process configuration has been successfully applied for the photoisomerisation of functionalized TCO in our research [56].

Flow rate effect

As can be seen in Figure 8.8d and be expected for a closed-loop recycle flow system, for a certain time of operation, larger flow rates result in a higher conversion. For instance, if the total flow rate is equal to 0.66 ml/min, after almost 3hr, more than 80% of *cis*-cyclooctene is converted. While, if we double the total flow rate to 1.2 ml/min, a conversion of more than 90 % can be reached within 3 hr. On the other hand, if the flow rate is kept lower, for instance 0.2 ml/min, after 3 hrs, only 50 % of *cis*-cyclooctene is converted. By increasing the total flow rate, although the stable equilibrium may not be reached in photo-microreactor, we get benefit from recycling the feed faster and the whole process speeds up. Therefore, comparing the higher flow rate case with the lower flow rate cases, indicates that in less time of operation, higher conversion is

achieved.



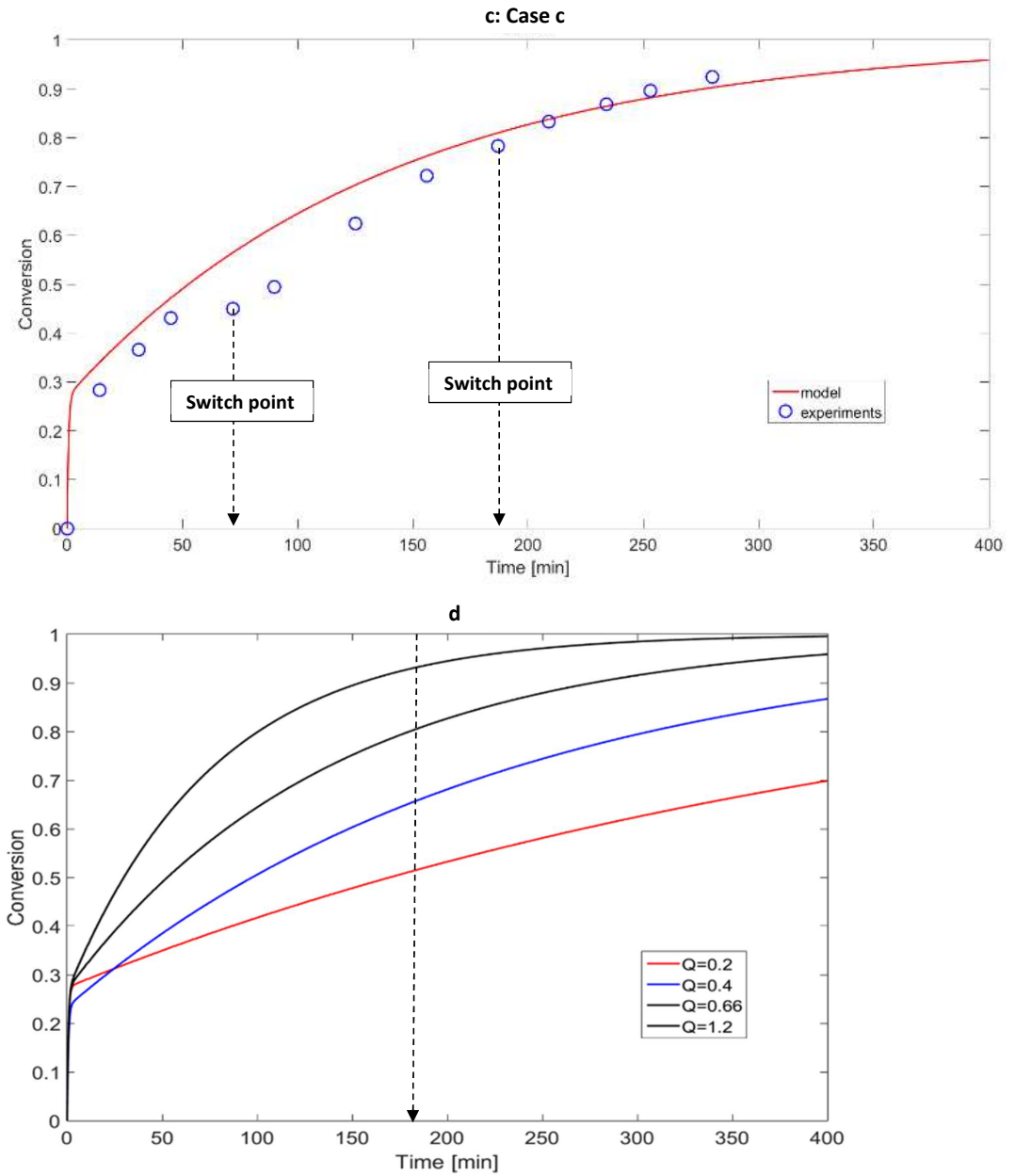


Figure 8.8. Validation of the model of combination of the photoreactor and adsorption column and comparing the results with three process configuration, (a) case a, (b) case b, (c) case c, (d) Total flow rate (ml/min) effect on *cis*-cyclooctene conversion

8.5 Conclusions

In this chapter, an integrated photo micro-flow adsorption was developed for product separation, with the option to do that in recycle mode. This was investigated to produce *trans*-cyclooctene from its *cis*-isomer. Here, the thermodynamic equilibrium is shifted by inserting an in-flow separation in a recycling flow mode, which makes better use of the given photoenergy (transport intensification). Further, a full theoretical study of in-flow separation in a recycling flow mode has been conducted. Moreover, different process design options to reach an optimum yield of *trans*-cyclooctene are proposed and experimentally tested. Radiolabeled *trans*-cyclooctenes are valuable in vivo click synthons for PET imaging.

First, the kinetics of the photoisomerisation of *cis*- to *trans*-cyclooctene was investigated in a microreactor. Results confirm that the conversion is limited by equilibrium to nearly 28%. The comparison of the reaction rate constants, k_1 and k_{-1} , shows that the reaction rate from *trans*- to *cis*- is higher than *cis*- to *trans*-cyclooctene.

Moreover, an in-depth study of the TCO adsorption on $\text{AgNO}_3/\text{SiO}_2$ was done. The results indicate that the adsorption of TCO on AgNO_3 follows the Langmuir isotherm model. The reaction rate is governed by the equilibrium surface reaction. The analysis of the adsorption kinetic data demonstrated that the kinetics can be approximated with a pseudo-second order rate equation. The maximum adsorption capacity of the *trans*-isomer adsorbed per gram AgNO_3 is equal to $44.25 \text{ mg}_{\text{trans}}/\text{g}_{\text{silvernitrate}}$.

The dynamic behavior of the adsorption column was experimentally studied and modeled according to the local equilibrium theory. The results of the model calculations show good agreement with the experimental data. Based on the model, it is possible to predict the breakthrough curve and saturation time of the mentioned adsorption column.

Finally, after optimization of each sub process, i.e. photoisomerisation and adsorption, three different integrated process designs for photoisomerisation of the *cis* to *trans*-isomer was mathematically modeled. According to the calculated model, it is important to remark that by increasing the flow rate a higher conversion of *cis*-isomer was achieved. By increasing the total flow rate, the time that the flow is passing through connecting parts is reduced and also, speeding up the feed recycling gives an advantage. Furthermore, the three different process configurations were tested experimentally. Comparing three cases, case (c) (Figure 8.8), shows improvement of the total conversion of the *cis*-isomer. 90% conversion was achieved after 250 min. In case (c) two parallel photo-microreactors and parallel packed beds in switching mode were applied. Switching the packed bed as soon as it reaches saturation results in obtaining higher conversion in less time. Numbering up the sub processes gives a good promise for scaling up this integrated process.

It is worth mentioning that in this closed-loop system, solvent can be added only once at the beginning. In this system solvent is only carrier medium and is not consumed or converted, thus by recycling, solvent is also recovered and transferred back to the system. As soon as the amount of *cis*-isomer reaches to 0.05 of initial concentration, fixed amount of *cis*-isomer can be added to the initial feed vessel which already contains enough solvent. Therefore, with this closed-loop design, it is possible to reduce the amount of solvent usage to only once.

8.6 Acknowledgements

We kindly acknowledge the European Research Council for the Advanced Grant on “Novel Process Windows—Boosted Micro Process Technology” No 267443.

8.7 References

- [1] E. D. G. Fleuren *et al.*, "Theranostic applications of antibodies in oncology," *Molecular Oncology*, vol. 8, no. 4. pp. 799–812, 2014.
- [2] L. E. Lamberts *et al.*, "Antibody positron emission tomography imaging in anticancer drug development," *J. Clin. Oncol.*, vol. 33, no. 13, pp. 1491–1504, 2015.
- [3] R. J. Hargreaves, "The role of molecular imaging in drug discovery and development," *Clinical Pharmacology and Therapeutics*, vol. 83, no. 2. pp. 349–353, 2008.
- [4] H. H. Pien, A. J. Fischman, J. H. Thrall, and A. G. Sorensen, "Using imaging biomarkers to accelerate drug development and clinical trials," *Drug Discov. Today*, vol. 10, no. 4, pp. 259–266, 2005.
- [5] C. Denk *et al.*, "Development of a ¹⁸F-Labeled Tetrazine with Favorable Pharmacokinetics for Bioorthogonal PET Imaging," *Angew. Chemie Int. Ed.*, vol. 53, no. 36, pp. 9655–9659, 2014.
- [6] K. Serdons, A. Verbruggen, and G. M. Bormans, "Developing new molecular imaging probes for PET," *Methods*, vol. 48, no. 2. pp. 104–111, 2009.
- [7] M. L. Blackman, M. Royzen, and J. M. Fox, "Tetrazine ligation: Fast bioconjugation based on inverse-electron-demand Diels-Alder reactivity," *J. Am. Chem. Soc.*, vol. 130, no. 41, pp. 13518–13519, 2008.
- [8] N. K. Devaraj, R. Upadhyay, J. B. Haun, S. A. Hilderbrand, and R. Weissleder, "Fast and sensitive pretargeted labeling of cancer cells through a tetrazine/trans-cyclooctene cycloaddition," *Angew. Chemie - Int. Ed.*, vol. 48, no. 38, pp. 7013–7016, 2009.
- [9] E. M. F. Billaud *et al.*, "Pretargeted PET Imaging Using a Bioorthogonal (18)F-Labeled trans-Cyclooctene in an Ovarian Carcinoma Model.," *Bioconjug. Chem.*, vol. 28, no. 12, pp. 2915–2920, 2017.
- [10] C. Wolf, *Dynamic Stereochemistry of Chiral Compounds*. 2007.
- [11] J. S. Swenton, "Photoisomerization of cis-cyclooctene to trans-cyclooctene," *J. Org. Chem.*, vol. 34, no. 10, pp. 3217–3218, 1969.
- [12] M. Royzen, G. P. A. Yap, and J. M. Fox, "A Photochemical Approach to Functionalized trans - Cyclooctenes Driven by Metal Complexation," pp. 1–30.
- [13] C. Jiménez-Gonzalez *et al.*, "Key green engineering research areas for sustainable manufacturing: A perspective from pharmaceutical and fine chemicals manufacturers," *Org. Process Res. Dev.*, vol. 15, no. 4, pp. 900–911, 2011.
- [14] P. Poechlauer *et al.*, "Pharmaceutical Roundtable Study Demonstrates the Value of Continuous Manufacturing in the Design of Greener Processes," *Org. Process Res. Dev.*, vol. 17, no. 12, pp. 1472–1478, 2013.
- [15] L. Vaccaro, D. Lanari, A. Marrocchi, and G. Strappaveccia, "Flow approaches towards sustainability," *Green Chem.*, vol. 16, no. 8, pp. 3680–3704, 2014.
- [16] E. E. Coyle and M. Oelgemöller, "Micro-photochemistry: photochemistry in microstructured reactors. The new photochemistry of the future?," *Photochem. Photobiol. Sci.*, vol. 7, no. 11, p. 1313, 2008.
- [17] J. P. Knowles, L. D. Elliott, and K. I. Booker-Milburn, "Flow photochemistry: Old light through new windows," *Beilstein J. Org. Chem.*, vol. 8, pp. 2025–2052, 2012.

- [18] Y. Su, N. J. W. Straathof, V. Hessel, and T. Noël, "Photochemical Transformations Accelerated in Continuous-Flow Reactors: Basic Concepts and Applications," *Chem. – A Eur. J.*, vol. 20, no. 34, pp. 10562–10589, 2014.
- [19] D. Cambié, C. Bottecchia, N. J. W. Straathof, V. Hessel, and T. Noël, "Applications of Continuous-Flow Photochemistry in Organic Synthesis, Material Science, and Water Treatment," *Chem. Rev.*
- [20] T. Noël, *Photochemical Processes in Continuous-Flow Reactors*. World Scientific, 2017.
- [21] M. W. Losey, M. A. Schmndt, and K. F. Jensen, "Microfabricated multiphase packed-bed reactors: Characterization of mass transfer and reactions," *Ind. Eng. Chem. Res.*, vol. 40, no. 12, pp. 2555–2562, 2001.
- [22] K. F. Jensen, "Microreaction engineering — is small better?," *Chem. Eng. Sci.*, vol. 56, no. 2, pp. 293–303, 2001.
- [23] M. Shang, T. Noël, Y. Su, and V. Hessel, "High Pressure Direct Synthesis of Adipic Acid from Cyclohexene and Hydrogen Peroxide via Capillary Microreactors," *Ind. Eng. Chem. Res.*, vol. 55, no. 10, pp. 2669–2676, 2016.
- [24] J. R. H. Carucci *et al.*, "Ethylene oxide formation in a microreactor: From qualitative kinetics to detailed modeling," in *Industrial and Engineering Chemistry Research*, 2010, vol. 49, no. 21, pp. 10897–10907.
- [25] M. Jiang, Y. Qi, Y. L. Cui, L. Zhao, and S. Liu, "Removal and Recovery of Chromium from Aqueous Solutions by Reduction-Absorption Microreactor," *Water. Air. Soil Pollut.*, vol. 228, no. 1, 2017.
- [26] E. Shahbazali, M. Spapens, H. Kobayashi, S. Ookawara, T. Noël, and V. Hessel, "Connected nucleophilic substitution-Claisen rearrangement in flow – Analysis for kilo-lab process solutions with orthogonality," *Chem. Eng. J.*, vol. 281, pp. 144–154, 2015.
- [27] E. Shahbazali, T. Noel, and H. Volker, "Photo-claisen rearrangement of allyl phenyl ether in micro-flow: influence of phenyl core substituents and vision on orthogonality," *J. Flow Chem.*, vol. 6, no. 3, pp. 252–259, 2016.
- [28] V. Hessel, I. Vural Gürsel, Q. Wang, T. Noël, and J. Lang, "Potential Analysis of Smart Flow Processing and Micro Process Technology for Fastening Process Development: Use of Chemistry and Process Design as Intensification Fields," *Chemical Engineering and Technology*, vol. 35, no. 7, pp. 1184–1204, 2012.
- [29] V. Hessel, I. Vural Gürsel, Q. Wang, T. Noël, and J. Lang, "Potential Analysis of Smart Flow Processing and Micro Process Technology for Fastening Process Development: Use of Chemistry and Process Design as Intensification Fields," *Chem. Eng. Technol.*, vol. 35, no. 7, pp. 1184–1204, Jul. 2012.
- [30] V. Hessel, "Novel Process Windows - Gate to Maximizing Process Intensification via Flow Chemistry," *Chem. Eng. Technol.*, vol. 32, no. 11, pp. 1655–1681, Nov. 2009.
- [31] V. Hessel, D. Kralisch, N. Kockmann, T. No??l, and Q. Wang, "Novel process windows for enabling, accelerating, and uplifting flow chemistry," *ChemSusChem*, vol. 6, no. 5, pp. 746–789, 2013.
- [32] T. Noël, T. J. Maimone, and S. L. Buchwald, "Accelerating palladium-catalyzed C-F bond formation: Use of a microflow packed-bed reactor," *Angew. Chemie - Int. Ed.*, vol. 50, no. 38, pp. 8900–8903, 2011.
- [33] J. R. Naber and S. L. Buchwald, "Packed-bed reactors for continuous-flow C-N cross-coupling," *Angew. Chemie - Int. Ed.*, vol. 49, no. 49, pp. 9469–9474, 2010.

- [34] T. Noël, S. Kuhn, A. J. Musacchio, K. F. Jensen, and S. L. Buchwald, "Suzuki-miyaura cross-coupling reactions in flow: Multistep synthesis enabled by a microfluidic extraction," *Angew. Chemie - Int. Ed.*, vol. 50, no. 26, pp. 5943–5946, 2011.
- [35] Y. I. Hiroshi Tsuneishi, Tadao Hakushi, "Singlet- versus triplet-sensitized enantiodifferentiating photoisomerization of cyclooctene: remarkable effects of spin multiplicity upon optical yield," *J. Chem. SOC., Perkin Trans. 2*, pp. 1601–1605, 1996.
- [36] M. R. Wilson and R. E. Taylor, "Strained alkenes in natural product synthesis," *Angew. Chemie - Int. Ed.*, vol. 52, no. 15, pp. 4078–4087, 2013.
- [37] E. J. Molga and K. R. Westerterp, "Principles of chemical reaction engineering," *Ullmann's Encycl. Ind. Chem.*, 2013.
- [38] H. S. Fogler, "Elements of chemical reaction engineering," *Chem. Eng. Sci.*, vol. 42, p. 1000, 1999.
- [39] K. Y. Foo and B. H. Hameed, "Insights into the modeling of adsorption isotherm systems," *Chem. Eng. J.*, vol. 156, no. 1, pp. 2–10, 2010.
- [40] J. Aracil, J. L. Casillas, and M. Martinez, "Modelling and Solving Fixed-bed Adsorption," vol. 1, no. January 1992, pp. 533–544, 1993.
- [41] C. Costa and A. Rodrigues, "Design of cyclic fixed-bed adsorption processes. Part I: Phenol adsorption on polymeric adsorbents," *AIChE J.*, vol. 31, no. 10, pp. 1645–1654, 1985.
- [42] L. Fournel, P. Mocho, R. Brown, and P. Le Cloirec, "Modeling breakthrough curves of volatile organic compounds on activated carbon fibers," *Adsorption*, vol. 16, no. 3, pp. 147–153, 2010.
- [43] A. A. C. M. B. K.R. Westerterp, W. P. M. van Swaaij, *Chemical reactor design and operation*. Wiley, 1991.
- [44] T. FUNAZUKURI, N. NISHIMOTON, and N. WAKAO, "Binary Diffusion-Coefficients of Organic-Compounds in Hexane, Dodecane, and Cyclohexane at 303.2-333.2-K and 16.0 Mpa," *J. Chem. Eng. Data*, vol. 39, pp. 911–915, 1994.
- [45] M. Siahpoosh, S. Fatemi, and A. Vatani, "Mathematical modeling of single and multi-component adsorption fixed beds to rigorously predict the mass transfer zone and breakthrough curves," *Iran. J. Chem. Chem. Eng.*, vol. 28, no. 3, pp. 25–44, 2009.
- [46] C. L. Chuang, P. C. Chiang, and E. E. Chang, "Modeling VOCs adsorption onto activated carbon," *Chemosphere*, vol. 53, no. 1, pp. 17–27, 2003.
- [47] J. F. Wehner and R. H. Wilhelm, "Boundary conditions of flow reactor (Reprinted from Chem Engng, vol 6, pg 89-93, 1956)," *Chem. Eng. Sci.*, vol. 50, no. 24, pp. 3885–3888, 1995.
- [48] J. Lin and L. Wang, "Comparison between linear and non-linear forms of pseudo-first-order and pseudo-second-order adsorption kinetic models for the removal of methylene blue by activated carbon," *Front. Environ. Sci. Eng. China*, vol. 3, no. 3, pp. 320–324, 2009.
- [49] J. P. Simonin, "On the comparison of pseudo-first order and pseudo-second order rate laws in the modeling of adsorption kinetics," *Chem. Eng. J.*, vol. 300, pp. 254–263, 2016.
- [50] Y. S. Ho and G. McKay, "Pseudo-second order model for sorption processes," *Process Biochem.*, vol. 34, no. 5, pp. 451–465, 1999.
- [51] H. Qiu, L. Lv, B. Pan, Q. Q. Zhang, W. Zhang, and Q. Q. Zhang, "Critical review in adsorption kinetic models," *J. Zhejiang Univ. Sci. A*, vol. 10, no. 5, pp. 716–724, 2009.

- [52] T. Shahwan, "Sorption kinetics: Obtaining a pseudo-second order rate equation based on a mass balance approach," *J. Environ. Chem. Eng.*, vol. 2, no. 2, pp. 1001–1006, 2014.
- [53] X. Song, Y. Zhang, C. Yan, W. Jiang, and C. Chang, "The Langmuir monolayer adsorption model of organic matter into effective pores in activated carbon," *J. Colloid Interface Sci.*, vol. 389, no. 1, pp. 213–219, 2013.
- [54] M. U. Dural, L. Cavas, S. K. Papageorgiou, and F. K. Katsaros, "Methylene blue adsorption on activated carbon prepared from *Posidonia oceanica* (L.) dead leaves: Kinetics and equilibrium studies," *Chem. Eng. J.*, vol. 168, no. 1, pp. 77–85, 2011.
- [55] Y. Matsui, N. Ando, H. Sasaki, T. Matsushita, and K. Ohno, "Branched pore kinetic model analysis of geosmin adsorption on super-powdered activated carbon," *Water Res.*, vol. 43, no. 12, pp. 3095–3103, 2009.
- [56] E. M. F. Billaud *et al.*, "Micro-flow photosynthesis of new dienophiles for inverse-electron-demand Diels–Alder reactions. Potential applications for pretargeted in vivo PET imaging," *Chem. Sci.*, vol. 8, no. 2, pp. 1251–1258, 2017.
- [57] M. A. Vannice and W. H. Joyce, "Acquisition and Evaluation of Reaction Rate Data," pp. 38–86, 2005.
- [58] M. A. Vannice, *Kinetics of catalytic reactions*. Springer, 2005.
- [59] P. Y. Lanfrey, Z. V. Kuzeljevic, and M. P. Dudukovic, "Tortuosity model for fixed beds randomly packed with identical particles," *Chem. Eng. Sci.*, vol. 65, no. 5, pp. 1891–1896, 2010.
- [60] J. H. Dymond and L. A. Woolf, "Tracer diffusion of organic solutes in n-hexane at pressures up to 400 MPa," *J. Chem. Soc. Faraday Trans. 1 Phys. Chem. Condens. Phases*, vol. 78, no. 3, p. 991, 1982.
- [61] J. H. Dymond and L. a. Woolf, "Tracer diffusion of organic solutes in n-hexane at pressures up to 400 MPa," *J. Chem. Soc. Faraday Trans. 1*, vol. 78, no. 3, p. 991, 1982.

8.8 Supplementary Material

S1. Experimental section

General reactant information

Cis-cyclooctene, methyl benzoate, n-dodecane, AgNO₃/Silica (10% loading, +230 mesh size), ammonium hydroxide (28% NH₃ in H₂O), 1,3,5 trimethoxy benzene, n-hexane, diethyl ether and dichloromethane were purchased from Sigma-Aldrich chemical company and used as received. The solvent purity were all according to HPLC grade (>95%). Ultrapure water (HPLC grade, 18.2 MΩ at 25°C) was used.

Trans-cyclooctene preparation

The general procedure to produce *trans*-cyclooctene (TCO) was followed by using the setup which was applied in case 3 (section 4.5.1). In the photoisomerisation of *cis* into *trans*-cyclooctene, 0.06 g (0.55 mmol) of TCO and 0.136 g (1mmol) of methyl benzoate were dissolved in 25 ml of (1: 99 diethyl ether: n-hexane) solvent. The solution was stirred in the inlet vessel and pumped through the micro flow setup (case 3). On average, each 70 minutes the packed bed was changed to a fresh bed. Prior to discharge of the used column, the bed was flushed with solvent (1% ether in n-hexane), dried with compressed air and

stored in an Erlenmeyer flask. Each packed bed approximately contained 200-220 mg of AgNO_3 impregnated silica gel and was mixed with 1 mm borosilicate glass beads in a mass ratio 1.66:1. The experiment was carried out for about 3 hours and the final yield was above 80% (using n-dodecane as internal standard).

Trans-cyclooctene adsorbed on packing powder was extracted by the following procedure. First, the powder was stirred with a mixture of 10 ml ammonium hydroxide solution (28% NH_3 in H_2O) and 10 ml of dichloromethane for about 5 min. Then, the powder was filtered and the filtrate was transferred to a separating funnel. The organic layer was separated and the aqueous phase was extracted by dichloromethane three times (each time 10 ml). The organic layers were combined, washed with water and dried by using MgSO_4 . After filtration, the residue was concentrated under reduced pressure to provide concentrated *trans*-cyclooctene. The yield (80%) was determined by $^1\text{H-NMR}$ using 1,3,5 trimethoxybenzene as an internal standard.

Batch operation for determination of the adsorption isotherm

The batch adsorption experiment was performed in 25 ml glass Erlenmeyer flask at a fixed temperature, 23°C. The first experiment was done by concentrating the pure TCO in n-hexane to a volume of approximately 5 ml. Then 0.192 mmol of 1,3,5 trimethoxybenzene (internal standard for $^1\text{H-NMR}$) was added. Based on the $^1\text{H-NMR}$ result, the amount of TCO was calculated. Then, a fixed amount (0.2 g) of $\text{AgNO}_3/\text{silica}$ was added to the solution. Subsequently, the Erlenmeyer was shaken at 100 rpm in a temperature controlled shaker, for a period of 4 hours. Next, the mixture was kept in stagnant mode to let the particles sediment. From the solution a sample (0.2 ml) was taken for $^1\text{H-NMR}$ analysis. The result is one point in the TCO adsorption isotherm. Afterwards, 3 ml of n-hexane was added to the solution and was shaken again at the same condition as previous for a period of 4 hours and consequently another sample was taken for $^1\text{H-NMR}$ analysis. This procedure was repeated for several times and every time a certain amount of solvent was added and after shaking a sample was taken for $^1\text{H-NMR}$ analysis.

The amount of solute (B) adsorbed per gram dry of adsorbent at equilibrium, q_B (g_B/g), was calculated according to Equation S8.1.

$$q_B = \frac{V}{W} (C_{B_0} - C_{B_e}) \quad (\text{S8.1})$$

Where, C_{B_0} (g/dm³) and C_{B_e} (g/dm³) are respectively the initial and equilibrium concentrations of the solute (B) in the liquid phase, V (dm³) is the solution volume, and W (g) is the weight of the dry adsorbent.

Photo-microreactor kinetics study experiment

In order to perform a kinetic study of the photoisomerization, *cis*-cyclooctene (0.0234 g, 0.2 mmol), methyl benzoate (0.054 g, 0.4 mmol) and n-dodecane (0.014 g, 0.082 mmol) are dissolved in 10 ml n-hexane and mixed well. This solution is pumped in to the photo-microreactor (FEP tubing, 2m) without passing the packed bed. The reaction mixture is not recycled. The flow rate is varied between 0.02-1.0 ml/min, corresponding to mean residence times of 10-0.20 min. The samples are collected for GC analyses at the outlet of photo-microreactor for each flow rate.

Breakthrough curve prediction experiment

The experiment was done by concentrating pure TCO in n-hexane to a volume of 12.75 ml. Then 0.02141 g 1,3,5 trimethoxybenzene (internal standard for $^1\text{H-NMR}$) was added. Based on the $^1\text{H-NMR}$ result, the amount of TCO was calculated which was equal to 0.04 g (0.028 mol/dm^3). Then the solution was diluted to 20 ml ($[\text{TCO}], 0.018 \text{ mol/dm}^3$). The packed bed (stainless steel, ID 4.5 mm, L 25 mm) was packed with 0.2 g $\text{AgNO}_3/\text{silica}$ and 0.12 g glass beads (1 mm), similarly to the previous section. The inlet solution is pumped through the packed bed at the flow rate of 1 ml/min. The outlet of the packed bed was connected to a FEP tube, from which samples were collected for analyses. All packed bed space times have been determined assuming a bed porosity of 0.5.

Characterization

Results of the flow experiments were characterized by gas chromatography (GC-FID; Varian 430-GC) equipped with a CP-Sil 5 CB capillary column, length 30 m (0.25 mm ID, film thickness 1 μm). The carrier gas was helium (1 mL/min, split ratio 1:80). The oven temperature was maintained at 50 $^\circ\text{C}$ for 5 min and then increased to 200 $^\circ\text{C}$ at a rate of 10 $^\circ\text{C}/\text{min}$. The injector temperature was fixed at 250 $^\circ\text{C}$, and the detector temperature at 275 $^\circ\text{C}$. The results from batch experiments and breakthrough curve experiments were characterized by nuclear magnetic resonance spectroscopy ($^1\text{H-NMR}$). Nuclear magnetic resonance spectra were recorded on a Varian 400 MHz instrument. All, $^1\text{H-NMR}$ are reported in chemical shift (δ , part per million (ppm)), and were measured relative to the signal of tetramethylsilane (0 ppm) in the deuterated solvent, unless otherwise stated.

S2. Kinetics of photoisomerisation

If C_{cis} and C_{trans} denote *cis*-cyclooctene and *trans*-cyclooctene concentration, respectively, the rate equation assuming first order kinetics becomes:

$$r_{cis} = k_1 C_{cis} - k_{-1} C_{trans} \quad (\text{S8.2})$$

$$C_{trans} + C_{cis} = C_t \quad (\text{S8.3})$$

$$r_{cis} = (k_1 + k_{-1}) C_{cis} - k_{-1} C_t \quad (\text{S8.4})$$

The conversion of *cis*-isomer can be defined as:

$$X = 1 - \frac{C_{cis}}{C_{cis,0}} \quad (\text{S8.5})$$

For a batch process integration of $\frac{dC_{cis}}{dt} = (k_1 + k_{-1}) C_{cis} - k_{-1} C_t$ leads to Equation 8.1.

S3. Internal mass transfer resistance calculation

In order to study internal mass transfer limitation or effect of pore diffusion on adsorption rate, Weisz-Prater Criteria is used [57].

Silver nitrate/silica pore size is around 60 A (6nm) and considered as meso or microporous. Here, the assumption is silver nitrate nano crystals make the first layer in the silica pores and after some time the

entrance of the pores is plugged in with silver nitrate nano crystals. Therefore, we assume the silver nitrate/silica like a core shell morphology.

Under isothermal conditions at steady state, the observed rate of reaction of the TCO within the AgNO_3 is equal to the diffusion rate across the surface of the particle into the AgNO_3 layer. Since the AgNO_3 layer thickness is much less than the particle diameter, it is assumed that AgNO_3 layer is a two dimensional flat plate.

Other assumptions that are made are as follows,

- Diffusion of TCO within AgNO_3 can be represented by Fick's first law and an over-all invariant effective diffusion coefficient,

$$\text{flux} = -D_{eff} \left(\frac{dC}{dx} \right)$$

- Adsorption involves a single component, TCO

Therefore, a mass balance on the differential volume element:

$$r_{obs} \cdot V = A \cdot D_{eff} \left(\frac{dC}{dx} \right)_{x=\delta} \quad (S8.6)$$

And for a two dimensional slab that $V = \delta \cdot A$:

$$\frac{r_{obs} \cdot \delta}{D_{eff}} = \left(\frac{dC}{dx} \right)_{x=\delta} \quad (S8.7)$$

From literature [57], it is known that

$$\left(\frac{dC}{dx} \right)_{x=\delta} \leq \frac{\beta C_{trans,\delta}}{\delta} \quad (S8.8)$$

where, $\beta C_{trans,\delta}$ is the maximum acceptable decrease in TCO concentration within the AgNO_3 layer.

$C_{trans,\delta}$ is the concentration of TCO at the liquid-solid interface of the boundary layer outside the particle. However, this value is unknown. Therefore, the Weisz-Prater criterion is estimated with the bulk concentration (at this stage it is assumed that there is no external mass transfer).

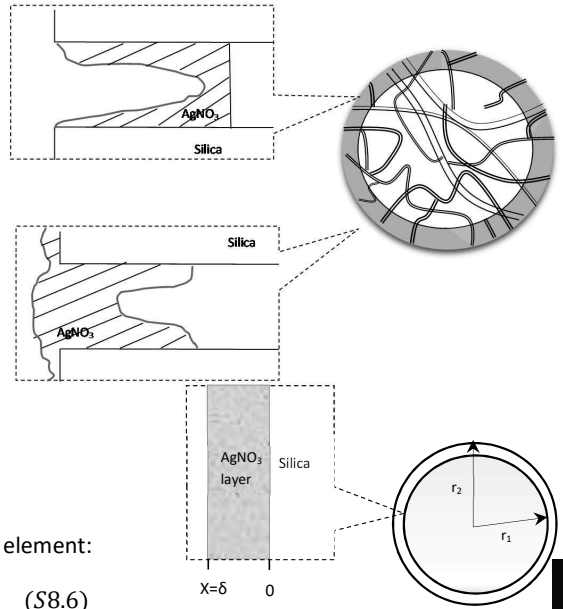
Then Equation S8.8 becomes

$$\frac{r_{obs} \cdot \delta^2}{D_{eff} \cdot C_{trans,\delta}} \leq \beta \quad (S8.9)$$

where

$$\eta = 1 - \frac{n_{obs} \beta}{4} \quad (S8.10)$$

The observed order of adsorption in the regime of pore diffusion controls is:



$$n_{obs} = \frac{1+n}{2} \quad (S8.11)$$

where n is the true order of reaction. According to the literature [58] if $\eta \geq 0.95$ is acceptable, Weisz-Prater Criterion becomes:

$$\frac{\rho_{AgNO_3} \cdot r_{obs} \cdot \delta^2}{D_{eff} \cdot C_{trans,\delta}} \cdot \frac{n+1}{2} \leq 0.2 \quad (S8.12)$$

If the Weisz-Prater criterion is obeyed (less than 0.2), internal mass transfer limitation is negligible.

The $AgNO_3$ /silica in the shell that is used is 10% wt.

Here, first it is assumed that the 10% loading is distributed homogenously on all silica particles (later on, the impact of not distributed evenly is addressed). Therefore, for the first assumption:

$$M_{AgNO} = 0.1M_{total} \quad (S8.13)$$

$$\rho_{AgNO_3} \cdot V_{AgNO_3} \cdot N_t = 0.1\rho_{total} \cdot V_{total} \cdot N_t \quad (S8.14)$$

where, N_t is the total number of silica particles.

and for a spherical particle $AgNO_3$ layer thickness is:

$$\delta = r_2 - r_1 \quad (S8.15)$$

thus,

$$\frac{4\pi(r_2^3 - r_1^3)}{3} \rho_{AgNO_3} = 0.1 \frac{4\pi r_2^3}{3} \rho_{total} \quad (S8.16)$$

If, $\rho_{AgNO_3} = 4.35 \frac{g}{ml}$ and true density of silica = $\rho_{silica} = 2.2 \frac{g}{ml}$. The true density of silica is considered as the density of silica particles without particle porosity, ε_p . For now it is assumed that $\varepsilon_p = 0.2$

and

$$\rho_{total} = 0.1\rho_{AgNO_3} + 0.9\rho_{silic} (1 - \varepsilon_p) = 2.77 \frac{g}{ml}$$

If $r_2 = 30 \mu m$ (according to the $AgNO_3$ impregnated on silica particle mesh size of 230+ which is provided with the supplier) and by solving the Equation S8.16, $AgNO_3$ layer thickness is

$$\delta = r_2 - r_1 = 0.5 \mu m$$

As it is stated in the manuscript the adsorption kinetic rate is considered to be pseudo-second order, therefore,

$$\frac{dq_{B_t}}{dt} = k''(q_{B_e} - q_{B_t})^2 \quad (S8.17)$$

The maximum adsorption rate is obtained if $q_t = 0$, which is then equal to:

$$\frac{dq_{B_t}}{dt} = k''q_{B_e}^2 \equiv r_{obs} \quad (S8.18)$$

$k''q_e^2$ is calculated from the Figure 8.5 (in the chapter)

The parameters being used to calculate the Weisz-Prater Criterion, are listed in Table S8.1.

Table S8.1. Parameter used in the Weisz-Prater criteria calculation

parameter	value
D_{eff}	2×10^{-10} (m ² /s)
$kq_{B_e}^2 \equiv r_{obs}$	4.58×10^{-3} (g _{trans} /g _{AgNO₃} ·s ⁻¹)
δ	0.5×10^{-6} (m)
$C_{trans,\delta}$	6 (g/dm ³)
n	2
ρ_{AgNO_3}	4.35 (g/ml)
ρ_{silica}	2.2 (g/ml)

Therefore, the Weisz-Prater Criterion is calculated as:

$$\frac{4.35 \left(\frac{g_{AgNO_3}}{ml} \right) \times 4.58 \left(\frac{mg_{trans}}{g_{AgNO_3} \cdot s} \right) \times (0.5 \times 10^{-6})^2 (m^2)}{2 \times 10^{-10} \left(\frac{m^2}{s} \right) \times 6 \left(\frac{mg_{trans}}{ml} \right)} \cdot \frac{3}{2} = 0.0062 \ll 0.2 \quad (S8.19)$$

Also, the Weisz-Prater Criterion is calculated for different silica porosity and presented in Table S8.2.

Table S8.2. Different silica porosity and the calculated Weisz-Prater Criteria

ϵ_p	Weisz-Prater Criterion
0.5	0.0027
0.2	0.0062
0.15	0.0061
0.1	0.0067
0.05	0.0073

In the above mass balance calculation, it is assumed that the 10% loading of AgNO₃ is distributed homogeneously on all silica particles. Now, it is assumed that this loading is unevenly distributed over the particles. Therefore, the volume of AgNO₃ per unit surface is larger. Then, for the same mass of AgNO₃, if the shell layer thickness of AgNO₃ is larger (for example 5 times), the adsorption rate of TCO per volume of AgNO₃ decreases by the same factor as increasing the layer thickness. Finally, the Weisz-Prater modulus increases with the same factor too. However, with even a factor of 10, the result for the Weisz-Prater modulus is far from the limit for intra-particle diffusion limitation.

Until now, we have considered that the AgNO₃ layer has a certain inherent porosity at a density of 4.35 g/cm³. In the following case, it is assumed that the AgNO₃ layer is distributed over the silica particles with a higher porosity, ϵ_{AgNO_3} (which is in addition to the inherent porosity). Consequently, this has an effect on the values of effective diffusivity, density of the AgNO₃ layer, and finally, the AgNO₃ layer thickness.

The density of the AgNO₃ layer (considering the porosity term) is calculated as ($\rho_{AgNO_3} (1 - \epsilon_{AgNO_3})$).

Effective diffusivity is defined as:

$$D_{eff} = \frac{\varepsilon_{AgNO_3}}{\tau} D \quad (S8.20)$$

Where, τ and D are tortuosity and diffusion coefficient of TCO in the solvent, respectively.

Tortuosity is calculated according to Equation S8.21 [59]. In this equation, particle sphericity factor, ϕ_s , is considered to be 1.

$$\tau = 1.23 \frac{(1 - \varepsilon_{AgNO_3})^{4/3}}{\varepsilon_{AgNO_3} \phi_s^2} \quad (S8.21)$$

The $AgNO_3$ shell layer thickness increases with higher porosity; however, the effective diffusivity also increases with the porosity. Therefore, this does not result in a significant increase in the Weisz modulus (Equation S8.12).

In order to present the impact of the increase in porosity, the Weisz-Prater Criterion is calculated for different silver nitrate porosities. The results are presented in Table S8.3.

Table S8.3. The impact of silver nitrate porosity on Weisz modulus

ε_{AgNO_3}	τ	$D_{eff} [m^2/s]$	$\delta [m]$	Weisz modulus
0.1	10.68	3×10^{-10}	5.9×10^{-7}	0.052
0.2	4.56	1.3×10^{-10}	6.5×10^{-7}	0.013
0.3	2.54	3.5×10^{-10}	7.3×10^{-7}	0.0053
0.5	0.97	1.5×10^{-9}	10^{-6}	0.0016
0.7	0.35	5.9×10^{-9}	1.6×10^{-6}	0.0006

According to the calculated values, it can be seen that an increase in ε_{AgNO_3} would result in a decrease in the Weisz modulus. And for the case where $\varepsilon_{AgNO_3} = 0.1$, which is the worst case scenario, the value for the Weisz-Prater modulus is approaching the limit.

Therefore, considering all the aforementioned cases and the estimated Weisz-Prater modulus for each case, the absence of internal mass transfer limitation was confirmed.

S4. External mass transfer resistance calculation

Parameter used in Sherwood number calculation, Sh Number and external mass transfer coefficient (Equation 8.6 and 8.7) are summarized in Table S8.4.

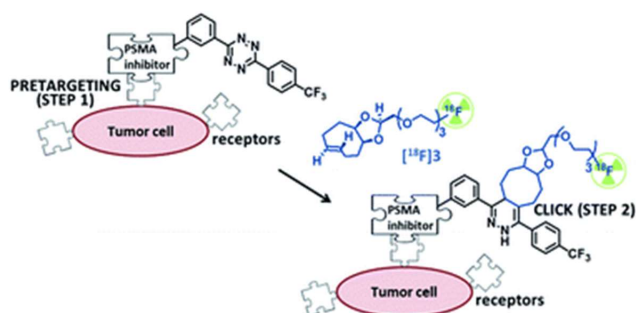
Table S8.4. Parameters used in Sherwood Nr. And mass transfer resistance calculation

parameter	Value
ϕ_s	1 [59]
u	0.00104 (m/s)
d_p	60×10^{-6} (m)
D	3×10^{-9} (m ² /s)* [44], [60]
ξ	10 [43]
ε_b	0.5
$a = 6(1 - \varepsilon_b)/d_p$	50000 (m ² /m ³)
ρ/μ	655/0.000325 (m ² /s) @25°C
$Re_p = ud_p\rho/\mu$	0.126
Sh	0.693
$k_c \cdot a = D \cdot Sh \cdot a/d_p$	1.733 (1/s)

*Here, reported D is based on an average of binary diffusion coefficients of some organic compounds in n-hexane at 303.2 K [44], [61]

CHAPTER 9

Micro-Flow Photosynthesis of New Dienophiles for Inverse-Electron-Demand Diels-Alder Reactions. Application for Pretargeted *in vivo* PET Imaging



This chapter is based on:

Billaud, E. M. F., Shahbazali E. , Ahamed, A. , Cleeren F., Noël, T., Koole, M. , Verbruggen, A. , Hessel, V., and Bormans, G., Chem. Sci., 2017, 8, 1251–1258

9.1 Introduction

As stated in chapter 6, pretargeting approaches can be based on an inverse-electron-demand Diels-Alder (IEDDA) click reaction between 1,2,4,5-tetrazines and trans-cyclooctene (TCO) derivatives [1]. Indeed, this fast, selective, high-yield, biocompatible, and bioorthogonal reaction has already proven to be suitable for this kind of applications, both *in vitro* and *in vivo* [2]–[8], even using tetrazines labeled with fluorine-18 [9], [10]. However, to the best of our knowledge, no *in vivo* pretargeting PET imaging results have been reported on using a ^{18}F -labeled TCO derivative, an alternative to ^{18}F -labeled tetrazines which suffer from some limitations due to their lipophilic nature. Some radiolabeling procedures were developed for a ^{18}F TCO compound (^{18}F **1**, Figure 9.1) [11], [12], but they were only applied for the construction of ^{18}F -labeled probes [13], [14].

Wyffels *et al.* explored biodistribution of ^{18}F **1** in healthy mice, from 5 to 240 min p.i.) [12]. Results demonstrated renal and hepatobiliary clearance of radioactivity, slow blood clearance, as well as increasing bone uptake values (from 60 min p.i.) [12]. The bone uptake is probably due to defluorination and is an indication of tracer instability. Therefore, we aimed to develop new TCO derivatives, with improved *in vivo* stability, favorable pharmacokinetics, and high reactivity for IEDDA reactions.

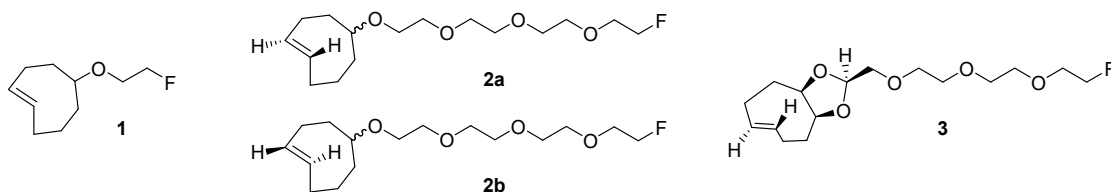


Figure 9.1. Chemical structure of TCO derivative **1** reported by other groups [11], [12] and newly developed dienophiles **2a**, **2b**, and **3**.

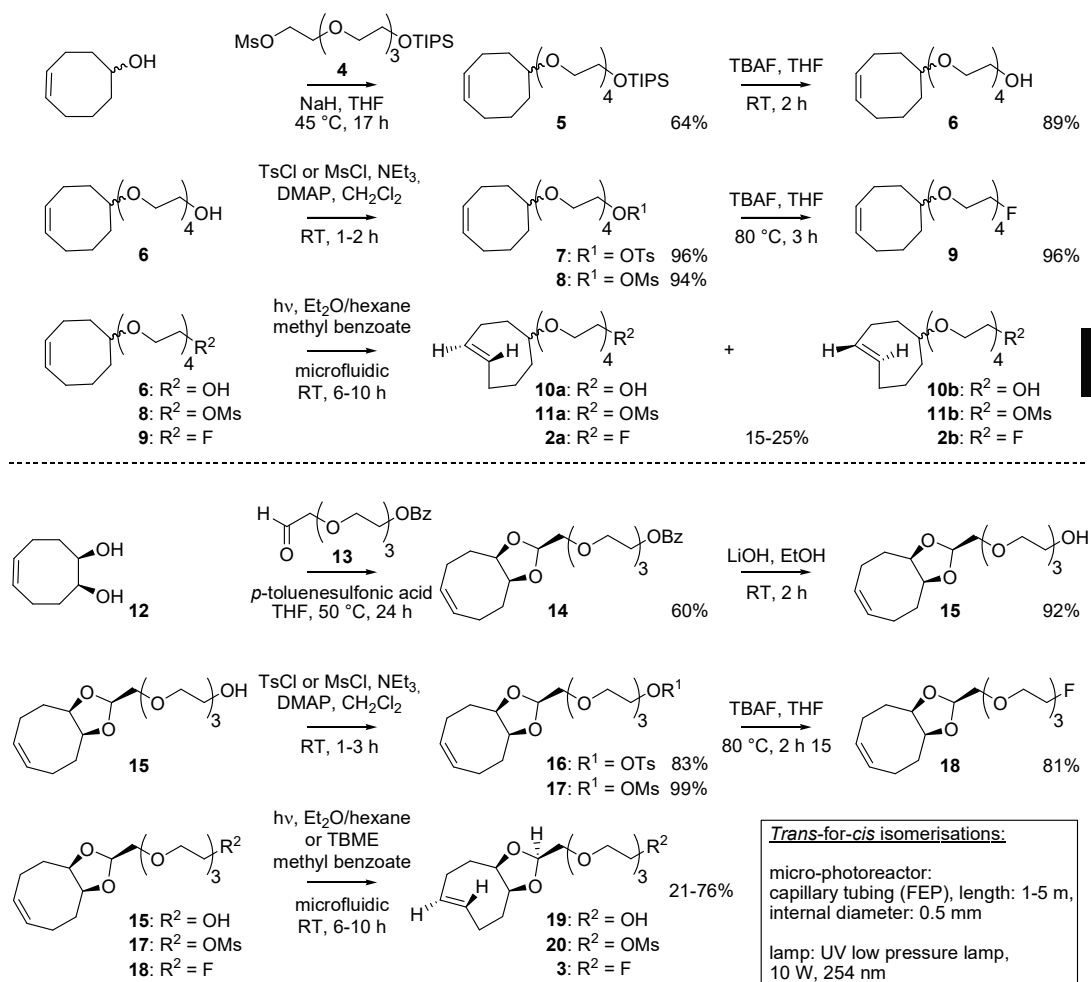
The compounds **2a**, **2b** and **3** derivatised with polyethylene glycol (PEG) chains (Figure 9.1) has been synthesized at KULeuven. With the aim to increase their hydrophilicity and their stability towards enzymatic degradations [8], [15]. A conformationally-strained dioxolane-fused trans-cyclooctene (**3**) has been developed, encouraged by the results recently reported by Fox *et al.* [16]. Indeed, it was demonstrated that this type of strained trans-cyclooctenes reacts faster with 3,6-diphenyl-s-tetrazine than non strained analogs, and displays excellent chemical stability in aqueous solutions and plasma. Moreover, dioxolane-fused trans-cyclooctenes can be prepared easily through diastereoselective synthesis.

In this chapter we report (i) the syntheses of new TCO derivatives, via a trans-to-cis photoisomerization step using the micro-flow process; (ii) the reaction kinetics of these new

dienophiles with a tetrazine, as well as their stability in aqueous solution. Since the scope of this thesis is related to micro-flow chemistry, for the rest of the research which was done at KULeuven, it is referred to the published article [17]; (iii) the radiolabeling of the most promising TCO derivative, [^{18}F]3; (iv) in vitro and in vivo stability and biodistribution studies of [^{18}F]3; (v) in vitro and in vivo pretargeting experiments using [^{18}F]3.

9.2 Syntheses

New dienophiles **2a**, **2b** and **3** were prepared as shown in Scheme 9.1. First, the corresponding *cis*-derivatives **9** and **18** were synthesized, in 6 and 7 steps respectively.



Scheme 9.1. Syntheses of dienophiles **2a**, **2b** and **3**. THF: tetrahydrofuran, MsCl: mesyl chloride, TsCl: tosyl chloride, DMAP: 4-(dimethylamino)pyridine, TBME: tert-butyl methyl ether

PEG synthon **4** was obtained in two steps, starting from tetraethylene glycol: protection of one hydroxyl group using triisopropylsilyl (TIPS) chloride followed by mesylation of the other hydroxyl group. Then, synthon **4** was used for nucleophilic substitution on *cis*-cyclooctenol, to yield derivative **5**. The choice of TIPS as the hydroxyl protecting group was important to obtain a good yield in this step. After deprotection using tetrabutylammonium fluoride (TBAF), the hydroxyl group of compound **6** was replaced by fluorine (**9**) *via* a sulfonate intermediate.

For the synthesis of **18**, PEG synthon **13** was first prepared in two steps, starting from tetraethylene glycol: after protection of one hydroxyl group using benzoyl chloride (BzCl), the other hydroxyl was oxidized into an aldehyde in the presence of Dess-Martin periodinane reagent. In parallel, oxidation of 1,5-cyclooctadiene into diol **12** was carried out using cetyltrimethylammonium permanganate. Then, PEG synthon **13** and diol **12** were involved in an acetalization, leading to dioxolane **14**. The stereochemistry of **14** was determined according to Darko *et al.* [18] After deprotection using LiOH, the hydroxyl group of compound **15** was replaced by fluorine (**18**) *via* a sulfonate intermediate.

Trans-to-*cis* isomerization of hydroxy-derivatives **6**, **15**, sulfonate precursors for radiofluorination **7**, **8**, **16**, **17**, and fluoro-derivatives **9**, **18** was performed using the micro-flow photochemistry process. The basic design of the setup was based on the work explained on chapter 6 for photochemical synthesis of functionalized *trans*-cyclooctenes driven by metal complexation. For the *trans*-to-*cis* isomerization of our compounds, we used the aforementioned micro-flow setup, since the short characteristic inner diameter of the microreactor allows a high overall absorption even at larger concentration (high quantum yield) which increases the gross conversion rate largely and reduces the reaction time from hours to minutes for typical photo-flow processes. In addition, process scale-up is facilitated by the numbering-up of several flow microcapillaries with (almost) identical performance. Two microreactors in parallel, coiled around the UV lamp, were used and flow was adjusted to result in 2 to 3 min irradiation time (Figure 9.2). Although Fox *et al.* [19] used 8 lamps of 35 W (light intensity of 12800 $\mu\text{W}\cdot\text{cm}^{-2}$), a UV lamp of 10 W (light intensity of 21-24 $\mu\text{W}\cdot\text{cm}^{-2}$) provided sufficient power for the isomerization reaction in our micro-photochemistry setting. In-flow separation process based on Ag complexation was also optimized, by using several packed beds made of AgNO_3 -impregnated silica gel and glass beads. During the experiment, the flow was switched after a certain time (30-90 min) from one packed bed to another, in order to avoid saturation. After the experiment, packed beds were removed and stirred with NH_4OH solution to liberate the *trans*-compound from Ag^+ . With this continuous-flow method using microreactors, 85% conversion can be achieved for the *cis*-to-*trans* isomerization of cyclooctenol in 3 h (Supporting Information), compared to a reported 73% in 8 h or 70% in 3 h for non-microfluidic productions [19], [20]. For the new functionalized cyclooctene derivatives, photoisomerization yields reached 76% for a 6 h experiment, with fluoro-compound **3**. For tosylate (OTs) precursors **7** and **16**, the corresponding *trans*-derivatives were unstable,

therefore, less reactive but more stable mesylate (OMs) precursors **8** and **17** were synthesized. After isomerization of mesylate **8**, only **11b** could be isolated but was quite unstable (data not shown). However, *trans*-derivative mesylate **20** was obtained with 44% yield for a 6 h isomerization process.

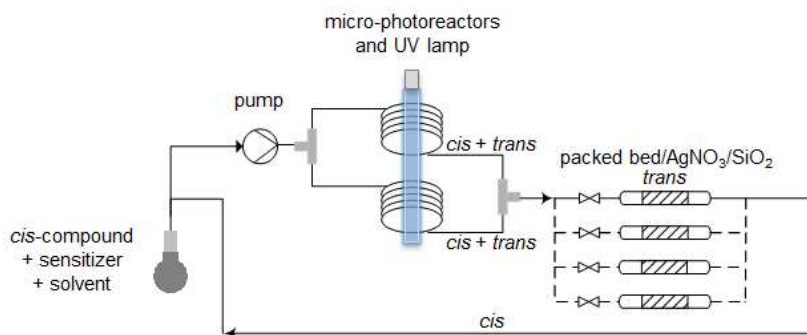


Figure 9.2. Microfluidic device optimized for *trans*-for-*cis* isomerization of functionalized cyclooctene derivatives

9.3 Conclusions

In summary, three TCO derivatives for IEDDA reactions were developed, and compound **3** was selected for pretargeting applications. *Trans*-**3** has been prepared via diastereoselective synthesis, and the *trans*-to-*cis* isomerization step has been performed by micro-flow photochemistry with 76% yield. The innovative microfluidic setup reported here can be applied as continuous process which is promising for process scale-up.

9.4 References

- [1] M. L. Blackman, M. Royzen, and J. M. Fox, "Tetrazine ligation: Fast bioconjugation based on inverse-electron-demand Diels-Alder reactivity," *J. Am. Chem. Soc.*, vol. 130, no. 41, pp. 13518–13519, 2008.
- [2] N. K. Devaraj, R. Upadhyay, J. B. Haun, S. A. Hilderbrand, and R. Weissleder, "Fast and sensitive pretargeted labeling of cancer cells through a tetrazine/trans-cyclooctene cycloaddition," *Angew. Chemie - Int. Ed.*, vol. 48, no. 38, pp. 7013–7016, 2009.
- [3] T. Reiner and B. M. Zeglis, "The inverse electron demand Diels-Alder click reaction in radiochemistry," *Journal of Labelled Compounds and Radiopharmaceuticals*. 2014.
- [4] R. Rossin *et al.*, "In vivo chemistry for pretargeted tumor imaging in live mice," *Angew. Chemie - Int. Ed.*, 2010.
- [5] G. Budin, H. J. Chung, H. Lee, and R. Weissleder, "A magnetic gram stain for bacterial detection," *Angew. Chemie - Int. Ed.*, 2012.
- [6] R. Rossin *et al.*, "Highly reactive trans-cyclooctene tags with improved stability for diels-alder chemistry in living systems," *Bioconjug. Chem.*, 2013.
- [7] Z. B.M. *et al.*, "A pretargeted PET imaging strategy based on bioorthogonal diels-alder click chemistry," *J. Nucl. Med.*, 2013.
- [8] B. M. Zeglis *et al.*, "Optimization of a pretargeted strategy for the PET imaging of colorectal carcinoma via the modulation of radioligand pharmacokinetics," *Mol. Pharm.*, 2015.
- [9] N. K. Devaraj, G. M. Thurber, E. J. Keliher, B. Marinelli, and R. Weissleder, "Reactive polymer enables efficient in vivo bioorthogonal chemistry," *Proc. Natl. Acad. Sci.*, 2012.
- [10] C. Denk *et al.*, "Development of a ¹⁸F-Labeled Tetrazine with Favorable Pharmacokinetics for Bioorthogonal PET Imaging," *Angew. Chemie Int. Ed.*, vol. 53, no. 36, pp. 9655–9659, 2014.
- [11] Z. Li *et al.*, "Tetrazine-trans-cyclooctene ligation for the rapid construction of 18F labeled probes," *Chem. Commun.*, 2010.
- [12] L. Wyffels *et al.*, "In vivo evaluation of 18F-labeled TCO for pre-targeted PET imaging in the brain," *Nucl. Med. Biol.*, 2014.
- [13] T. Reiner, E. J. Keliher, S. Earley, B. Marinelli, and R. Weissleder, "Synthesis and in vivo imaging of a18F-labeled PARP1 inhibitor using a chemically orthogonal scavenger-assisted high-performance method," *Angew. Chemie - Int. Ed.*, 2011.
- [14] R. Selvaraj *et al.*, "Tetrazine-trans-cyclooctene ligation for the rapid construction of integrin alpha v beta 3 targeted PET tracer based on a cyclic RGD peptide," *Bioorganic Med. Chem. Lett.*, 2011.
- [15] G. Molineux, "Pegylation: Engineering improved pharmaceuticals for enhanced therapy," *Cancer Treat. Rev.*, 2002.
- [16] A. Darko *et al.*, "Conformationally Strained trans-Cyclooctene with Improved Stability and Excellent Reactivity in Tetrazine Ligation.," *Chem. Sci.*, vol. 5, no. 10, pp. 3770–3776, 2014.
- [17] E. M. F. Billaud *et al.*, "Micro-flow photosynthesis of new dienophiles for inverse-electron-demand Diels–Alder reactions. Potential applications for pretargeted in vivo PET imaging," *Chem. Sci.*, vol. 8, no. 2, pp. 1251–1258, 2017.
- [18] A. Darko *et al.*, "Conformationally strained trans-cyclooctene with improved stability and excellent

reactivity in tetrazine ligation," *Chem. Sci.*, 2014.

- [19] M. Royzen, G. P. A. Yap, and J. M. Fox, "A photochemical synthesis of functionalized trans-cyclooctenes driven by metal complexation," *J. Am. Chem. Soc.*, 2008.
- [20] D. Svatunek *et al.*, "Efficient low-cost preparation of trans-cyclooctenes using a simplified flow setup for photoisomerization," *Monatshefte fur Chemie*, 2016.

9.5 Supplementary material

9.5.1 Material and general methods

All reagents and solvents were purchased from Sigma-Aldrich, Fisher Scientific, TCI or Acros Organics. Distilled water and ultrapure water (18.2 MΩ·cm at 25°C, 0.22 μm filtration) were used. Unless otherwise noted, moisture-sensitive reactions were conducted under dry nitrogen atmosphere. Thin layer chromatography (TLC) was performed on silica-based plates (silica gel on TLC aluminum foils, 60 Å, Sigma-Aldrich) and visualized with UV light (254 nm) or developed with potassium permanganate dyeing agent. Column chromatography was carried out on silica gel (0.060-0.200 mm, 60 Å, Acros Organics). Nuclear magnetic resonance (NMR) spectra (400 MHz for ¹H, 101 MHz for ¹³C and 376 MHz for ¹⁹F) and 2D-NMR (¹H-¹H COSY, ¹H-¹³C HSQC) were recorded for each compound on a Bruker AVANCE II 400 Ultrashield instrument (Bruker), with chemical shift values expressed in ppm relative to TMS (δH 0.00 and δC 0.0) or residual chloroform (δH 7.26 and δC 77.2) as standard. High-resolution mass spectrometry (HRMS) was achieved using a Dionex Ultimate 3000 LC System (Thermo Fisher Scientific) coupled in series to an ultra-high resolution time-of-flight mass spectrometry (TOF-HRMS) (MaXis impact, Bruker), equipped with orthogonal electrospray ionization (ESI) interface.

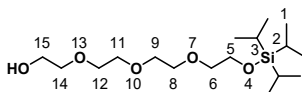
Continuous flow setup: The micro-photoisomerization reactions were performed using the setup represented in Figure 9.2. The setup mainly consists of HPLC pump (Knauer Azura P4.1S), capillary tube which is made of fluorinated ethylene propylene (FEP 1548L; Upchurch Scientific), low pressure amalgam lamp (TS23-212; Dinies Technologies GmbH) and a tubular packed bed reactor (stainless steel, ID 4.5 mm). The photoisomerization solution was pumped from the inlet solution flask that was stirred with magnetic stirrer to the micro-photoreactor (FEP capillary tube). The micro-photoreactor was wound around the UV lamp and placed in a safety oven. The outlet from the photoreactor was then entered into the packed bed which was packed with AgNO₃ impregnated silica gel as packing. The AgNO₃/Silica mesh was 230+. The AgNO₃/silica particles were mixed with 1 mm and 212-300 μm borosilicate glass beads (the amount of packings and glass beads are given in the photoisomerization of each compound separately) and then introduced to the packed bed with funnel. The inert glass beads were used to avoid particle agglomeration which leads to channeling of the flow inside the packed bed. The inlet and outlet of the packed bed attached frits with a pore size of 10 μm to maintain the packing material inside the reactor. The outlet of the packed bed was recycled back to the inlet solution flask through a 0.2 m long FEP capillary tube.

Semi-preparative HPLCs were performed on a VWR-Hitachi LaChrom Elite system equipped with a L2130 pump and a L2400 UV detector.

9.5.2 Syntheses

Synthesis of (Z)-5-(2-(2-(2-(2-fluoroethoxy)ethoxy)ethoxy)ethoxy)cyclooct-1-ene **9** and 2-(2-(2-(2-(Z)-cyclooct-4-enyloxy)ethoxy)ethoxy)ethyl methanesulfonate **8**

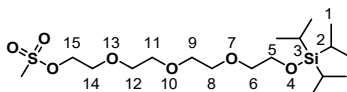
3,3-diisopropyl-2-methyl-4,7,10,13-tetraoxa-3-silapentadecan-15-ol (**23**)



A solution of sodium hydride (60% in mineral oil; 386 mg; 9.65 mmol; 1.25 eq.) in anhydrous tetrahydrofuran (20 mL) was stirred at RT for 5 min under N₂ atmosphere. Tetraethylene glycol (2.67 mL; 15.45 mmol; 2 eq.) was added dropwise at 0 °C and the reaction mixture was stirred for 5 more min before addition of triisopropylsilyl chloride (1.65 mL; 7.72 mmol; 1 eq.). The resulting mixture was stirred at RT for 1 h and the reaction was stopped by addition of water (30 mL). The mixture was extracted with ethyl acetate (3 x 30 mL). The organic layers were combined, washed with brine, dried over magnesium sulfate, filtered and evaporated

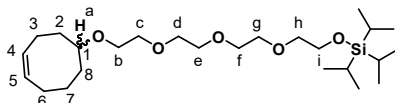
under reduced pressure. The crude product was purified by column chromatography (silica, ethyl acetate/*n*-heptane, 75:25) to yield 23 (1.91 g; 5.45 mmol) as a colorless oil. Yield: 71%. Rf (silica; ethyl acetate/*n*-heptane 75:25 v/v) 0.39; HRMS/ESI m/z $[M+H]^+$ = 351.2587 (calculated for $C_{17}H_{38}O_5Si$: 351.2561); 1H NMR ($CDCl_3$) 1.02-1.09 (m, 21H, CH_3 -1, H-2), 2.62 (bs, 1H, OH), 3.54-3.58 (m, 4H, CH_2 -6, 14), 3.62-3.63 (m, 8H, CH_2 -8, 9, 11, 12), 3.67-3.69 (m, 2H, CH_2 -15), 3.81 (t, 2H, J = 5.6 Hz, CH_2 -5); ^{13}C NMR ($CDCl_3$) 12.1 (3C, C-2), 18.0 (6C, C-1), 61.8 (C-15), 63.1 (C-5), 70.5 (C-8 or 9 or 11 or 12), 70.8 (C-8 or 9 or 11 or 12), 70.8 (C-8 or 9 or 11 or 12), 70.8 (C-8 or 9 or 11 or 12), 70.9 (C-8 or 9 or 11 or 12), 72.6 (C-14 or 6), 72.9 (C-14 or 6).

3,3-diisopropyl-2-methyl-4,7,10,13-tetraoxa-3-silapentadecan-15-yl methanesulfonate 4



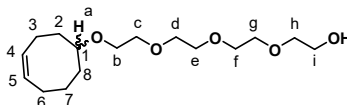
To a solution of compound 23 (1.45 g; 4.14 mmol), distilled *N,N*-diisopropylethylamine (865 μ L; 4.96 mmol; 1.2 eq.), and 4-(dimethylamino)pyridine (51 mg; 0.41 mmol; 0.1 eq.) in dry dichloromethane (50 mL) was added mesyl chloride (384 μ L; 4.96 mmol; 1.2 eq.) under N_2 atmosphere. The reaction mixture was stirred at RT for 1 h and then poured into a saturated aqueous sodium hydrogencarbonate solution (50 mL). The organic layer was separated and the aqueous phase was extracted with dichloromethane (2 x 50 mL). The organic layers were combined, dried over magnesium sulfate, filtered and evaporated under reduced pressure. The crude product was purified by column chromatography (silica, dichloromethane/ethyl acetate 90:10) to yield 4 (1.65 g; 3.85 mmol) as a pale yellow oil. Yield: 93%. Rf (silica; dichloromethane/ethyl acetate 90:10 v/v) 0.40; HRMS/ESI m/z $[M+H]^+$ = 429.2386 (calculated for $C_{18}H_{40}O_7Si$: 429.2337); 1H NMR ($CDCl_3$) 1.02-1.11 (m, 21H, CH_3 -1, H-2), 3.04 (s, 3H, CH_3 -S), 3.56 (t, 2H, J = 5.5 Hz, CH_2 -6), 3.60-3.65 (m, 8H, CH_2 -8, 9, 11, 12), 3.74-3.76 (m, 2H, CH_2 -14), 3.82 (t, 2H, J = 5.5 Hz, CH_2 -5), 4.34-4.36 (m, 2H, CH_2 -15); ^{13}C NMR ($CDCl_3$) 12.1 (3C, C-2), 18.1 (6C, C-1), 37.8 (CH_3 -S), 63.1 (C-5), 69.2 (C-14 or 15), 69.4 (C-14 or 15), 70.7 (C-8 or 9 or 11 or 12), 70.8 (2C, C-8 or 9 or 11 or 12), 70.9 (C-8 or 9 or 11 or 12), 72.9 (C-6).

(2)-15-(cyclooct-4-en-1-yloxy)-3,3-diisopropyl-2-methyl-4,7,10,13-tetraoxa-3-silapentadecane 5



A dispersion of sodium hydride (60% in mineral oil; 396 mg; 9.91 mmol) in anhydrous tetrahydrofuran (10 mL) was stirred at RT for 5 min under N_2 atmosphere. 5-hydroxy-1-cyclooctene (500 mg; 3.96 mmol) in anhydrous tetrahydrofuran (10 mL) was dropwise added and the reaction mixture was stirred for 45 min at 45 $^{\circ}C$ under N_2 atmosphere. Compound 4 (1.40 g; 3.27 mmol) in anhydrous tetrahydrofuran (10 mL) was then added and the resulting mixture was stirred at 45 $^{\circ}C$ overnight under N_2 atmosphere. Back to RT, the reaction was stopped by addition of water (50 mL). The mixture was extracted with ethyl acetate (3 x 50 mL). The organic layers were combined, dried over magnesium sulfate, filtered and evaporated under reduced pressure. The crude product was purified by column chromatography (silica, dichloromethane/ethyl acetate, 100:0 \rightarrow 80:20) to yield 5 (960 mg; 2.09 mmol) as a colorless oil. Yield: 64%. Rf (silica; dichloromethane/ethyl acetate 90:10 v/v) 0.39; HRMS/ESI m/z $[M+H]^+$ = 459.3514 (calculated for $C_{25}H_{50}O_5Si$: 459.3500); 1H NMR ($CDCl_3$) 1.04-1.11 (m, 21H, CH_3 , CH -Si), 1.34-1.43 (m, 1H, H-7), 1.45-1.54 (m, 1H, H-2), 1.63-1.85 (m, 3H, H-7, H-8, H-8), 1.89-1.97 (m, 1H, H-2), 1.98-2.05 (m, 1H, H-3), 2.08-2.16 (m, 2H, H-6, H-6), 2.28-2.37 (m, 1H, H-3), 3.33-3.38 (m, 1H, H-a), 3.48-3.67 (m, 14H, CH_2 -b, c, d, e, f, g, h), 3.83 (t, 2H, J = 5.6 Hz, CH_2 -i), 5.53-5.68 (m, 2H, H-4, H-5); ^{13}C NMR ($CDCl_3$) 12.2 (3C, C-Si), 18.1 (6C, CH_3), 22.9 (C-3), 25.7 (C-6 or 7), 26.0 (C-6 or 7), 33.5 (C-8), 34.3 (C-2), 63.1 (C-i), 67.9 (C-b), 70.8 (C-c, d, e, f or g), 70.8 (C-c, d, e, f or g), 70.9 (C-c, d, e, f or g), 71.0 (C-c, d, e, f or g), 71.1 (C-c, d, e, f or g), 72.9 (C-h), 81.1 (C-1), 129.5 (C-4 or 5), 130.2 (C-4 or 5).

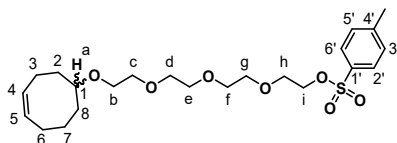
(2)-2-(2-(2-(2-(cyclooct-4-en-1-yloxy)ethoxy)ethoxy)ethoxy)ethanol 6



To a solution of compound 5 (800 mg; 1.74 mmol) in anhydrous tetrahydrofuran (20 mL) was added a solution of tetrabutylammonium fluoride 1 M in tetrahydrofuran (2.62 mL; 2.62 mmol; 1.5 eq.). The mixture was then stirred at RT for 2 h. The reaction was quenched by addition of a saturated aqueous sodium hydrogencarbonate solution (50 mL), followed by water

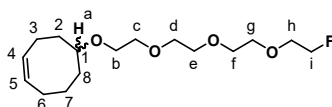
(25 mL) and then by ethyl acetate (30 mL). The organic layer was separated and the aqueous phase was extracted with ethyl acetate (2 x 30 mL). The organic layers were combined, dried over magnesium sulfate, filtered and evaporated under reduced pressure. The crude product was purified by column chromatography (silica, ethyl acetate/ethanol, 95:05) to yield **6** (465 mg; 1.54 mmol) as a colorless oil. Yield: 89%. Rf (silica, ethyl acetate/ethanol, 95:05) 0.41; HRMS/ESI m/z [M+H]⁺ = 303.2183 (calculated for C₁₆H₃₀O₅: 303.2166); ¹H NMR (CDCl₃) 1.30-1.42 (m, 1H, H-7), 1.45-1.55 (m, 1H, H-2), 1.64-1.85 (m, 3H, H-7, H-8, H-8), 1.89-1.96 (m, 1H, H-2), 1.99-2.07 (m, 1H, H-3), 2.10-2.17 (m, 2H, H-6, H-6), 2.29-2.38 (m, 1H, H-3), 2.66 (bs, 1H, OH), 3.34-3.39 (m, 1H, H-a), 3.50-3.66 (m, 14H, CH₂-b, c, d, e, f, g, h), 3.72 (m, 2H, CH₂-i), 5.54-5.69 (m, 2H, H-4, H-5); ¹³C NMR (CDCl₃) 22.9 (C-3), 25.7 (C-7), 26.0 (C-6), 33.5 (C-8), 34.3 (C-2), 62.0 (C-i), 67.9 (C-b), 70.6 (C-c, d, e, f or g), 70.8 (3C, C-c, d, e, f or g), 71.1 (C-c, d, e, f or g), 72.7 (C-h), 81.2 (C-1), 129.6 (C-4 or 5), 130.2 (C-4 or 5).

(Z)-2-(2-(2-(2-(cyclooct-4-en-1-yloxy)ethoxy)ethoxy)ethoxy)ethyl 4-methylbenzenesulfonate 7



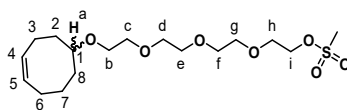
To a solution of compound **6** (270 mg; 0.89 mmol), distilled triethylamine (299 μ L; 2.14 mmol; 2.4 eq.), and 4-(dimethylamino)pyridine (22 mg; 0.18 mmol; 0.2 eq.) in dry dichloromethane (10 mL) was added tosyl chloride (204 mg; 1.07 mmol; 1.2 eq.) under N₂ atmosphere. The reaction mixture was stirred at RT for 2 h. The mixture was poured into a saturated aqueous sodium hydrogencarbonate solution (20 mL). After extractions with dichloromethane (3 x 20 mL), the organic layers were combined, dried over magnesium sulfate, filtered and evaporated under reduced pressure. The crude product was purified by column chromatography (silica, ethyl acetate/heptane 5:5) to yield **7** (388 mg; 0.85 mmol) as a colorless oil. Yield: 96%. Rf (silica; ethyl acetate/heptane 5:5) 0.33; HRMS/ESI m/z [M+H]⁺ = 457.2283 (calculated for C₂₃H₃₆O₇S: 457.2255); ¹H NMR (CDCl₃) 1.33-1.43 (m, 1H, H-7), 1.44-1.53 (m, 1H, H-2), 1.63-1.84 (m, 3H, H-7, H-8, H-8), 1.88-1.96 (m, 1H, H-2), 1.98-2.07 (m, 1H, H-3), 2.09-2.15 (m, 2H, H-6, H-6), 2.28-2.37 (m, 1H, H-3), 2.44 (s, 3H, CH₃), 3.32-3.37 (m, 1H, H-a), 3.50-3.63 (m, 12H, CH₂-b, c, d, e, f, g), 3.68 (t, 2H, J = 4.8 Hz, CH₂-h), 4.15 (t, 2H, J = 4.8 Hz, CH₂-i), 5.54-5.68 (m, 2H, H-4, H-5), 7.33 (d, 2H, J = 8.3 Hz, H-3', H-5'), 7.79 (d, 2H, J = 8.3 Hz, H-2', H-6'); ¹³C NMR (CDCl₃) 21.7 (CH₃), 22.7 (C-3), 25.7 (C-7), 25.9 (C-6), 33.5 (C-8), 34.2 (C-2), 67.7 (C-b), 68.7 (C-h), 69.3 (C-i), 70.6 (C-c, d, e, f or g), 70.7 (C-c, d, e, f or g), 70.7 (C-c, d, e, f or g), 70.8 (C-c, d, e, f or g), 70.9 (C-c, d, e, f or g), 81.0 (C-1), 128.0 (2C, C-2', 6'), 129.5 (C-4 or 5), 129.9 (2C, C-3', 5'), 130.1 (C-4 or 5), 133.1 (C-1'), 144.9 (C-4').

(Z)-5-(2-(2-(2-(2-(2-fluoroethoxy)ethoxy)ethoxy)ethoxy)cyclooct-1-ene 9



To a solution of compound **7** (115 mg; 0.25 mmol) in dry tetrahydrofuran (1.5 mL) was added a solution of tetrabutylammonium fluoride 1 M in tetrahydrofuran (1.26 mL; 1.26 mmol; 5 eq.) under N₂ atmosphere. The reaction mixture was heated at 80 °C for 3 h. Back to RT, the mixture was poured into a saturated aqueous sodium hydrogencarbonate solution (20 mL). After extractions with dichloromethane (3 x 20 mL), the organic layers were combined, dried over magnesium sulfate, filtered and evaporated under reduced pressure. The crude product was purified by column chromatography (silica, ethyl acetate/heptane 5:5 → 1:0) to yield **9** (72 mg; 0.24 mmol) as a colorless oil. Yield: 96%. Rf (silica; ethyl acetate/heptane 5:5) 0.46; HRMS/ESI m/z [M+H]⁺ = 305.2138 (calculated for C₁₆H₂₉FO₄: 305.2123); ¹H NMR (CDCl₃) 1.31-1.42 (m, 1H, H-7), 1.43-1.51 (m, 1H, H-2), 1.60-1.82 (m, 3H, H-7, H-8, H-8), 1.87-1.95 (m, 1H, H-2), 1.96-2.04 (m, 1H, H-3), 2.07-2.13 (m, 2H, H-6, H-6), 2.26-2.35 (m, 1H, H-3), 3.30-3.36 (m, 1H, H-a), 3.46-3.65 (m, 12H, CH₂-b, c, d, e, f, g), 3.71 (dt, 2H, J = 4.2 Hz, 3JH-F = 29.6 Hz, CH₂-h), 4.53 (dt, 2H, J = 4.2 Hz, 2JH-F = 47.7 Hz, CH₂-i), 5.51-5.66 (m, 2H, H-4, H-5); ¹³C NMR (CDCl₃) 22.7 (C-3), 25.7 (C-7), 25.9 (C-6), 33.4 (C-8), 34.2 (C-2), 67.7 (C-b), 70.5 (d, 2J_{C-F} = 20 Hz, C-h), 70.7 (2C, C-c, d, e, f or g), 70.7 (C-c, d, e, f or g), 70.9 (C-c, d, e, f or g), 70.9 (C-c, d, e, f or g), 81.0 (C-1), 83.2 (d, 1J_{C-F} = 168 Hz, C-i), 129.5 (C-4 or 5), 130.1 (C-4 or 5).

2-(2-(2-(2-(Z)-cyclooct-4-enyloxy)ethoxy)ethoxy)ethoxy)ethyl methanesulfonate 8



To a solution of compound 6 (100 mg; 0.33 mmol), distilled triethylamine (111 μ L; 0.79 mmol; 2.4 eq.), and 4-(dimethylamino)pyridine (8 mg; 66 μ mol; 0.2 eq.) in dry dichloromethane (10 mL) was added mesyl chloride (31 μ L; 0.40 mmol; 1.2 eq.) under N₂ atmosphere. The reaction mixture was stirred at RT for 1 h 15. The mixture was poured into a saturated aqueous sodium hydrogencarbonate solution (25 mL). After extractions with dichloromethane (3 x 20 mL), the organic layers were combined, dried over magnesium sulfate, filtered and evaporated under reduced pressure. The crude product was purified by column chromatography (silica, ethyl acetate) to yield 8 (118 mg; 0.31 mmol) as a pale yellow oil. Yield: 94%. R_f (silica; ethyl acetate) 0.57; HRMS/ESI m/z [M+H]⁺ = 381.1951 (calculated for C₁₇H₃₂O₇S: 381.1942); ¹H NMR (CDCl₃) 1.34-1.45 (m, 1H, H-7), 1.46-1.55 (m, 1H, H-2), 1.64-1.85 (m, 3H, H-7, H-8, H-8), 1.89-1.97 (m, 1H, H-2), 1.99-2.08 (m, 1H, H-3), 2.10-2.17 (m, 2H, H-6, H-6), 2.29-2.38 (m, 1H, H-3), 3.07 (s, 3H, CH₃), 3.33-3.39 (m, 1H, H-a), 3.49-3.68 (m, 12H, CH₂-b, c, d, e, f, g), 3.75-3.77 (m, 2H, CH₂-h), 4.36-4.38 (m, 2H, CH₂-i), 5.54-5.69 (m, 2H, H-4, H-5); ¹³C NMR (CDCl₃) 22.7 (C-3), 25.7 (C-7), 25.9 (C-6), 33.4 (C-8), 34.2 (C-2), 37.8 (CH₃), 67.7 (C-b), 69.1 (C-h), 69.4 (C-i), 70.6 (C-c, d, e, f or g), 70.7 (2C, C-c, d, e, f or g), 70.7 (C-c, d, e, f or g), 71.0 (C-c, d, e, f or g), 81.0 (C-1), 129.5 (C-4 or 5), 130.1 (C-4 or 5).

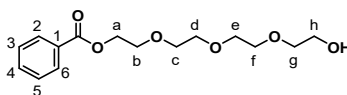
Synthesis of (2*s*,3*aR*,9*aS*,Z)-2-((2-(2-(2-fluoroethoxy)ethoxy)ethoxy)methyl)-3*a*,4,5,8,9,9*a*-hexahydrocycloocta[d][1,3]dioxole 18 and 2-(2-2-(((2*s*,3*aR*,9*aS*,Z)-3*a*,4,5,8,9,9*a*-hexahydrocycloocta[d][1,3]dioxol-2-yl)methoxy)ethoxy)ethyl methanesulfonate 17

(2*1S*,2*R*)-cyclooct-5-ene-1,2-diol 12

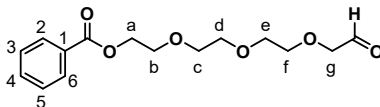


To a solution of 1,5-cyclooctadiene (6.22 mL; 50.7 mmol) in tert-butanol (15 mL) was dropwise added a solution of cetyltrimethylammonium permanganate[1] (20.45 g; 50.7 mmol) in water/tert-butanol (1:4; 75 mL). The mixture was stirred at RT for 4 h. The mixture was diluted with dichloromethane (100 mL) and with an aqueous solution of sodium hydroxide (5%, 100 mL), and then stirred for 15 min. The layers were separated and the aqueous phase was extracted with dichloromethane (3 x 150 mL). The organic layers were combined, dried over magnesium sulfate, filtered and evaporated under reduced pressure. The crude product was purified by column chromatography (silica, ethyl acetate) to yield 12 (1.22 g; 8.58 mmol) as a white solid. Yield: 17%; R_f (silica, ethyl acetate) 0.37; ¹H NMR (CDCl₃) 1.76-1.85 (m, 2H, H-3, H-8), 1.97-2.08 (m, 4H, H-3, H-8, H-4, H-7), 2.14 (s, 2H, OH), 2.47-2.54 (m, 2H, H-4, H-7), 3.98-4.00 (m, 2H, H-1, H-2), 5.65-5.67 (m, 2H, H-5, H-6); ¹³C NMR (CDCl₃) 23.1 (2C, C-4, 7), 32.1 (2C, C-3, 8), 75.2 (2C, C-1, 2), 130.1 (2C, C-5, 6).

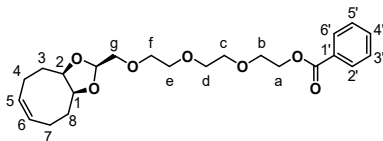
2-(2-(2-(2-hydroxyethoxy)ethoxy)ethoxy)ethyl benzoate 24



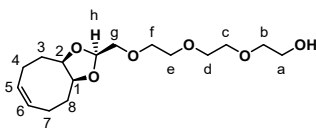
To a solution of tetraethylene glycol (3.93 mL; 22.77 mmol; 1.6 eq.) in anhydrous dichloromethane (120 mL) were successively added distilled N,N-diisopropylethylamine (3.72 mL; 21.34 mmol; 1.5 eq.) and 4-(dimethylamino)pyridine (174 mg; 1.42 mmol; 0.1 eq.) under N₂ atmosphere. Benzoyl chloride (2.00 g; 14.23 mmol) in anhydrous dichloromethane (15 mL) was then added dropwise and the mixture was stirred at RT overnight under N₂ atmosphere. The mixture was then poured into water (200 mL). The organic layer was separated and the aqueous phase was extracted with dichloromethane (3 x 100 mL). The organic layers were combined, dried over magnesium sulfate, filtered and evaporated under reduced pressure. The crude product was purified by column chromatography (silica, ethyl acetate/dichloromethane/ethanol 67:29:4) to yield 24 (2.48 g; 8.31 mmol) as a pale yellow oil. Yield: 58%. R_f (silica; ethyl acetate/dichloromethane/ethanol 67:29:4 v/v/v) 0.37; HRMS/ESI m/z [M+H]⁺ = 299.1453 (calculated for C₁₅H₂₂O₆: 299.1489); ¹H NMR (CDCl₃) 2.48 (bs, 1H, OH), 3.57 (m, 2H, CH₂-g), 3.64-3.71 (m, 10H, CH₂-c, d, e, f, h), 3.83 (t, 2H, J = 4.9 Hz, CH₂-b), 4.47 (t, 2H, J = 4.9 Hz, CH₂-a), 7.40-7.44 (m, 2H, H-3, 5), 7.52-7.56 (m, 1H, H-4), 8.04-8.06 (m, 2H, H-2, 6); ¹³C NMR (CDCl₃) 61.9 (C-h), 64.2 (C-a), 69.4 (C-b), 70.5 (C-c or d or e or f), 70.8 (C-c or d or e or f), 70.8 (C-c or d or e or f), 70.9 (C-c or d or e or f), 72.6 (C-g), 128.4 (2C, C-3, 5), 129.8 (2C, C-2, 6), 130.3 (C-1), 133.1 (C-4), 166.7 (C=O).

2-(2-(2-(2-oxoethoxy)ethoxy)ethoxy)ethyl benzoate 13

To a solution of compound 24 (300 mg; 1.01 mmol) in dichloromethane (15 mL) was added Dess-Martin Periodinane (512 mg; 1.21 mmol; 1.2 eq.). The reaction mixture was stirred at RT for 2.5 h. The reaction was quenched with sodium thiosulfate (382 mg; 2.41 mmol; 2.4 eq.) in a saturated solution of sodium bicarbonate (15 mL). The mixture was separated, and the aqueous phase was extracted with dichloromethane (2 x 25 mL). The organic layers were combined, dried over magnesium sulfate, filtered and evaporated under reduced pressure. The crude product was purified by column chromatography (silica, ethyl acetate/dichloromethane 30:70 → 70:30) to yield 13 (196 mg; 0.66 mmol) as a colorless oil. Yield: 65%. Rf (silica; ethyl acetate/dichloromethane 50:50 v/v) 0.33; HRMS/ESI m/z [M+H]⁺ = 297.1282 (calculated for C₁₅H₂₀O₆: 297.1333); ¹H NMR (acetone-d₆) 3.62-3.68 (m, 8H, CH₂-c, d, e, f), 3.82-3.84 (m, 2H, CH₂-b), 4.12 (d, 2H, J = 0.8 Hz, CH₂-g), 4.44-4.46 (m, 2H, CH₂-a), 7.49-7.53 (m, 2H, H-3, 5), 7.63 (tt, 1H, J = 7.5 Hz, J = 1.6 Hz, H-4), 8.04 (dd, 2H, J = 8.3 Hz, J = 1.2 Hz, H-2, 6), 9.65 (s, 1H, CHO); ¹³C NMR (acetone-d₆) 65.0 (C-a), 69.8 (C-b), 71.3 (C-c or d or e or f), 71.3 (C-c or d or e or f), 71.4 (C-c or d or e or f), 71.8 (C-c or d or e or f), 77.4 (C-g), 129.4 (2C, C-3, 5), 130.3 (2C, C-2, 6), 131.4 (C-1), 133.9 (C-4), 166.8 (O-C=O), 201.7 (H-C=O).

2-(2-(2-(((2s,3aR,9aS,Z)-3a,4,5,8,9,9a-hexahydrocycloocta[d][1,3]dioxol-2-yl)methoxy)ethoxy)ethoxy)ethyl benzoate 14

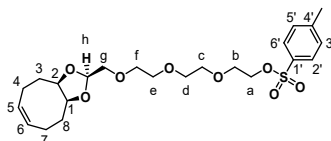
To a solution of compound 12 (190 mg; 1.34 mmol) in anhydrous tetrahydrofuran (10 mL) were successively added compound 13 (396 mg; 1.34 mmol; 1.0 eq) and p-toluenesulfonic acid monohydrate (127 mg; 0.67 mmol; 0.5 eq.). The reaction mixture was heated at 50 °C for 24 h under N₂ atmosphere. Back to RT, the solution was diluted with ethyl acetate (25 mL) and with a saturated aqueous solution of sodium bicarbonate (25 mL). After separation, the aqueous phase was extracted with ethyl acetate (2 x 25 mL). The organic layers were combined, dried over magnesium sulfate, filtered and evaporated under reduced pressure. The crude product was purified by column chromatography (silica, ethyl acetate/dichloromethane 10:90 → 40:60) to yield 14 (337 mg; 0.80 mmol) as a colorless oil. Yield: 60%. Rf (silica; ethyl acetate/dichloromethane 20:80 v/v) 0.46; HRMS/ESI m/z [M+H]⁺ = 421.2228 (calculated for C₂₃H₃₂O₇: 421.2221); ¹H NMR (CDCl₃) 1.92-1.98 (m, 2H, H-3, H-8), 2.01-2.10 (m, 4H, H-3, H-8, H-4, H-7), 2.45-2.50 (m, 2H, H-4, H-7), 3.56 (d, 2H, J = 4.2 Hz, CH₂-g), 3.64-3.70 (m, 8H, CH₂-c, d, e, f), 3.82-3.84 (m, 2H, CH₂-b), 4.12-4.15 (m, 2H, H-1, H-2), 4.46-4.48 (m, 2H, CH₂-a), 4.96 (t, 1H, J = 4.2 Hz, H-h), 5.58-5.60 (m, 2H, H-5, H-6), 7.41-7.45 (m, 2H, H-3', 5'), 7.53-7.57 (tt, 1H, J = 7.4 Hz, J = 1.6 Hz, H-4'), 8.04-8.06 (m, 2H, H-2', 6'); ¹³C NMR (CDCl₃) 23.6 (2C, C-4, C-7), 28.6 (2C, C-3, C-8), 64.3 (C-a), 69.4 (C-b), 70.7 (C-c or d or e or f), 70.8 (C-c or d or e or f), 70.8 (C-c or d or e or f), 71.3 (C-c or d or e or f), 73.2 (C-g), 79.2 (2C, C-1, C-2), 100.8 (C-h), 128.4 (2C, C-3', C-5'), 129.3 (2C, C-5, C-6), 129.8 (2C, C-2', C-6'), 130.2 (C-1'), 133.1 (C-4'), 166.7 (C=O). The stereochemistry was determined according to A. Darko *et al.*[3]

2-(2-(2-(((2s,3aR,9aS,Z)-3a,4,5,8,9,9a-hexahydrocycloocta[d][1,3]dioxol-2-yl)methoxy)ethoxy)ethoxy)ethanol 15

To a solution of compound 14 (322 mg; 0.77 mmol) in absolute ethanol (2.0 mL) was added lithium hydroxide monohydrate (48 mg; 1.15 mmol; 1.5 eq.). The mixture was stirred at RT for 2 h. The mixture was then poured in a saturated aqueous solution of sodium chloride (20 mL), with water (6 mL) and a 5% aqueous solution of sodium carbonate (2 mL). After extractions with dichloromethane (3 x 20 mL), the organic layers were combined, dried over magnesium sulfate, filtered and evaporated under reduced pressure. The crude product was purified by column chromatography (silica, ethyl acetate) to yield 15 (223 mg; 0.71 mmol) as a colorless oil. Yield: 92%. Rf (silica; ethyl acetate) 0.24; HRMS/ESI m/z [M+H]⁺ = 317.1963 (calculated for C₁₆H₂₈O₆: 317.1959); ¹H NMR (CDCl₃) 1.89-1.94 (m, 2H, H-3, H-8), 1.96-2.06 (m, 4H, H-3, H-8, H-4, H-7), 2.41-2.45 (m, 2H, H-4,

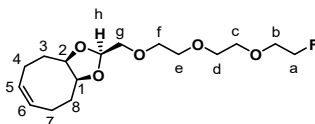
H-7), 2.70 (bs, 1H, OH), 3.53 (d, 2H, J = 4.1 Hz, CH₂-g), 3.55-3.62 (m, 8H, CH₂-c, d, e, f), 3.64-3.67 (m, 4H, CH₂-a, b), 4.07-4.11 (m, 2H, H-1, H-2), 4.92 (t, 1H, J = 4.2 Hz, H-h), 5.54-5.55 (m, 2H, H-5, H-6); ¹³C NMR (CDCl₃) 23.5 (2C, C-4, C-7), 28.6 (2C, C-3, C-8), 61.8 (C-a), 70.4 (C-c or d or e or f or g), 70.6 (C-c or d or e or f or g), 70.7 (C-c or d or e or f or g), 71.1 (C-c or d or e or f or g), 72.6 (C-c or d or e or f or g), 73.1 (C-b), 79.2 (2C, C-1, C-2), 100.8 (C-h), 129.3 (2C, C-5, C-6).

2-(2-(2-(((2*S*,3*aR*,9*aS*,*Z*)-3*a*,4,5,8,9,9*a*-hexahydrocycloocta[d][1,3]dioxol-2-yl)methoxy)ethoxy)ethoxy)ethyl 4-methylbenzenesulfonate 16



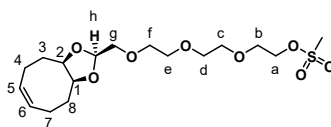
To a solution of compound 15 (400 mg; 1.26 mmol), distilled triethylamine (423 μ L; 3.03 mmol; 2.4 eq.), and 4-(dimethylamino)pyridine (31 mg; 0.25 mmol; 0.2 eq.) in dry dichloromethane (15 mL) was added tosyl chloride (289 mg; 1.52 mmol; 1.2 eq.) under N₂ atmosphere. The reaction mixture was stirred at RT for 3 h. The mixture was poured into a saturated aqueous sodium hydrogencarbonate solution (35 mL). After extractions with dichloromethane (3 x 25 mL), the organic layers were combined, dried over magnesium sulfate, filtered and evaporated under reduced pressure. The crude product was purified by column chromatography (silica, ethyl acetate/heptane 5:5 \rightarrow 1:0) to yield 16 (494 mg; 1.05 mmol) as a colorless oil. Yield: 83%. R_f (silica; ethyl acetate/heptane 5:5) 0.36; HRMS/ESI m/z [M+NH₄]⁺ = 488.2371 (calculated for C₂₃H₃₄O₈S: 488.2313); ¹H NMR (CDCl₃) 1.95-1.97 (m, 2H, H-3, H-8), 2.05-2.07 (m, 4H, H-3, H-8, H-4, H-7), 2.44-2.49 (m, 5H, CH₃, H-4, H-7), 3.55-3.69 (m, 12H, CH₂-b, c, d, e, f, g), 4.14-4.16 (m, 4H, CH₂-a, H-1, H-2), 4.96 (t, 1H, J = 4.2 Hz, H-h), 5.60 (s, 2H, H-5, H-6), 7.34 (d, 2H, J = 7.8 Hz, H-3', H-5'), 7.79 (d, 2H, J = 8.1 Hz, H-2', H-6'); ¹³C NMR (CDCl₃) 21.7 (CH₃), 23.5 (2C, C-4, C-7), 28.6 (2C, C-3, C-8), 68.7 (C-b), 69.3 (C-a), 70.6 (2C, C-c or d or e or f or g), 70.8 (C-c or d or e or f or g), 71.2 (C-c or d or e or f or g), 73.2 (C-c or d or e or f or g), 79.2 (2C, C-1, C-2), 100.7 (C-h), 128.0 (2C, C-2', C-6'), 129.3 (2C, C-5, C-6), 129.9 (2C, C-3', C-5'), 133.1 (C-1'), 144.8 (C-4').

(2*S*,3*aR*,9*aS*,*Z*)-2-((2-(2-(2-fluoroethoxy)ethoxy)ethoxy)methyl)-3*a*,4,5,8,9,9*a*-hexahydrocycloocta[d][1,3]dioxole 18



To a solution of compound 16 (175 mg; 0.37 mmol) in dry tetrahydrofuran (1.5 mL) was added a solution of tetrabutylammonium fluoride 1 M in tetrahydrofuran (1.86 mL; 1.86 mmol; 5 eq.) under N₂ atmosphere. The reaction mixture was heated at 80 °C for 2 h 15. Back to RT, the mixture was poured into a saturated aqueous sodium hydrogencarbonate solution (20 mL). After extractions with dichloromethane (3 x 20 mL), the organic layers were combined, dried over magnesium sulfate, filtered and evaporated under reduced pressure. The crude product was purified by column chromatography (silica, ethyl acetate/heptane 5:5) to yield 18 (94 mg; 0.30 mmol) as a colorless oil. Yield: 81%. R_f (silica; ethyl acetate/heptane 5:5) 0.50; HRMS/ESI m/z [M+NH₄]⁺ = 336.2228 (calculated for C₁₆H₂₇F₅O₅: 336.2181); ¹H NMR (CDCl₃) 1.93-1.98 (m, 2H, H-3, H-8), 2.02-2.09 (m, 4H, H-3, H-8, H-4, H-7), 2.45-2.50 (m, 2H, H-4, H-7), 3.57 (d, 2H, J = 4.2 Hz, CH₂-g), 3.64-3.71 (m, 9H, H-b, CH₂-c, d, e, f), 3.77 (t, 1H, J = 4.2 Hz, H-b), 4.12-4.16 (m, 2H, H-1, H-2), 4.55 (dt, 2H, J = 4.2 Hz, 2JH-F = 47.7 Hz, CH₂-a), 4.97 (t, 1H, J = 4.2 Hz, H-h), 5.58-5.60 (m, 2H, H-5, H-6); ¹³C NMR (CDCl₃) 23.6 (2C, C-4, C-7), 28.6 (2C, C-3, C-8), 70.5 (d, 2J_{C-F} = 20 Hz, C-b), 70.6 (C-c or d or e or f), 70.7 (C-c or d or e or f), 70.9 (C-c or d or e or f), 71.2 (C-c or d or e or f), 73.2 (C-g), 79.2 (2C, C-1, C-2), 83.2 (d, 1J_{C-F} = 170 Hz, C-a), 100.8 (C-h), 129.3 (2C, C-5, C-6).

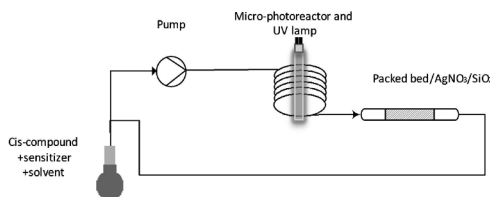
2-(2-(2-(((2*S*,3*aR*,9*aS*,*Z*)-3*a*,4,5,8,9,9*a*-hexahydrocycloocta[d][1,3]dioxol-2-yl)methoxy)ethoxy)ethoxy)ethyl methanesulfonate 17



To a solution of compound **15** (150 mg; 0.47 mmol), distilled triethylamine (159 μ L; 1.14 mmol; 2.4 eq.), and 4-(dimethylamino)pyridine (12 mg; 95 μ mol; 0.2 eq.) in dry dichloromethane (10 mL) was added mesyl chloride (44 μ L; 0.57 mmol; 1.2 eq.) under N₂ atmosphere. The reaction mixture was stirred at RT for 1 h 30. The mixture was poured into a saturated aqueous sodium hydrogencarbonate solution (25 mL). After extractions with dichloromethane (3 x 20 mL), the organic layers were combined, dried over magnesium sulfate, filtered and evaporated under reduced pressure. The crude product was purified by column chromatography (silica, ethyl acetate/dichloromethane 8:2) to yield **17** (185 mg; 0.47 mmol) as a pale yellow oil. Yield: 99%. R_f (silica; ethyl acetate) 0.50; HRMS/ESI m/z [M+NH₄]⁺ = 412.2000 (calculated for C₁₇H₃₀O₈: 412.2000); ¹H NMR (CDCl₃) 1.93-1.99 (m, 2H, H-3, H-8), 2.01-2.12 (m, 4H, H-3, H-8, H-4, H-7), 2.45-2.51 (m, 2H, H-4, H-7), 3.07 (s, 3H, CH₃), 3.56 (d, 2H, J = 4.2 Hz, CH₂-g), 3.62-3.70 (m, 8H, CH₂-c, d, e, f), 3.75-3.77 (m, 2H, CH₂-b), 4.13-4.16 (m, 2H, H-1, H-2), 4.36-4.38 (m, 2H, CH₂-a), 4.96 (t, 1H, J = 4.2 Hz, H-h), 5.59-5.61 (m, 2H, H-5, H-6); ¹³C NMR (CDCl₃) 23.5 (2C, C-4, C-7), 28.6 (2C, C-3, C-8), 37.8 (CH₃), 69.0 (C-b), 69.4 (C-a), 70.5 (C-c or d or e or f), 70.6 (C-c or d or e or f), 70.6 (C-c or d or e or f), 71.2 (C-c or d or e or f), 73.1 (C-g), 79.1 (2C, C-1, C-2), 100.7 (C-h), 129.3 (2C, C-5, C-6).

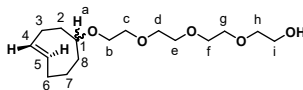
Photoisomerisations

(E)-2-(2-(2-(2-(cyclooct-4-en-1-yloxy)ethoxy)ethoxy)ethoxy)ethanol **10a** and **10b**



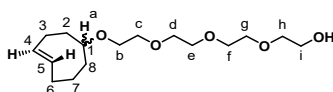
To a solution of compound **6** (364 mg; 1.20 mmol) in a mixture of diethyl ether:hexane (4:1, 50 mL) was added methyl benzoate (377 mg; 2.77 mmol; 2.3 eq.). The reaction mixture was pumped through the microreactor (FEP capillary tubing, length 2.5 m; ID 0.5 mm) and then to a column filled with silica impregnated with silver nitrate (314 mg) and glass beads (200 mg of 1mm beads and 70 mg of 212-300 μ m beads), at an average flow rate of 0.2 mL.min⁻¹, to achieve a residence time of 2.5 min in the reactor. After 10 h of experiment, the packed bed was washed with diethyl ether/hexane (4:1), and then the column was emptied in an Erlenmeyer flask. The silica was stirred with ammonium hydroxide (10 mL) and dichloromethane (10 mL) for 5 min. After filtration, the filtrate was transferred to an extraction funnel. The organic phase was separated, and the aqueous phase was extracted with dichloromethane (3 x 15 mL). The organic layers were combined, dried over MgSO₄, filtered and evaporated under reduced pressure. The crude products were purified by column chromatography (silica gel, ethyl acetate/ethanol 100:0 then 97:3) to yield **10a** (major isomer) and **10b** (minor isomer) as colorless oils. The stereochemistry was determined according to M. Royzen *et al.*^[6]

MINOR compound **10b**:



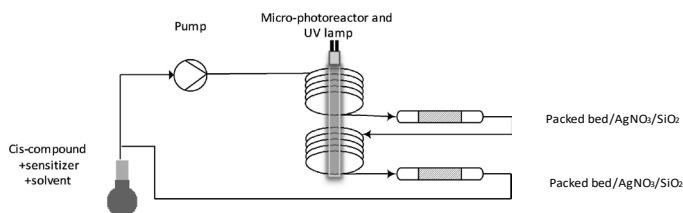
m = 20 mg. Yield: 6%. R_f (silica; ethyl acetate) 0.30; HRMS/ESI m/z [M+H]⁺ = 303.2187 (calculated for C₁₆H₃₀O₅: 303.2166); ¹H NMR (CDCl₃) 1.10-1.16 (m, 1H, H-8), 1.42-1.48 (m, 1H, H-2), 1.68-1.72 (m, 1H, H-7), 1.76-1.83 (m, 2H, H-6, H-7), 1.97-1.99 (m, 1H, H-3), 2.11-2.22 (m, 2H, H-6, H-8), 2.28-2.32 (m, 2H, H-2, H-3), 2.84 (bs, 1H, OH), 3.44-3.49 (m, 1H, H-b), 3.56-3.71 (m, 16H, H-a, H-b, CH₂-c, d, e, f, g, h, i), 5.43-5.49 (m, 1H, H-4), 5.57-5.63 (m, 1H, H-5); ¹³C NMR (CDCl₃) 27.7 (C-7), 29.9 (C-3), 33.1 (C-8), 34.7 (C-6), 40.4 (C-2), 61.9 (C-i), 68.4 (C-b), 70.5 (C-c, d, e, f or g), 70.8 (C-c, d, e, f or g), 70.8 (C-c, d, e, f or g), 70.9 (C-c, d, e, f or g), 71.0 (C-c, d, e, f or g), 72.7 (C-h), 75.0 (C-1), 131.5 (C-4), 136.0 (C-5).

MAJOR compound **10a**:

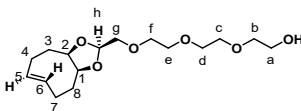


$m = 33$ mg. Yield: 9%. Rf (silica; ethyl acetate) 0.15; HRMS/ESI m/z $[M+H]^+ = 303.2200$ (calculated for $C_{16}H_{30}O_5$: 303.2166); 1H NMR ($CDCl_3$) 1.46-1.49 (m, 2H, H-7, H-8), 1.79-1.85 (m, 2H, H-2, H-8), 1.88-1.96 (m, 2H, H-6, H-7), 2.05-2.09 (m, 1H, H-2), 2.18-2.22 (m, 1H, H-3), 2.32-2.34 (m, 2H, H-3, H-6), 2.53 (bs, 1H, OH), 2.98-3.00 (m, 1H, H-a), 3.41-3.44 (m, 1H, H-b), 3.50-3.64 (m, 13H, H-b, CH_2 -c, d, e, f, g, h), 3.69-3.70 (m, 2H, CH_2 -i), 5.32-5.38 (m, 1H, H-5), 5.52-5.58 (m, 1H, H-4); ^{13}C NMR ($CDCl_3$) 31.9 (C-7), 33.1 (C-3), 34.6 (C-6), 37.8 (C-8), 40.8 (C-2), 61.8 (C-i), 67.5 (C-b), 70.3 (C-c, d, e, f or g), 70.6 (2C, C-c, d, e, f or g), 70.7 (C-c, d, e, f or g), 70.9 (C-c, d, e, f or g), 72.8 (C-h), 86.2 (C-1), 132.3 (C-5), 135.5 (C-4).

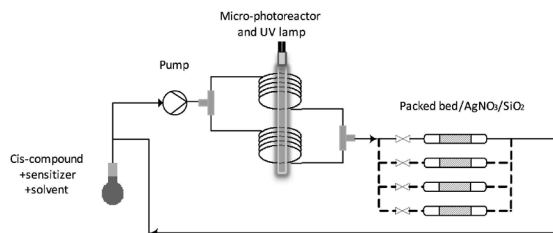
2-(2-(2-(((2*S*,3*aR*,9*aS*,*E*)-3*a*,4,5,8,9,9*a*-hexahydrocycloocta[*d*][1,3]dioxol-2-yl)methoxy)ethoxy)ethoxy)ethanol 19



To a solution of compound **15** (85 mg; 0.27 mmol) in *tert*-butyl methyl ether (25 mL) was added methyl benzoate (201 mg; 1.48 mmol; 5.5 eq.). The reaction mixture was pumped through a first microreactor (FEP capillary tubing, length 2.5 m; ID 0.5 mm) followed by a first column filled with silica impregnated with silver nitrate (324 mg) and glass beads (35 mg of 212-300 μ m beads and 110 mg of 1 mm beads), then through a second reactor (FEP capillary tubing, length 1.0 m; ID 0.5 mm) followed by a second column filled with silica impregnated with silver nitrate (160 mg) and glass beads (37 mg of 212-300 μ m beads and 120 mg of 1 mm beads), at a flow rate of 0.1 mL \cdot min $^{-1}$, to achieve a residence time of 2.5 min in the first reactor and 1 min in the second reactor. After 10 h of experiment, the packed beds were washed with *tert*-butyl methyl ether, and then the columns were emptied in an Erlenmeyer flask. The silica was stirred with ammonium hydroxide (5 mL) and dichloromethane (5 mL) for 5 min. After filtration, the filtrate was transferred to an extraction funnel. The organic phase was separated, and the aqueous phase was extracted with dichloromethane (3 \times 10 mL). The organic layers were combined, dried over $MgSO_4$, filtered and evaporated under reduced pressure to yield **19** (18 mg; 57 μ mol) as a colorless oil. Yield: 21%. HRMS/ESI m/z $[M+H]^+ = 317.1984$ (calculated for $C_{16}H_{28}O_6$: 317.1959); 1H NMR ($CDCl_3$) 1.48-1.57 (m, 1H, H-3 or 8), 1.64-1.72 (m, 1H, H-3 or 8), 1.79-1.91 (m, 2H, H-3 or 8, and H-4 or 7), 2.07-2.28 (m, 3H, H-4 or 7, H-3 or 8, and H-4 or 7), 2.35-2.42 (m, 1H, H-4 or 7), 3.55 (t, 2H, $J = 4.1$ Hz, CH_2 -g), 3.58-3.72 (m, 12H, CH_2 -a, b, c, d, e, f), 3.87-3.96 (m, 2H, H-1, H-2), 4.89 (t, 1H, $J = 4.1$ Hz, H-h), 5.46-5.71 (m, 2H, H-5, H-6); ^{13}C NMR ($CDCl_3$) 25.7 (C-4 or 7), 31.4 (C-4 or 7), 33.9 (C-3 or 8), 38.8 (C-3 or 8), 61.9 (C-a), 70.4 (C-c or d or e or f), 70.7 (C-c or d or e or f), 70.8 (C-c or d or e or f), 71.1 (C-c or d or e or f), 72.7 (C-b or C-g), 72.8 (C-b or C-g), 80.7 (C-1 or 2), 82.7 (C-1 or 2), 100.3 (C-h), 131.3 (C-5 or 6), 136.5 (C-5 or 6). The stereochemistry was determined according to A. Darko *et al.*^[3]

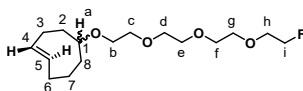


(*E*)-5-(2-(2-(2-(2-fluoroethoxy)ethoxy)ethoxy)ethoxy)cyclooct-1-ene 2*a* and 2*b*



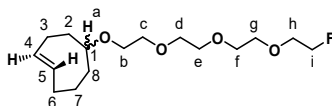
To a solution of compound **9** (82 mg; 0.27 mmol) in a mixture of diethyl ether:hexane (1:1, 25 mL) was added methyl benzoate (169 mg; 1.24 mmol; 4.6 eq.). The reaction mixture was pumped through two microreactors (FEP capillary tubing, length 5.0 m; ID 0.5 mm) in parallel followed by four columns in parallel (switch from one column to another every 90 min) filled with silica impregnated with silver nitrate (200-220 mg in each column) and glass beads (100-120 mg of 1 mm beads in each column), at a flow rate of 1.0 mL·min⁻¹, to achieve a residence time of 2.0 min in both reactors. After 6 h of experiment, the packed beds were washed with diethyl ether/hexane (1:1), and then the column was emptied in an Erlenmeyer flask. The silica was stirred with ammonium hydroxide (5 mL) and dichloromethane (5 mL) for 5 min. After filtration, the filtrate was transferred to an extraction funnel. The organic phase was separated, and the aqueous phase was extracted with dichloromethane (3 x 10 mL). The organic layers were combined, washed with water, dried over MgSO₄, filtered and evaporated under reduced pressure. The crude products were purified by column chromatography (silica gel, ethyl acetate/heptane 2:8 then 5:5) to yield **2a** (major isomer) and **2b** (minor isomer) as colorless oils. The stereochemistry was determined according to M. Royzen *et al.*^[6]

Minor compound **2b**:



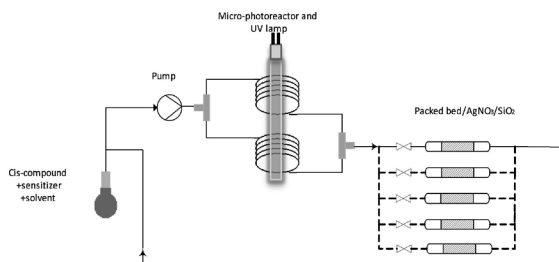
m = 4 mg. Yield: 5%. Rf (silica, ethyl acetate/heptane 2:8) 0.21; HRMS/ESI *m/z* [M+H]⁺ = 305.2149 (calculated for C₁₆H₂₉FO₄: 305.2123); ¹H NMR (CDCl₃) 1.11-1.17 (m, 1H, H-8), 1.43-1.50 (m, 1H, H-2), 1.69-1.71 (m, 1H, H-7), 1.78-1.86 (m, 2H, H-6, H-7), 1.98-2.01 (m, 1H, H-3), 2.14-2.31 (m, 4H, H-6, H-8, H-2, H-3), 3.45-3.49 (m, 1H, H-b), 3.56-3.59 (m, 2H, H-a, H-b), 3.66-3.69 (m, 11H, H-h, CH₂-c, d, e, f, g), 3.78-3.80 (m, 1H, H-h), 4.56 (d, 2H, ²J_{H-F} = 47.2 Hz, CH₂-i), 5.44-5.50 (m, 1H, H-4), 5.59-5.65 (m, 1H, H-5); ¹³C NMR (CDCl₃) 27.7 (C-7), 29.9 (C-3), 33.2 (C-8), 34.7 (C-6), 40.4 (C-2), 68.4 (C-b), 70.6 (d, ²J_{C-F} = 20 Hz, C-h), 70.8 (C-c, d, e, f or g), 71.0 (C-c, d, e, f or g), 71.0 (C-c, d, e, f or g), 71.0 (2C, C-c, d, e, f or g), 75.0 (C-1), 83.3 (d, ¹J_{C-F} = 168 Hz, C-i), 131.4 (C-4), 136.0 (C-5).

Major compound **2a**:

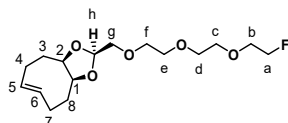


m = 16 mg. Yield: 20%. Rf (silica, ethyl acetate/heptane 2:8) 0.11; HRMS/ESI *m/z* [M+H]⁺ = 305.2143 (calculated for C₁₆H₂₉FO₄: 305.2123); ¹H NMR (CDCl₃) 1.47-1.50 (m, 2H, H-7, H-8), 1.76-1.82 (m, 2H, H-2, H-8), 1.90-1.97 (m, 2H, H-6, H-7), 2.07-2.11 (m, 1H, H-2), 2.20-2.24 (m, 1H, H-3), 2.34-2.36 (m, 2H, H-3, H-6), 3.00-3.03 (m, 1H, H-a), 3.42-3.45 (m, 1H, H-b), 3.51-3.68 (m, 12H, H-b, H-h, CH₂-c, d, e, f, g), 3.77-3.79 (m, 1H, H-h), 4.56 (d, 2H, ²J_{H-F} = 47.7 Hz, CH₂-i), 5.33-5.40 (m, 1H, H-5), 5.54-5.60 (m, 1H, H-4); ¹³C NMR (CDCl₃) 31.9 (C-7), 33.2 (C-3), 34.7 (C-6), 37.9 (C-8), 41.0 (C-2), 67.6 (C-b), 70.5 (d, ²J_{C-F} = 20 Hz, C-h), 70.8 (3C, C-c, d, e, f or g), 71.0 (2C, C-c, d, e, f or g), 83.3 (d, ¹J_{C-F} = 170 Hz, C-i), 86.2 (C-1), 132.4 (C-5), 135.5 (C-4).

(2*s*,3*a*R,9*a*S,E)-2-((2-(2-fluoroethoxy)ethoxy)ethoxy)methyl)-3*a*,4,5,8,9,9*a*-hexahydrocycloocta[d][1,3]dioxole 3

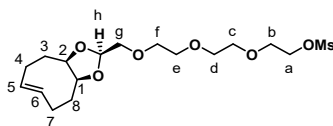


To a solution of compound **18** (37 mg; 0.12 mmol) in *tert*-butyl methyl ether (10 mL) was added methyl benzoate (70 mg; 0.51 mmol; 4.3 eq.). The reaction mixture was pumped through two microreactors (FEP capillary tubing, length 5.0 m; ID 0.5 mm) in parallel followed by five columns in parallel (switch from one column to another every 75 min) filled with silica impregnated with silver nitrate (200–220 mg in each column) and glass beads (100–120 mg of 1 mm beads in each column), at a flow rate of 0.66–1.0 mL·min⁻¹, to achieve an average residence time of 3.0 min in both reactors. After 6 h of experiment, the packed beds were washed with *tert*-butyl methyl ether, and then the columns were emptied in an Erlenmeyer flask. The silica was stirred with ammonium hydroxide (5 mL) and dichloromethane (5 mL) for 5 min. After filtration, the filtrate was transferred to an extraction funnel. The organic phase was separated, and the aqueous phase was extracted with dichloromethane (3 x 10 mL). The organic layers were combined, washed with water, dried over MgSO₄, filtered and evaporated under reduced pressure to yield **3** (29 mg; 91 μmol) as a colorless oil. Yield: 76%. HRMS/ESI *m/z* [M+NH₄]⁺ = 336.2217 (calculated for C₁₆H₂₇FO₅: 336.2181); ¹H NMR (CDCl₃) 1.48–1.58 (m, 1H, H-3 or 8), 1.62–1.73 (m, 1H, H-3 or 8), 1.80–1.92 (m, 2H, H-3 or 8, and H-4 or 7), 2.08–2.28 (m, 3H, H-4 or 7, H-3 or 8, and H-4 or 7), 2.36–2.44 (m, 1H, H-4 or 7), 3.55 (dd, 2H, *J* = 4.2 Hz, *J* = 3.0 Hz, CH₂-g), 3.64–3.71 (m, 9H, H-b, CH₂-c, d, e, f), 3.78 (m, 1H, H-b), 3.87–3.96 (m, 2H, H-1, H-2), 4.56 (dt, 2H, *J* = 4.1 Hz, ²*J*_{H-F} = 47.7 Hz, CH₂-a), 4.89 (t, 1H, *J* = 4.2 Hz, H-h), 5.47–5.66 (m, 2H, H-5, H-6); ¹³C NMR (CDCl₃) 25.8 (C-4 or 7), 31.4 (C-4 or 7), 33.9 (C-3 or 8), 38.9 (C-3 or 8), 70.5 (d, ²*J*_{C-F} = 20 Hz, C-b), 70.7 (C-c or d or e or f), 70.8 (C-c or d or e or f), 71.0 (C-c or d or e or f), 71.3 (C-c or d or e or f), 72.8 (C-g), 80.7 (C-1 or 2), 82.7 (C-1 or 2), 83.3 (d, ¹*J*_{C-F} = 168 Hz, C-a), 100.4 (C-h), 131.4 (C-5 or 6), 136.5 (C-5 or 6); ¹⁹F NMR (CDCl₃) -222.9. The stereochemistry was determined according to A. Darko *et al.*^[3]

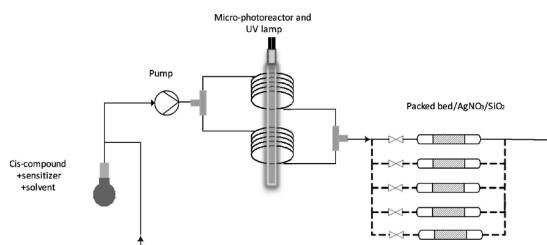


2-(2-(2-(((2*s*,3*aR*,9*aS*,*E*)-3*a*,4,5,8,9,9*a*-hexahydrocycloocta[d][1,3]dioxol-2-yl)methoxy)ethoxy)ethoxy)ethyl methanesulfonate **20**

To a solution of compound **17** (61 mg; 0.16 mmol) in a mixture of diethyl ether:hexane (3:7, 10 mL) was added methyl benzoate (114 mg; 0.84 mmol; 5.3 eq.). The reaction mixture was pumped through two microreactors (FEP capillary tubing, length 5.0 m; ID 0.5 mm) in parallel followed by five columns in parallel (switch from one column to another every 75 min) filled with silica impregnated with silver nitrate (200–220 mg in each column) and glass beads (100–120 mg of 1 mm beads in each column), at a flow rate of 1.0–1.2 mL·min⁻¹, to achieve an average residence time of 2.5 min in both reactors. After 6 h of experiment, the packed beds were washed with diethyl ether:hexane (3:7), and then the columns were emptied in an Erlenmeyer flask. The silica was stirred with ammonium hydroxide (5 mL) and dichloromethane (5 mL) for 5 min. After filtration, the filtrate was transferred to an extraction funnel. The organic phase was separated, and the aqueous phase was extracted with dichloromethane (2 x 10 mL). The organic layers were combined, washed with water, dried over MgSO₄, filtered and evaporated under reduced pressure and then under N₂ flow. The crude product was purified by semi-preparative HPLC (Column Waters XBridge C18, 5 μm, 4.6 x 150 mm; flow rate: 1.0 mL·min⁻¹; UV detection: 210 nm; Solvent A: Ammonium acetate buffer, 50 μM, pH 8; Solvent B: EtOH; Isocratic A/B 74:26). The solvents were evaporated using a lyophilisator to yield **20** as a pale yellow oil (27 mg; 69 μmol). Yield: 44%. HRMS/ESI *m/z* [M+NH₄]⁺ = 412.2002 (calculated for C₁₇H₃₀O₈S: 412.2000); ¹H NMR (CDCl₃) 1.54–1.59 (m, 1H, H-3 or 8), 1.63–1.73 (m, 1H, H-3 or 8), 1.80–1.93 (m, 2H, H-3 or 8, and H-4 or 7), 2.05–2.30 (m, 3H, H-4 or 7, H-3 or 8, H-4 or 7), 2.36–2.44 (m, 1H, H-4 or 7), 3.08 (s, 3H, CH₃), 3.54 (dd, 2H, *J* = 4.2 Hz, *J* = 2.1 Hz, CH₂-g), 3.63–3.67 (m, 8H, CH₂-c, d, e, f), 3.75–3.77 (m, 2H, CH₂-b), 3.87–3.97 (m, 2H, H-1, H-2), 4.37–4.39 (m, 2H, CH₂-a), 4.89 (t, 1H, *J* = 4.2 Hz, H-h), 5.47–5.66 (m, 2H, H-5, H-6). ¹³C NMR (CDCl₃) 25.7 (C-4 or 7), 31.4 (C-4 or 7), 33.9 (C-3 or 8), 37.8 (CH₃), 38.7 (C-3 or 8), 69.1 (C-b), 69.4 (C-a), 70.6–71.2 (4C, C-c, d, e, f), 72.8 (C-g), 80.7 (C-1 or 2), 82.6 (C-1 or 2), 100.3 (C-h), 131.3 (C-5 or 6), 136.4 (C-5 or 6). The stereochemistry was determined according to A. Darko *et al.*^[3]

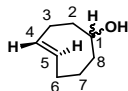


Trans-cyclooctenol



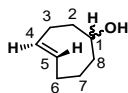
To a solution of *cis*-cyclooctenol (40 mg; 0.32 mmol) in a mixture of diethyl ether:hexane (1:4, 15 mL) was added methyl benzoate (95 mg; 0.70 mmol; 2.2 eq.). The reaction mixture was pumped through two microreactors (FEP capillary tubing, length 5.0 m; ID 0.5 mm) in parallel followed by five columns in parallel (switch from one column to another every 30-45 min) filled with silica impregnated with silver nitrate (200-220 mg in each column) and glass beads (100-120 mg of 1 mm beads in each column), at a flow rate of 0.66-0.80 mL·min⁻¹, to achieve an average residence time of 3.0 min in both reactors. After 3.25 h of experiment, the packed beds were washed with diethyl ether/hexane (1:4), and then the column was emptied in an Erlenmeyer flask. The silica was stirred with ammonium hydroxide (5 mL) and dichloromethane (5 mL) for 5 min. After filtration, the filtrate was transferred to an extraction funnel. The organic phase was separated, and the aqueous phase was extracted with dichloromethane (3 x 10 mL). The organic layers were combined, washed with water, dried over MgSO₄, filtered and evaporated under reduced pressure. The crude products were purified by column chromatography (silica gel, ethyl acetate/*n*-heptane 1:4) to yield *trans*-cyclooctenol major isomer and *trans*-cyclooctenol minor isomer as colorless oils. The stereochemistry was determined according to M. Royzen *et al.*^[6]

Minor compound:



m = 6 mg. Yield: 15%. R_f (silica; ethyl acetate/heptane 1:4 v/v) 0.37; ¹H NMR (CDCl₃) 1.21-1.30 (m, 2H, OH, H-8), 1.61-1.70 (m, 1H, H-2), 1.75-1.87 (m, 3H, H-6, H-7, H-7), 2.06-2.17 (m, 2H, H-3, H-8), 2.19-2.27 (m, 2H, H-2, H-6), 2.32-2.42 (m, 1H, H-3), 4.02-4.06 (m, 1H, H-1), 5.55-5.58 (m, 2H, H-4, H-5); ¹³C NMR (CDCl₃) 27.8 (C-7), 29.4 (C-3), 34.2 (C-6 or C-8), 34.2 (C-6 or C-8), 43.1 (C-2), 67.5 (C-1), 133.2 (C-4 or C-5), 134.4 (C-4 or C-5).

Major compound:



m = 28 mg. Yield: 70%. R_f (silica, ethyl acetate/heptane 1:4 v/v) 0.19; ¹H NMR (CDCl₃) 1.25 (s, 1H, OH), 1.54-1.71 (m, 3H, H-7, H-8, H-8), 1.89-1.98 (m, 4H, H-2, H-2, H-6, H-7), 2.23-2.36 (m, 3H, H-3, H-3, H-6), 3.43-3.48 (m, 1H, H-1), 5.34-5.42 (m, 1H, H-5), 5.53-5.61 (m, 1H, H-4); ¹³C NMR (CDCl₃) 31.4 (C-7), 32.8 (C-3), 34.5 (C-6), 41.2 (C-8), 44.7 (C-2), 77.9 (C-1), 132.9 (C-5), 135.2 (C-4).

CHAPTER 10

Conclusions

10.1 Conclusions and Research Highlights

10.1.1 Conclusions

The thesis aimed at a study of a chemical reaction under highly intensified micro-flow conditions under the auspices of novel process windows (NPW). The thesis was performed together with 4 others (and a post-doc research) in the framework of an ERC Advanced Grant and was the last to start. The thesis of Dr. Shang investigated safe processing under harsh conditions (high-T, high-c) with a harmful reactant, hydrogen peroxide; in the sense of a traditional microreactor topic, i.e. transfer intensification. The thesis of Dr. Stouten investigated a modern kind of transfer intensification through use of a master solvent, supercritical carbon dioxide applied to a new catalyst concept which is the Support Ionic Liquid Phase (SILP) / Supported Aqueous Phase (SAP). The thesis of Borukhova investigated the classical means of flow chemistry NPW activation, which is chemical intensification) (high-T and high-c), and added a high-p and solvent-free intensification. Expanding the benefits of the latter to multi-step syntheses, some synergistic potential was released beyond the sums of chemical intensification. This has termed process-design intensification and was systematically investigated by Dr. Iris Vural-Gürsel. Cost, energy and life-cycle assessment analyses were done at all scales, ranging from the pharma to the bulk chemistry level. Most modern compact, modular containers were considered as ideal platform for manufacturing under intensified / micro-flow conditions. This thesis made the first consideration to NPW transfer intensification with regard to micro-flow separation.

This is the topic of this thesis, the last cornerstone in the bundle of ERC NPW research. More than the proof-of-concept for integrated reaction and separation given by Dr. Iris Vural-Gürsel, deep theoretical analysis thereof is given, the question of orthogonality been tackled, and recycle flow introduced to account for the need of multiple-stage operation. As in the thesis of Dr. Iris Vural-Gürsel, process designs satisfying the pilot-scale on the separation (and reaction) side are proposed.

Concerning the reaction, a non-thermal activation, UV-photo flow, was chosen. Here, the emphasis was not on the establishment of a photo flow chemistry, but rather on the NPW aspects of transfer intensification for such reaction types. For example, to operate under highest photon flux ('reactor-on-lamp'), and with segmented flow as 'nanoliter cuvette' (even under inverted-flow conditions). As in the thesis of Dr. Borukhova, the aim was on multi-step synthesis, but different and as said, the focus was on achieving orthogonality. Here, the superiority of using a photo- versus thermal reaction could be shown. Finally and as said, process design development by integration of micro-flow reaction and separation was done. A real-life application of such processing to produce an ingredient for a medical treatment has been given, as did the thesis of Dr. Borukhova for the production of an active pharmaceutical ingredient. Last, but not least,

automated UHPLC analysis using a new type of fast, minute-volume autosampler was developed, which was targeted towards PAT analysis as quality-control instrument in pharmaceutical manufacturing.

Thus, the thesis is complementary to the four other ones of the ERC grant and managed to investigate proprietary NPW challenges for the first time.

There was even more hope, which has only partially materialized due to the inability to make collaboration further with a Russian partner in Nizhy-Novgorod (as a cause of non-release of a grant joint project and associated guest professorship). The Claisen rearrangement is one of the best investigated reactions and looks back on 100 years investigation. This includes very fundamental studies of the reaction mechanism. Modern quantum-mechanistic modelling and Noble-Prize awarded femto-second spectroscopic studies (Ahmed H. Zewail, California Institute of Technology, Pasadena, USA) has given deep insight in all stages of bonding breakage and formation, including the transition states – femtochemistry: “chemistry in slow motion”. The Russian partner, Prof. Zelentsov, is a specialist in quantum-mechanical modelling of chemistries and was himself active in microreactor photochemistry. Hope of the envisioned collaboration was to use the existing deep insight into the Claisen rearrangement for a target, ‘calculated’ use of NPW principles for chemical intensification and to monitor that by the above named means – quantum-mechanical modelling and modern chemical analysis. This has not been realized, yet three extended reviews deal with the subject and provide a think-tank assessment and statement to the scientific community. For this, an own chapter was inserted, as it is part of the scientific outcome of this thesis.

10.1.2 Research Highlights

Beyond the scope of the NPW innovation, the thesis has delivered the following highlights:

Construct of ideas for rational NPW- and flow chemistry

- (‘White paper’, consisting of two reviews (three, considering a translated version), on the use of computational modelling and most modern mechanistic reaction analysis to identify and control impact factors, relevant for an intensified flow process chemistry, at the example of the Claisen rearrangement.

Transfer intensification

- Intensifying the photoreaction under highest photon flux and developing an analysis for quantifying it through actinometry.
- Intensifying the photoreaction by using segmented flows with their intensification capabilities for photoreactions, (i) liquid layers capping the Taylor gas bubbles which are

much thinner than any practical microchannel, and acting as ‘nanoliter-cuvettes’; (ii) enforced mass transport through recirculation and thus constant surface refreshment, and (iii) and test for coiled inverted flows to make use of Dean forces to strengthen (ii).

Chemical intensification

- Developing a synthesis path for di-substituted aromates which has chemical diversity for reasons of (i) synthesis of all possible regioisomers, by developing both thermal and photo-chemical pathways in flow, and (ii) flexibility in choice of reactant by developing a two-step (substitution-rearrangement) flow synthesis.
- Orthogonality: demonstration of the superior issue of the photo-Claisen rearrangement, as the unwanted side reactions of non-compatible molecules are larger when operating under thermal conditions. Such finding have led to the construct of ideas of the ‘Compartmentalized Factories’ of the EU FET-Open project ONE-FLOW (started in 2017), coordinated by TU Eindhoven.

Process-design intensification

Adsorption

- First research (paper) on micro-flow adsorption and its use for product separation. One of the few researches (papers) in the field of liquid-phase recycle operation by micro-flow.
- Systematic kinetic study and full theoretical study of the underlying effects, which was an enabler for the next point.
- Proposal and evaluation of process designs of integrated photo-reaction and adsorption on a pilot-scale; addressing the main issue of automatic (in-line) adsorption media renewal.

Reactive absorption

- Proposal of similar process designs of integrated photo-reaction and reactive absorption (ion exchanger) on a pilot-scale and experimental validation on a lab-scale; addressing the main issue of automatic (in-line) adsorption media renewal.

PAT-targeted UPHLC online-analysis:

- Holistic analysis of suitability of UHPLC as PAT tool in automated, on-line fashion; providing challenges and chances as opportunities for follow-up researches
- Proof-of-concept for fast, minute-volume autosampler as missing link
- Use of statistical analysis for flow process automation beyond the reported kinetic analysis, with the statistical approaches common for PAT development

Real-life application

- Development of a UV-photo flow process for real-life molecules (TCO and TCO derivatives)
- Enabling application of them for PET imaging and proof of that.

Dissemination beyond thesis core subject

Metallic Nanoparticles Made in Flow and their Catalytic Applications in Organic Synthesis

Based on:

Shahbazali, E., Hessel, V., Noël, T. & Wang, Q. (2014). Metallic nanoparticles made in flow and their catalytic applications in organic synthesis. *Nanotechnology Reviews*, 3(1), 65-86

Shahbazali, E., Hessel, V., Noël, T., Metallic nanoparticles made in flow and their catalytic applications in organic synthesis. Chapter 3 in *Catalytic Reactors*, (eds. Basudeb Saha) Walter de Gruyter GmbH & Co, 2016

Since these two paper reviews are in addition to this thesis, here only the abstract is given. For more information, it is referred to the published paper or the related published book chapter.

Abstract

This paper reviews recent developments on the synthesis of noble metal nanoparticles in micro and millifluidic devices and their catalytic application in organic flow synthesis. A variety of synthesis methods using microfluidics is presented for gold, silver, palladium, platinum, and copper nanoparticles, including the formation in single-phase flows and multiphase flows. In the field of organic chemistry, metal nanoparticles can be used as catalysts. This can lead to remarkably improved reaction performance in terms of minimizing the reaction time and higher yields. In this context, various applications of those metal nanoparticles as catalysts in microfluidic devices are highlighted at selected examples. As a new direction and operational window, nanocatalysts may be synthesized in situ in flow and directly utilized in an organic synthesis. This allows making use of highly active, yet unstable catalyst species, which may only have a very short life of a few seconds - a kind of flashed nanocatalyst organic synthesis.

List of Publications

List of Publications

Journal articles

1. Shahbazali, E., Su, Y., Noël, T., Hessel, V. (2018). UV-Photo-flow intensification - Taylor Flow for Enhancing Photo-microreactors. To be submitted to Chemical Engineering Journal
2. Shahbazali, E., Billaud, E., Meuldijk, J., Bormans, G., Noël, T. & Hessel, V. (2018). Photo isomerization of cis-cyclooctene to trans-cyclooctene: Integration of a micro flow reactor and separation by specific adsorption. Industrial and Engineering Chemistry Research (submitted)
3. Shahbazali, E., Escriba Gelonch, M., Honing, M. & Hessel, V. (2018). Quality-in(Process)Line (QuiProLi) process intensification for a micro-flow UV-photo synthesis enabled by online UHPLC analysis. Tetrahedron, 74 (25), 3143-3151
4. Billaud, E., Shahbazali, E., Ahamed, M., Cleeren, F., Noël, T., Koole, M., Verbruggen, A., Hessel, V. & Bormans, G. (2017). Micro-flow photosynthesis of new dienophiles for inverse-electron-demand Diels-Alder reactions: potential applications for pretargeted in vivo PET imaging. Chemical Science, 8(2), 1251-1258.
5. Shahbazali, E., Noël, T. & Hessel, V. (2016). Photo-Claisen rearrangement of allyl phenyl ether in micro-flow: influence of phenyl core substituents and vision on orthogonality. Journal of Flow Chemistry, 6(3), 252-259.
6. Shahbazali, E., Spapens, M.R.P., Kobayashi, H., Ookawara, S., Noël, T. & Hessel, V. (2015). Connected nucleophilic substitution-Claisen rearrangement in flow: analysis for kilo-lab process solutions with orthogonality. Chemical Engineering Journal, 281, 144-154.
7. Hessel, V., Shahbazali, E., Noël, T. & Zelentsov, S. (2014). Claisen-Umlagerung im Rühr- und Durchflussbetrieb : Verstaendnis des Mechanismus und Steuerung der Einflussgroessen : the Claisen rearrangement in flow and batch processing : mechanism exploration and control over influencing factors. Chemie, Ingenieur, Technik, 86(12), 2160-2179.
8. Zelentsov, S., Hessel, V., Shahbazali, E. & Noël, T. (2014). The Claisen rearrangement – part 1: mechanisms and transition states, revisited with quantum mechanical calculations and ultrashort pulse spectroscopy. ChemBioEng Reviews, 1(5), 230-240.
9. Hessel, V., Shahbazali, E., Noël, T. & Zelentsov, S. (2015). The Claisen rearrangement - part 2: impact factor analysis of the Claisen rearrangement, in batch and in flow. ChemBioEng Reviews, 1(6), 244-261.
10. Shahbazali, E., Hessel, V., Noël, T. & Wang, Q. (2014). Metallic nanoparticles made in flow and their catalytic applications in organic synthesis. Nanotechnology Reviews, 3(1), 65-86.

Book Chapter

1. Shahbazali, E., Hessel, V., Noël, T., Metallic nanoparticles made in flow and their catalytic applications in organic synthesis. Chapter 3 in *Catalytic Reactors*, (eds. Basudeb Saha) Walter de Gruyter GmbH & Co, 2016

Conference contributions

1. Shahbazali, E., Noël, T. & Hessel, V. Taylor flow for enhancing micro photoreactors (IMRET, China, Beijing, September 2016)
2. Shahbazali, E., Noël, T., Meuldijk, J., Hessel, V., Billaud, E., Ahamed, M. & Bormans, G. (2015). Micro-flow based photoisomerization and in-flow separation process. (MicroNanoConference, The Netherlands, Amsterdam, December 2015)
3. Shahbazali, E., Tsompanoglou, T., Noël, T., Meuldijk, J., Hessel, V., Billaud, E., Ahamed, M. & Bormans, G. Micro-flow based photoisomerization and in-flow separation process. (CHAINS, The Netherlands, Veldhoven, 2015)
4. Shahbazali, E. & Hessel, V. Novel process windows as gate opener towards green chemistry. Advances in innovative experimental methodology or simulation tools used to create, test, control and analyze systems, materials and molecules (NEXTLAB 2014), Rueilmalmaison, France, 2-4 April 2014)
5. Billaud, E., Shahbazali, E., Ahamed, M., Cleeren, F., Noël, T., Hessel, V., Koole, M., Verbruggen, A. & Bormans, G. New dienophiles for the inverse-electron-demand Diels-Alder reaction and for pretargeted PET imaging. (WMIC, New York, 2016)

Acknowledgement

Here, I am sitting behind my computer and thinking of my life during the past 8 years. Back to 2010, the first time I got an email saying that I had been accepted for PDEng at TU Eindhoven, I was very excited and delighted. I knew a new path was opened in front of me. I came to Eindhoven, my new city. Since then my life changed entirely. Studying abroad has its own “pros” and “cons”, it requires a very brave personality. Achieving PDEng was not enough for me as an ambitious person, therefore, I decided to continue as a PhD researcher. Today that I am here at the end of this journey, I would say I couldn't make it without all the people were with me during these years. I had the pleasure to work among talented, inspiring and most importantly kind people who supported me in different aspects.

Foremost, I would like to thank my promoter and first supervisor Prof. Volker Hessel for providing me this opportunity. I still remember the first time at 2012 that I came to your office, you were speaking about process chemistry and as an engineer I was not that sure if this was suited for me. But, you trusted me. I appreciate your trust in my capabilities that allowed me to learn, work and grow. Thanks to your good network and reputation, from that I benefited working with well-known analytical company, Agilent. I learned from you how to build a research story. You were always available even if I would send an email during the night, I would get a quick reply back, and not many supervisors would do that.

I would like to express my gratitude to my co supervisors, Dr. Timothy Noël and Prof. Jan Meuldijk. Tim, thank you for your support, I am grateful for having you as my daily supervisor and your great expertise in photochemistry. Your friendly attitude turned these challenging years into a nice experience for me. Jan, thank you for your time and availability and for the productive discussions during our meetings. You were always very much supportive to me and strengthen much the engineering depth of my research, especially for the adsorption chapter. I really appreciate your input and scientific comments in my papers.

I would also like to thank the committee members: prof. Emiel Hensen, prof. Holger Löwe, prof. Maarten Honing, prof. Martin van Sint Annaland, and dr. Stefan Meskers for dedicating their time to the careful reading of my thesis and for participating in my defense.

To Carlo, thank you for making sure that our work environment was a safe place. To Peter and Marlies, thank you for your help in the lab, especially with the last phase of my project which was involved with Agilent HPLC. To Erik, thank you, you were the best technician that our group could have.

Thank you Denise, without you I would still be lost in the administration rules for PhD defense application. You were really helpful, by providing quick answers to all my questions. Also, I would like to thank Jose. Jose you were one of the best secretaries I have ever met. I never forget your kind messages and gifts throughout the time that I was sick at home.

To my besties, Catherine, Smitha, Shamayita and Teresa, girls I can write a book about you... but here I just say without you I could not handle all these years. Popo, I already started to cry... It is difficult to write about you and our friendship. I think this is the 5th time I am writing this paragraph and stop just because I get too emotional (Ela re...)... My Katoo, you are the sweetest angel ever. I will never forget what you did for me during the last months of my PhD. I won't forget your generosity that you shared your flat with me. Ela re now some more funny things, Katoo, from now on who would come to my office and say "mikrouliiii may I ask you something?" or who would come and ask "Mikrouli do you have something sweet? And àààgain you! :D I will never ever forget your gesture when you were saying your Greek expressions, like take... and leave me alone, which now I am applying it in my daily life a lot ;) Anyhow, my English has been strongly influenced by a Greek girl! Thanks for all the funs we had together and your translated expressions especially when we really needed. The trip to Athens was a memorable trip, thanks to Georgia and Costas. Georgia, when you are reading this part just laugh, your daughter is adorable. My dear cool officemate Smitha, thank you for being there for me and sharing nice memories with me. I miss that. You were always trying to calm me down whenever I was sad, angry or disappointed. You are the best assistant ever! I still count on your corrections on my writings, don't think you can get rid of me ;) Shamayita, you are one of the calmest scientists I have ever met. I learned a lot from you. Thanks for all the moments we shared especially the dinners also with Shauvik. Martini, I will miss your shopping attitude. I should have hired you and Catherine as my stylish assistants, for instance, now I don't know what to wear in my defense :\ Girls loooooook, we need to have a reunion every year! This time should be in California! We have to go and tease Katoo ;).

Thanks to my dear friends, Bhaskar, Carlos and Marc from whom I gained a lot of knowledge. Thanks to the all scientific discussions we had. Bhaskar, you are a very kind and strong person. I learned a lot from you how to be strong and work professionally. Marc, I enjoyed working with you, especially in the last part of my thesis.

To the rest of the SFPs, SCRs and also PPDs (my late co-workers), thank you all for all the activities and fun we had together. During the four years (+2 years of PDEng) a lot of people have finished their studies, and a lot of new PhD students have come. It was a pleasure having you as colleagues and friends.

I am very thankful to dr. Emilie Billaud and prof. Guy Bormans from KU Leuven for their contribution and the collaboration that we had, which concluded in very valuable results and publications.

To my students Max and Dora, thank you for your commitment and enthusiasm during the project which resulted in fruitful publications.

To my friends, Samaneh and Hossein, Maryam and Pouya, Raheleh and Adam, Azar and Hamid, Shohreh and Marco, Mona thank you guys for all the moments that we shared together.

To my dear Ana and Faysal, thank you, you were among the first initiator of this journey. Ana, my dear soulmate, without you I couldn't start this step of my life. Thank you for being there for me. I will never forget the nice trip together to Portugal that your lovely parents hosted me.

Last but foremost, to my family, to my route and my origin. Again, tears are coming...

Mamani va babayi e azizam, to you that whoever, wherever I am now, I owe you all. I am the luckiest ever that I have you as my parents. I cannot find any words to express my feeling. If not for your care and sacrifice, I wouldn't be standing as a doctorate candidate today. You gave me wings and taught me how to soar up into the sky and expand my horizon. You sacrificed your own happiness, just so that I could be happy. I know how much you wanted me to finish my PhD. You were always encouraged me to aim the best. It may take a lifetime, but I'll do everything to repay for what you have done for me. Mamanie golam, I am very very sorry that I was not there to help you. I love you both to death.

To my love, Arash, thank you for all your support, motivation, patience and sacrifice. Without having you next to me this book wouldn't come to an end. Thank you for being my inspiration from the first time we met. You were always on my side even at the very difficult time.

To my lovely sis, Maryam, and my brother in law, Arash, and my little angel, Ario, thanks for supporting me from the distance. Maryami, thank you for being there for me, I cannot say how grateful I am that I have you, sisi joonam.

Also, thanks to my parents in law, who were always ready to help and support.

And finally, thanks to whoever that played a role in my journey and I have forgotten to mention.

Elnaz Shahbazali
Herent, August 2018

About the author

Elnaz Shahbazali was born in Tehran (1982), Iran. In 2006, she received her MSc degree in Chemical Engineering-separation processes and transport phenomena- at Sharif University of Technology in Iran. In 2010 she moved to the Netherlands to pursue a Professional Doctorate in Engineering (Process and Product Design) at Eindhoven University of Technology. She obtained her PDEng degree in 2012 by working on “New route to SiC” for her individual design project. In October 2012, she started her PhD project at Eindhoven University of Technology in the group of Micro Flow Chemistry and Process Technology under the supervision of Prof. Volker Hessel. Her PhD project on rearrangement and isomerization in continuous micro-flow was funded by the European Research Council (ERC) advanced grant on “Novel Process Windows – Boosted Micro Process Technology”. The focus of her PhD is to develop integrated process design solutions under the highly chemically intensified (under Novel Process Window) conditions. The results of her research are described in this dissertation and in 10 peer reviewed journal papers. She has presented her research findings orally as well as with posters in several conferences.

As the next step in her career, she joined ExxonMobil Chemical Europe Inc. as Senior Process Development Engineer at the Europe Technology Center based in Machelen, Belgium from 2018.

